ARLCB-SP-85009

PROCEEDINGS OF THE

FOURTH U S ARMY SYMPOSIUM ON GUN DYNAMICS

VOLUME II OF II

HILTON INN OF THE PALM BEACHES
RIVIERA BEACH, FL

7-9 MAY 1985

SPONSORED BY

US ARMY ARMAMENT RESEARCH AND DEVELOPMENT CENTER
LARGE CALIBER WEAPON SYSTEMS LABORATORY
BENET WEAPONS LABORATORY
WATERVLIET, N. Y. 12189

DISCLAIMER

The findings in this report are not to be construed as an official Department of the Army position unless so designated by other authorized documents.

The use of trade name(s) and/or manufacture(s) does not constitute an official indorsement or approval.

DISPOSITION

Destroy this report when it is no longer needed. Do not return it to the originator.

PROCEEDINGS OF THE

FOURTH US ARMY SYMPOSIUM ON GUN DYNAMICS

HILTON INN OF THE PALM BEACHES
RIVIERA BEACH, FL

7–9 MAY 1985

EDITORS:

DR. THOMAS E. SIMKINS,
BENET WEAPONS LABORATORY, LCWSL AMCCOM

DR. J. VASILAKIS,
BENET WEAPONS LABORATORY, LCWSL, AMCCOM

SPONSORED BY

US ARMY ARMAMENT RESEARCH AND DEVELOPMENT CENTER
LARGE CALIBER WEAPON SYSTEMS LABORATORY
BENET WEAPONS LABORATORY
WATERVLIET, N. Y. 12189

SECURITY CLASSIFICATION OF THIS PAGE (When Data Entered)

REPORT DOCUMENTATION PAGE

READ INSTRUCTIONS BEFORE COMPLETING FORM

1. REPORT NUMBER: ARLCB-SP-85009	2. GOVT ACCESSION NO.: AD-A162 135
3. RECIPIENT'S CATALOG NUMBER:	
4. TITLE (and Subtitle): PROCEEDINGS, FOURTH U.S. ARMY SYMPOSIUM ON GUN DYNAMICS VOL II of II.	5. TYPE OF REPORT & PERIOD COVERED: Final
	6. PERFORMING ORG. REPORT NUMBER:
7. AUTHOR(s): Editors: Dr. T. E. Simkins, Dr. J. Vasilakis	8. CONTRACT OR GRANT NUMBER(s):
9. PERFORMING ORGANIZATION NAME AND ADDRESS: US Army Armament Research & Development Center, Benet Weapons Laboratory, SMCAR-LCB-TL, Watervliet, NY 12189-5000	10. PROGRAM ELEMENT, PROJECT, TASK AREA & WORK UNIT NUMBERS: N. A.
11. CONTROLLING OFFICE NAME AND ADDRESS: US Army Armament Research & Development Center, Large Caliber Weapon Systems Laboratory, Dover, NJ 07801-5001	12. REPORT DATE: May 1985 13. NUMBER OF PAGES: 236
14. MONITORING AGENCY NAME & ADDRESS (if different from Controlling Office):	15. SECURITY CLASS. (of this report): Unclassified 15a. DECLASSIFICATION/DOWNGRADING SCHEDULE:

16. DISTRIBUTION STATEMENT (of this Report)

Approved for public release; Distribution unlimited

17. DISTRIBUTION STATEMENT (of the abstract entered in Block 20, if different from Report)

18. SUPPLEMENTARY NOTES

Presented at the Fourth U.S. Army Symposium on Gun Dynamics, 7-9 May 1985, at the Hilton Inn of the Palm Beaches, Riviera Beach, Florida.

19. KEY WORDS (Continue on reverse side if necessary and identify by block number)

Acquisition
Ballistics
Barrel Vibration
Dynamics
Precision
Stabilization
Target Acquisition

20. ABSTRACT (Continue on reverse side if necessary and identify by block number)

This represents a compilation of thirty-four technical papers concerning analyses, design, measurement, and automation of gun dynamics. The authors represent a cross-section of the scientific and technical community, including universities, industrial, and Government research laboratories.

DD FORM 1 JAN 73 1473 EDITION OF 1 NOV 65 IS OBSOLETE UNCLASSIFIED

SECURITY CLASSIFICATION OF THIS PAGE (When Data Entered)

TABLE OF CONTENTS

Page

VOLUME I

Page

GENERAL SESSION II.

CHAIRMAN:
Gary Anderson, Army Research Office

*This paper arrived too late to be included with the papers in this session. It is the last paper in Volume II.

FOREWORD

The precision of a gun system clearly involves the dynamics of the gun carrier, ground characteristics, and interior and exterior ballistics. It is a problem of enormous complexity and is often divided into different phases for investigative purposes. While the division of the task is convenient and often necessary, one should always keep in mind that the different phases interact and the dynamic forces are usually coupled. This fact necessitates an interactive process or, better yet, a complete system approach, if at all possible, to the precision problem.

During recent years, one has witnessed great strides in various branches of continuum mechanics, kinematic designs, and numerical and computer techniques for solving problems of great complexity as well as in the areas of experimental mechanics and instrumentation. It appears feasible now more than ever to gain understanding and to improve the design of gun systems for greater accuracy by exploiting the new technological advances. The present Symposium represents the continuing interest of the U.S. Army in this direction.

These proceedings contain nearly thirty-five papers presented at the Symposium held at the Hilton Inn of the Palm Beaches, Riviera Beach, FL, during 7-9 May 1985. The papers represent the current research efforts on gun dynamics and its effect on precision and design by industrial, university, and Department of Defense Laboratories in the United States and two allied nations - the United Kingdom and the Federal Republic of West Germany.

The editors gratefully acknowledge the work of Ellen Fogarty in preparing volumes I and II of Gun Dynamics, and her assistance in the collection of the papers and the required clearances.

LIST OF ATTENDEES

Gary L. Anderson
Army Research Office
P.O. Box 12211
Research Triangle Park, NC 27709-2211

Robert S. Becker
S&D Dynamics
755 New York Avenue
Huntington, NY 11743

Gerald A. Benedetti
Sandia National Laboratories
East Avenue
Livermore, CA 94550-0096

Willard R. Benson
Aerojet Ordnance Company
Rockaway Townsquare Office Park
33 Mt. Hope Avenue, Suite 103
Rockaway, NJ 07866

Philip Benzkofer
Armament Research & Development Center
SMCAR-SCA
Dover, NJ 07801-5001

John Bostonian III
Armament Research & Development Center
SMCAR-LCU-SI
Dover, NJ 07801-5001

Robert X. Brennan
Armament Research & Development Center
SMCAR-LCN
Dover, NJ 07801-5001

Jack Brooks
Armament Research & Development Center
SMCAR-LCS
Dover, NJ 07801-5001

David N. Bulman
Royal Military College of Science
Land Systems Group
Shrivenham
Swindon Wilts SN6 8LA England

Bruce P. Burns
Ballistic Research Laboratory
AMXBR-IBD
Aberdeen Proving Ground, MD 21005-5066

S. H. Chu
Armament Research & Development Center
SMCAR-LCA
Dover, NJ 07801-5001

Kok Chung
Armament Research & Development Center
SMCAR-LC
Dover, NJ 07801-5001

Susan A. Coates
Ballistic Research Laboratory
AMXBR-IBD
Aberdeen Proving Ground, MD 21005-5066

Herbert E. Cohen
Army Materiel Systems Analysis Activity
AMSY-MP
Aberdeen Proving Ground, MD 21005-5071

P. A. Cox
Southwest Research Institute
6220 Culebra Road
P.O. Drawer 28510
San Antonio, TX 78284

Thomas E. Davidson
Armament Research & Development Center
SMCAR-LC
Dover, NJ 07801-5001

Thomas Dolce
Army Materiel Systems Analysis Activity
AMXSY-GB
Aberdeen Proving Ground, MD 21005-5071

Patricia M. Dutko
Armament Research & Development Center
SMCAR-LCA-G
Dover, NJ 07801-5001

Thomas F. Erline
Ballistic Research Laboratory
AMXBR-IBD
Aberdeen Proving Ground, MD 21005-5066

Roger K. Fancett
Royal Armament Research & Development
Establishment
Fort Halstead
Seven Oaks, Kent TN14 7BP
England

Stephen G. Floroff
Armament Research & Development Center
SMCAR-LCW-E
Dover, NJ 07801-5001

Jeffrey M. Fornoff
Armament Research & Development Center
SMCAR-TSB
Dover, NJ 07801-5001

Paul L. Fritch
Armament Research & Development Center
SMCAR-LC
Dover, NJ 07801-5001

Robert F. Gartner
Honeywell, Inc.
5901 South County Road 18
Edina, MN 55436-5000

Ronald Gast
Armament Research & Development Center
Benet Weapons Laboratory
Watervliet, NY 12189-5000

Daniel Gleason
Air Force Institute of Technology
Wright Patterson Air Force Base
Dayton, OH 45433

John Groff
Army Materiel Systems Analysis Activity
AMXSY-GB
Aberdeen Proving Ground, MD 21005-5071

Richard G. Hasenbein
Armament Research & Development Center
Benet Weapons Laboratory
Watervliet, NY 12189-5000

Bailey T. Haug
Ballistic Research Laboratory
AMXBR-IBD
Aberdeen Proving Ground, MD 21005-5066

David High
Hercules, Inc.
Allegany Ballistic Laboratory
P.O. Box 210
Cumberland, MD 21502

Tonney Hung
Armament Research & Development Center
SMCAR-SCS-E
Dover, NJ 07801-5001

Sidney S. Jacobson
Armament Research & Development Center
SMCAR-TDT
Dover, NJ 07801-5001

W. P. C. King
Royal Military College of Science
School of Mechanical Materials & Civil Engineering
Shrivenham
Swindon Wilts SN6 8LA England

Herbert B. Kingsbury
University of Delaware
Department of Mechanical & Aerospace Engineering
Newark, DE 19711

Bruce Knutelsky
Armament Research & Development Center
SMCAR-LCA-M
Dover, NJ 07801-5001

George Kobori
FMC Corporation - Ordnance Division
1105 Coleman Avenue
Box 1201
San Jose, CA 95108

Frank Kuhl
Armament Research & Development Center
SMCAR-SCF-RE
Dover, NJ 07801-5001

Scott Langlie
FMC Corporation
Northern Ordnance Division
4800 E. River Road
Minneapolis, MN 55421

Neil A. Lapetina
Sandia National Laboratories
East Avenue
Livermore, CA 94550-0096

Norman T. Lionetti
Armament Research & Development Center
SMCAR-LCW-E
Dover, NJ 07801-5001

Rurik K. Loder
Ballistic Research Laboratory
AMXBR-IBD
Aberdeen Proving Ground, MD 21005-5066

John M. Miller
Harry Diamond Laboratories
DELHD-DE-FT
2800 Powder Mill Road
Adelphia, MD 20783-1197

Albert H. Mitchell
Armament Research & Development Center
SMCAR-SCA
Dover, NJ 07801-5001

Lionel Pasiuk
Naval Sea Systems Command
SEA-62R41
Washington, D.C. 20362-5101

Edward M. Patton
Battelle, Pacific Northwest Labs
Battelle Road
Richland, WA 99352

P. H. G. Penny
Royal Armament Research & Development Establishment
Chobham Lane
Chertsey, Surrey KT16 OEE
England

Robert Peterson
Armament Research & Development Center
SMCAR-SCS-EW
Rock Island, IL 61299-7300

George Pflegl
Armament Research & Development Center
Benet Weapons Laboratory
Watervliet, NY 12189-5000

S. E. Powell
Royal Military College of Science
Land Systems Group
Shrivenham
Swindon Wilts SN6 8LA England

Robert J. Radkiewicz
Armament Research & Development Center
SMCAR-SCS-EW
Rock Island, IL 61299-7300

Frederick E. Saxe
Armament Research & Development Center
SMCAR-LCA-M
Dover, NJ 07801-5001

Edward M. Schmidt
Ballistic Research Laboratory
AMXBR-IBD
Aberdeen Proving Ground, MD 21005-5066

Jimmy Q. Schmidt
Ballistic Research Laboratory
AMXBR-IBD
Aberdeen Proving Ground, MD 21005-5066

Mark J. Seymour
Hunting Engineering Limited
Reddings Wood, Ampthill
Bedfordshire MK45 2HD England

Thomas E. Simkins
Armament Research & Development Center
Benet Weapons Laboratory
Watervliet, NY 12189-5000

Martin T. Soifer
S&D Dynamics
755 New York Avenue
Huntington, NY 11743

G. D. Stilley
Honeywell, Inc.
5901 S. County Road 18
Edina, MN 55436-5000

Martin Thomas
Royal Armament Research & Development Establishment
Chobham Lane
Chertsey, Surrey KT16 OEE
England

Philip E. Townsend
Armament Research & Development Center
SMCAR-SCS
Dover, NJ 07801-5001

Tien-Yu Tsui
Army Materials & Mechanics Research Center
Watertown, MA 02172

David C. Uhrig
Air Force Armament Laboratory
Guns and Projectiles Branch
AFALT/DLJG
Eglin Air Force Base, FL 32542

John D. Vasilakis
Armament Research & Development Center
Benet Weapons Laboratory
Watervliet, NY 12189-5000

Cris Watson
Ballistic Research Laboratory
AMXBR-IBD
Aberdeen Proving Ground, MD 21005-5066

Emma M. Wineholt
Ballistic Research Laboratory
AMXBR-IBD
Aberdeen Proving Ground, MD 21005-5066

Julian J. Wu
US Army Research, Development, & Standardization Group (UK)
Box 65
FPO, NY 09510

Adam Zak
Aeronautical & Astronautical Engr Dept.
University of Illinois
104 S. Mathews Avenue
Urbana, IL 61801-2997

William T. Zepp
Armament Research & Development Center
SMCAR-LCW-S
Dover, NJ 07801-5001

John R. Zimmerman
Armament Research & Development Center
SMCAR-TSE-L
Dover, NJ 07801-5001

Kathleen L. Zimmerman
Ballistic Research Laboratory
AMXBR-IBD
Aberdeen Proving Ground, MD 21005-5066

TITLE: Technology Review on Projectile Gun Disengagement

Dr. Rurik K. Loder
USA Ballistic Research Laboratory
Aberdeen Proving Ground, MD 21005-5006

Dr. Roger K. Fancett
Royal Armament Research and Development Establishment
Fort Halstead, Sevenoaks, Kent TN14 7BP

ABSTRACT:

This paper outlines the importance of an accurate projectile launch definition to gun accuracy, projectile-gun dynamics models, and gun system diagnostics; reviews the technology which is available for the investigation of the projectile disengagement mechanism from the gun barrel; discusses the relevant instrumentation and measurement methods; and describes the ongoing research efforts, thus providing the introduction and basis to the other papers.

This paper was unavailable at the time the Proceedings were published. For further information, contact the authors.

TITLE: Description of the Joint BRL-RARDE 40-mm Experiment to Define Projectile Launch

Jimmy Q. Schmidt
U.S. Army Ballistic Research Laboratory, Aberdeen Proving Ground, MD 21005-5006
Thomas O. Andrews
Royal Armament Research and Development Establishment, Fort Halstead, UK

ABSTRACT:

Acquistion of data pertaining to the launch parameters of a projectile is very important for understanding the underlying causes of projectile-gun system inaccuracy. These experimental data are also necessary in the validation of the theoretical modelling of projectile-gun systems. During the past several years, the Ballistic Research Laboratory has been developing a new technique to measure projectile and gun tube motion during the launch of the projectile. As part of the ongoing program, the Ballistic Research Laboratory, US and the Royal Armament Research and Development Establishment, UK, recently conducted a joint collaborative firing experiment with a 40-mm gun. The primary purpose of the experiment was to assess the BRL system by performing paralliel measurements using standard electrooptical methods. This paper presents a brief description of the measurement techniques used, the firing experiment, and a brief discussion of the preliminary results.

BIOGRAPHY:

PRESENT ASSIGNMENT: Electronic Development Technician, Ballistic Research Laboratory, Aberdeen Proving Ground, MD, 21005-5006

PAST EXPERIENCE: Thirty-five years of electronic experience which includes Radar system repair (1948-1956), Design of speciallized High Frequency receivers and Phase Locked tracking filters used for Upper Ionosphere research (1956-1972), Ultrasonic testing of simulated rocket propellant including the design of the ultrasonic test equipment (1972-1976). Design of special measurement techniques related to interior and launch ballistics of projectile-gun systems in particular the RFO or Muzzleschmidt technique to measure projectile velocity, exit, and transverse displacement (1976-present).

DESCRIPTION OF THE JOINT BRL-RARDE 40-MM EXPERIMENT TO DEFINE PROJECTILE LAUNCH

MR. JIMMY Q. SCHMIDT
U.S. ARMY BALLISTIC RESEARCH LABORATORY
ABERDEEN PROVING GROUND, MD 21005-5006

MR. THOMAS O. ANDREWS
ROYAL ARMAMENT RESEARCH AND DEVELOPMENT ESTABLISHMENT
FORT HALSTEAD, UK

1. INTRODUCTION

In May 1982 a new measurement technique [1] which provides measurements of projectile transverse displacement during muzzle exit was presented by the Ballistic Research Laboratory (BRL), at the Third U.S. Army Symposium on Gun Dynamics. This new technique is a four sensor coil arrangement derived from the Radio Frequency Oscillator (RFO) velocimeter commonly referred to as the "Muzzleschmidt". This method aroused considerable interest among the visiting delegation of the Royal Armament Research and Development Establishment (RARDE), from the United Kingdom (UK), because of its high potential of providing the experimental means for defining the projectile launch.

The importance of accurately defining projectile launch parameters and some of the previous experimental methods used to obtain such data are discussed in the opening paper of the Session," Technology Review on Projectile Disengagement" by Dr. R.K. Loder (BRL) and Dr. Roger K. Fancett (RARDE).

During subsequent discussions between BRL and RARDE personnel it was evident that both the US and the UK would benefit from a joint BRL/RARDE program to assess the ability and accuracy of the Schmidt displacement transducers to measure both the projectile motion with respect to the gun muzzle and the gun muzzle motion with respect to the ground during the projectile-barrel disengagement. BRL would provide measurements using the Muzzleschmidt technique while the UK made measurements using their optical methods. By performing the test in the UK, RARDE personnel would be able to obtain a direct comparison of the measurement techniques and to assess the relative merits of each. The US while also obtaining the direct comparison would in effect obtain a dynamic calibration of the BRL method. This would be highly desirable since the sensitivity of the RFO sensor to mechanical displacement is at least an order of magnitude greater than what is easily obtained with a mechanical test calibrator.

SCHMIDT, ANDREWS

In May 1983, Mr. J.Q. Schmidt, BRL, visited RARDE to coordinate with Mr. T.O. Andrews and consider all the technical details and the time table for preparing and conducting the joint firing experiment. This joint experiment was carried out at RARDE in June 1984. This paper covers the experimental aspect of the joint collaborative firing experiment. A paper on the data analysis will be given later in this Session.

The objective of this trial, fired in RARDE/GR2's range at Fort Halstead using a 40-mm gun, was to compare the results obtained from Radio Frequency inductive loop devices, developed at BRL, with the results of observations using optical devices developed in the UK by Hunting Engineering Ltd. (HEL) and by RARDE.

2. GENERAL OUTLINE OF THE TEST

A total of twenty-one 40-mm L60 ogival nosed projectiles were fired at velocities of approximately 500 m/sec, using the RARDE Ord. Q.F. 40/70 gun. One half of the projectiles were essentially unmodified and the other half deliberately unbalanced to provide a yaw in excess of the maximum yaw normally encountered with this projectile-gun system. Twelve of the rounds had a 0.254 mm undercut from 5.00 mm behind the bourrelet to 5.00 mm in front of the rotating band. This undercut is used to accurately relate longitudinal points on the recorded waveform corresponding to longitudal points on the projectile.

BRL provided the instrumentation for the measurements of the displacement of the projectile with respect to the bore axis during shot exit using the Muzzleschmidt technique. Measurements were made at two locations, one at the muzzle, and one 2.54 cm forward of the first sensor. The use of dual sensors allows the rate of yaw determination. BRL also provided a gun tube motion measurement with respect to ground during shot exit, using a modified Muzzleschmidt detector. Shot exit time was obtained by the BRL projectile displacement sensor. Since the gun tube motion after shot exit may exceed the clearance between the gun tube and the tube motion sensor, RARDE built a mechanical sliding platform to pull the gun tube motion sensor clear of the gun after shot exit.

RARDE provided measurements of gun tube motion at two stations some distance to the rear of the BRL sensor mounting collar, using the HEL electrooptical device incorporating a collimated light beam and knife edges. During the latter stages of the test RARDE measured the projectile in-bore yaw, using Peter Fuller's laser and optical grating method. In addition to the specific test requirements, RARDE also measured breech pressure, projectile velocity, and target strike. RARDE provided the data recording facility. Projectile displacements were recorded on Nicolet digital oscilloscopes with backup recording by a high speed digital data logger. Tube motion measurements, both BRL and RARDE, plus shot exit time were recorded on a second data logger with backup recording on an analog tape. Data recorded on the data loggers were transferred to the Nicolet oscilloscope for storage on floppy disc. This enabled BRL to hand carry the recorded data back for processing. The RARDE in-bore yaw data were recorded on film.

One of the prime areas of concern was the mechanical compatibility which

is quite often taken too lightly. When fabricating parts to fit a gun tube based on mechanical drawings, quite often problems are encountered such as improper thread mating and unexpected variation in tolerances. To eliminate any last minute problems, RARDE fabricated the mounting collar in the UK based on BRL requirements, assured proper fitting of the collar to the gun tube and sent it to BRL for the sensor and electronics to be installed.

3. MEASUREMENT TECHNIQUES

As previously mentioned, BRL's measurements are based on the RFO (Muzzleschmidt) technique while RARDE's measurements on optical methods. Each method has its relative merits and, by conducting parallel measurements, a better assessment of each method is obtained. In addition, in view of the information exchange program between the US and the UK, the expertise gained by the parallel test will be valuable in future information exchanges.

A. BRL, Dual Projectile Displacement Measuring System (Muzzleschmidt)

Several years ago the RFO technique was developed by BRL to provide a method for measuring projectile velocity directly at the muzzle, primarily on rapid fire guns or moving gun systems. The basic concept is quite simple, an inductive loop excited by a radio frequency oscillator and clamped to the muzzle face detects the metallic parts of the projectile as it passes through it [2]. The detected signal is an electrical pulse representative of the geometric configuration of the projectile. Knowing the projectile length, the measurement of the time duration of the detected pulse provides a measurement of muzzle velocity. Experience gained in the development of the RFO velocimeter lead to the development of the RFO system to measure projectile transverse displacement during muzzle exit [3]. The basic operation of the system is explained in detail in the reference so only a very brief explanation will be given here.

In the RFO displacement measuring system, the single circular sensor used in the velocity measuring system is replaced by a four segment sensor which is configured to provide two semi-circular loops in the horizontal plane and two semi-circular loops in the vertical plane as shown in Figure 1. Each sensor loop is responsive to the proximity of the metallic parts of the projectile to it. By electronically differencing the signal from the left and right loops a measurement of the projectile displacement from the center axis is obtained as a function of time. Vertical projectile displacement is obtained in the identical way. The displacements from the center axis in the horizontal and vertical plane as a function of time yield the angle and the orientation of the projectile yaw. By electronically summing the detected signals, a pulse is obtained from which velocity can be computed or used simply as a very precise muzzle exit time.

Shown in Figure 2 is the basic block diagram of the sensors and the summing and differencing circuits. The detected waveforms shown correspond to the detected signal of a cylindrical projectile perfectly aligned in the horizontal plane. Should the projectile be displaced from center but have no yaw, a positive or negative pulse would be obtained, the polarity being dependent on the direction of the displacement from the axis and the magnitude

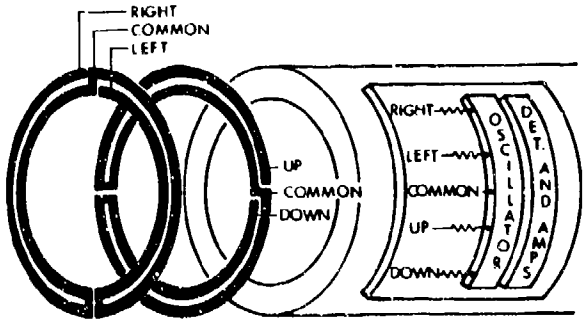

Figure 1. The Basic Sensor Coil Configuration for Measuring Projectile Displacement

corresponding to the amount of displacement. The signal shown in the vertical channel represents the projectile with a fixed yaw in the vertical plane as indicated by the linear slope of the pulse. If a rate of yaw were present at the time the projectile was passing the sensor, the slope would be non-linear. The summed signal is used to provide a profile of the pulse to assess the acquired data, obtain muzzle velocity, and for use as a muzzle exit trigger. The summed signal is used to trigger the recording device. This is necessary because the differenced signals can be either positive or negative-going or even essentially zero, depending on the orientation of the projectile as it passes through the sensor.

By using two sensors, spaced a known distance apart, the rate of yaw can be obtained from the simultaneous displacement measurements of the front and rear section of the projectile. This of course is an oversimplification of the complexity of the analysis, when one considers the complex motion caused by the longitudinal displacement, the spin of the projectile, the rate of yaw during disengagement, gun tube motion, and minute sensor to gun displacements caused by stress waves being propagated down the gun tube. A complete mathematical analysis of the projectile motion will be given in the data analysis paper to follow this paper.

Shown in Figure 3 is the block diagram of the dual projectile displacement measuring system. The sensor and amplifier assemblies are contained in two electronic housing boxes mounted on the collar at the gun muzzle. The horizontal and vertical difference signals plus the horizontal summed signal from each sensor are coupled to the recording facility via co-axial cables. Unity gain isolation amplifiers in the recording facility are used to minimize 50 Hz ground loop currents. The horizontal and vertical difference signals from each sensor were recorded on Nicolet digital oscilloscopes, using the horizontal summed signal as a trigger.

B. BRL, Gun Tube Motion Measurement System

Since the measurements of projectile displacement are with respect to the gun tube on which the sensors are mounted, gun tube motion measurements relative to ground must be made in order to accurately determine projectile

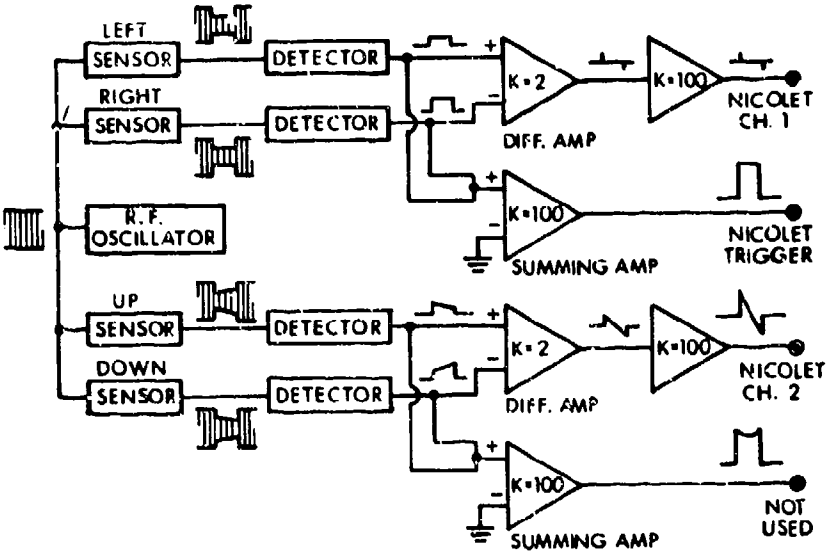

Figure 2. Block Diagram of the Signal Processing Circuit

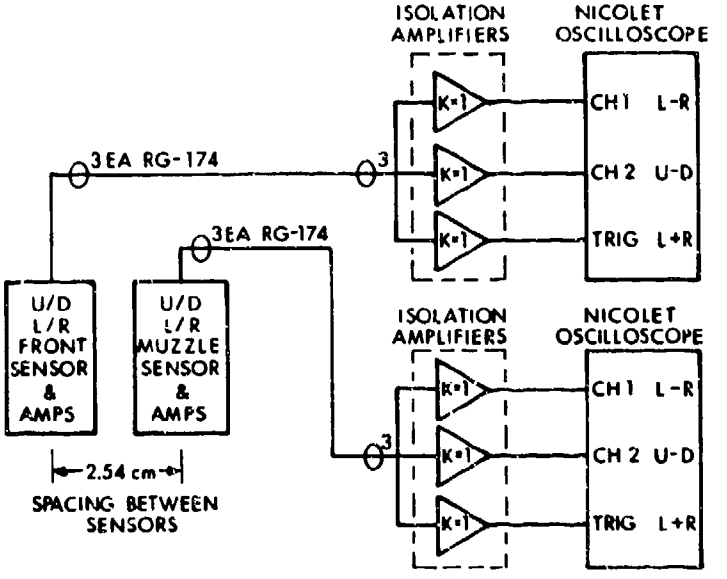

Figure 3. Block Diagram of the Dual Projectile Displacement Measuring System

motion in reference to ground. The RFO technique can also be used to measure gun tube motion. By fabricating identical sensors and circuitry as used to measure projectile displacement and mounting them in a metal loop surrounding the gun tube, accurate measurements of tube motion can be obtained in the

horizontal and vertical planes. Ideally, the clearance between the gun tube and the sensor ring should be large enough that the gun tube would not strike the sensor when counter-recoiling to the rest position. If the spacing between the sensor ring and the muzzle face, or in this case the mounting collar, is increased, the radiated field depth is greater, permitting the sensor to be further from the gun. This causes a loss of definition of the signal which is undesirable for projectile measurements; however, for tube motion measurements an accurate definition of the longitudinal displacement of the gun is actually not necessary. This permits increasing the spacing between sensors for gun tube motion measurements. By placing two additional rings of printed circuit (PC) substrate between the horizontal and vertical sensors and one between each sensor and the metal mounting collar, the radiated field depth was increased to provide measurements with a sensor ring which is 10.0 mm larger in diameter than the gun.

Electrically, the sensor and associated circuitry were identical with that used to measure projectile displacement with the exception of a lesser signal bandwidth requirement. Mechanically, the sensor consists of a vertically oriented sensor loop mounting attached to a small box housing the electronics. The box was mounted to an adjustable base providing horizontal and vertical adjustments to position the sensor loops equidistant from the outer surface of the gun. Shown in Figure 4 is the basic configuration used for gun tube motion measurements.

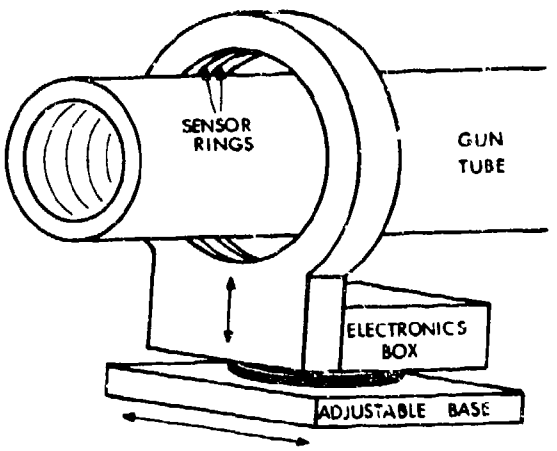

Figure 4. The Basic BRL Configuration Used for Gun Tube Motion Measurements

Since this was the first test of the RFO technique to measure the transverse motion of the gun tube at projectile exit and the required sensitivity was unknown, it was decided that 5.0 mm clearance would be sufficient for tube displacement before and immediately after muzzle exit. However, provisions had to be made to pull the sensor forward several centimeters after projectile exit so that the tube , after recoil, did not strike the sensor. It may be possible to increase the diameter of the sensor

rings sufficiently to prevent interaction between the tube and the sensor in future tests.

C. RARDE, Gun Tube Motion Measurement Technique

One optical method to measure gun tube motion is the use of a collimated light beam passing over a knife edge and partially illuminating a large area light sensitive diode through a narrow slit [4]. To measure transverse gun tube motion, knife edges (razor blades) are mounted to the gun tube parallel to the tube axis and perpendicular to the light beam. The razor blade is positioned to partially block the light beam passing through the slit masking the photo-diode. If the razor is mounted in a vertical position, partially obscuring the light beam, than any vertical tube motion will move the razor blade and cause a lesser or greater amount of light to strike the sensor. The detected signal is amplified and recorded. The signal is proportional to the gun tube motion in the vertical plane. By using two light sources and sensors positioned orthogonally, both the horizontal and vertical components of tube motion can be measured. The basic test set up used to measure tube motion is shown in Figure 5.

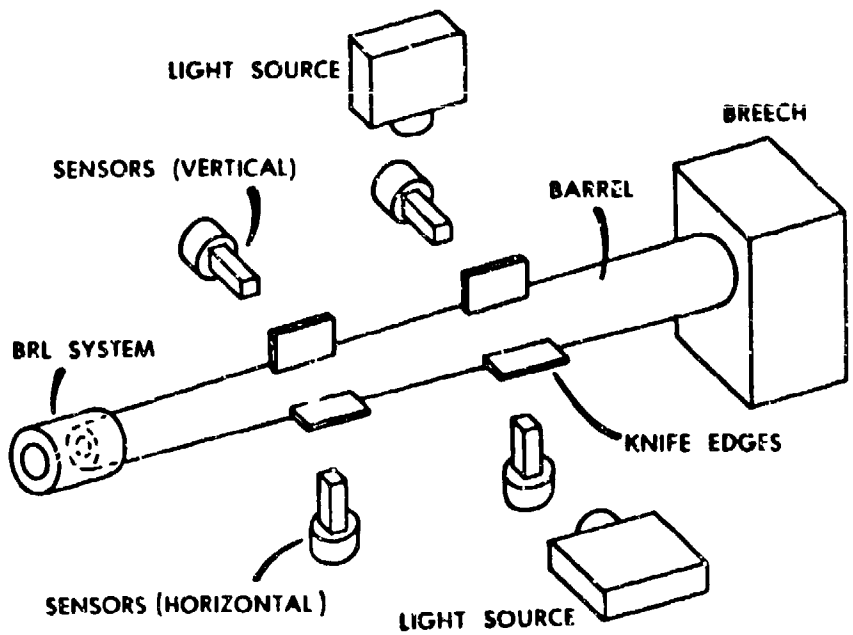

Figure 5. The Basic Electrooptical System To Measure Gun Tube Motion

D. RARDE, Projectile In-bore Yaw Measurement System

This system determines the in-bore yaw of a projectile by the deflection of a parallel beam of laser light reflected from its nose [5]. The light from a 16mW HeNe laser (wavelength 0.000632 mm) is focused by a lens fitted to the laser to give a point source of light in the focal plane of a concave mirror

300 mm in diameter (focal length 1220 mm, 48 inches). The lens is chosen so that the mirror produces a beam of parallel light about 25 mm in diameter.

This beam of light, Figure 6, is reflected by plane mirrors to lie along the bore axis. It is then reflected back by a reflective optical grating fixed to the nose of the projectile and set to be accurately perpendicular to the projectile's axis. The grating has equal widths of reflecting and non-reflecting surface, the reflecting strips being spaced at intervals of

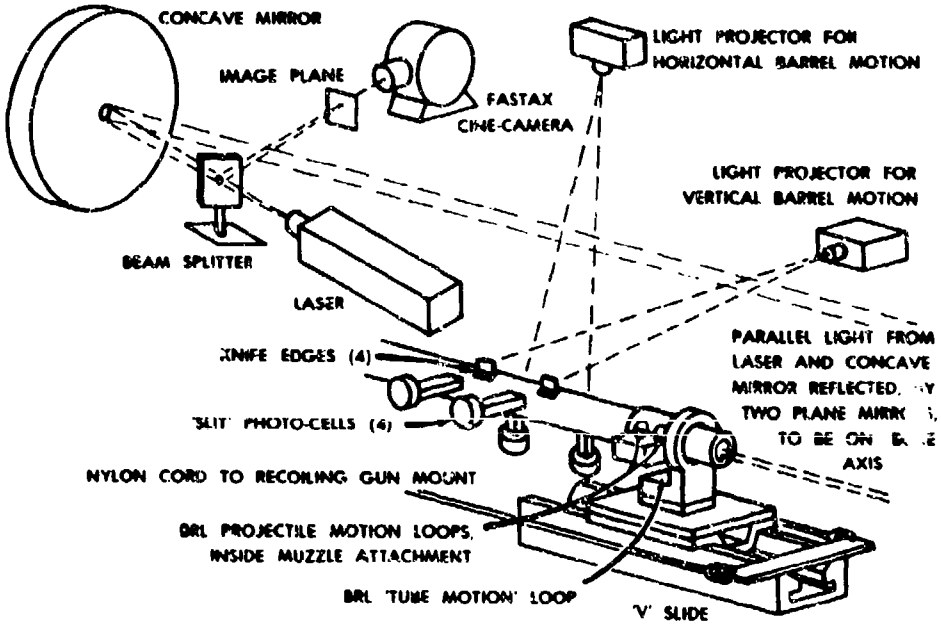

Figure 6. The Complete Instrumentation Layout

0.4233 mm. The area of the grating is divided into two, with the grating lines on one half being perpendicular to the lines on the other half. The reflected light then consists of a central beam and four beams representing the two first-order diffraction beams from each half of the grating. When these beams, which return via the plane mirrors to the concave mirror, are brought to a focus they produce five spots in the form of a "quincunx" (5-spot die pattern).

A half-silvered mirror is placed between the laser and the concave mirror to act as a beam splitter. This reflects the returning beams away from the laser to where the spots can be recorded on a cine film, at about 6000 frames per second. The ends of fibre optic light guides are positioned in the focal plane of the camera to provide reference points for film reading and film orientation.

The angular divergence of the beams producing the spot pattern depends only on the grating spacing and on the laser wavelength and so provides an automatic yaw angle calibration. With the laser and gratings used for this

trial, each outer spot is at an angle of 0.0855 degrees from the central spot; but, as a yaw angle of 0.1 degrees will deflect the spot pattern as a whole by 0.2 degrees, the yaw scale is obtained by taking the diagonal pairs of outer spots as being 0.0855 degrees apart.

If the light beam reflected down the bore is truly parallel, then deflection due to yaw, as viewed in the focal plane of the concave mirror, is independent of the projectile's travel. Any change in scale which may occur will be shown by a corresponding change in the spot pattern size.

E. Data Recording

The prime consideration in choosing the method of recording the trials data was the need to provide copies of the data for BRL in a form suitable for analysis in the United States, and preferably available to be taken to BRL immediately at the end of the trial. This requirement involved more effort than all other aspects of RARDE's preparation for the trial.

The recording system assembled was largely digital, with an analog tape recorder as back-up for the low-frequency records, i.e., barrel motion and chamber pressure, with one projectile profile as a synchronizing signal. Three Nicolet Explorer III two-channel digital oscilloscopes were used to make the primary high-frequency recordings of the outputs of the Schmidt displacement transducers, with a Datalabs DL2800 transient recorder as back-up. The primary low-frequency records were made using an eight channel Datalabs DL1200 transient recorder.

A Digital Equipment Corp. MINC 11/03 computer was used to control the transfer of data from the Datalabs recorders into one of the Nicolet oscilloscopes and the recording of all the data on Nicolet disks. This could readily be done in a few minutes between rounds. As opportunity offered the data were copied from the Nicolet disks onto MINC disks for later analysis at RARDE so that the Nicolet disks were available to be taken to BRL for analysis.

4. DETAILS OF THE BRL SENSORS

As agreed, preliminary and final drawings of the mounting for the projectile displacement sensor were exchanged between BRL and RARDE. The mounting collar was then fabricated by RARDE. During the time the collar was being fabricated, the electronics were constructed as far as possible without the sensor assembly. Upon receipt of the collar, sensor rings were fabricated by BRL. Each sensor consist of three rings constructed from PC substrate. Approximately 0.6 mm of copper was removed from the ID of the rings and the adjacent ring undercut by the thickness of the copper clad as shown in Figure 7. This placed the ID of the sensor rings behind a protective layer of PC substrate and provided a seal when epoxied together. This protective layer was to prevent any metallic parts of the rotating band from striking the sensor elements. After the sensor loops were formed from the copper clad and leads attached, the sensor rings were epoxied into the sensor housing and held in place by rings which screwed into the housing.

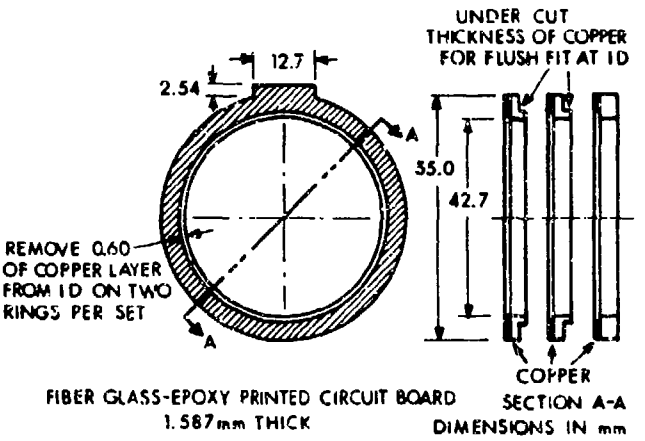

Figure 7. Projectile Displacement Sensor Rings Before Sensor Loop Formation

The complete sensor mounting collar was then assembled and connected to the oscillator circuitry. The electronics for the muzzle sensor were housed in a box on one side of the collar, while the electronics for the front sensor were housed in a box on the opposite side.

The muzzle attachment consisted of a collar screwed onto the muzzle with a ring bolted to the forward surface containing two sets of BRL loops, one close to the muzzle face and the other 25.4 mm further forward, for the observation of the position of the projectile. A further ring bolted to the front of the attachment provided a measuring surface for the "tube motion" loop.

Shown in Figure 8 is a drawing of the collar assembly and the relative positions of the sensor elements and the gun tube.

The complete projectile sensor assembly was electrically checked out and mounted on a dummy gun tube. Sensitivity checks were made using a mechanical calibrator consisting of a steel cylinder with the diameter of the projectile, which was inserted into the sensor area. The steel cylinder was displaced from the center line of the bore axis in 0.127 mm increments and measurements were made in the radial direction every thirty degrees by inserting the face plate of the calibrator into guide pin holes. The following sensitivities were measured.

Muzzle Sensor	Front Sensor
Left - Right 8.6 V/mm	Left - Right 8.32 V/mm
Up - Down 8.58 V/mm	Up - Down 7.76 V/mm

With sensitivities in the order of 8.0 V/mm it is easy to see the need for an extremely precise mechanical calibrator which at this time is not available. Therefore, at the present time, the calibration constants are obtained via statistical data analysis. More precise calibration relations

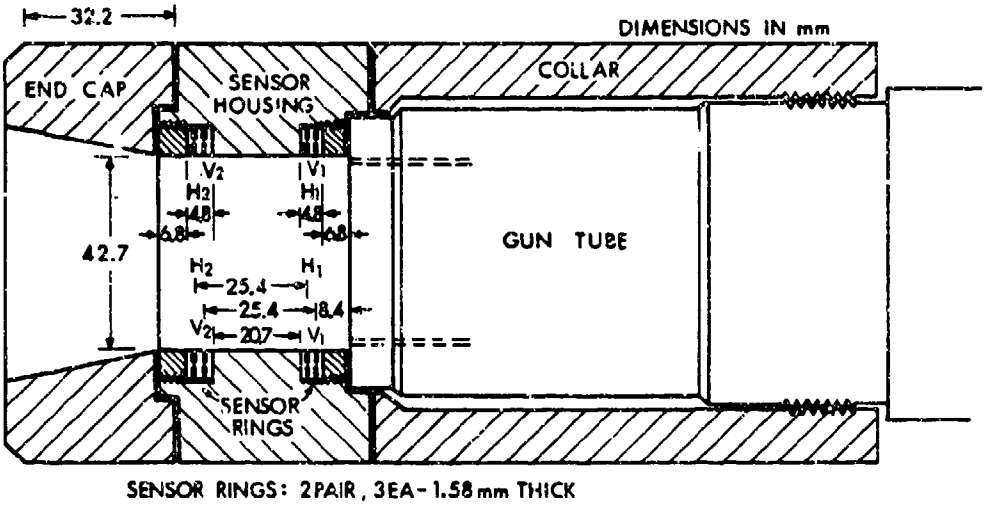

Figure 8. Relative Positions of Projectile Sensors and Gun Tube

based on the statistical analysis are used in the actual data analysis of the recorded data.

Shown in Figure 9 is the complete projectile sensor assembly before mounting to the gun tube. The assembly replaces the flash hider which is normally screwed onto the gun.

The tube motion sensor performs electrically identical to the projectile sensor; however, in this case the sensor surrounds the muzzle collar rather than the emerging projectile. Since longitudinal definition is not necessary for tube motion measurements, and a greater spacing is required between the sensor and the gun, the spacing between the sensor elements was increased. Instead of three PC rings with a one PC ring spacing between elements as used for the projectile sensor, six PC rings were used with the sensing elements spaced two PC substrate thicknesses apart. This provided a usable depth of the radiated electromagnetic field of at least 6.00 mm.

The tube motion sensor was mounted to the dummy gun tube fixture with the projectile sensor collar. Calibration was performed by recording the horizontal and vertical output voltages while repositioning the sensor assembly with its horizontal and vertical adjustments on the base. Again this is a rather crude method to calibrate, but at this time no other calibration rig is available. The horizontal sensitivity was found to be 5.2 V/mm and the vertical sensitivity was 4.8 V/mm. These sensitivities were with reduced gain in the amplifier. Additional gain can be provided by the amplifier but this would limit the dynamic range of the measurement because of the amplifier output limiting due to the voltage swing. This sensitivity provides a dynamic range of tube motion of approximately ± 2.5mm. Figure 10 is a photograph of the completed tube motion sensor.

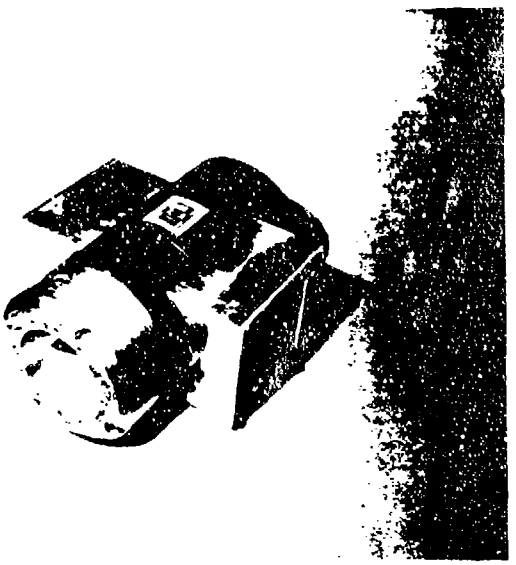

Figure 9. Complete Projectile Sensor Assembly

5. DETAILS OF THE TEST

The actual firing tests were conducted at the RARDE test range during the two week period of 29 May through 12 June 1984. Interfacing the BRL equipment to the RARDE facility proceeded extremely well with no problems being encountered either mechanically or electrically. The following data were recorded, the longitudinal position given here being only approximate.

BRL, Projectile Horizontal Displacement at the Muzzle (Muzzle L-R)
BRL, Projectile Vertical Displacement at the Muzzle (Muzzle U-D)
BRL, Projectile Summed Horizontal Displacement at the Muzzle (Muzzle L+R)
BRL, Projectile Horizontal Displacement 2.54 cm forward of the Muzzle Sensor (Front L-R)
BRL, Projectile Vertical Displacement 2.54 cm forward of the Muzzle Sensor (Front U-D)
BRL, Projectile Summed Horizontal Displacement 2.54 cm forward of the Muzzle Sensor (Front L+R)
BRL, Vertical Tube Motion at the Muzzle (BRL U-D)
BRL, Horizontal Tube Motion at the Muzzle (BRL L-R)
BRL, Projectile Muzzle Exit
RARDE, Vertical Tube Motion, 32.5 cm from the Muzzle (HEL Front Vertical)
RARDE, Horizontal Tube Motion, 32.5 cm from the Muzzle (HEL Front Horizontal)
RARDE, Vertical Tube Motion, 44.5 cm from the Muzzle (HEL Rear Vertical)
RARDE, Horizontal Tube Motion 44.5 cm from the Muzzle (HEL Rear Horizontal)
RARDE, Breech Pressure
RARDE, Projectile Velocity
RARDE, Projectile In-bore Yaw
RARDE, Projectile Strike Coordinates at the Target

Figure 10. The Complete Tube Motion Sensor Assembly

In addition to these primary recordings, all projectile and tube motion measurements were put on backup recording devices to prevent loss of data.

Shown in Figure 11 is the BRL and RARDE instrumentation attached to the 40-mm gun. The laser set up to measure in-bore yaw is not shown in this photograph.

Nineteen rounds were fired during the two week test period with two additional rounds being fired by RARDE, after the BRL personnel left, to obtain additional projectile in-bore data with Fuller's optical lever/grating system. The projectiles were all fired at a velocity of approximately 525 m/sec. As previously mentioned some rounds fired were standard projectile configurations and some rounds were deliberately unbalanced. Details of the gun and projectile configuration fired are given below.

The gun and ammunition used were chosen because a considerable volume of data had been obtained for these firing conditions in previous trials.

Gun: 40-mm L70, Barrel No. E3169, with 1 in 18 twist of rifling, muzzle face machined to remove chamfer, BRL sensor assembly fitted to muzzle in place of "Flash Hider." Adapted into 6 Pdr. 7 cwt breech rings and recoil mechanism mounted on range stand.

Charge: All, 95 grams SC/Z, 0.02 mm scroll propellant.

Ignition: No. 12 MK4 Percussion.

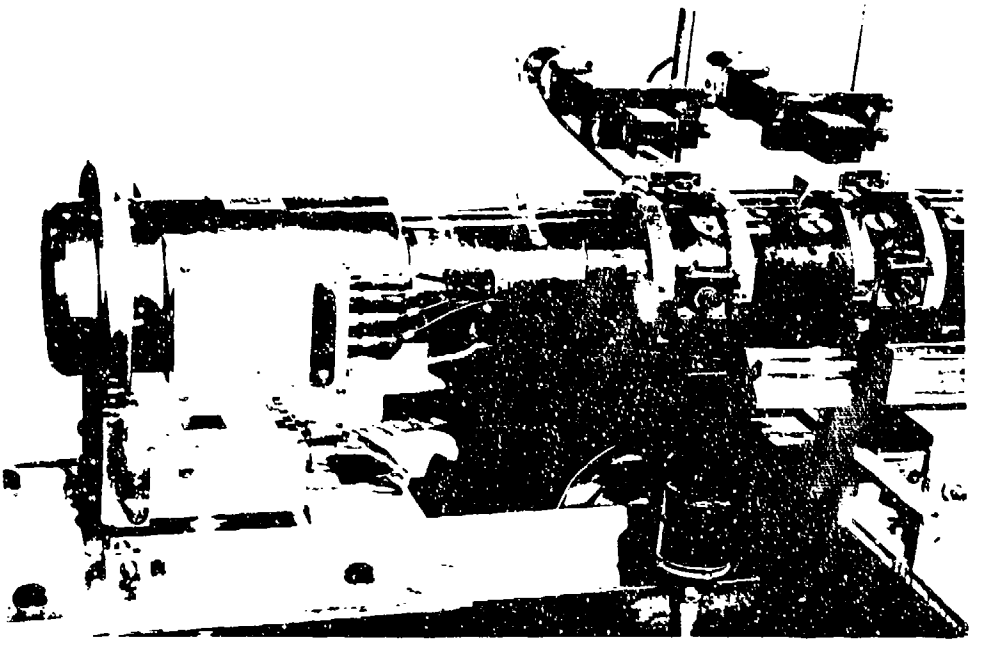

Figure 11. BRL and RARDE Instrumentation Attached to the 40-mm Gun

Projectiles:

All — A shell body, 40 mm/T Mk 4, Part No. SX252, fitted with a steel base plug of local manufacture in place of a tracer.

Type A — Fitted with an ogival aluminum alloy nose plug and filled with 88 grams of H.E. Substitute wax giving a total weight of approximately 865 grams. The center of gravity is 64.6 mm from the base of the shell.

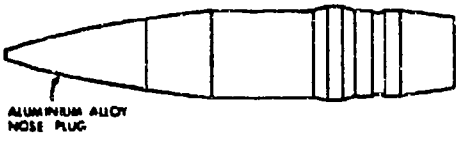

B — As A, but with the outer surface of the body turned down to form an "undercut" 0.25 mm deep from 5 mm behind the shoulder to 5 mm in front of the driving band, a length varying between 34.62 mm and 35.05 mm. This reduces the shell weight by 8 grams and moves the center of gravity 0.17 mm towards the base.

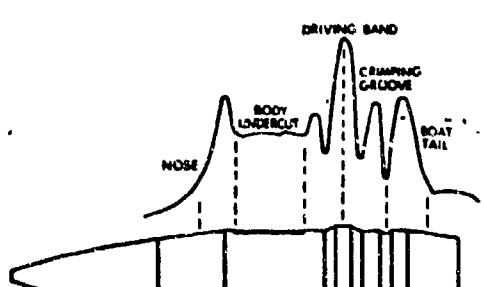

C As A, but deliberately unbalanced, with a 9.53 mm (3/8") diameter steel rod, 77.4 mm long, placed against one side of the shell cavity, the cavity then being filled with Bees Wax, of density 0.95 gram/ml, rather than H.E. Substitute wax of density 1.674 gram/m;. The rod weighs 43 grams, and the Bees Wax filling 45 grams, giving the same weight of filling (88 grams) and the same total shell weight. With a cavity diameter of 27.53 mm and a rod diameter of 9.53 mm the rod axis is 9 mm from the shell axis. The center of gravity of the complete shell is 0.39 mm off axis and possibly 0.1 mm nearer the base than in type A.

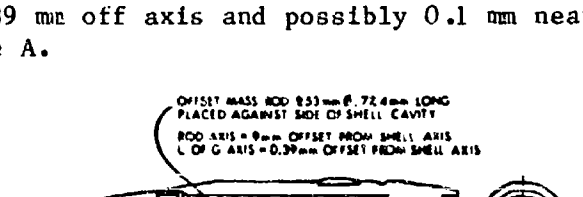

D With a machined outer surface as B, and unbalanced as C.

E As A, but with the aluminum alloy nose plug replaced by a flat steel nose plug fitted with a reflective optical grating for in-bore yaw measurement. These shells also had a second groove machined in the body, behind the crimping groove, to take a rubber obturating ring, to reduce the obscuration by gas leakage of the light reflected from the optical grating. The total shell weight is still 865 grams but the center of gravity is possible 0.6 mm nearer the base than in type A.

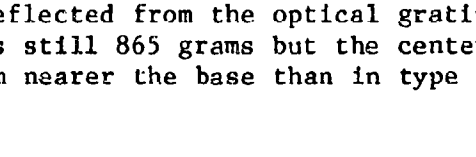

F With a machined outer surface as B, and with an optical grating and obturating ring as E.

G With a machined outer surface as B, and unbalanced as C, with an optical grating and obturating ring as E.

6. PRELIMINARY RESULTS

Since the analysis of the recorded signals for the projectile and tube motion is quite complex and covered in detail in the following papers in this session, no attempt is made to present precise data analysis or assessment of the comparative results. However, preliminary assessment of several rounds of the recorded data gives some insight on the quality of the data recorded as well as the general trends in the behavior of various configurations of the projectile fired.

Comparison of the recorded data of tube motion seems to indicate that the tube motion of similar rounds is fairly consistant. The unbalancing of the projectile mass distribution produces a distinctly different motion near muzzle exit yet is very similar within its particular grouping. Unbalancing the projectile in the opposite direction produces an opposite effect but still similar within its particular grouping. Since only six rounds were fired with the center of gravity (CG) offset in the vertical plane (three with the CG up and three with the CG down), there is not enough data to come to any firm conclusion. Even with a greater number of data rounds statistical analysis is necessary before any real degree of confidence can be placed on the results.

This is also true of the analysis of the projectile motion. Quick look comparison of the projectile motion of the unbalanced rounds shows some similarity within their particular grouping (three rounds with the CG offset up and three rounds with the CG offset down). However, examination of the records of the balanced rounds shows a wide variation in the apparent amount of projectile yaw. Since these measurements are relative to the gun tube and the gun tube motion during the launch phase of the projectile is distinctly different for balanced rounds versus unbalanced rounds, complete analysis is again necessary.

Data from the single BRL tube motion sensor provides only transverse tube displacement and not the angle of the tube axis relative to the line of sight. In general, however, the transverse tube motion during and immediately after projectile exit using balanced rounds is small as compared to when unbalanced rounds are fired.

Shown in Figure 12 are the recorded difference signals of projectile displacement at the muzzle sensor for a balanced round with a slight undercut from 5.00 mm behind the bourrelet to 5.00 mm in front of the rotating band. The recorded vertical signal indicates that the projectile is well centered in the vertical plane with virtually no indication of projectile yaw relative to the gun tube. The recording of the horizontal displacement indicates the projectile is displaced from the center axis but, as in the case of the vertical signal, with very little indication of projectile yaw. It should be noted that these measurements are made with respect to the center axis of the sensors and there can be a slight displacement between the center axis of the sensor and the center axis of the gun tube. This will be taken into account in the actual data reduction. The signal is clearly defined from the front of the bourrelet to the rotating band. Figure 13 shows the horizontal summed signal of the same round. The undercut, the rotating band, and the groove for crimping the case to the projectile are clearly defined.

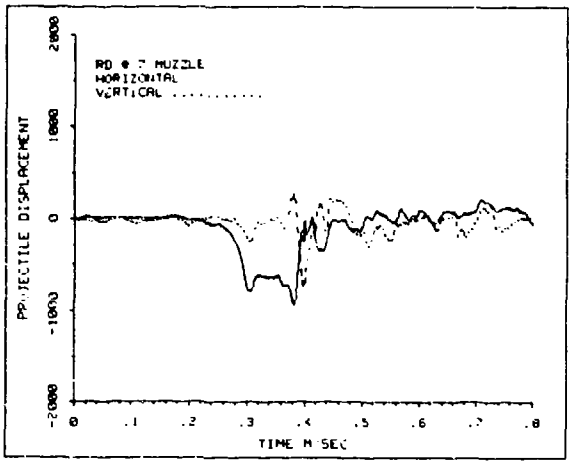

Figure 12

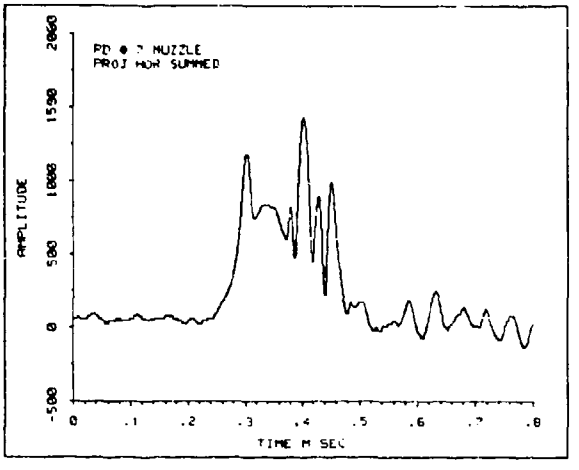

Figure 13

The recorded signal of the projectile displacement at the front sensor for the same round, Figure 14, shows a substantial amount of yaw in both the horizontal and vertical planes. Since this yaw interpretation is relative to the gun tube and the front of the projectile has disengaged from the gun, it must be resolved as to whether the amount of yaw is completely projectile related or whether the muzzle of the gun is moving and affecting the trajectory of the projectile. Both sets of information are important to gun tube accuracy, since, even if the projectile was perfectly aligned with the gun tube axis but the tube axis has actually moved, the trajectory will be affected.

Shown in Figure 15 is the front-summed signal. Here again the longitudinal reference points such as undercut, rotating band and groove are very clearly defined. The difference in signal amplitude in the rotating band area can be attributed to the relative response of the sensor to the copper band as compared to the steel projectile case and any asymmetrical engraving of the band. These are only typical records of the test and direct correlation between the projectile yaw and the location of the projectile center of gravity or gun tube motion will have to be resolved in the complete analysis of data.

A rough indication of the angle and the angle of orientation of yaw can be obtained from this quick look data. The data were recorded on the ± 4 volt range or 8 volts total range of a Nicolet oscilloscope. The 12 bit resolution of the Nicolet oscilloscope provides approximately 2 mV per point, therefore the measured voltage can be read from the plot. A more accurate quick look method is to read the voltage differential of the slope from the Nicolet recordings. This provides a voltage differential, from the beginning of the undercut to the end of it, of 668 mV for the horizontal and 678 mV for the vertical signal. This agrees roughly with what can be read from the plot in Figure 14 when plotted to this scale. The length of the undercut on this

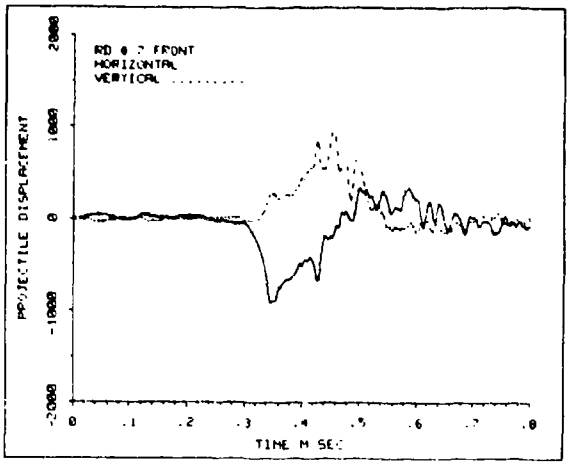

Figure 14

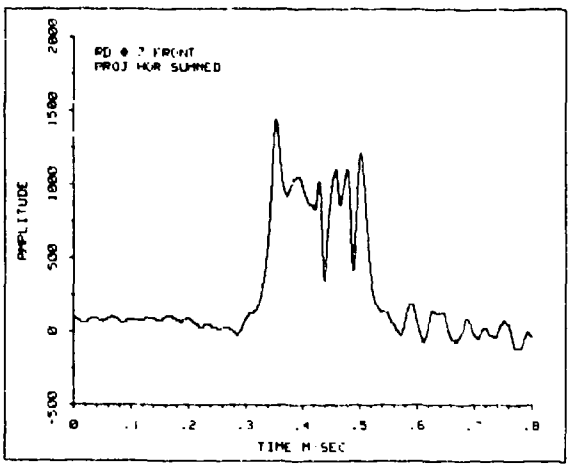

Figure 15

projectile was 35.05 mm. Taking into account the substrate thickness of the sensor, the recorded values were measured after the raised shoulder of the projectile had passed the sensor by the thickness of the substrate in front and before the rear raised shoulder passed by sensor by one substrate thickness. Therefore the baseline is actually 35.05 mm minus the thickness of two substrates (3.175 mm) or 31.875 mm. Using a horizontal sensitivity of 8.32 V/mm and a vertical sensitivity of 7.76 V/mm. The horizontal and vertical component calculates to be 0.0813 mm and 0.0889 mm. By transposing these values to zero and solving for the vector the displacement calculates to be 0.120 mm down and to the left, looking downrange, at an angle of 42.4 degrees or 222.4 degrees from the twelve O'Clock position. The actual angle of yaw is then simply calculated to be 0.216 degrees using the arctangent function. This of course is an oversimplification of the analysis but still gives a rough indication of the orientation of the projectile during the launch phase.

The tube motion data acquired appears to be very good. The BRL loop and RARDE sliding mount arrangement worked very well. After each round was fired it was a simple matter to slide the sensor loop back into position. As a common reference, prior to each shot, the sensor was slid back so the rear of the metal loop was 2.0 mm in front of the joint between the end cap and the sensor housing.

Figures 16 through 20 are examples of tube motion data at the muzzle as detected by the BRL sensor. Only the BRL data are presented, because the RARDE measurements were made well to the rear of the muzzle and require extrapolation of the data to obtain motion at the muzzle. Shown in the following examples are gun tube motion with a balanced projectile and with projectiles unbalanced and loaded in the gun with the center of gravity (CG) up, down, left, and right. These records are the actual recorded signals not yet converted to actual displacements.

Shown in Figure 16A are the horizontal and vertical displacements of the tube when firing a balanced round. Also shown is the precise muzzle exit time of the projectile. Figure 16B is the same measurement with the X and Y scale

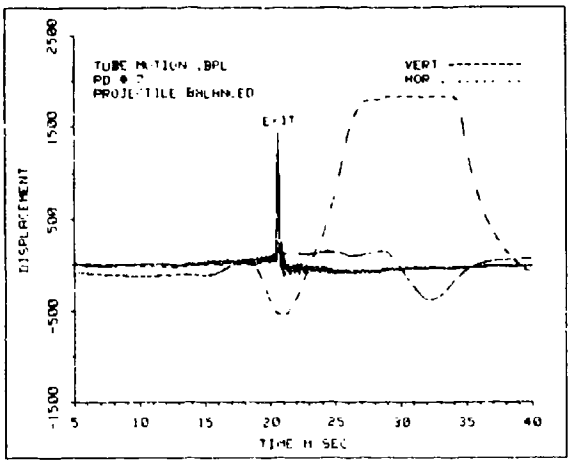

Figure 16A

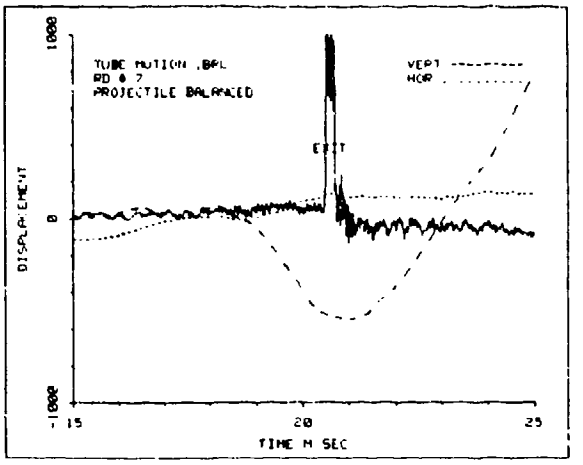

Figure 16B

expanded to show more detail at muzzle exit time. As can be seen, even though the gun has moved before projectile exit, especially in the vertical plane, there is very little movement during the actual time of exit. There are noticeable difference when examining the records of an unbalanced round. In Figures 17A and 17B it can be seen that the gun tube is moving down at the time of projectile exit and abruptly swings up during projectile exit. The same effect is noticeable in the horizontal plane during exit, the muzzle abruptly moves left. Several other motions are noticeable. The projectile during its in-bore travel rotates three full turns plus one hundred and forty degrees. With the unbalanced projectile there is a modulation of the tube displacement for approximately three and one half cycles before exit indicating that the unbalanced projectile causes the muzzle to move in unison with the spin as the projectile traverses the gun tube. This modulation starts at approximately the start of projectile motion although it is hard to ascertain from the visual interpretation of these records. Also by comparing records of balanced versus unbalanced projectiles, it appears that this same modulation is detectable on the summed projectile signal (muzzle exit pulse). The higher frequency modulation is probably caused by the stress waves generated during engraving of the band. Figure 18A and 18B show the displacement caused by an unbalanced round but loaded with the CG to the right. The same effects are noticeable although in the opposite direction. In the vertical plane the gun tube motion going down increases during projectile exit while in the horizontal plane the tube abruptly moves right. It appears the effect of the projectile unbalance is forcing the tube into the direction of the CG offset of the projectile and then as the projectile disengages, the tube abruptly swings the opposite direction. For example, with the projectile making approximately three and one half turns during in-bore travel and the CG offset before firing to the left, the CG of the projectile would be to the right at muzzle exit. If this forced the gun tube

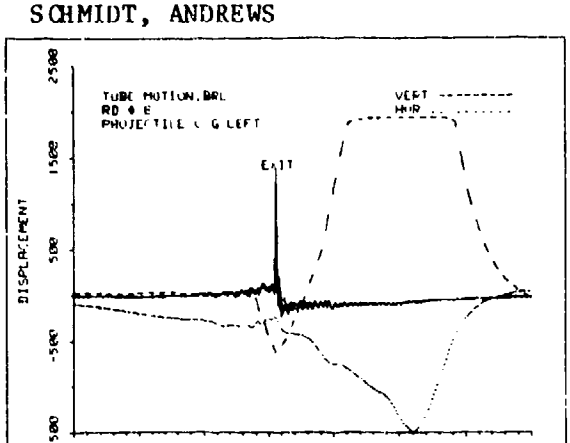

Figure 17A

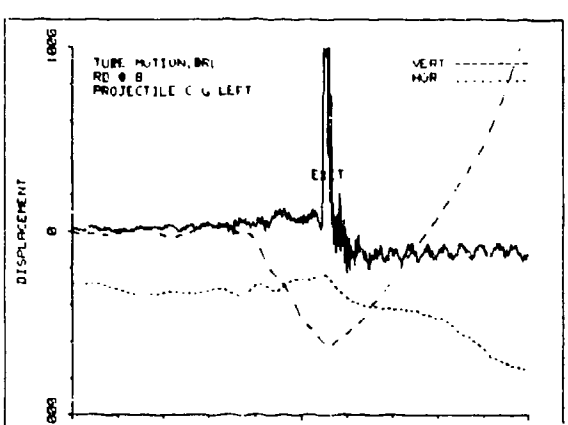

Figure 17B

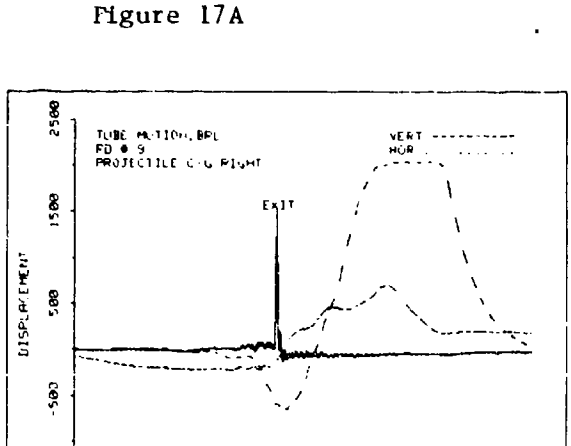

Figure 18A

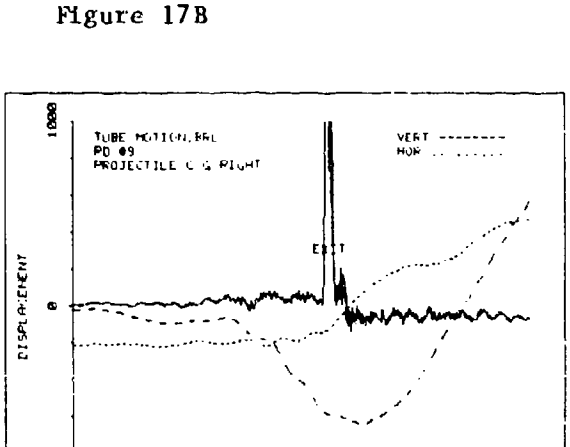

Figure 18B

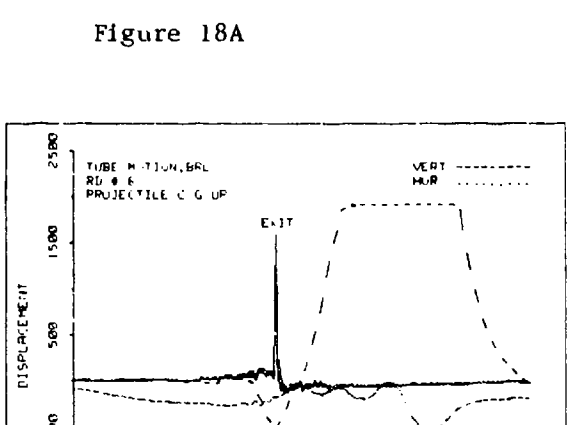

Figure 19A

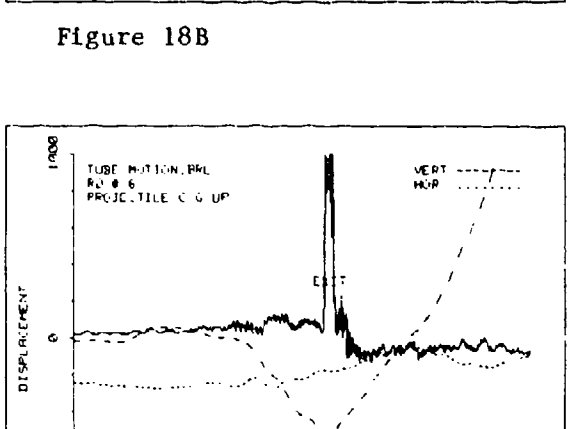

Figure 19B

muzzle right then upon release, it would swing left. This same effect is evident in the tube motion record when the projectile was loaded with the CG to the right. Also noticeable in these two examples is how long after projectile exit the tube motion continues in that same direction. The same sort of effect is evident in the records shown in Figures 19 and 20, although

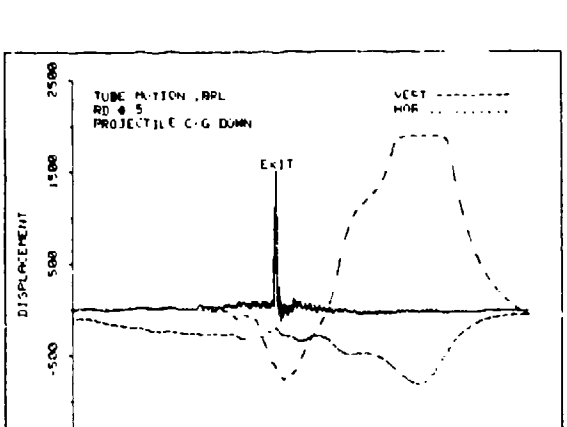

Figure 20A

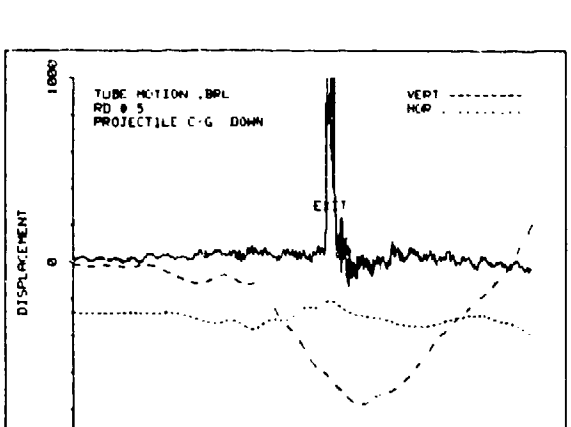

Figure 20B

the major difference in motion is in the vertical plane which seems to confirm the cause of motion. In these cases the projectile CG was initially positioned up and down. Once again this is an oversimplification of the required analysis but it should provide some insight on how the tube motion is related to other factors such as projectile in-bore motion. Also, with further analysis it should be possible to calculate the tube motion at the points in time the projectile displacement was measured. This should ascertain how much of the measured yaw is in reference to ground and how much apparent yaw is due to tube motion.

Shown in Figures 21, and 22, are composite plots of the horizontal and vertical tube motion for a balanced round, an unbalanced round with the CG to the left, and an unbalanced round with the CG to the right. Approximate projectile exit times are shown with "tick" marks since a plot of the muzzle exit signal would have made the displacement records hard to read. However, the records clearly show the same effect producing tube motion in opposite directions. Hopefully, further analysis will either confirm this effect or determine what the actual cause is. Since the tube records are very clean, further details should be obtainable. The records presented here are shown on an arbitrary scale, which is sufficient for providing an example of the motion.

A typical record of the observed in-bore yaw, from Round 21, is shown in Figure 23. This does not show the behavior of the projectile during the last full turn of the rifling, but it appears by then to have settled down to a constant yaw of the maximum allowed by its fit within the bore, turning at the

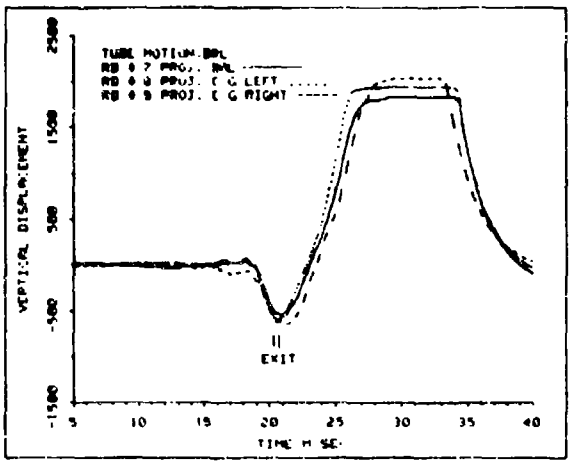

Figure 21A

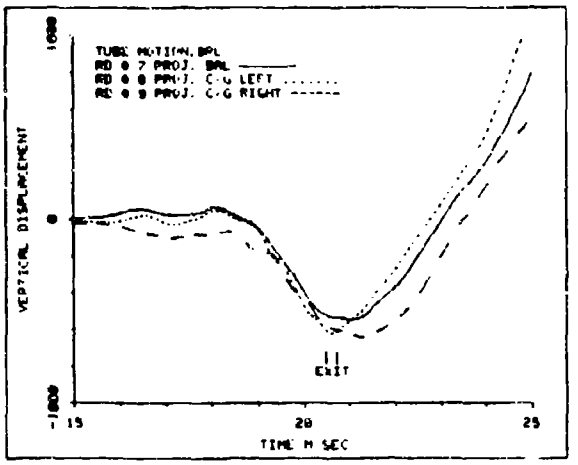

Figure 21B

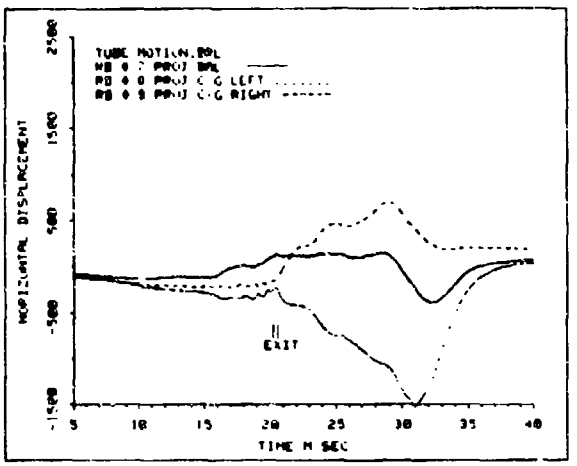

Figure 22A

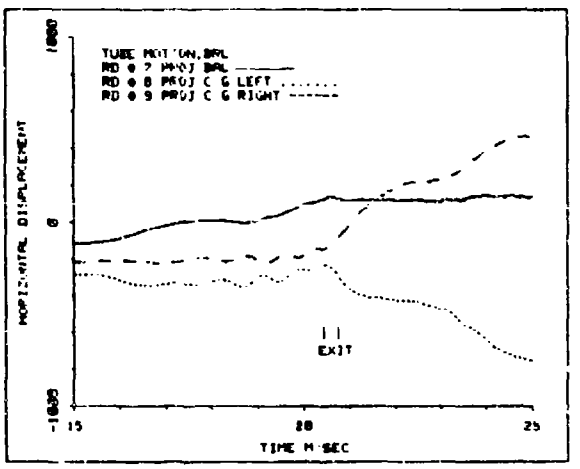

Figure 22B

rifling rate. The clearance between the projectile and the bore allows a maximum in-bore yaw of the order of 0.2 degrees to 0.25 degrees. The initial angular motion, until this yaw angle is reached, occurs before the first linear motion (7.5 milliseconds before time zero). The hesitations and reversals of the precession of the yaw which follow may be due to variations in the contact force and the frictional force between the shoulder of the projectile and the bore; the last occurs shortly after the time of peak pressure.

The result shown in Figure 23 exhibits a considerable difference in scale between the vertical and horizontal directions. This may arise from curvature of the supposedly plane mirrors. One of these, situated necessarily on the bore axis, is destroyed by the shot, it cannot be supported anywhere but at its edges.

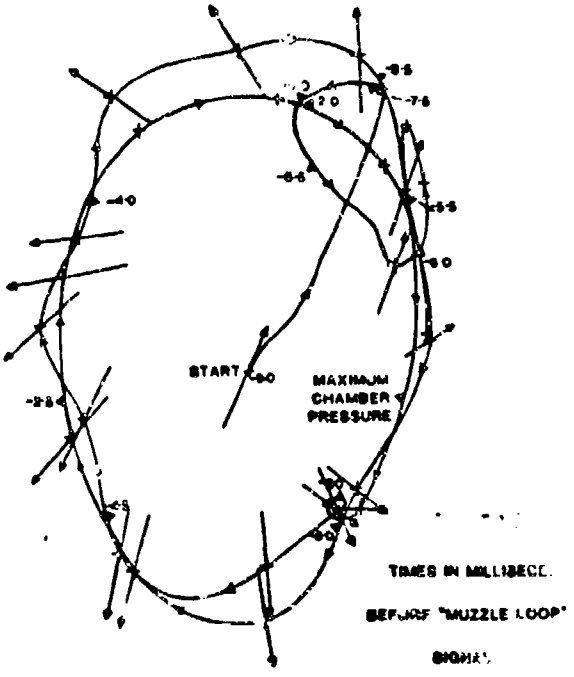

In-BORE YAW, ROUND 31.

(ARROW LENGTH REPRESENTS 0.0888 DEG.)

Figure 23.

7. SUMMARY

At this time all preliminary analysis results indicate that the joint test was very successful; but, how successful really is never known until the data analysis is completed. The quality of the data appears to be very good and, with few exceptions, all the data desired are recorded. No problems were encountered in interfacing the BRL and RARDE systems or performing the test. In fact, the only problem in the whole program was a delay caused by the exchange of drawings which were temporarily sidetracked in the official US communication channel.

This was the first time that tube motion measurements were made using the Schmidt displacement transducers and a great deal of information was obtained which should be useful in future test. Based on the apparent high quality of the tube motion data, future tube motion measurements using the Schmidt displacement transducer will employ at least two sensors to obtain the angle of tube displacement at muzzle exit. The recorded signals of the projectile displacements are also of good quality and it is hoped that comparison with the in-bore laser measurements made by RARDE will further confirm the BRL measurements. Future tests will be conducted using a symmetrical mounting collar with the projectile measurement electronics located off of the gun. This will provide a symmetrical measuring surface for dual tube motion measurements and protect the electronics.

REFERENCES

1. J.Q. Schmidt, "Radio Frequency Oscillator Technique for Measuring Projectile Velocity and Orientation at Muzzle Exit," Proceedings of the Third US Symposium on Gun Dynamics, Rensselaerville, NY, 11-14 May 1982.

2. J.Q. Schmidt, "A Radio Frequency Oscillator Technique for Measuring Projectile Muzzle Velocity," ARBRL-TR-02158, US Army Ballistic Research Laboratory, Aberdeen Proving Ground, MD 21005, April 1979 (AD #B0389261).

3. J.Q. Schmidt, "A Radio Frequency Oscillator Technique for Measuring Projectile Transverse Displacement at Muzzle Exit," ARBRL-TR-02448, US Army Ballistic Research Laboratory, Aberdeen Proving Ground, MD 21005, November 1982 (AD #A122757).

4. P Brown, "Report on 40-mm Gun Barrel Vibration Trials Fired at RARDE, at Halstead" (A Reduced Version of HE/Shock/36), Systems Experimental Group, Hunting Engineering Ltd., United Kingdom, April 1980.

5. P.W.W. Fuller, "Measurements of In-bore Yaw of Projectiles," Proceedings of the 5th International Symposium on Ballistics, Toulouse, France, Royal Armament Research and Defense Establishment (RARDE) Fort Halstead, United Kingdom, April 1980.

TITLE: Results of the Joint BRL-RARDE 40-mm Firing Experiment to Define Projectile Launch

Dr. Rurik K. Loder and Emma M. Wineholt
USA Ballistic Research Laboratory
Aberdeen Proving Ground, MD 21005-5006

Dr. Roger K. Fancett
Royal Armament Research and Development Establishment
Fort Halstead, Sevenoaks, Kent TN14 7BP

ABSTRACT:

Using the BRL and the two HEL displacement data sets individually as well as combined, the muzzle motion of the instrumented 40-mm L70 cannon is determined and evaluated for the total interior ballistic cycle from the initiation of the firing until shortly after the projectile has left the muzzle. The validity of the indirectly calculated muzzle recoil is examined by comparing it with recoil data obtained by an earlier experiment with the same gun and ammunition. The time window corresponding to the projectile-gun disengagement is expanded to the same temporal resolution as used in the analysis of the projectile motion, and the linear displacement vector and the pointing direction of the coordinate system which moves with the muzzle are computed as functions of time.

The projectile motion - the vectors for the linear displacement of the center of mass and the angular orientation of the axis and their derivatives with respect to time - during the projectile gun disengagement time is computed by employing the previously described data analysis program to the two recorded data sets, graphically presented with respect to both the muzzle and the ground frame of reference, and discussed. The axial component of the projectile velocity obtained from the analysis of the Schmidt displacement transducers is compared with the velocity recorded downrange and the velocity gain in the muzzle blast regime is estimated. The projectile yaw, i.e., the orientation of the vector for the projectile axis with respect to the velocity vector of the center of the mass, is displayed with the data from Fuller's optical lever arrangement overlaid, whenever applicable.

The variations in the initial condition - projectile unbalance and its orientation in the gun chamber - are correlated to the linear and angular motion of the muzzle and the projectile immediately before and after the projectile separation from the gun barrel and related to the recorded impact location on the target.

This paper was unavailable at the time the Proceedings were published. For further information, contact the authors.

TITLE: Data Analysis Procedure for the Schmidt Displacement Transducer to Extract Projectile Launch and Muzzle Motion

Dr. Rurik K. Loder and Emma M. Wineholt
USA Ballistic Research Laboratory
Aberdeen Proving Ground, MD 21005-5006

ABSTRACT:

This paper delineates the analysis concept and procedure used in the development of the data analysis program. The projectile-related analysis program contains: (i) the data base describing the frame of reference, the bore geometry of the muzzle in reference to the locations of the two sensors used in the experiment, the contour geometry of the projectile, and the recorded data; (ii) the analysis of a subset of data to establish points of reference for the temporal alignment of the projectile contour with the data sequence and to extract the axial component of the projectile motion; (iii) the analysis of the remaining data to spatially align the coordinate systems of the two displacement sensors, extract the transverse displacement of the center of the projectile contour from the sensor axis from the data in the presence of large amplitude colored noise, and convert these displacements into the vectorial description of the motion of the projectile's center of mass and the angular motion of projectile's axis about the direction given by the velocity vector of the center of mass; and (iv) the utilization of the results of the anteceding analysis to determine the pivotal location on the projectile axis and the orientation of the tube axis with respect to the frame of reference, represent the projectile motion with respect to the tube axis, and estimate the asymmetry of rotating band engraving. The frame of reference is the coordinate system given by one of the two sensor systems and, hence, moves with the muzzle. The analysis program allows the superposition of the muzzle motion and the description of the projectile motion with the respect to the frame of reference in which the muzzle motion is defined.

The analysis program for the muzzle displacement data is straightforward. The data are converted into displacements and superimposed on the displacement equation for a moving, flexural beam in the least squares sense. Essentially, the transverse displacements of the muzzle section of the gun barrel are set forth as polynomials in the axial position, with the coefficients varying in time and satisfying the end conditions for a free beam at the muzzle face. Since the sensor position with respect to the muzzle is a function of gun recoil, the correlations between the data and the model parameters are expressed such that five of the six degrees of freedom are obtained. Only the rotation about the bore axis is not extractable. The program permits the analyis of data sets from one or more measurement stations. If the data of only one station are used, the muzzle section is considered a rigid base which moves in space.

This paper was unavailable at the time the Proceedings were published. For further information, contact the authors.

TITLE: Results of the Joint BRL-RARDE 40-mm Firing Experiment to Define Projectile Launch

Dr. Rurik K. Loder
USA Ballistic Research Laboratory
Aberdeen Proving Ground, MD 21005-5006

Dr. Roger K. Fancett
Royal Armament Research and Development Establishment
Fort Halstead, Sevenoaks, Kent TN14 7BP

ABSTRACT:

Results from the 37-mm and 40-mm caliber firings are used to evaluate the performance of the Schmidt displacement transducer for the measurement of the muzzle motion as well as the projectile dynamics during the final phase of the interior ballistic cycle. Limitations and shortcomings in the current instrumentation design and measurement technique which includes the data analysis procedure are discussed, together with possible avenues of its improvement and research in progress.

This paper was unavailable at the time the Proceedings were published. For further information, contact the authors.

*SIMKINS, PFLEGL, AND SCANLON

TITLE: Corroborative Measurements of the Transverse Motion of a Gun Tube During Firing

T. E. Simkins, G. A. Pflegl, and R. D. Scanlon
U.S. Army Armament, Munitions, and Chemical Command
Armament Research and Development Center
Large Caliber Weapon Systems Laboratory
Benet Weapons Laboratory
Watervliet, NY 12189-5000

ABSTRACT:

This work presents new measurements of transverse motion of the 30 mm (GAU-8) gun tube first reported at the Third Gun Dynamics Symposium in 1982. The measurements are unique and fully corroborated through the use of two independent measuring devices. In particular, the work discusses three items of interest. First, there definitely exists a 'base-line' transverse tube movement, the cause of which has yet to be determined. The magnitude of this motion is of the same order as that due to other causes intentionally introduced for study. Second, intentionally introducing an eccentric breech mass produces muzzle displacements in good agreement with theoretical models, provided the base-line component is accounted for. Finally, the muzzle rotation created by the moving projectile - though insignificant when operating alone - is strongly coupled to, and capable of greatly modifying the rotation due to other causes. This coupling does not appear to strongly affect muzzle displacement. It is concluded that predictions from gun dynamics models which agree well with displacement measurements, may err greatly when used to predict muzzle rotation, the quantity of which is of central interest.

BIOGRAPHY:

PRESENT ASSIGNMENT: Chief, Applied Mathematics & Mechanics Section, Research Branch, Benet Weapons Laboratory, Large Caliber Weapon Systems Laboratory, Armament Research and Development Center, Watervliet, NY.

DEGREES HELD: Ph.D. - Mechanics, Rensselaer Polytechnic Institute, Troy, NY; B.S. - Mechanical Engineering, Northeastern University.

*SIMKINS, PFLEGL, SCANLON

CORROBORATIVE MEASUREMENTS OF THE TRANSVERSE MOTION OF A GUN TUBE DURING FIRING

T. E. SIMKINS, G. A. PFLEGL, AND R. D. SCANLON
U.S. ARMY ARMAMENT, MUNITIONS, AND CHEMICAL COMMAND
ARMAMENT RESEARCH AND DEVELOPMENT CENTER
LARGE CALIBER WEAPON SYSTEMS LABORATORY
BENET WEAPONS LABORATORY
WATERVLIET, NY 12189-5000

1. INTRODUCTION

The work herein reports further measurements of the transverse muzzle motion of an elastically suspended 30 mm gun tube. When last reported [1], there were significant but unexplained muzzle movements prior to shot ejection. As a result, the credibility of the measurements of these motions was brought into question and it was decided that further analysis could not be justified until fully corroborated measurements were in hand. It was decided that two completely independent methods of measuring muzzle displacement would be employed simultaneously and that close agreement of these measurements would be demanded for acceptability. This quest for corroborated - and hence believable - measurements was highly successful as the results herein will demonstrate.

Having the proper instrumentation and measurement techniques in hand, however, did not guarantee immediate success in totally explaining the motions of the 30 mm tube during firing - the central problem of gun dynamics to which we have finally been able to return. Latest measurements, although greatly improved from those reported in 1982 [1], still reveal an unexplained transverse movement of the tube prior to shot ejection. Furthermore, the magnitude of this motion is roughly the same as that which is to be studied from intentional causes such as tube curvature, tube and/or projectile eccentricity, etc. There can be little doubt that the cause of this underlying motion will be found, but as yet this is not the case.

2. EXPERIMENTAL DESIGN AND INSTRUMENTATION

Referring to Figure 1, the 30 mm/GAU-8 gun tube was suspended as described in Reference 1. Briefly, the tube is suspended by two pairs of wires from a virtually rigid overhead structure. The wires are 0.026 inch in diameter and each is approximately 50 inches in length. The recoiling tube thus behaves as an elastic bar-pendulum, stretching each wire approximately

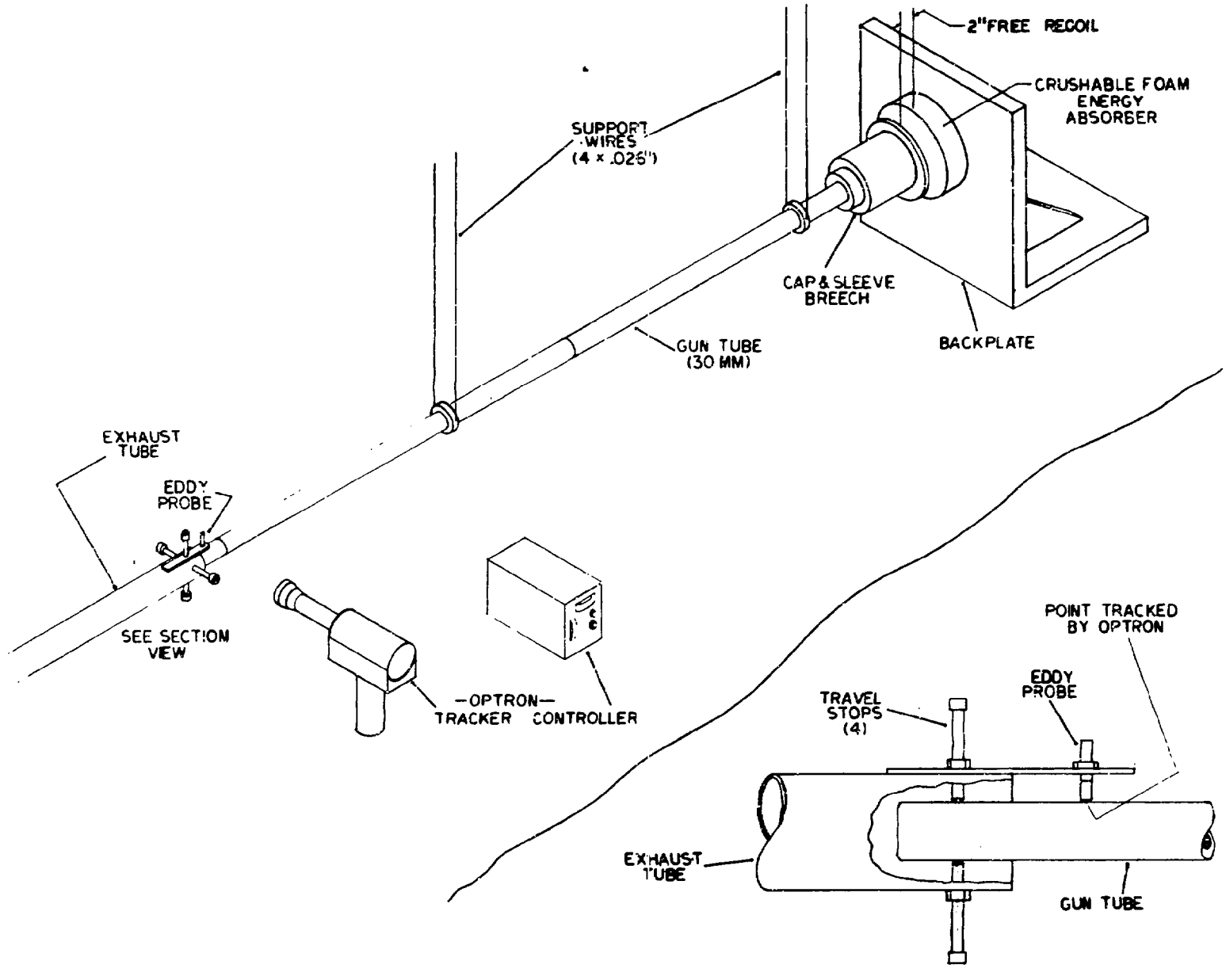

Figure 1. Elastically suspended 30 mm gun system.

0.010 inch at shot ejection. A NASTRAN model of this means of support indicates that the wire support loads create negligible transverse tube motion prior to shot ejection, i.e., that the suspension as modeled can be regarded as 'soft.' Following shot ejection, the recoil motion is arrested by contact between a circular buffer plate attached to the breech and a block of open-cell silica foam. (This foam has been found far superior to the 'styrafoam' used previously.)

The propellant charge used in these experiments is half that normally used in a standard GAU-8 round and yields a maximum pressure of about 10,000 psi. The round is separated from its case and manually started into the origin of rifling with a light tap. The cartridge case containing the propellant is then inserted and forced home as the threaded breech cap is tightened. The breech cap contains a small central recess into which an electrically actuated, propellant-driven firing pin is inserted.*

Instrumentation used to perform the measurements presented herein consists of two late model optical trackers (trade name - 'Optron'), and one so-called 'eddy probe' manufactured by Dymac Division of Scientific-Atlanta. One Optron is used with a light source which is interrupted as the shot leaves the muzzle. This, plus a breakwire mounted across the muzzle provides two independent measurements of the time of shot ejection. Agreement between the two is within 0.0002 seconds. It is hoped that in the future an inductance device will improve this measurement. The remaining Optron is used to record the vertical motion of the tube approximately six inches rearward of the muzzle. From this point the muzzle protrudes into a tube which exits through a wall of the room. The tube protects the instrumentation from muzzle flash and smoke. The end of this tube also serves as a mounting place for the eddy probe which is positioned 0.050 inch directly over the point of the tube being followed by the tracker. Thus the tracker and the eddy probe both follow the motion of the same point on the upper surface of the tube at all times. Owing to recoil, of course, different material surface points are being tracked in time, i.e., the measurement frame is Eulerian, not Lagrangian. This difference is of little consequence for the purpose at hand, however.

Measurements are monitored and recorded digitally on a four-channel Nicolet system. Approximately twenty milliseconds of data are recorded from each round using the muzzle breakwire and a trigger.

3. MEASUREMENTS OF GUN TUBE MOTION

Figure 2 shows the motion of the muzzle as measured by an optical tracker and by the eddy probe. Shot ejection is taken at t = 0.0. It is estimated that most of the time agreement is within 0.0002 inch (0.2 mils). Assuming sufficient care is taken to duplicate all of the preliminaries, a second shot will produce measurements in close agreement with those of the first shot. This is exemplified in Figure 3.

---

*These 'mini-actuators' are manufactured by ICI Americas, Inc., Atlas Aerospace Division, P.O. Box 819, Valley Forge, PA.

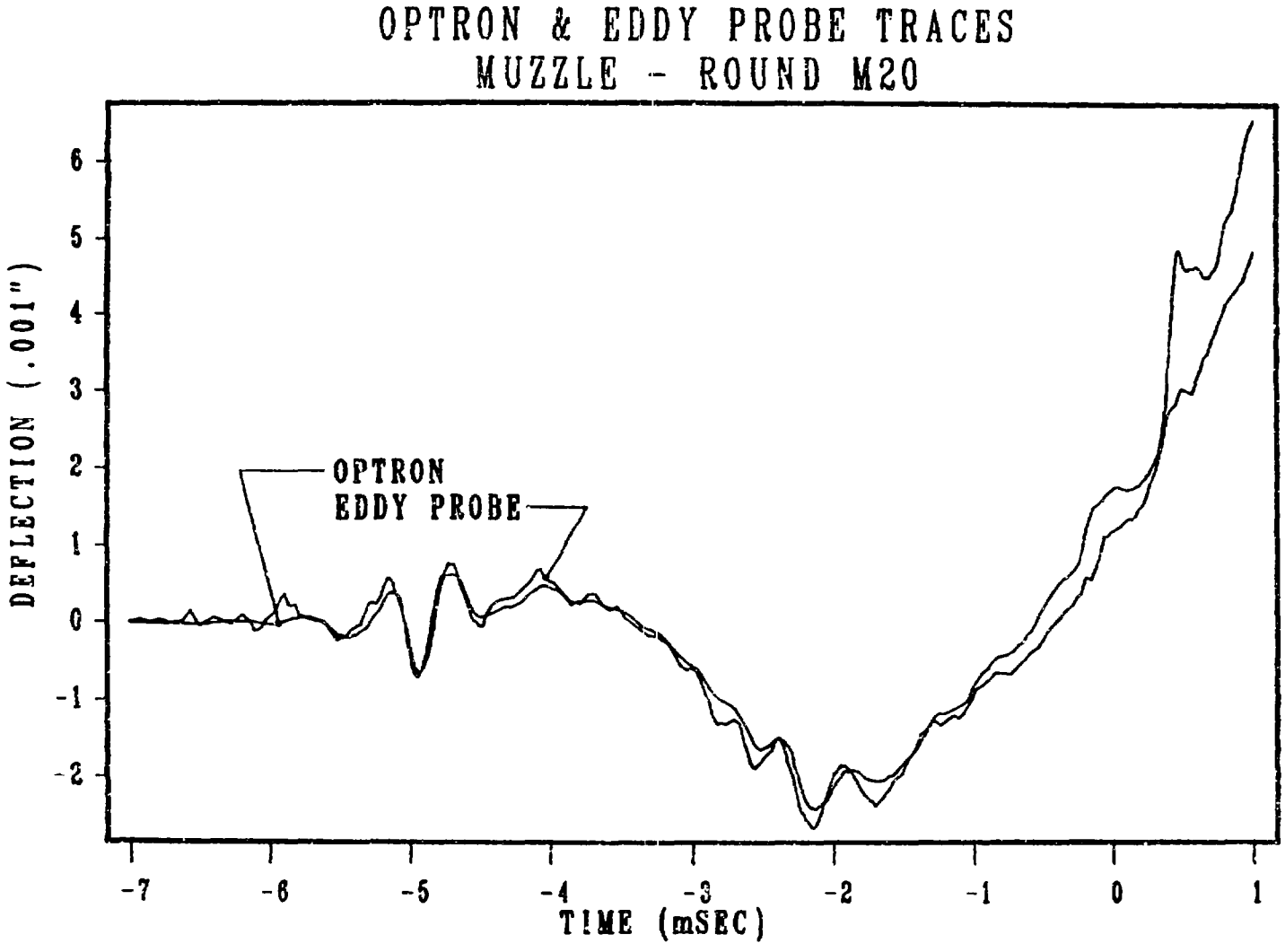
OPTRON & EDDY PROBE TRACES
MUZZLE - ROUND M20
DEFLECTION (.001")
6
5
4
3
2
1
0
-1
-2
OPTRON
EDDY PROBE
-7
-6
-5
-4
-3
-2
-1
0
1
TIME (mSEC)

Figure 2

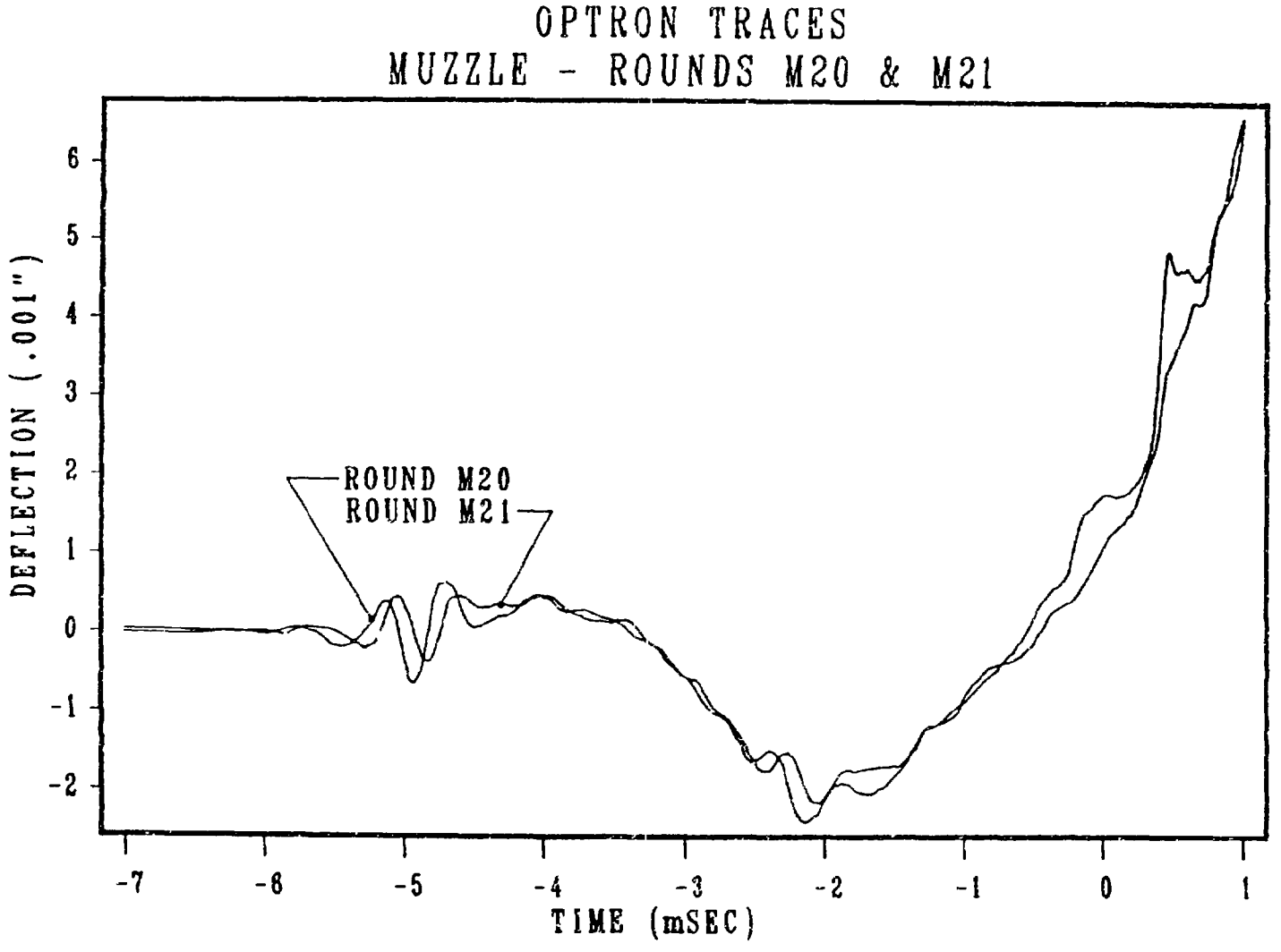
OPTRON TRACES
MUZZLE - ROUNDS M20 & M21
DEFLECTION (.001")
6
5
4
3
2
1
0
-1
-2
ROUND M20
ROUND M21
-7
-6
-5
-4
-3
-2
-1
0
1
TIME (mSEC)

Figure 3

*SIMKINS, PFLEGL, SCANLON

Presently there is no explanation as to the cause of the motions depicted in Figures 2 and 3, i.e., no eccentric masses have been applied to the tube, and the curvature of the tube 'as manufactured' is not sufficient (according to our two computer models) to create motion of this magnitude. Likewise, the support reactions applied by the wires are not supposed to change radically during recoil. (A thorough check of these reaction forces is presently underway.)

Figure 4 shows the displacement of the muzzle when an eccentric mass is added to the breech end of the tube. The eccentric mass is created by simply replacing the 7.75 lb circular buffer plate with an identical one whose center is located below the central axis of the tube. The weight of the entire recoiling mass is 90.8 lbs. The eccentric location of the buffer plate is 1.3 inches directly below the bore axis of the tube. In Figure 5 the response shown in Figures 2 and 3 is taken as a 'base-line' and subtracted from that of Figure 4. The result is in reasonable agreement with that predicted by a NASTRAN model of the system. This is shown in Figure 6.

4. MODEL VALIDATION

The agreement shown in Figure 6 is at least as close as that in Figure 2, if one disregards the higher frequency components of the motion (probably radial vibrations); i.e., the experimental measurements and the NASTRAN-predicted muzzle displacements agree to the same extent as our measurement devices. It would appear, therefore, that we have a useful and validated computer model. Assuming this to be the case, one of the most expected uses of a computer model of a gun system is to predict muzzle rotation. It is of much more interest to know muzzle rotation than it is to know muzzle displacement, target error being associated most strongly with the former. Can our NASTRAN model be trusted to predict muzzle rotation? The answer is very negative. One reason for this will be shown - the fact that our NASTRAN model does not account for moving projectile mass. Unfortunately, there may be others.

In Figures 7a through 7d the predicted muzzle response due to an eccentric breech mass with and without the presence of the moving projectile mass are compared. (These predictions were produced by a second computer code in which moving mass effects are easier to include.) It is observed that although there is close agreement between muzzle displacement predictions with and without moving mass effects, the prediction of the (all-important) muzzle rotations are totally different. Thus the effect of moving projectile mass cannot be ignored.

While it has been shown that moving projectile mass must be included in any mathematical model from which muzzle rotation predictions are expected, this is by no means a sufficient condition. Other effects normally overlooked and expected to be negligible, may have to be included also. Most important, one may not know what they are, or in what detail to describe them. For example, the muzzle rotation predicted when the moving projectile is included may well depend on the detail with which it is modeled. (In Figures 7c and 7d, the projectile was simply modeled as a moving point mass.) It may be

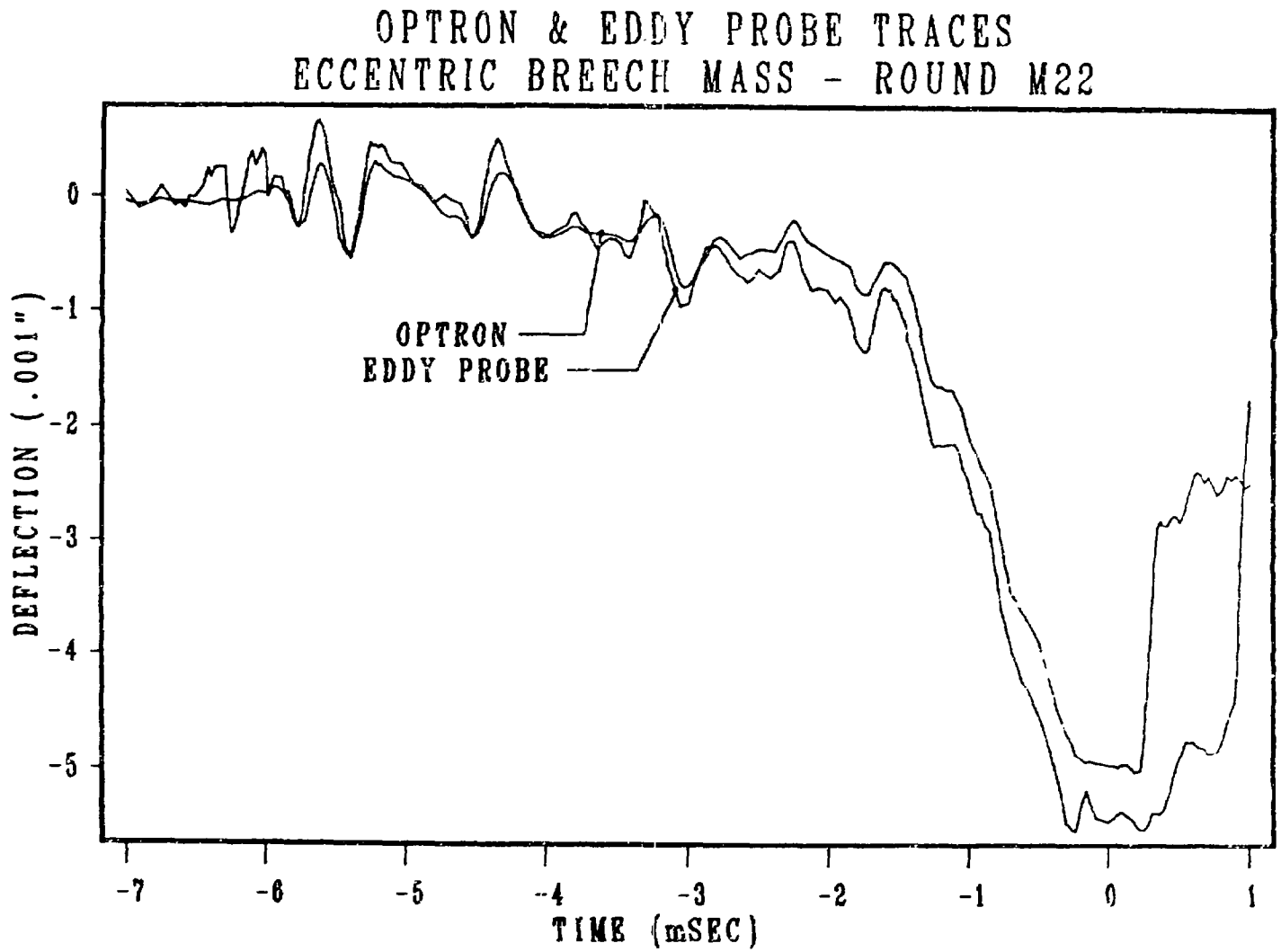
OPTRON & EDDY PROBE TRACES
ECCENTRIC BREECH MASS - ROUND M22
OPTRON
EDDY PROBE
DEFLECTION (.001")
0
-1
-2
-3
-4
-5
-7
-6
-5
-4
-3
-2
-1
0
1
TIME (mSEC)

Figure 4

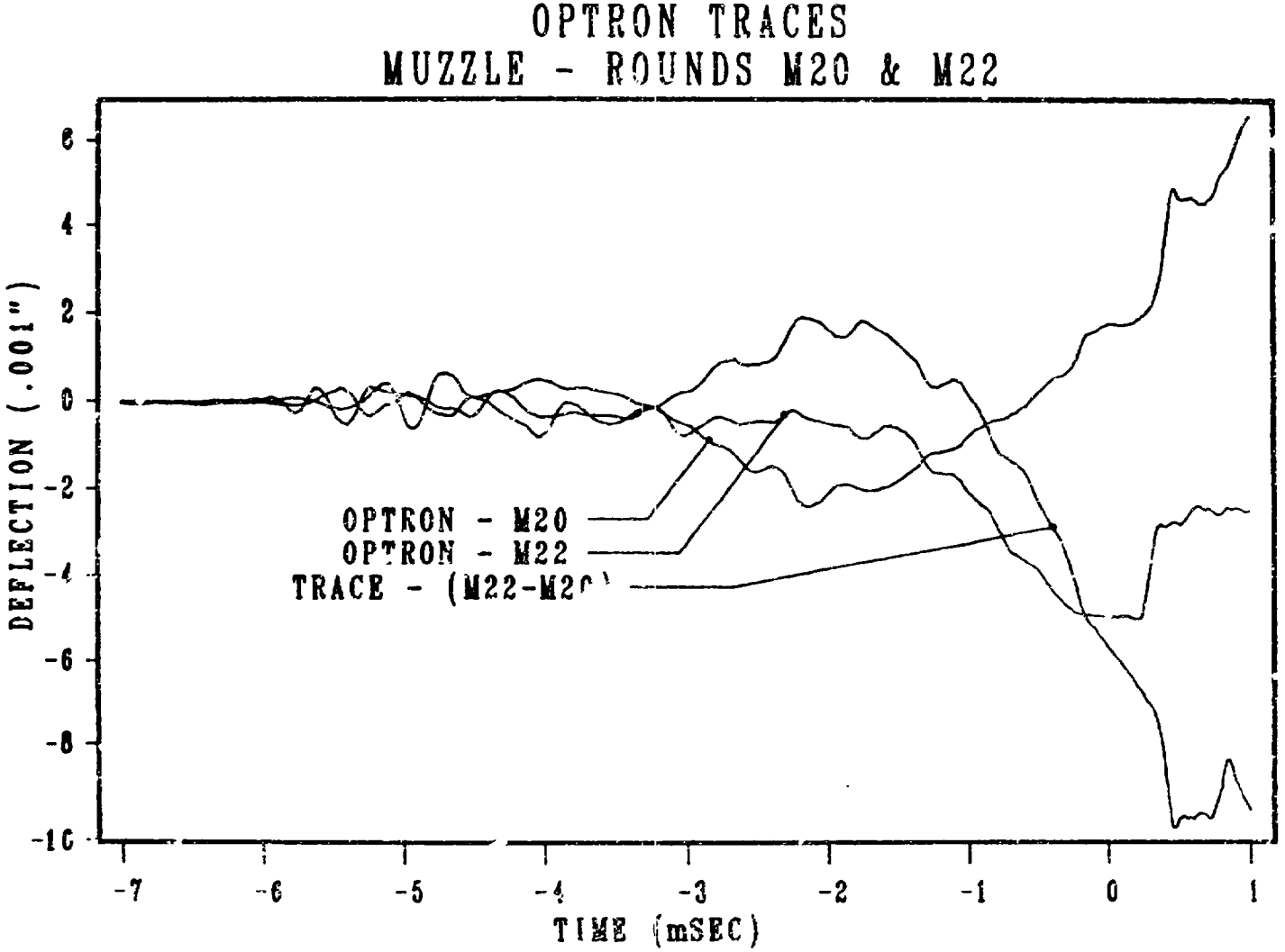
OPTRON TRACES
MUZZLE - ROUNDS M20 & M22
DEFLECTION (.001")
6
4
2
0
-2
-4
-6
-8
-10
OPTRON - M20
OPTRON - M22
TRACE - (M22-M20)
-7
-6
-5
-4
-3
-2
-1
0
1
TIME (mSEC)

Figure 5

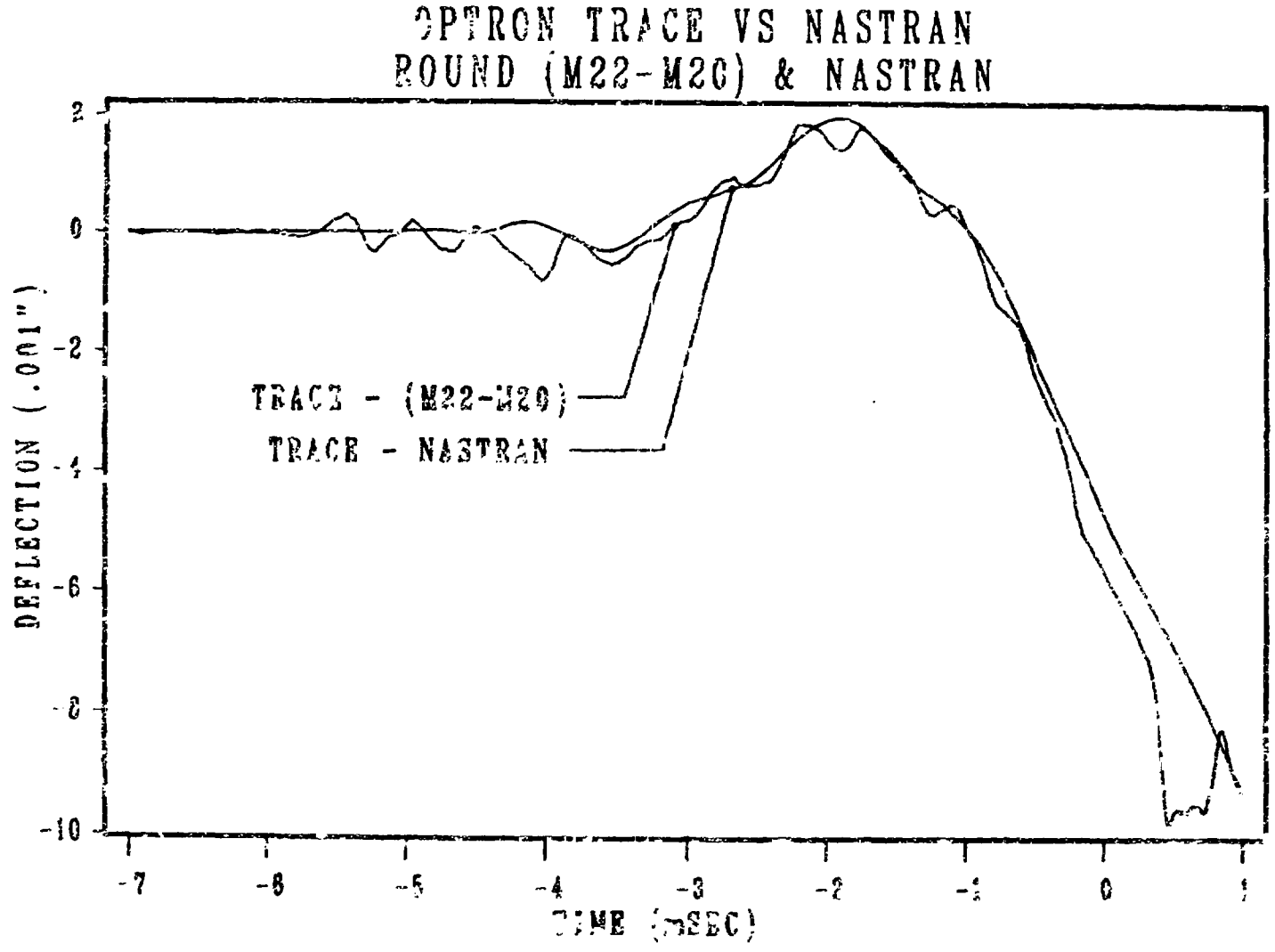
OPTRON TRACE VS NASTRAN
ROUND (M22-M20) & NASTRAN
TRACE - (M22-M20)
TRACE - NASTRAN
DEFLECTION (.001")
2
0
-2
-4
-6
-8
-10
-7
-6
-5
-4
-3
-2
-1
0
1
TIME (MSEC)

Figure 6

concluded, therefore, that the only way to be certain that a model can be trusted to predict muzzle rotations is by experimental verification - the very task one hoped to avoid! In conclusion, complete model validation requires measurement of displacement and rotation.

That the inclusion of moving projectile mass in any mathematical model of a gun system would have such a dramatic effect on predicting muzzle rotations may come as a surprise to some investigators. After all, predictions of muzzle motion due to a moving projectile mass in the absence of other load functions (such as eccentric breech mass, support reactions, curvature, etc.) have been virtually negligible. One must not forget, however, that the tube response due to combinations of load functions which are motion-dependent, is not simply the sum of the responses due to each load acting independently. Even though one is dealing in general with a linear model based on some particular linear partial differential equation (p.d.e.), the differential operator is altered every time a motion-dependent load is included or excluded. The operator must remain the same in order for linear superposition to hold. For example, consider the partial differential equations corresponding to Figures 7a through 7d. If the moving projectile mass and an eccentric breech mass are both included, the p.d.e. is

$$(EIy'')'' + \rho y = \varepsilon M\alpha(t)\delta'(x) - m_p(y+2\dot{y}'\dot{\xi}+\dot{\xi}^2y''+g)\delta(x-\xi) \qquad (1)$$

where $\alpha(t)$ is the recoil acceleration of a breech mass M located distance ε from the bore axis (see Figure 7a), m_p is the mass of the projectile located at a distance $\xi(t)$ from the breech end of the tube, y is the transverse displacement of the tube, δ is the Dirac function, and g is the gravitational constant. Note that the projectile mass creates a motion-dependent load function - it depends on y and its derivatives. The solution to Eq. (1) at the muzzle is shown in Figures 7a and 7b.

On the other hand, if the moving projectile is neglected

$$(EIy'')'' + \rho y = \varepsilon M\alpha(t)\delta'(x) \qquad (2)$$

and the solution is shown in Figures 7c and d. A quick glance shows that the displacement is hardly changed from Figure 7a, but the rotation (y') is completely different.

Now consider the case where the moving projectile is the only load acting). The p.d.e. is

$$(EIy'')'' + \rho y = -m_p(y+2\dot{y}'\dot{\xi}+\dot{\xi}^2y''+g)\delta(x-\xi) \qquad (3)$$

The muzzle displacement and rotation corresponding to this equation are shown in Figure 8. As can be seen, their magnitudes are very small. If these are added to those from Eq. (2), hardly any change to Figures 7c and 7d would result, demonstrating that solutions to Eqs. (2) and (3) cannot be summed to yield the solution to Eq. (1). This is shown in Figure 9. In effect, the motion-dependent term affects the operator of the p.d.e. and one cannot add solutions to equations with different operators.

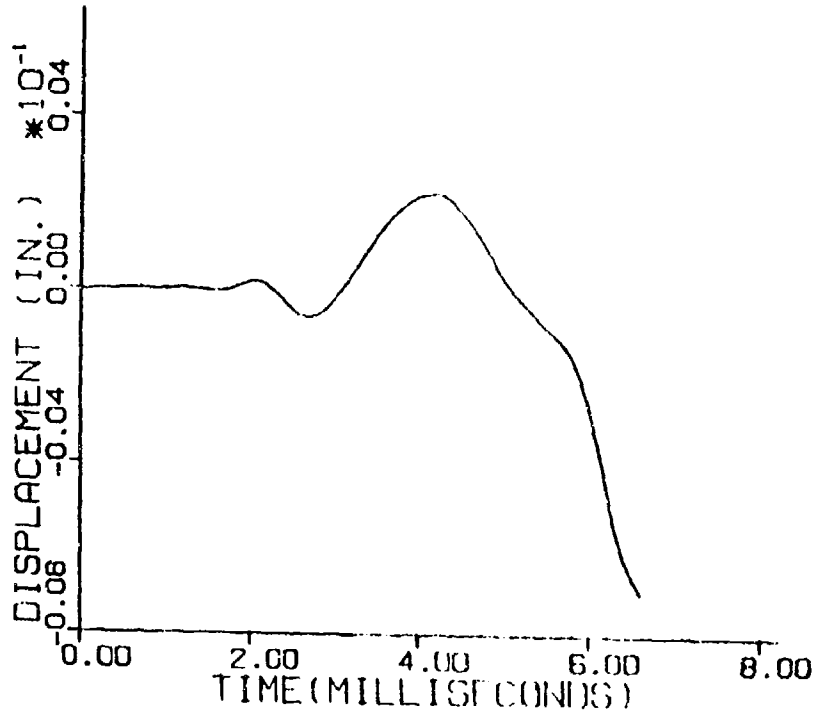

Figure 7a. Muzzle Displacement Due to Eccentric Breech Mass and Moving Projectile.

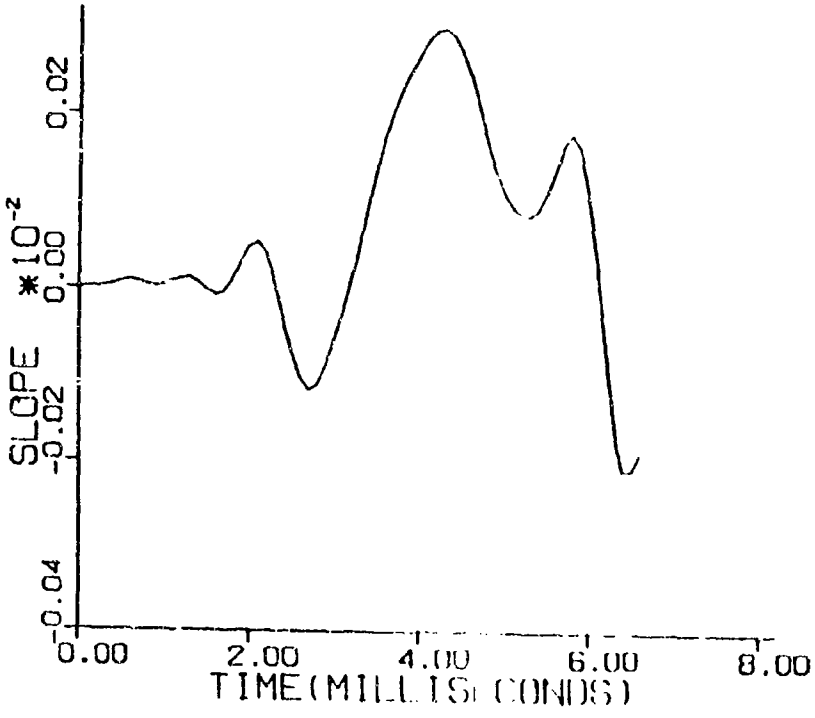

Figure 7b. Muzzle Rotation Due to Eccentric Breech Mass and Moving Projectile.

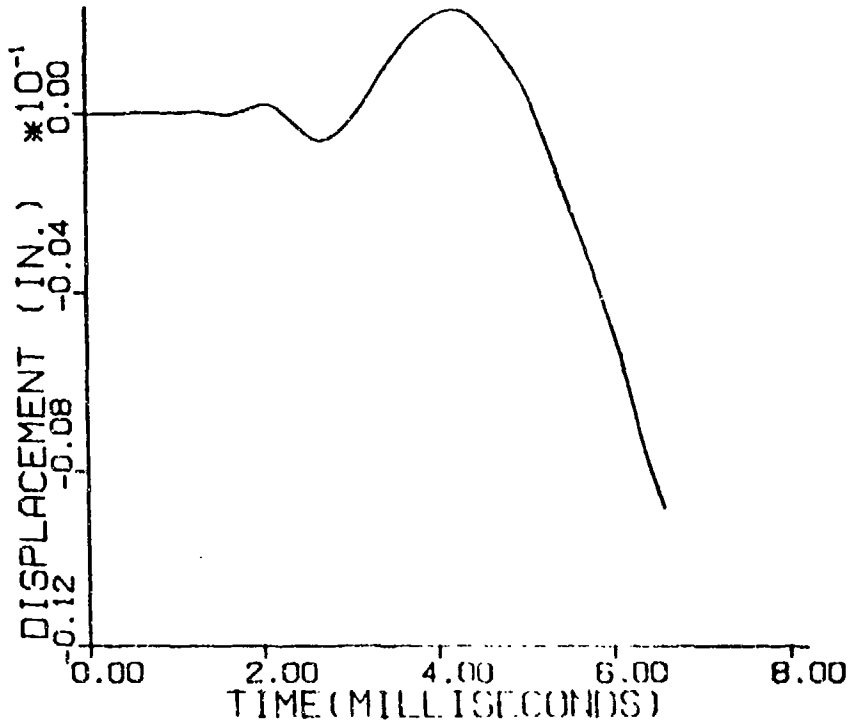

Figure 7c. Muzzle Displacement Due to Eccentric Breech Mass.

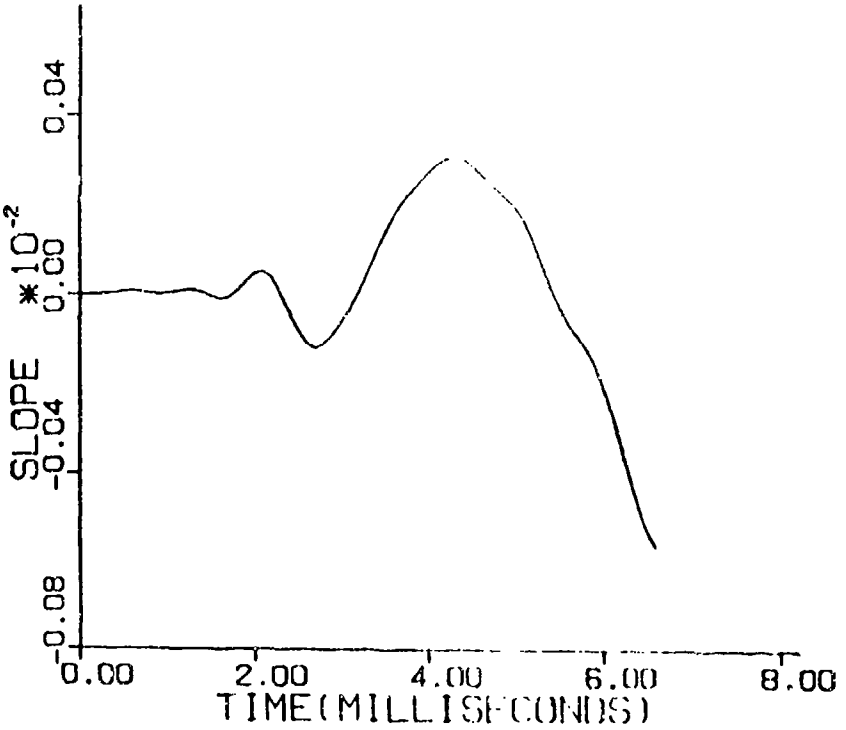

Figure 7d. Muzzle Rotation Due to Eccentric Breech Mass.

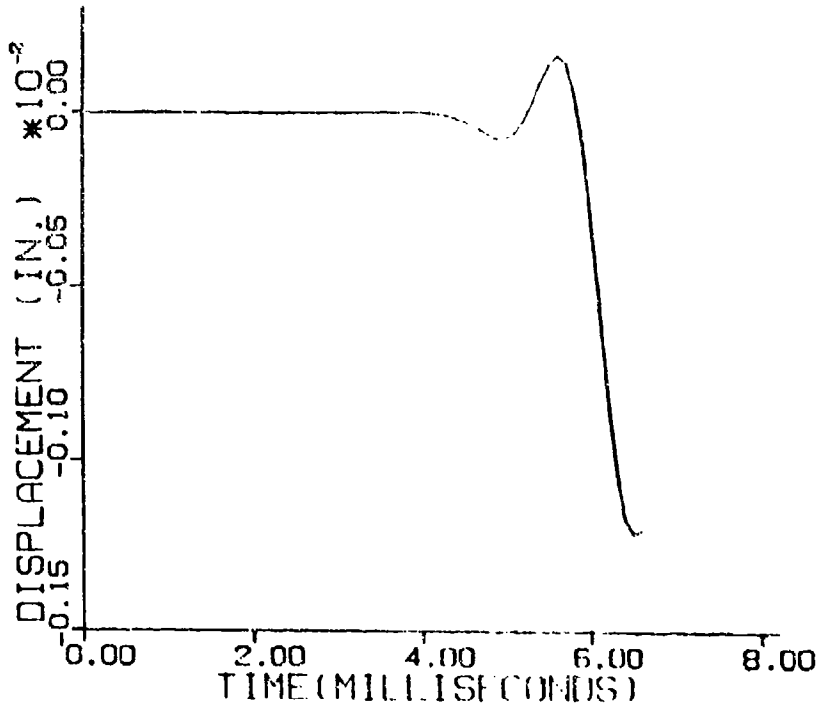

Figure 8a. Muzzle Displacement Due to Moving Projectile.

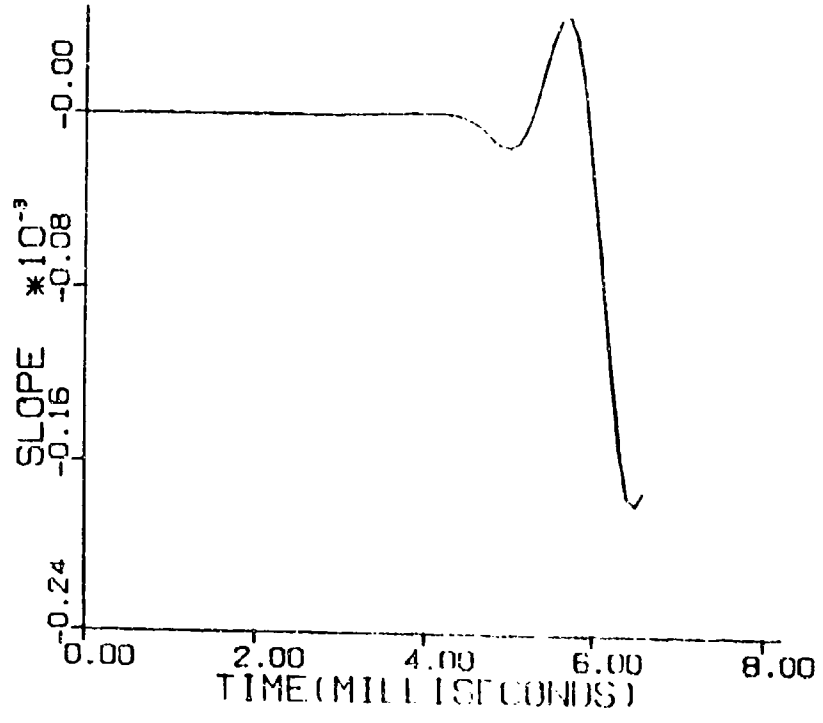

Figure 8b. Muzzle Rotation Due to Moving Projectile.

*SIMKINS, PFLEGL, SCANLON

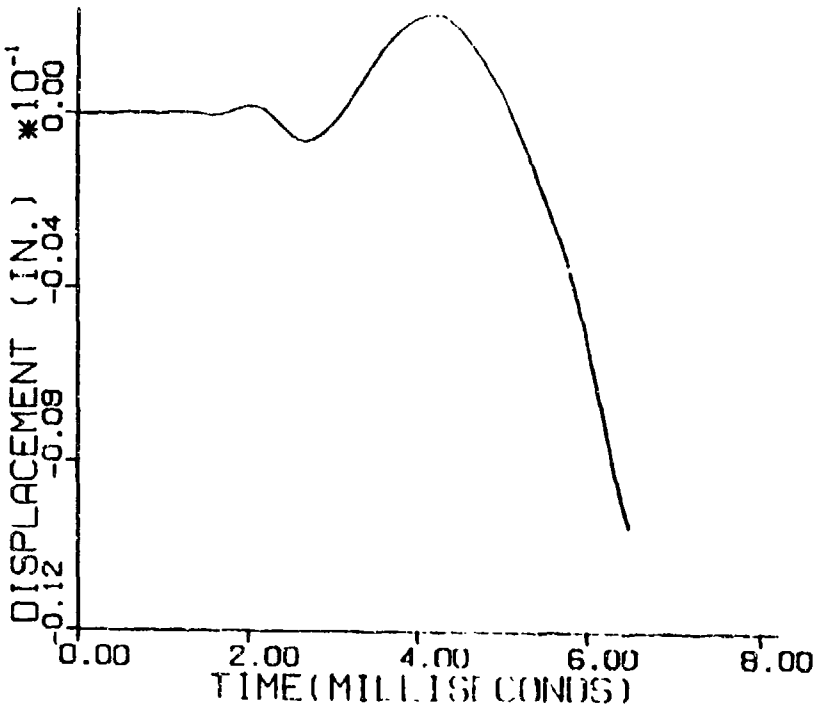

Figure 9a. Sum of Figures 7c and 8a.

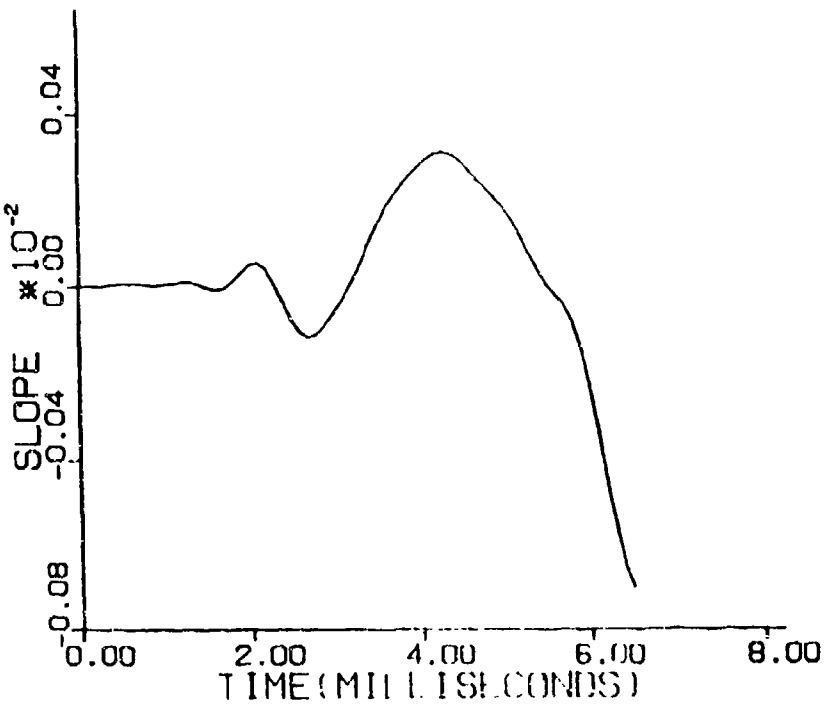

Figure 9b. Sum of Figures 7d and 8b.

*SIMKINS, PFLEGL, SCANLON

5. CONCLUSION

1. The measurement of transverse tube displacements during firing can now be accomplished with a high degree of confidence. Eddy probes and optical trackers may be expected to disagree as much as 0.0005 inch (0.0127 mm). Neither device can be assumed superior to the other, but eddy probes are relatively inexpensive - almost expendable, and very easy to use by comparison.

2. There is no way to know if all motion-dependent load functions have been accounted for in a given mathematical model or if those which have been accounted for have been described in sufficient detail. It has been shown herein that motion-dependent load functions, which are unimportant when acting alone, become very important when acting in concert with other loads. The importance of such motion-dependent loads cannot be assessed from their effects on tube displacement which may be minimal. Tube rotation, however, may depend significantly on the inclusion and proper description of these loads. Thus, a model should not be considered validated until displacement and rotation have been verified experimentally. Needless to say, all models must be validated to be of any use. In view of this, it is important to the future of analytical gun dynamics that means be found to obtain measurements of tube rotations - particularly at the muzzle. In addition, such measurements should be corroborated.

REFERENCES

1. Simkins, T. E., Scanlon, R. D., and Benedict, R., "Transverse Motion of an Elastically Supported 30 mm Gun Tube During Firing," Proceedings of the Third U.S. Army Symposium on Gun Dynamics, ARLCB-SP-82005, Vol. I, May 1982, pp. I-72 - I-95.

ABSTRACT

THOMASSON

TITLE: The Development of an Algorithm for Shot/Barrel Interaction Calculations

ABSTRACT:

Shot/barrel interaction calculations pose a calculation problem in that the dynamics of the shot are non linear and involve high frequencies, whilst the dynamics of the barrel are linear and involve for the most part, lower frequencies. Since the barrel involves a large number of degrees of freedom and the shot has only a few, the calculation of the combined motion by direct integration is constrained by the step size required by the shot motion. In order to avoid this problem and take advantage of the existing the SHOCK-AID package the SHOCK-AID modal solution technique is used for the barrel and an algorithm is developed to link this to the direct integration solution of the shot motio . The algorithm is currently being integrated into the SHOCK-AID package. This work has been carried out with the support of Procurement Executive, Ministry of Defence.

BIOGRAPHY:

PRESENT ASSIGNMENT: Senior Lecturer, College of Aeornautics, Cranfield Institute of Technology, Cranfield, Bedford, England.

DEGREES HELD: MSc, Cranfield Institute of Technology.

THE DEVELOPMENT OF AN ALGORITHM FOR SHOT/BARREL INTERACTION CALCULATIONS

PETER G. THOMASSON
CRANFIELD INSTITUTE OF TECHNOLOGY
CRANFIELD
BEDFORD MK43 OAL

INTRODUCTION

Whenever a gun is fired a projectile is propelled violently along the barrel, whilst at the same time the barrel recoils. The magnitude of the resultant accelerations can cause large forces and moments to be applied to the barrel in the lateral direction and these then produce flexural waves that travel along the barrel. As a result, by the time the projectile is launched, the muzzle may have considerable transverse velocity and displacement and thus the projectile departs in a slightly different direction to that which was intended.

A second effect is that whilst the shot travels up the barrel it may undergo considerable vibration relative to the barrel due to the finite stiffness of its driving bands, gyroscopic motions, shot/barrel clearances etc. Therefore even in a perfectly rigid barrel the shot may depart with considerable lateral disturbance due to its internal motion within the barrel.

In practice both of these effects are present at the same time and they are probably coupled together as well. The calculation of these effects poses some considerable computational difficulties. The vibrational frequencies of the shot whilst in the barrel are quite high, usually in excess of 1KHz, but the flexural motion of the barrel usually has a fundamental frequency of only a few Hz. As a result using standard numerical integration techniques, the equations of both the shot and the barrel would have to be solved using very small time steps, sufficiently small to ensure that the high frequencies of the projectile dynamics were handled in an accurate and stable manner. Typically step sizes of the order of 10μ secs would be required to compute the shot motion and on a computer such as the VAX the solution of the motion of the shot alone would take quite a considerable time. Add to this the model of the gun barrel with 100 or more degrees of freedom and the solution time would escalate considerably.

This report addresses the problem of how this excessive solution time can be reduced. In addition it attempts to use the already established SHOCK-AID solution techniques Ref. (2) in such a manner that advantage is taken of the ability of SHOCK-AID to model barrels simply and efficiently. The major problem however with the latter approach is that SHOCK-AID is based upon a modal superposition system that takes advantage of the linear nature of the flexural equations of the barrel. Motion of the shot is non linear and hence does not lend itself to modal style solution, and as a result some method has to be found to couple the modal solution of the barrel flexure with the numerical integraiton of the shot motion. Details of the shot model were given in Ref. (3) along with very brief details of the interaction technique. This paper considers the computational details of the shot/barrel interaction in detail. In order to demonstrate the nature of the problem and its solution, a simplified modal of shot/barrel interaction is considered so as to remove non essential detail from the problem.

2.0 An initial simplified model

The shot is a relatively small mass connected to the barrel via stiff springs, whereas the barrel is a very large mass having a relatively low stiffness. As a result the simplest model of the two elements combined together is a two mass spring system as shown below

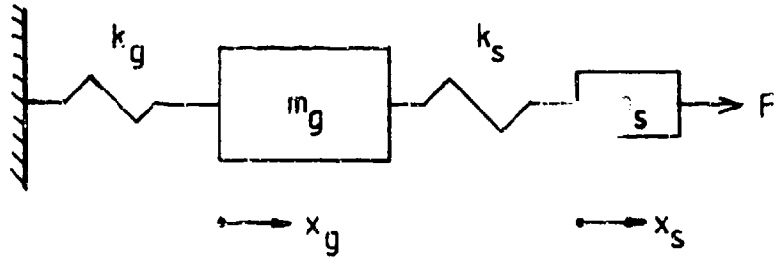

m_s and k_s represent the mass and stiffness of the shot whilst m_g and k_g represent the mass and stiffness of the gun. External forces applied to the shot (they may include dynamic effects such as gyroscopic forces etc.) are represented by F.

The equations of motion of the system are

$$\ddot{x}_g = -\frac{k_g - k_s}{m_g} x_g + \frac{k_s}{m_g} x_s$$

$$\ddot{x}_s = \frac{k_s}{m_s} x_g - \frac{k_s}{m_s} x_s + \frac{F}{m_s}$$

assuming $x_s(0) = x_g(0) = \dot{x}_s(0) = \ddot{x}_g(0) = 0$

and using Laplace Transforms we can write,

$$x_s = \frac{F}{m_s}\left[\frac{(k_g + k_s)/m_g}{w_1^2 w_2^2} + \frac{1}{(w_1^2 - w_2^2)}\left(\left(-1 + \frac{(k_g + k_s)/m_g}{w_1^2}\right)\cos w_1 t - \left(-1 + \frac{(k_g + k_s)/m_g}{w_2^2}\right)\cos w_2 t\right)\right] \quad (1)$$

$$x_g = \frac{k_s}{m_g}\frac{F}{m_s}\left[\frac{1}{w_1^2 w_2^2} + \frac{1}{(w_1^2 - w_2^2)}\left(\frac{1}{w_1^2}\cos w_1 t - \frac{1}{w_2^2}\cos w_2 t\right)\right] \quad (2)$$

and w_1 and w_2 are given by

$$2w^2 = -\left(\frac{k_s}{m_s} + \frac{(k_s + k_g)}{m_g}\right) \pm \sqrt{\left(\frac{k_s}{m_s} + \frac{(k_s + k_g)}{m_g}\right)^2 - 4\frac{k_s}{m_s}\frac{k_g}{m_g}} \quad (3)$$

Now in order that we have representative values for the constants in the above we assume the following:

k_s = 3.95 E10 N/m
m_s = 10 kg
k_g = 6.32 E8 N/m
m_g = 100 kg
F = 6.32 E5 N

These figures mean that the natural frequency of the shot mass on its own is about 10 KHz whilst that of the barrel element on its own is about 400 Hz. The load F produces a static deflection of the barrel element of 1mm.

Using the above data in equation (3) gives

$$w_1^2 \cong \frac{k_g}{m_g} \quad ; \qquad w_2^2 \cong \frac{k_s}{m_s} \tag{4}$$

and since $w_2^2 >> w_1^2$ we can write

$$x_g \cong \frac{F}{k_g}(1 - \cos w_1 t) \tag{5}$$

$$x_s \cong \frac{F}{k_g}(1 - \cos w_1 t - \frac{k_g}{k_s} \cos w_2 t) \tag{6}$$

and thus

$$x_s - x_g \cong \frac{F}{k_s} \cos w_2 t \tag{7}$$

In order to represent the shot barrel model using SHOCK-AID the obvious approach would be to solve the motion of the gun mass using the SHOCK-AID modal technique and solve the shot motion via a numerical solution such as Runge Kutta or a predictor/corrector technique. In order to link the two solutions some form of iterative scheme would be required.

If we denote the force in the shot spring by the letter f,i.e.

$$f = k_s(x_s - x_g) \tag{8}$$

then the equations of motion become,

$$m_g \ddot{x}_g = k_g x_g + f \tag{9}$$

$$m_s \ddot{x}_s = F - f \tag{10}$$

If we consider the barrel mass and spring alone we can write,

$$\ddot{x}_g = - \frac{k_g}{m_g} x_g + \frac{f}{m_g} = -w^2 x_g + \frac{f}{m_g} \tag{11}$$

and in order to solve (11) we need to know the variation of "f" with time,however, as equation (8) shows "f" is itself dependant upon the solution of (11).

Ignoring for the moment the implicit variation of "f" with "x_g" we can write the solution of (11) as,

$$x_g = x_g(0) + \int_0^t \frac{f(\tau)}{m_g} \frac{\sin w(t - \tau)d\tau}{w} \tag{12}$$

$$\dot{x}_g = v_g(0) + \int_0^t \frac{f(\tau)}{m_g} \cos w(t - \tau)d\tau \tag{13}$$

Let $b = f/m_g$ then expanding the integrals thus,

$$\int_0^t \frac{b(\tau)\sin w(t - \tau)d\tau}{w} = \frac{\sin wt}{w} \int_0^t b(\tau)\cos w\tau d\tau - \frac{\cos wt}{w} \int_0^t b(\tau)\sin w\tau d\tau \tag{14}$$

and the integrals can be represented by

$$\int_0^{t+\Delta t} b(\tau)\cos w\tau d\tau = J(t + \Delta t) = J(t) + \int_t^{t+\Delta t} b(\tau)\cos w\tau d\tau \tag{15}$$

$$\int_0^{t+\Delta t} b(\tau)\sin w\tau d\tau = k(t + \Delta t) = k(t) + \int_t^{t+\Delta t} b(\tau)\sin w\tau d\tau \tag{16}$$

A linear approximation to "b" is used by letting $b = mt + c$ over the step Δt, then,

$$m = \frac{b(t_o + \Delta t) - b(t_o)}{\Delta t} \tag{17}$$

$$c = b(t_o) - mt_o \tag{18}$$

We can thus write (15) and (16) as

$$J(t_o + \Delta t) = J(t_o) + JINC(t_o) \tag{19}$$

$$k(t_o + \Delta t) = k(t_o) + KINC(t_o) \tag{20}$$

where

$$JINC(t_o) = \int_{t_o}^{t_o+\Delta t} (m\tau + c)\cos w\tau d\tau = \left[\frac{m\cos w\tau}{w^2} + \frac{m\tau\sin w\tau}{w} + \frac{c\sin w\tau}{w}\right]_{t_o}^{t_o+\Delta t} \quad (21)$$

$$KINC(t_o) = \int_{t_o}^{t_o+\Delta t} (m\tau + c)\sin w\tau d\tau = \left[\frac{m\sin w\tau}{w^2} - \frac{m\tau\cos w\tau}{w} - \frac{c\sin w\tau}{w}\right]_{t_o}^{t_o+\Delta t} \quad (22)$$

and thus the final solution for x_g and v_g is,

$$x_g(t_o + \Delta t) = x_g(t_o) + \frac{\sin wt}{w}\left\{J(t_o) + JINC(t_o)\right\} - \frac{\cos wt}{w}\left\{k(t_o) + KINC(t_o)\right\} \quad (23)$$

$$v_g(t_o + \Delta t) = v_g(t_o) + \cos wt\left\{k(t_o) + KINC(t_o)\right\} + \sin wt\left\{J(t_o) + JINC(t_o)\right\} \quad (24)$$

The above equations represent a SHOCK-AID modal type solution to the motion of the gun mass.

Having produced a SHOCK-AID style solution for the gun element and a standard numerical solution for the shot, the next question is how to integrate the two calculations together. A possible scheme is as follows:

(i) Estimate the acceleration of the gun element over the interval $t_o \rightarrow t_o + \Delta T$

$$\dot{v}_g = (k_s x_g - f)/m_g \quad (26)$$

(ii) Compute the shot motion using the predicted motion of x_g^*

$$x_g^*(f) = x_g(t_o) + v_g(t_o)\Delta t + \tfrac{1}{2}\dot{v}_g(t_o)\Delta t^2 \quad (27)$$

to calculate the variation of "f" over the step $t_o \rightarrow t_o + \Delta T$. At the same time compute "avsf" the average value of f over the interval.

(iii) Compute the motion of the gun element using f = avsf as the applied spring force over the interval.

(iv) Compare $x_g(t_o + \Delta T)$ from step 3 above with $x_g^*(t + \Delta T)$. If they agree (within a suitable tolerance) then advance the solution otherwise re-estimate $\dot{v}_g$ at step 1 and repeat the calculations.

A program to implement the above was produced, It used the average force over the interval not a linear variation. Other representations of the force variation were investigated, but all versions of the program appeared to have a common draw back in that it was not in general possible to drive x_g and x_g^* into agreement. No matter how long the program iterated it always seemed to converge on a solution which had a small but steady error between x_g and x_g^*.

The problem was that the model was too simple in that it only uses two mass spring elements. A more representative model is a three element model. The reasons for this are explained in the next section.

3.0 Three Mass Spring System

As mentioned above a two mass/spring model for shot barrel interactions is too simple. The reason for this is that there are in fact THREE types of elements in such a problem. They are:

(i) The shot element or elements
(ii) The contact elements, i.e. those elements that the shot applies forces to directly.
(iii) Internal gun elements that have no direct contact with the shot.

The reason for treating each of the above elements differently is that they experience forces of very different frequency content. A shot element is subjected to very high frequencies due to its low mass and its high contact stiffnesses, an internal element on the other hand is only exposed to relatively low frequencies associated with the barrel dynamics. The contact element however is exposed to both the high and the low frequencies. As a result our three mass/spring model of barrel/shot interaction is as shown below.

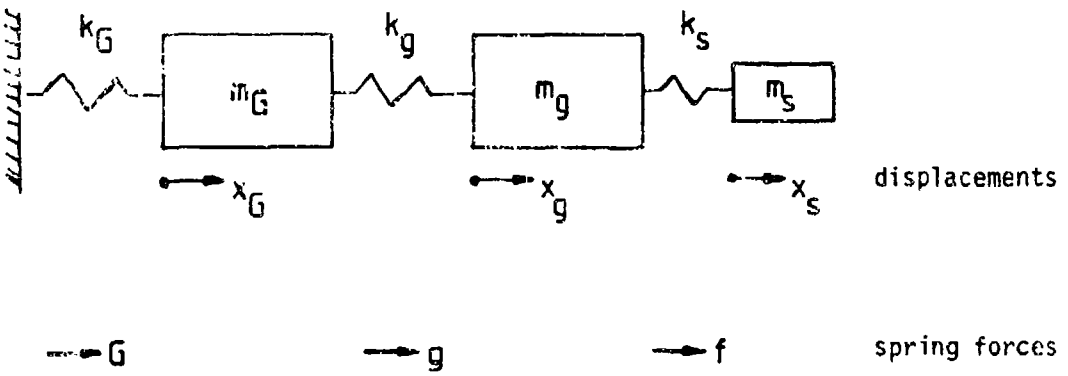

The two solutions (modal and numerical) now overlap in that the modal solution computes the motion of all the internal elements and all the contact elements, whilst the numerical solution computes the motion of all the contact elements and all the shot elements. In order to do this some assumptions are required about the behaviour of elements excluded from each calculation.

A possible solution scheme is as follows:

(i) Predict the motion of m_G over the next time step ΔT

$$x_G(t) = x_G(t_o) + \dot{x}_G(t_o)\Delta t + \ddot{x}_{G_{AV}} \frac{\Delta t^2}{2} \qquad (28)$$

$$t_o \leqslant t \leqslant t_o + \Delta T$$

$\ddot{x}_{G_{AV}}$ is a guess of the average acceleration over the interval ΔT, initially set this to $\ddot{x}_G(t_o)$.

(ii) Solve the equations of motion of masses m_g and m_s using the assumed $x_G(t)$ above so that spring force g can be calculated. This will use small time steps δT where in general $\delta T \ll \Delta T$. During this calculation monitor the variation of the spring force f and calculate f_{eqv}, an "equivalent" spring force that can be applied to the modal solution.

(iii) Apply f_{eqv} to the modal solution of the contact elements and the internal elements.

(iv) Compare $x_G(t + \Delta T)$ from (iii) with the predicted value from (i), if they agree within a reasonable tolerance then advance the solution another ΔT and repeat from (i); otherwise re-estimate $\ddot{x}_{G_{AV}}$ used in (i) and repeat the calculation.

In order to carry out the above, two items are required, these are an algorithm for calculating "f_{eqv}" and another for updating $\ddot{x}_{G_{AV}}$.

Considering the estimation of $\ddot{x}_{G_{AV}}$ first. The initial estimate of $\ddot{x}_{G_{AV}}$ is $\ddot{x}_G(t_o)$ since no data about the future variation of $\ddot{x}_G$ is available. On the next iteration however we have available $x_G(t_o + \Delta T)$ that was calculated by the modal solution and thus a reasonable estimate for $\ddot{x}_{G_{AV}}$ would be that value that would produce a predicted value of $x_G(t_o + \Delta T)$ equal to that observed. Thus using (28) we can say,

$$x_G(t_o + \Delta T) = x_G(t_o) + \dot{x}_G(t_o)\Delta t + \ddot{x}_{G_{AV}} \frac{\Delta t^2}{2} \qquad (29)$$

or

$$\ddot{x}_{G_{AV}} = 2(x_G(t_o + \Delta T) - x_G(t_o) - \dot{x}_G(t_o)\Delta t)/\Delta t^2 \qquad (30)$$

The calculation of "f_{eqv}" is a little more complicated. The standard SHOCK-AID modal solution assumes that the variation of applied force over the time step is linear. Thus the calculation of "f_{eqv}" must produce a linear force variation over the time step ΔT that is equivalent

to the (in general non-linear) variation of f over ΔT (f is available at intervals of ST).

The criteria of "equivalent" in this cas. is that the displacement and velocity of the large mass should be the same at the end of the long time step irrespective of whether the linear or non linear force is applied to it. This also means that both the potential and kinetic energies are the same for the "real" and the "equivalent" forces. In order that the two forces produce the same deflections and velocities at the end of the ΔT time step, examination of the SHOCK-AID equations shows that the values of the following two integrals must not change if either the "equivalent" or real forces are used.

$$\int_{t_0}^{t_0+\Delta T} f(t)\cos wt\,dt \quad ; \quad \int_{t_0}^{t_0+\Delta T} f(t)\sin wt\,dt \tag{31}$$

for all w's (w's are the gun system eigenvalues)

Now let $T_w = \frac{2\pi}{w}$ gun system period(s)

If $T_w \gg \Delta T$ then we can write

$$\int_{t_0}^{t_0+\Delta T} f(t)\cos\frac{2\pi t}{T_w}\,dt \cong \int_{t_0}^{t_0+\Delta T} f(t)dt \tag{32}$$

$$\int_{t_0}^{t_0+\Delta T} f(t)\sin\frac{2\pi t}{T_w}\,dt \cong \int_{t_0}^{t_0+\Delta T} f(t)\,\frac{2\pi t}{T_w}\,dt$$

$$\cong \frac{2\pi}{T_w}\int_{t_0}^{t_0+\Delta T} f(t)tdt \tag{33}$$

and the integral in (33) can be written,

$$\int_{t_o}^{t_o+\Delta T} f(t)tdt = \int_{t_o}^{t_o+\Delta T} td\left(\int_{t_o}^{t_o+\Delta T} f(\tau)d\tau\right)dt$$

$$= \Delta T\int_{t_o}^{t_o+\Delta T} f(t)dt - \int_{t_o}^{T+\Delta T}\int_{t_o}^{t} f(\tau)d\tau dt \qquad (34)$$

Thus the "real" and the "equivalent" forces must have the same values for the first and second integrals,

$$\int_{t_o}^{t_o+\Delta T} f(t)dt \quad \text{and} \quad \int_{t_o}^{t_o+\Delta T}\int_{t_o}^{t} f(\tau)d\tau dt \qquad (35)$$

If we call these two integrals for the "real" force I_f and II_f respectively, then we require for the linear equivalent force,

$$\int_{t_o}^{t_o+\Delta T} (mt + c)dt = \frac{m\Delta T^2}{2} + c_o\Delta T = I_f \qquad (36)$$

$$\int_{t_o}^{t_o+\Delta T} \left(\frac{mt^2}{2} + ct\right)dt = \frac{m\Delta T^3}{6} + \frac{c_o\Delta T^2}{2} = II_f \qquad (37)$$

where $c_o = (mt_o + c)$

These can be written

$$\begin{bmatrix} I_f \\ II_f \end{bmatrix} = \begin{bmatrix} \Delta T^2/2 & \Delta T \\ \Delta T^3/6 & \Delta T^2/2 \end{bmatrix}\begin{bmatrix} m \\ c_o \end{bmatrix} \qquad (38)$$

the determinant of (38) is $\Delta T^4/12$, and the inverse is,

$$\frac{12}{T^4}\begin{bmatrix} \Delta T^2/2 & -\Delta T \\ -\Delta T^3/6 & \Delta T^2/2 \end{bmatrix}$$

thus

$$m = \frac{6}{\Delta T^2} I_f - \frac{12}{\Delta T^3} II_f \tag{39}$$

$$c_o = -\frac{2}{\Delta T} I_f + \frac{6}{\Delta T^2} II_f \tag{40}$$

Direct implementation of equations (39) and (40) would mean that the equivalent force could be discontinuous, e.g.

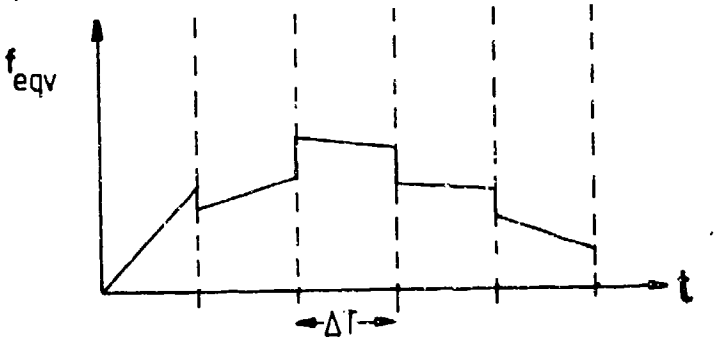

What is more in keeping with the original form of SHOCK-AID is for "c_o" to be determined by the previous time step. Then in that case, if the first integral is correct

$$m = \frac{2}{\Delta T^2} (I_f - c_o \Delta T) \tag{41}$$

and the value of the force at the end of the step is given by

$$m\Delta T + c_o = \frac{2}{\Delta T} (I_f - c\Delta T) + c_o$$

$$= \frac{2I_f}{\Delta T} - c_o \tag{42}$$

Alternatively if the second integral is correct

$$m = \frac{6}{\Delta T^3} (II_f - \frac{c_o \Delta T^2}{2}) \tag{43}$$

and

$$m\Delta T + c_o = \frac{6}{\Delta T^2} II_f - 2c_o \tag{44}$$

and thus it is not possible to satisfy both equations (42) and (44) at the same time if "c_o" is given by the previous step. The question therefore arises, if we can only satisfy one of the integrals which one is best?

If we satisfy the first integral then the cosine terms in the solution are correctly handled (see equation (32)) but there is an error in the sine expressions. From equations (33) and (34) the error in just using the first integral gives an error in the sine integral of,

$$\varepsilon = \frac{2\pi}{T_w}\left\{\int_{t_o}^{t_o+\Delta T}\int_{o}^{t} f(\tau)d\tau dt - \frac{m\Delta T^3}{6} - c_o\frac{\Delta T^2}{2}\right\}$$

where m is given by equation (42) for a c prescribed by the previous step.

Thus

$$\varepsilon = \frac{2\pi}{T_w}\left\{I_{ff} - \frac{\Delta T}{3} I_f - \frac{c_o\Delta T^2}{6}\right\} \tag{45}$$

It is not easy to tell from the above how the alternatives behave and a more convenient test is to assume that

$$f = \sin T \tag{46}$$

and observe how the different techniques approximate the function.

First of all using equations (46) we can write for a time step ΔT,

$$I_f = \cos(T) - \cos(T + \Delta T) \tag{47}$$

$$II_f = \sin(T) + \Delta T\cos(T) - \sin(T + \Delta T) \tag{48}$$

Using equations (39) and (40) in conjunction with (47) and (48) gives the results shown in Fig. 1. The curves show that for both large and small values of ΔT the approximation to f is well behaved, and the discontinuities are required in order to match the original function.

Using equations (41) and (42) with (47) and (48) removes the discontinuities but only the 1st integral is satisfied. Curves of the

results are shown in Fig. 2 for a range of ΔT values and the approximation is well behaved for all values of ΔT, there being larger discrepancies at large ΔT as would be expected.

If equations (43) and (44) are then used so as to satisfy the second integral only, the results shown in Fig. 3 are obtained. In this case the discrepancies are very large and somewhat surprisingly increase as ΔT decreases, there being some form of unstable behaviour apparent.

That this is indeed unstable behaviour can be illustrated as follows.

For the 1st integral case we can write equation (42) as

$$c_{i+1} = \frac{2I_f}{\Delta T} - c_i \tag{49}$$

and if $\Delta T \ll 1$ then $I_f = \Delta T \sin T = \Delta T \sin(i\Delta T)$

$$\therefore \quad c_{i+1} = 2\sin(i\Delta T) - c_i$$

and taking z transforms gives

$$z(c(z) - c_0) = \frac{2z\sin\Delta T}{z^2 - 2z\cos\Delta T + 1} - c(z)$$

or

$$c(z) = \frac{c_0 z}{(z+1)} + \frac{1}{(z+1)} \frac{2z\sin\Delta T}{(z^2 - 2z\cos\Delta T + 1)} \tag{50}$$

the poles of (50) are given by

$$z = -1 \quad \text{and} \quad z = \cos\Delta T \pm i \sin\Delta T$$

i.e. on the unit circle and thus the solution is stable.

For the second integral case equation (42) can be written,

$$c_{i+1} = \frac{6If}{\Delta T^2} - 2c_i \tag{51}$$

and if $\Delta T \ll 1$ then

$$\frac{II_f}{\Delta T^2} = \frac{\sin(i\Delta t)}{2} \tag{52}$$

and thus

$$c_{i+1} = 3\sin(i\Delta t) - 2c_i \tag{53}$$

and taking z transforms

$$z(c(z) - c_0) = \frac{3z\sin\Delta T}{z^2 - 2z\cos\Delta T + 1} - 2c(z)$$

or

$$c(z) = \frac{c_0 z}{(z+2)} + \frac{1}{(z+2)} \frac{3z\sin\Delta T}{(z^2 - 2z\cos\Delta T + 1)} \tag{54}$$

$z = -2$ and $z = \cos\Delta T \pm i \sin\Delta T$

i.e. outside the unit circle and therefore unstable.

Thus the conclusions are that ideally both integrals should be satisfied and the results will be valid for all step sizes, or for small steps the 1st integral alone can be satisfied. Satisfying the second integral alone results in unacceptable behaviour for all step sizes.

The preceding sections provide a basis for the solution of the three mass problem. The development is split into three phases as for the two mass problem. Firstly a modal solution is developed for the internal mass and the contact mass, making suitable assumptions regarding the motion of the shot mass. Secondly a numerical solution is derived for the motion of the shot mass and the contact mass, making suitable assumptions regarding the motion of the internal mass. Finally, the two are integrated together using the ideas of the previous paragraphs for $\ddot{x}_{G_{AV}}$ and f_{eqv}.

3.1 Modal Solution of Gun Masses

The equations of motion of the three mass model are,

$$m_G \ddot{x}_G = -G + g \tag{55}$$

$$m_g \ddot{x}_g = -g + f \tag{56}$$

$$m_s \ddot{x}_s = -f + F \tag{57}$$

where,

$$G = k_G x_G \tag{58}$$

$$g = k_g(x_g - x_G) \tag{59}$$

$$f = k_s(x_s - x_g) \tag{60}$$

The equations of motion of the gun masses alone are,

$$\begin{bmatrix} m_G & 0 \\ 0 & m_g \end{bmatrix} \begin{bmatrix} \ddot{x}_G \\ \ddot{x}_g \end{bmatrix} = \begin{bmatrix} (-k_G - k_g) & , & k_g \\ k_g & , & -k_g \end{bmatrix} \begin{bmatrix} x_G \\ x_g \end{bmatrix} + \begin{bmatrix} 0 \\ f \end{bmatrix} \tag{61}$$

or

$$\underset{\sim}{\ddot{x}} = M^{-1}k\underset{\sim}{x} + k\underset{\sim}{f} \tag{62}$$

and

$$M^{-1} = \begin{bmatrix} 1/m_G & 0 \\ 0 & 1/m_g \end{bmatrix} \tag{63}$$

$$M^{-1}k = \begin{bmatrix} \dfrac{-(k_G + k_g)}{m_G} & \dfrac{k_g}{m_G} \\ \dfrac{k_g}{m_g} & -\dfrac{k_g}{m_g} \end{bmatrix} \tag{64}$$

the eignvalues of (64) are g ven by

$$w^2 + \left(\frac{k_G + k_g}{m_G} + \frac{k_g}{m_g}\right) + \frac{k_G k_g}{m_g m_G} = 0 \tag{65}$$

i.e.

$$w_{1,2} = \tfrac{1}{2}\left[-\left(\frac{(k_G + k_g)}{m_G} + \frac{k_g}{m_g}\right) \pm \sqrt{\left(\frac{(k_G + k_g)}{m_G} + \frac{k_g}{m_g}\right)^2 - \frac{4k_G k_g}{m_g m_G}}\right.$$

The standard SHOCK-AID notation is

$$\ddot{\underset{\sim}{x}} + A\underset{\sim}{x} = \underset{\sim}{b}(t) \tag{66}$$

thus

$$A = -M^{-1}k \tag{67}$$

$$\underset{\sim}{b} = M^{-1}\underset{\sim}{f} \tag{68}$$

The left hand eigenvectors of A are

$$\begin{bmatrix} \underset{\sim}{U}_1' \\ \underset{\sim}{U}_2' \end{bmatrix} = \begin{bmatrix} \ell_e G_1 \ , \ 1 \\ \ell_e G_2 \ , \ 1 \end{bmatrix} \tag{69}$$

where

$$\ell_e G_{1,2} = \frac{m_G}{k_g}\left(\frac{k_g}{m_g} + w_{1,2}\right) \tag{70}$$

and the right hand eigenvectors are,

$$\underset{\sim}{V}_1 = \frac{1}{D_e t}\begin{bmatrix} 1 \\ -\ell_e G_2 \end{bmatrix} \quad , \quad \underset{\sim}{V}_2 = \frac{1}{D_e t}\begin{bmatrix} -1 \\ \ell_e G_1 \end{bmatrix} \tag{71}$$

where

$$D_e t = \ell_e G_1 - \ell_e G_2 \tag{72}$$

Let $\alpha_1 = \sqrt{-w_1}$ and $\alpha_2 = \sqrt{-w_2}$

The final solution is

$$\underset{\sim}{x}(t) = \underset{\sim}{U}_1\left\{\frac{1}{\alpha_1}\int_0^t \underset{\sim}{b}(\tau)\sin\alpha_1(t-\tau)d\tau\right\} V_1 + \underset{\sim}{U}_2\left\{\frac{1}{\alpha_2}\int_0^t \underset{\sim}{b}(\tau)\sin\alpha_2(t-\tau)d\tau\right\} V_2 \quad (73)$$

Equation (73) can be manipulated in a similar manner to equations (12) and (13) so as to produce marching integrals

3.2 Numerical Solution of Shot Motion

The equations of motion for the shot and the contact mass, assuming that m_G is motionless are,

$$g = k_g(x_g - x_G) \quad (74)$$

$$f = k_s(x_s - x_g) \quad (75)$$

$$\dot{v}_s = \frac{1}{m_s}(-f + F) \quad (76)$$

$$\dot{x}_s = v_s \quad (77)$$

$$\dot{v}_g = \frac{1}{m_g}(-g + f) \quad (78)$$

$$\dot{x}_g = v_g \quad (79)$$

A numerical solution to the motion of these two masses is used.

3.3 Coupled Solution

The two programs above were then integrated into one program using the interaction scheme outlined previously to produce a single program.

Basic data used in these programs is given below.

$m_G = 100, \quad m_g = 100, \quad m_s = 10$

$k_G = 6.32\ E8, \ k_g = 6.32\ E8, \ k_s = 3.95\ E10$

$F = 6.32\ E5, \ t \geq 0 \ ; \ F = 0, \ t < 0$

The program has two forms,

(i) that uses first integral only representation of f_{eqv}.

(ii) that uses both first and second integrals to represent f_{eqv}.

The results for the 1st integral case are given in Fig. (4) for modal solution time steps of 10 and 500 μ secs. The shot numerical integration time step was 1 μ sec in each case. For small time step ratios 10:1, Fig. (4a), the results are satisfactory but at large ratios 500:1, Fig. (4b), the solution is different. This can be noted by comparing the data calculation points (the corners on the graph every 500 μ sec) on Fig. (4b) with the same points on Fig. (4a). This is in line with what would be expected from the preceding results. Thus the 1st integral only algorithm is suitable for modest step size ratios but begins to break down when very high ratios are used.

The results for 1st and 2nd integrals are illustrated in Fig. (5) for step sizes ratios of 10:1 and 1000:1. Excellent agreement is obtained between the two cases, the solution points of the 1000μ sec step size calculation falling on top of those of the 10 μ sec step size calculation. Again this is what would be expected from the previous analysis.

4.0 Conclusions

An algorithm suitable for use as a SHOCK-AID interactive control routine has been developed that allows a numerical integration routine to be coupled to a modal solution technique such that each can have a different time step (in integer ratio). This means that the numerical integration can solve the fast dynamics of a few non linear degrees of freedom (the shot) with a small time step, whilst the modal SHOCK-AID solution can solve the slower dynamics of a much longer number of linear degrees of freedom (the barrel), using a much larger time step.

The algorithm, has been programmed into SHOCK-AID along with the full projectile model given in Ref. (3) and is at present undergoing validation tests.

5.0 References

(1) "SHOCK-AID users manual" M.D. Lipscombe and P.G. Thomasson, CIT/SHOCK/14 Cranfield Institute of Technology 1981.

(2) " A Consistent R & D assessment technique for the modelling of gun systems dynamics", B.A. Taylor and P.G. Thomasson. Proc 3rd US Army Symposium on Gun Dynamics, 1982.

(3) "A model for in-bore projectile dynamics including barrel interaction effects", P.G. Thomasson, Seventh International Symposium on Ballistics. The Hague, April 1983.

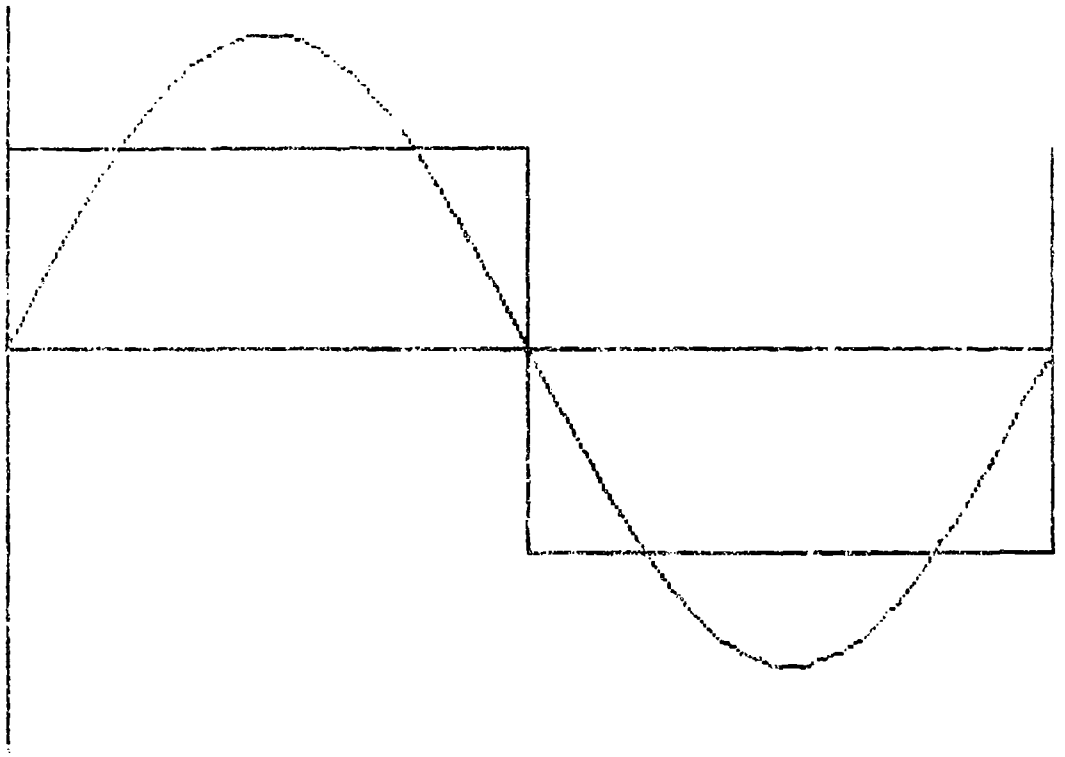

FIGURE 1a 1st and 2nd integrals satisfied, 2 steps/cycle

THOMASSON

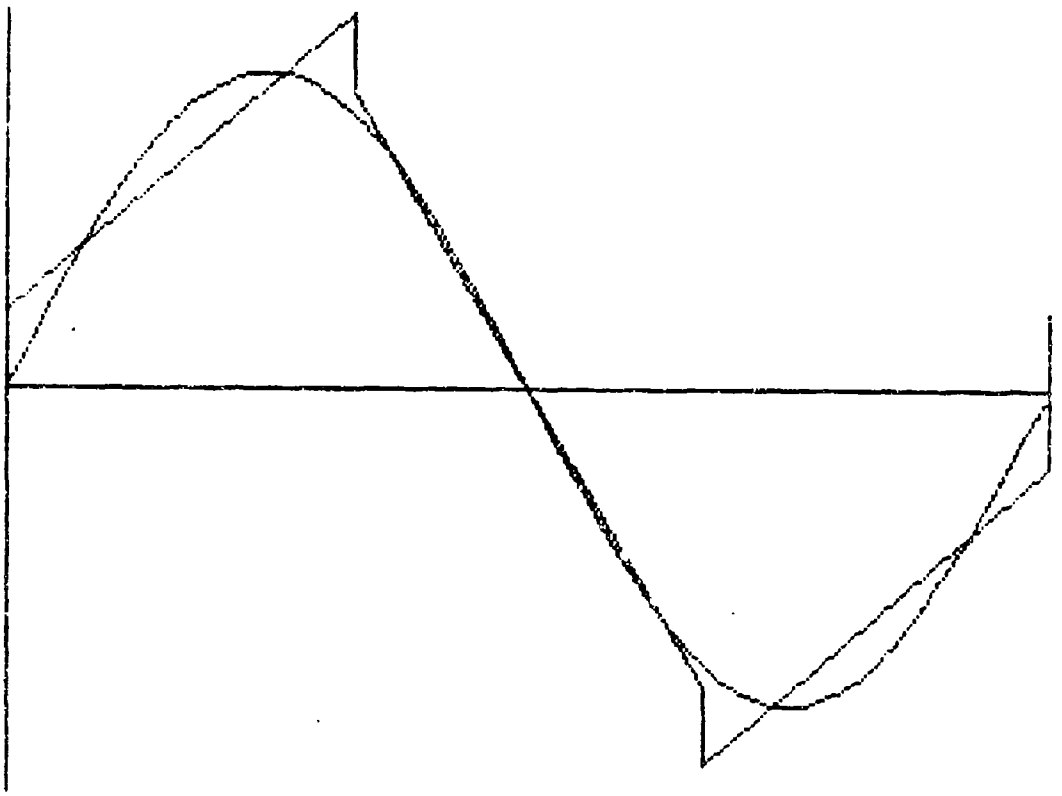

FIGURE 1b 1st and 2nd integrals satisfied, 3 steps/cycle

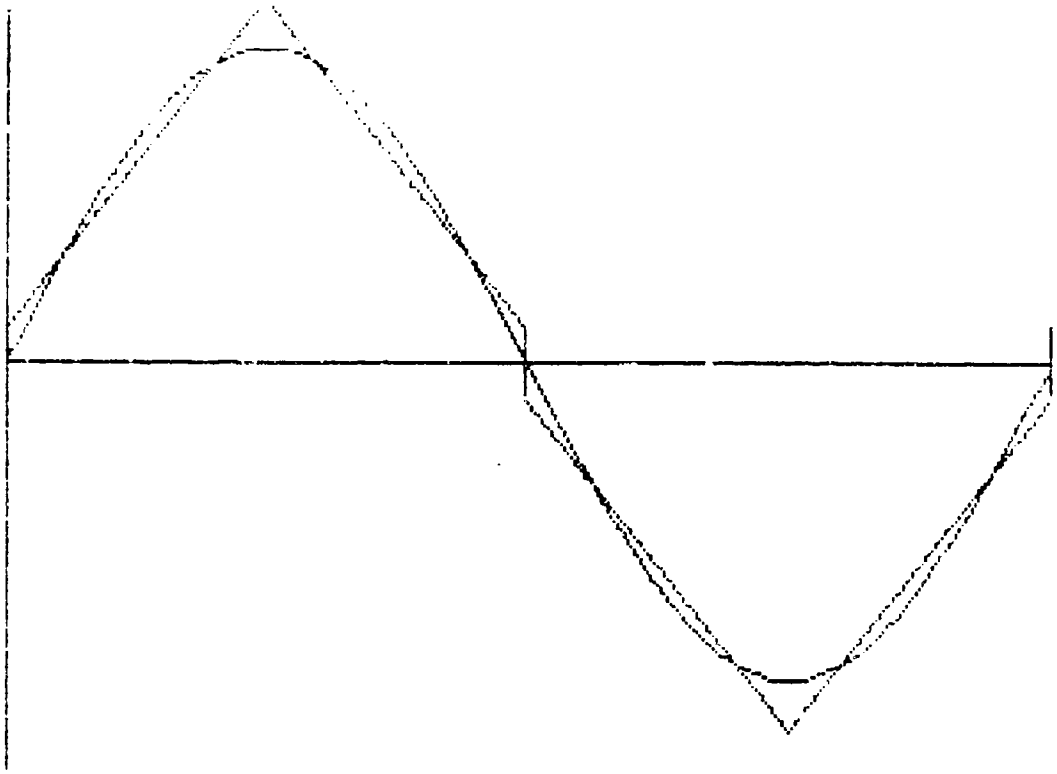

THOMASSON

FIGURE 1c 1st and 2nd integrals satisfied, 4 steps/cycle

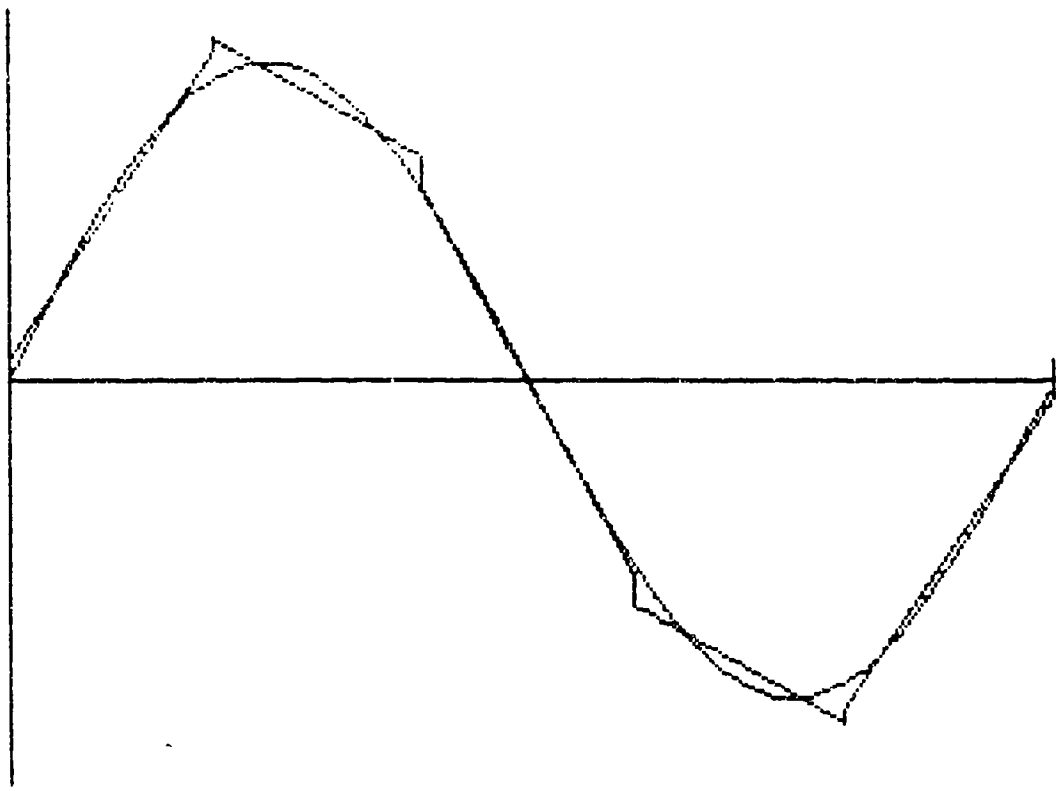

THOMASSON

FIGURE 1d 1st and 2nd integrals satisfied, 5 steps/cycle

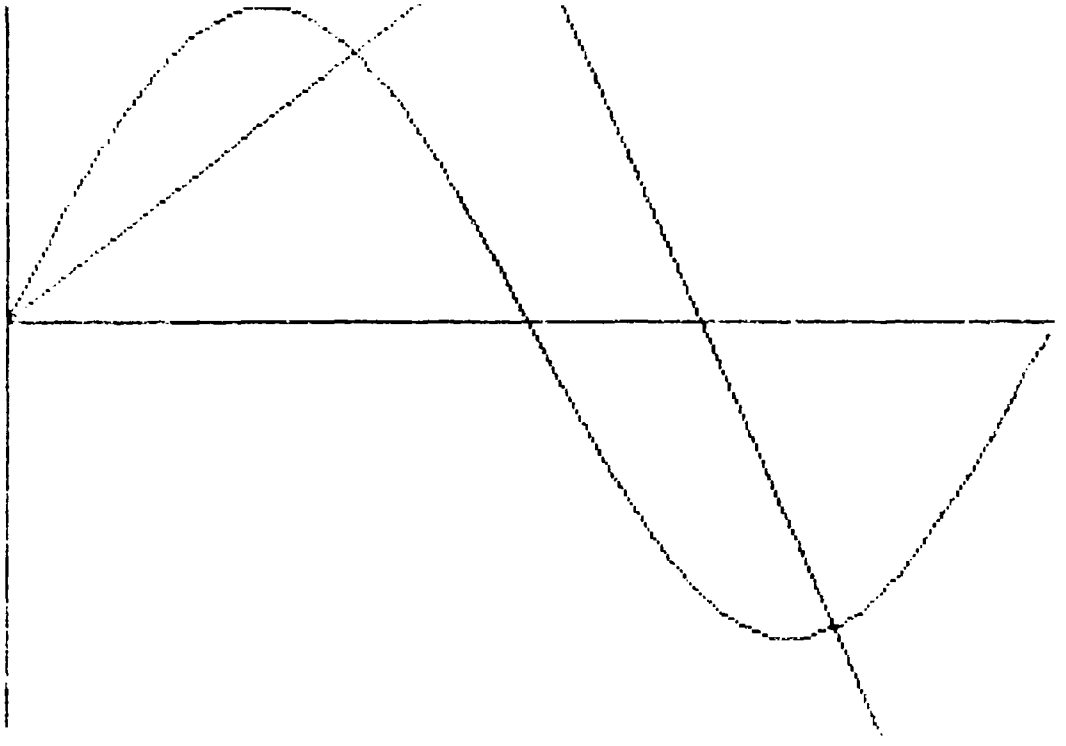

FIGURE 2a 1st integral only satisfied, 2 steps/cycle

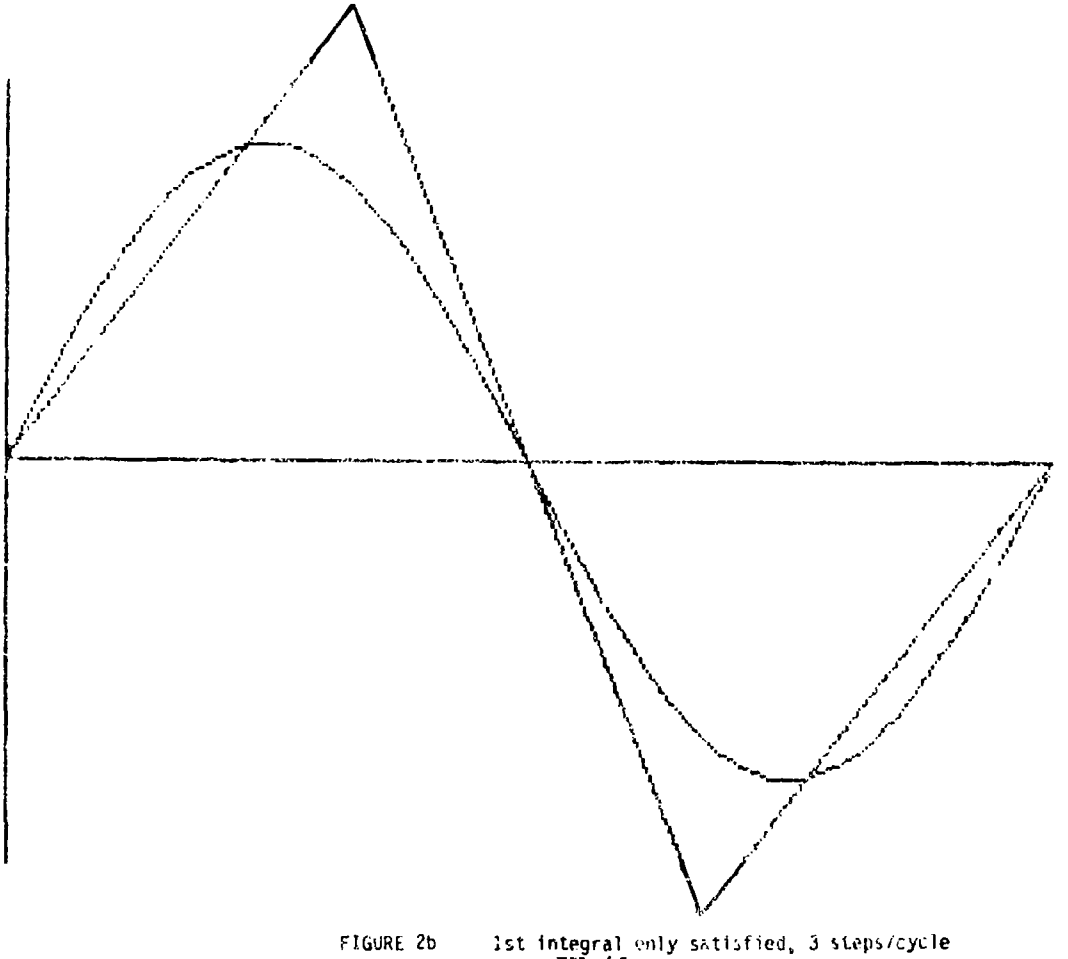

FIGURE 2b 1st integral only satisfied, 3 steps/cycle

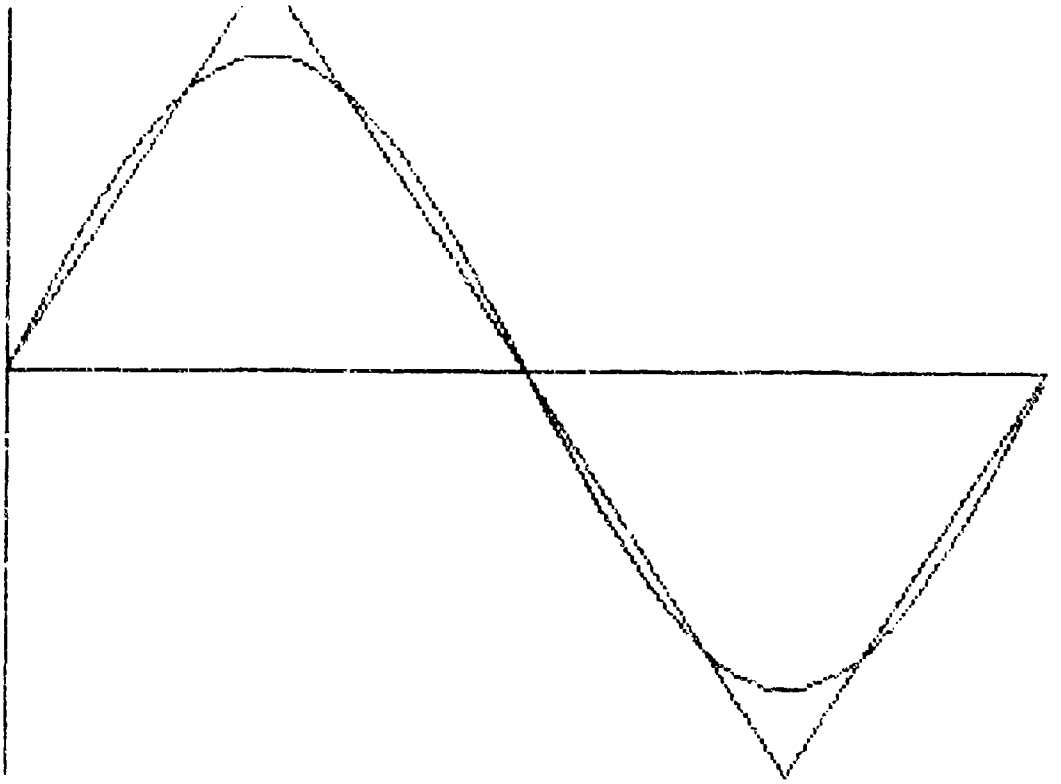

FIGURE 2c 1st integral only satisfied, 4 steps/cycle

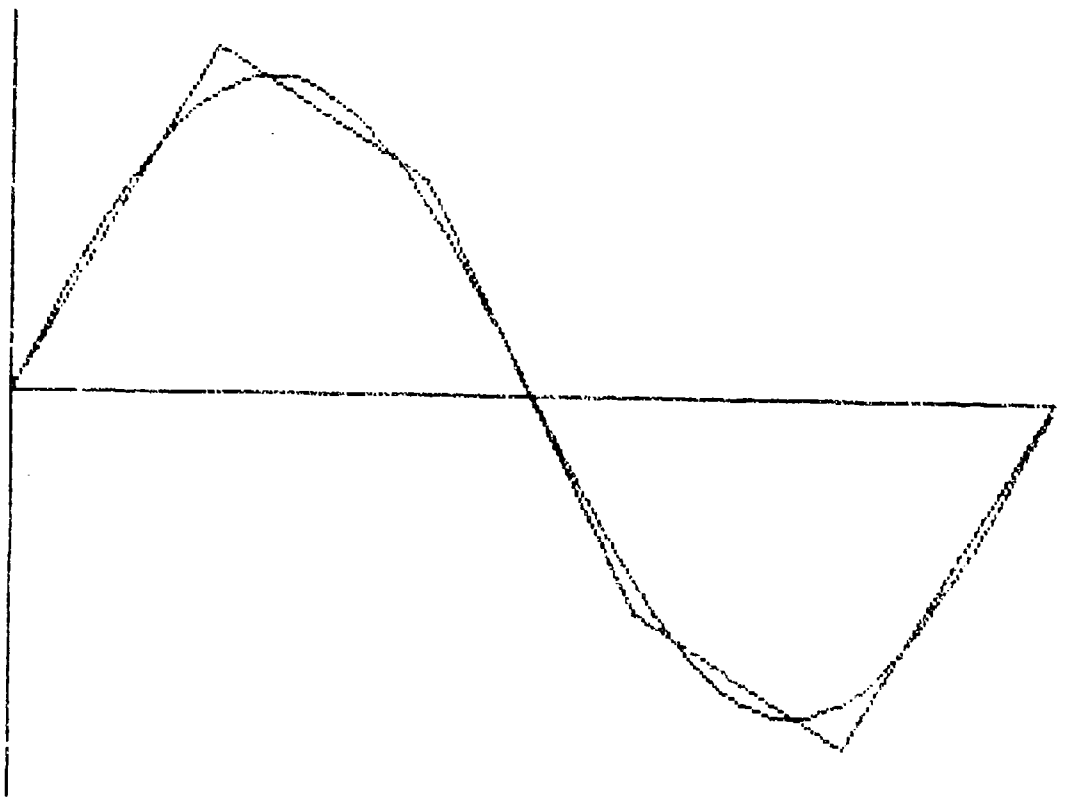

FIGURE 2d 1st integral only satisfied, 5 steps/cycle

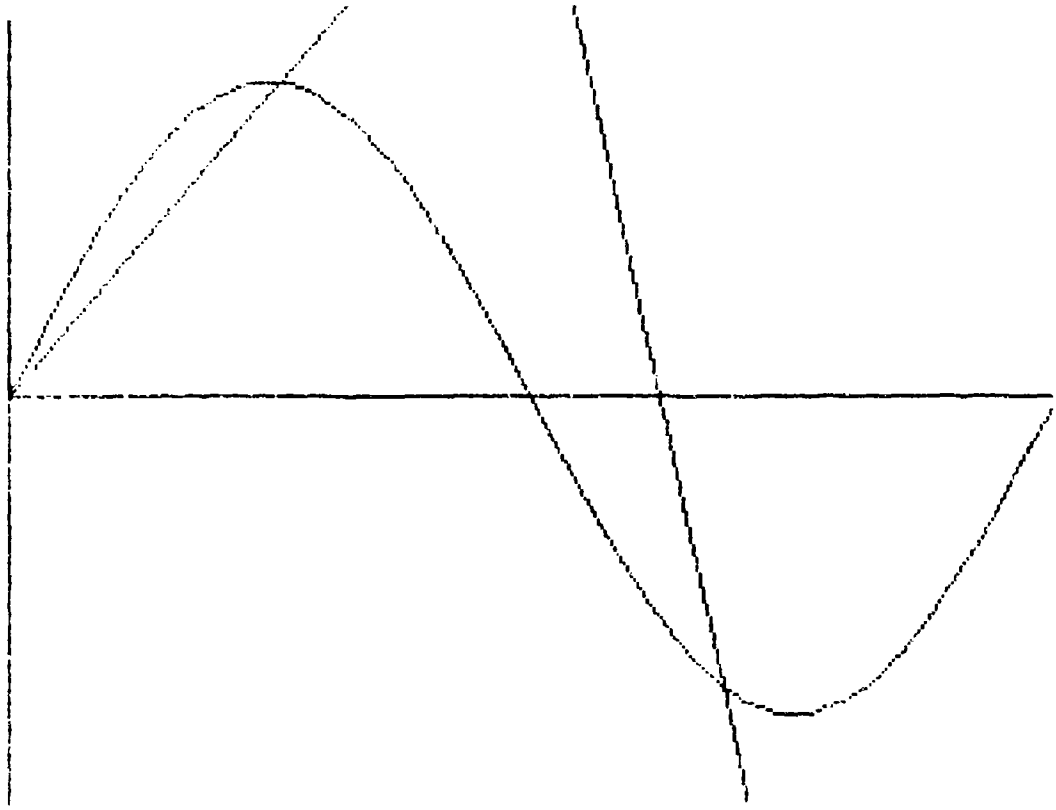

FIGURE 3a 2nd integral only satisfied, 2 steps/cycle

THOMASSON

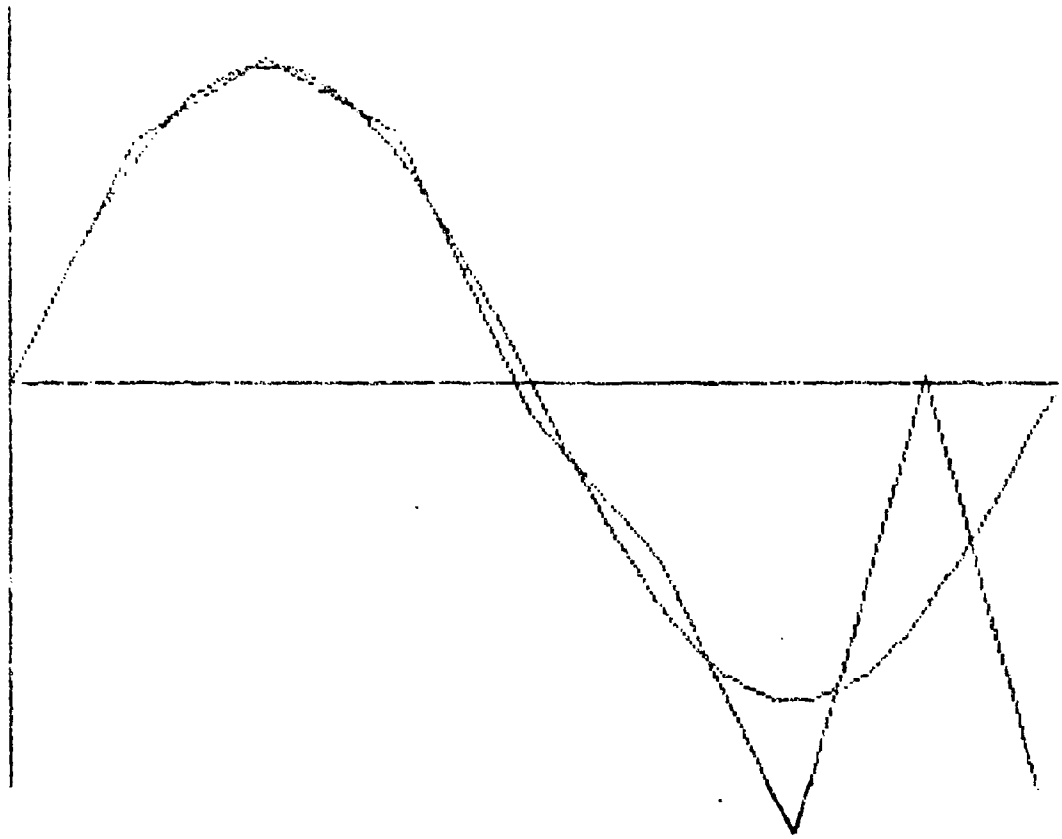

FIGURE 3b 2nd integral only satisfied, 8 steps/cycle

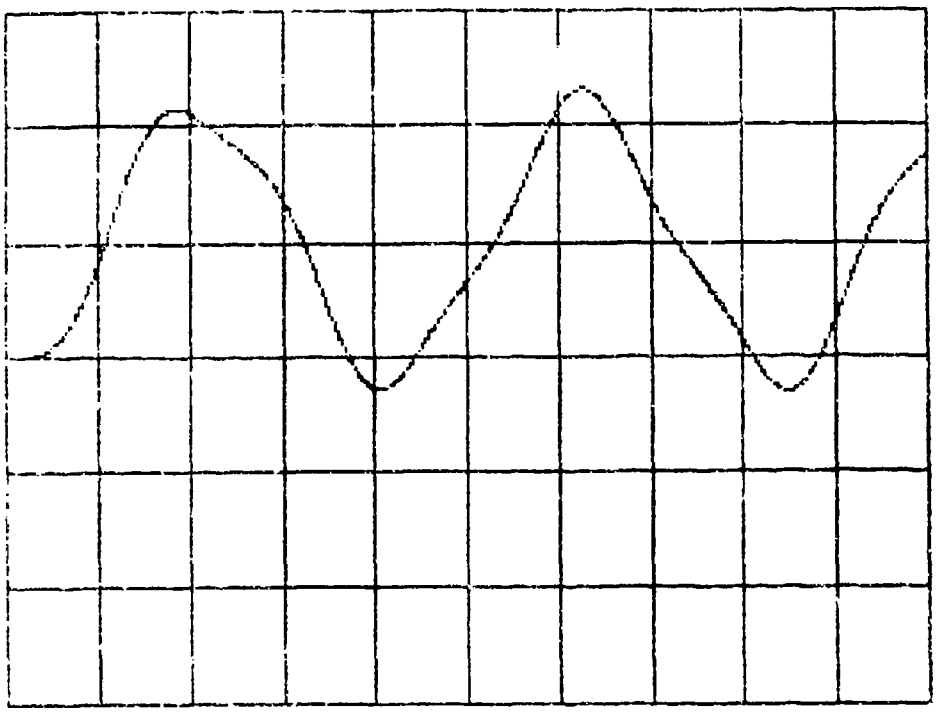

FIGURE 4a x_G/3E-3 vs t/0.01, δt = 10E-7, ΔT = 10E-6

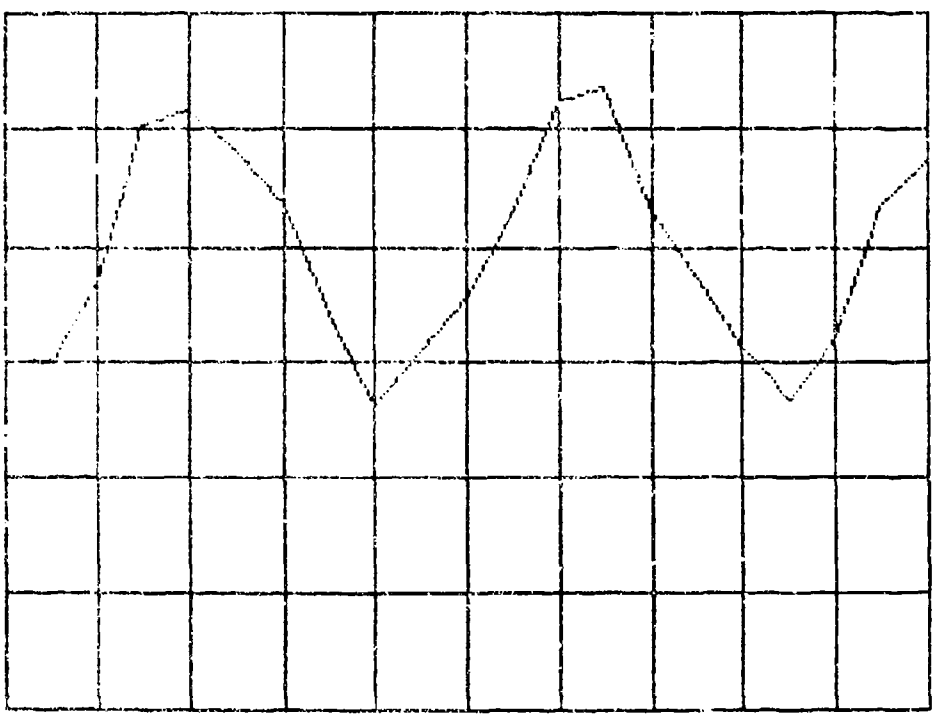

FIGURE 4b x_G/3E-3 vs t/0.01, δt _ 10E-7, Δt = 5E-4

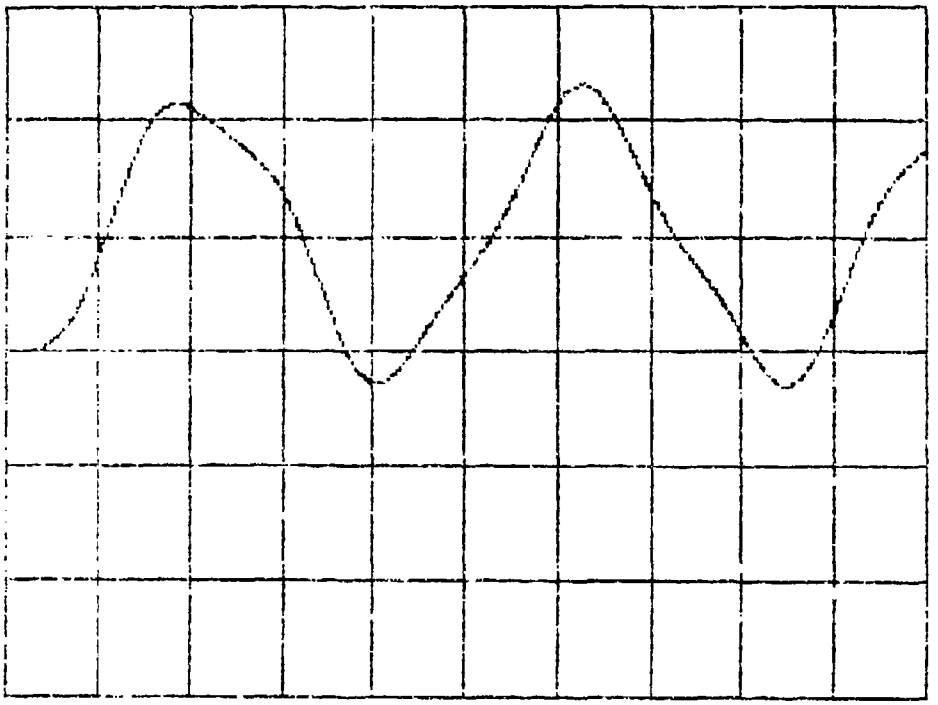

FIGURE 5a x_G/3E-3 vs t/0.01, δt = 10E-7, ΔT 0 10E-6

THOMASSON

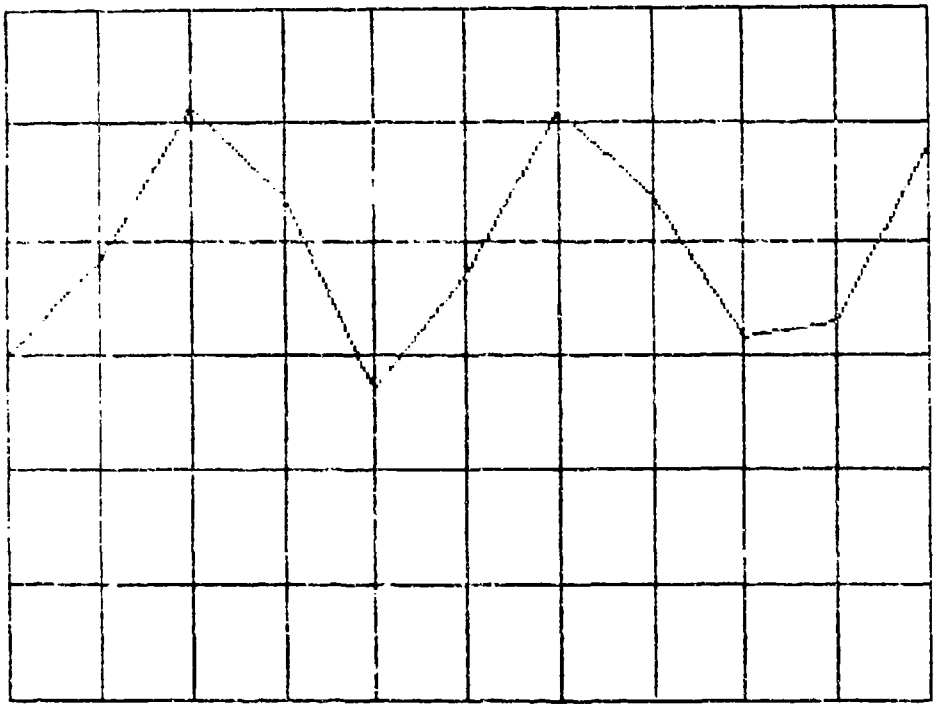

FIGURE 5b x_G/3E-e vs t/0.01, δt = 10E-7, ΔT = 10E-4

ABSTRACT

*SEYMOUR, VANCE

TITLE: Recent Advances in the SHOCK-AID Gun Modelling Capability**

ABSTRACT:

This paper addresses the use of the SHOCK-AID computer code together with a recently developed subroutine for modelling the effect of barrel curvature profiles on the dynamic response of the gun system. It is pointed out that attempting to incorporate such details at the Finite Element stage suffers from two serious defects: Firstly, a problem of numerical accuracy; secondly, continuous recreation of a basic model during parameter sweeps. The basic mathematical theory is presented followed by the computer realization. No analysis of error is presented in this paper.

***BIOGRAPHY:**

PRESENT ASSIGNMENT: Systems Engineer, Advanced Technology Group, Hunting Engineering Limited.

QUALIFICATION: BSc Applied Science, Royal Military College of Science, Wiltshire, England.

** This programme of work was supported in the United Kingdom by the Procurement Executive of the Ministry of Defence.

*SEYMOUR, VANCE

INTRODUCTION

1. Gun systems are generally analysed by treating the barrel as a large elastic structure with many degreees of freedom, whilst the remainder of the system is viewed as a set of driving mechanisms.

2. Generally these mechanisms are interactive with mutual loads depending on the current displacment and state of motion of the whole system. SHOCK-AID (Reference 1) is a suite of computer routines for simulating the response of gun systems under general firing conditions. It has been designed in a modular fashion to accomodate evolutionary enhancements and, in particular, contains the facility for a user to introduce new mechanisms via an Interactive Control Routine (ICR).

3. A number of mechanisms have been considered for ICR applications. For example:

   a. A Shot/Barrel ICR to simulate realistic loads on the barrel as the shot progresses toward the muzzle. This ICR has been outlined at previous symposia (Reference 2).

   b. A Barrel/Cradle ICR to simulate the contact/impact mechanism as the barrel recoils through the cradle bearings (Reference 3).

4. This report describes the development of an ICR for predicting the effect of barrel curvature on gun response. Barrel curvature arises in many ways: Gravity droop; differential cooling; manufacturing set; etc. A problem arises in simulating barrel curvature numerically (eg: using finite elements or differences), since the effect of curvature will be swamped by numerical approximations unless the model is prohibitively detailed. Furthermore, the performance of parameter sweeps involves the generation of a new model for each distinct curvature profile. The Barrel Curvature ICR described here provides for the imposition of small deviations in the barrel profile as an input file and interactively corrects for the resultant changes in mass distribution as the event evolves. In this respect it differs from other ICR's in proividing a correction for geometrical effects rather than adding further loading mechanisms.

THEORY

5. Until now gun barrels have been represented in SHOCK-AID by beam elements with forces being applied to an undisplaced configuration. There are two problem types that can be dealt with by the Barrel Curvature ICR:

   a. Any initial shape of the structure must be included in the model explicitly at the finite element modelling stage. For example, to model the differing curvatures on a set of barrels due to manufacturing set a corresponding set of models, one model for each curvature would have to be created.

b. Calculations performed in the main SHOCK-AID response routine are based upon the physical geometry of the undisplaced nodes. This may cause an approximation when the response of the beam is calculated because it does not account for the modified mass distribution.

ASSUMPTIONS

6. In order to overcome these difficulties the following assumptions are made in the formulation of the ICR:

a. The effect of small changes in mass distribution can be modelled by the imposition of appropriate correcting couples to the undisplaced configuration. The corrections concern inertial and external loads only.

b. For the purpose of calculating the correction the beam element may be treated as being rigid. Although this is not strictly necessary it is an extremely convenient simplification.

c. The correcting couple can be applied as a self-equilibrated pair of forces applied to the ends of a beam element. This, of course, relies on the assumption of rigidity.

d. The correcting couple is based upon the state of motion of the beam elements at the previous time step and any externally applied loads.

e. The mass matrix is assumed to be banded. Again this is not a necessary but a convenient simplification.

MATHEMATICAL FORMULATION

7. Figure 1 shows the displaced and undisplaced beams and their associated loading geometries.

8. Consider the vector from A to the point of action

$$\underset{\sim}{r} = -\alpha \underset{\sim}{F}_1 = l - \beta \underset{\sim}{F}_2$$

Then the length of the beam can be written as

$$\underset{\sim}{l} = \beta \underset{\sim}{F}_2 - \alpha \underset{\sim}{F}_1$$

or in matrix form

$$\begin{pmatrix} -\alpha \\ \beta \end{pmatrix} = [\underset{\sim}{F}_1 , \underset{\sim}{F}_2]^{-1} \underset{\sim}{l} \qquad 1$$

From the point of action to the beam is denoted by

$$\underset{\sim}{d} = \underset{\sim}{r} + \underset{\sim}{x} = \alpha \underset{\sim}{F}_1 + \underset{\sim}{x}$$

hence couple $c = \underset{\sim}{d} \Lambda \underset{\sim}{R} = \alpha (\underset{\sim}{F}_1 + \underset{\sim}{x}) \Lambda (\underset{\sim}{F}_1 + \underset{\sim}{F}_2)$

$$= \alpha (\underset{\sim}{F}_1 \Lambda \underset{\sim}{F}_2) + \underset{\sim}{x} \Lambda (\underset{\sim}{F}_1 + \underset{\sim}{F}_2) \qquad 2$$

9. Similarly when an element is rotated by as shown in Figure 1, so the couple acting is:

$$c_\theta = \alpha_\theta (\underset{\sim}{F}_1 \Lambda \underset{\sim}{F}_2) + \underset{\sim}{x}_\theta \Lambda (\underset{\sim}{F}_1 + \underset{\sim}{F}_2) \qquad 3$$

where $\begin{pmatrix} \alpha_\theta \\ \beta_\theta \end{pmatrix} = [\underset{\sim}{F}_1 , \underset{\sim}{F}_2]^{-1} \underset{\sim}{l}_\theta$

We know that

$$\underset{\sim}{x}_\theta = \begin{pmatrix} \cos\theta & \sin\theta \\ -\sin\theta & \cos\theta \end{pmatrix} \underset{\sim}{x}$$

Using equation 1 and expanding putting $\underset{\sim}{F}_1 = \frac{f_1}{f_2}$ and $\underset{\sim}{F}_2 = \frac{g_1}{g_2}$

i.e. $$\alpha = \frac{g_1 l_2 - g_2 l_1}{f_1 g_2 - f_2 g_1}$$

Similarly for the rotating beam it can be shown that

$$\alpha_\theta = \frac{-(g_1 l_1 + g_2 l_2) \sin\theta + (g_1 l_2 - g_2 l_1)\cos\theta}{f_1 g_2 - f_2 g_1}$$

10. It follows that by subtracting the couple calculated for the undisplaced beam from that for displaced beam we can evaluate the couple discrepancy

$$\delta_c = c_\theta - c$$

Combining equations 2 and 3 the expression for the couple discrepancy becomes

$$\delta_c = (\alpha_\theta - \alpha) (\underset{\sim}{F}_1 \Lambda \underset{\sim}{F}_2) + (\underset{\sim}{x}_\theta - \underset{\sim}{x}) \Lambda (\underset{\sim}{F}_1 + \underset{\sim}{F}_2) \qquad 4$$

IMPLEMENTATION

11. The implementation of the ICR is illustrated in Figure 2. The routine is called from the main SHOCK-AID loading module. The global model data is passed on initial entry to the ICR. The routine then loops through

all the elements along the barrel successively extracting local mass and geometry data, calculating the required correction couple and applying the appropriate statically equivalent self-equilibrated force pairs.

12. The following is a list of requirements regarding tasks to be performed by the Barrel Curvature ICR.

a. The ICR should allow initial displacements for one series of connected nodes.

b. Displacements and accelerations should be used to calculate couples, Equation 4.

c. The response routine (in SHOCK-AID) force vector should be modified according to the couple calculated for the beam between pairs of nodes.

d. Absolute position data must be produced for output using plotting routines.

e. Geometric, connectivity, acceleration, displacement and mass data must all be available.

13. The last requirement, e, implies certain modifications to the SHOCK-AID data structure. A new data structure has therefore been developed to provide facilities for all forseeable applications.

CONCLUSION

14. The Barrel Cuvature ICR provides a simple and effective solution to the problems associated with parameter sweeping on model geometry, and also corrects for the approximations concerning mass redistribution inherent in linear finite element techniques. It constitutes an example of the way in which, with the enhanced data structure, SHOCK-AID can cope with complex geometries and and boundary conditions in a realistic manner.

REFERENCES

1. Taylor B.A, Thomasson P.G., A Consistent R and D Technique for the Modelling of Gun System Dynamics, Proc. 3rd US Army Symposium on Gun Dynamics, 1982.

2. A Model for In Bore Projectile Dynamics including Barrel Interaction Effects, P.G. Thomasson. Presented at the KTA6 Workshop meeting of the TTCP Panel W2 at BRL, USA October 1983.

3. AIHG/155/99, The Use of Springs to Model the Effect of Cradle Bearing Forces in the Chieftain Finite Element model, E.G. Nicoll, March 1984.

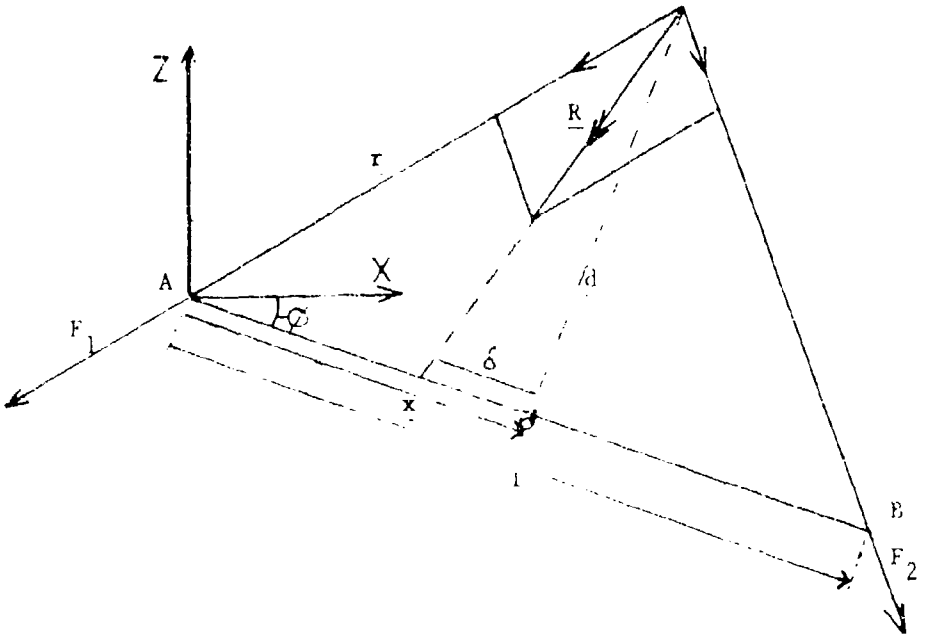

Rotating through θ

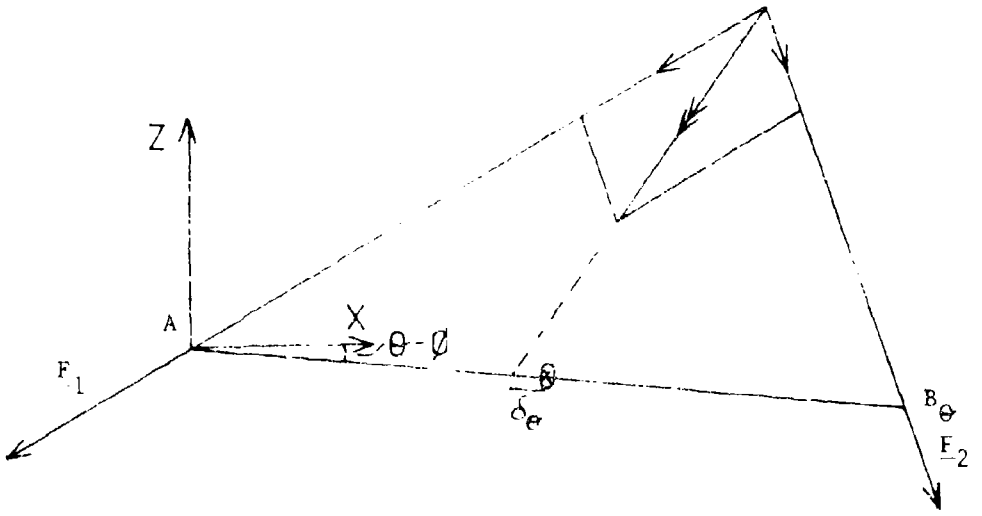

Figure 1. Force System Acting on an Element in both the Undisplaced and the Displaced Configuration.

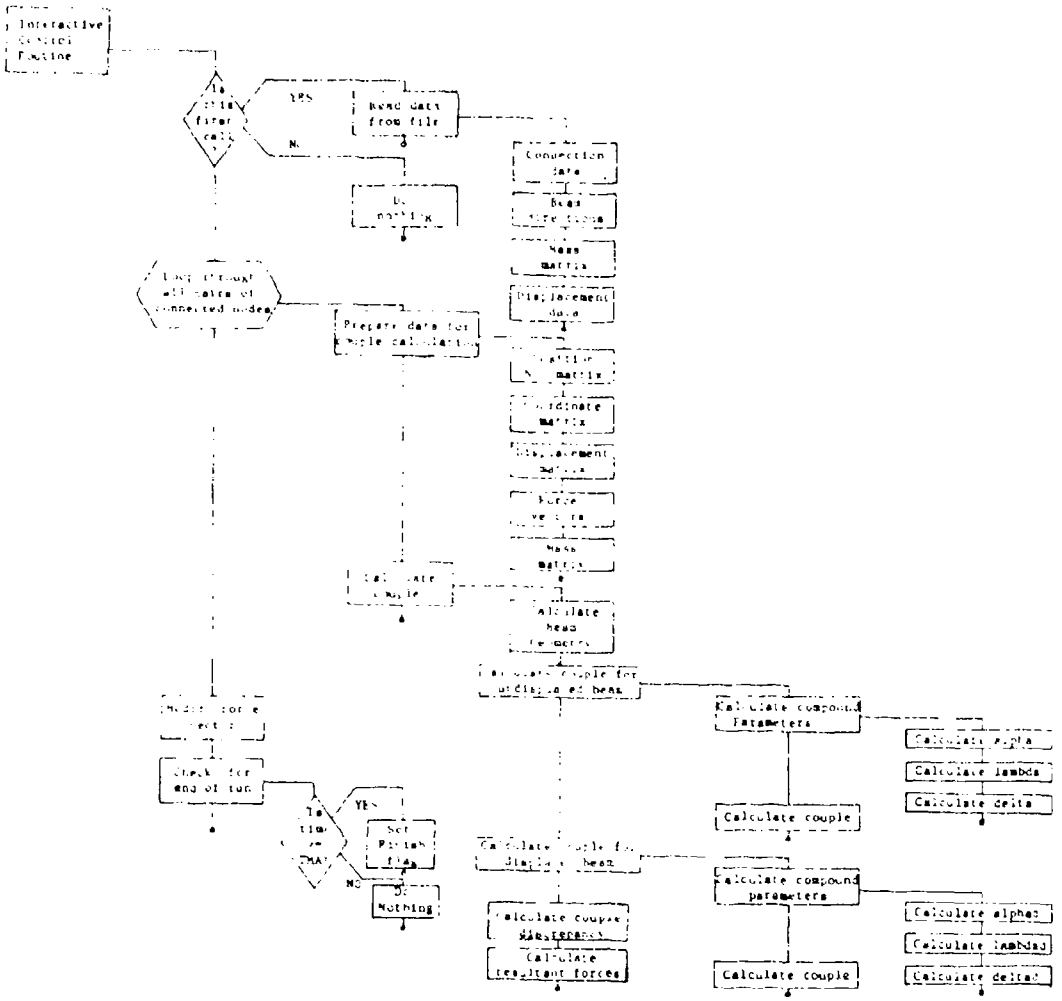

Figure 2. Structure Diagram for the Barrel Curvature Interactive Control Routine.

AUTHOR'S LAST NAME: BULMAN

TITLE: THE EFFECT OF BEARING CLEARANCE AND BARREL EXPANSION ON BARREL RESPONSE

ABSTRACT:

A number of mathematical models have been developed to study the motion of a gun barrel during the firing phase. Most of these models have considered fixed or elastic bearings with no clearance and also assumed that the initial forcing term comes from the recoil of the gun. It can be shown that bearing clearance, plus an input from the expansion of the barrel, has an important effect on the barrel response.

BIOGRAPHY:

PRESENT ASSIGNMENT: Reader in Dynamics of Physical Systems
Head of Land Systems
Royal Military College of Science, Shrivenham

PAST EXPERIENCE:

DEGREES HELD: BSc(1st) PhD MI Mech E CEng

Introduction

The prediction of barrel behaviour during the firing phase has in the past been approached in two distinct ways. The first, that of finite element analysis to determine mode shapes and frequencies, followed by the use of these to give the transient response(1,2). The second, the solution of the basic Euler-Bernoulli, or Timoshenko, beam equations by a finite difference or other technique (3,4). In both of these methods difficulties arise when non-linearities are introduced particularly nonlinear bearing stiffnesses, clearances, or damping.

In order to overcome these difficulties a dedicated package has been produced which treats the barrel as a multi-degree of freedom spring mass system. The resultant set of second order differential equations are then integrated directly. This technique enables non-linearities to be introduced easily and previous investigations have included the effect of bearing elasticity, bearing clearance, bearing and barrel damping (5) and more recently shot barrel interaction effects by Powell (6).

This paper describes the principles of the programme written for the SIMulation of BArrel Dynamics, SIMBAD, and in particular the inclusion and investigation of the effect which barrel expansion has upon the barrel response. The barrel is assumed to expand within the bearings until the clearance is taken up. This can be introduced to the barrel model as either a forced displacement at a bearing, or more realistically, a generalised force derived from the bearing stiffness.

Barrel Simulation

In the simulation package the barrel is divided into a number of Euler-bernoulli beam elements with three degrees of freedom at each

end. These relate to the transverse displacement, the longitudinal displacement, and the angular displacement. This provides a typical single plane analysis which is considered adequate for symmetrical barrels and shot barrel interaction effects of non-spinning projectiles.

Following entry of the barrel external and internal profiles, the barrel is automatically divided into a number of elements as specified by the user. This also takes account of bearing position. The resultant equations are assembled into a stiffness matrix in the same way as a finite element stiffness matrix would be composed. The fina basic equation is of the form:

$$[F] = [K]\ [\delta]$$

where [K] is the stiffness matrix

[δ] represents all of the degrees of freedom and

[F] represents the external forces at each node which can include inertia forces, damping forces, bearing forces, etc.

The present system allows a maximum of 25 elements (78 degrees of freedom) but experience has shown that a solution generally converges at between 20 and 25 elements.

If the inertia effects are included the equations become

$$[Ft] = [M]\ [\ddot{\delta}] + [K]\ [\delta]$$

Where [M] is the mass matrix of the system which in the package is calculated automatically together with the stiffness matrix. Additional masses such as breech mass and moment of inertia is added to the mass matrix and the resultant set of simultaneous differential equations solved by a second order Runge-Kutta technique. During this process it is relatively simple to suppress a displacement, or impose a prescribed displacement.

The applied external force vector [F] allows bearing elasticity and bearing clearance to be simulated with ease. Bearing clearance and non-linear bearing elasticity is accomplished by the use of a simply entered data file representing the force applied to the barrel as a function of barrel displacement.

The standard programme contains the following:

a. The effect of offset breech.

b. The effect of offset muzzle reference sight.

c. Simple selection of bearing position.

d. Angular and linear damping.

e. Bearing dampers.

f. Pin jointed bearings.

g. Non linear or linearis elastic bearings with and without clearance.

h. Simplified representation of barrel droop.

The generalised forcing term is a data file representing the pressure time curve which produces the recoil acceleration of the barrel. Other routines which have been incorporated for special case studies include the effect of buffer imbalance, shot barrel interaction, and the subject of this paper.

The package automatically produces a results file and allows plotting of muzzle transverse displacement, transverse velocity, angular displacement, angular velocity, jump, and the barrel shapes at 20 time intervals.The shape of the barrel can also be displayed in 'slow motion'.

The programme was written on a Hewlett Packard HP16 desk top computer, but has also been implemented on the HP9000 series.

Barrel Expansion Effects

Previous bearing representations have generally either assumed a pin joint, a linearly elastic bearing or an elastic bearing with a set clearance. The latter of these is probably the more realistic, but it still does not take account of the fact that during firing this clearance is changing as the barrel expands. Also, the expansion itself will tend to make the centre line of the barrel move relative to the bearing. This latter case on its own, can be represented simply as a prescribed displacement at a bearing node, such that the displacement of the node equals the barrel expansion. This represents an unrealistic, idealistic case of expansion on a solid bearing. However, when it is realised that the change in radius for free expansion of a typical 120 mm gun is of the order of 0.33 mm, it is of interest to examine the case as a base line.

The complete case is more complex because conditions change as the clearance is taken up or the barrel loses contact with either side of the bearing. Effectively the model of the barrel represents the motion of the centre line of the bore. The expansion, or increase in barrel radius at the bearings, can then be added or subtracted to give the effect which the expansion has upon the bearings. If the barrel is initially sitting on the bottom of the bearing then four separate conditions need to be considered. The initial starting position is shown in Diagram 1, and from this point the displacement of the barrel centre line at the bearing is Xc. The displacement of the lowest surface is therefore Xc - Ex, and of the top surface Xc + Ex.

The four separate conditions are now:

1. When $Xc - Ex > 0$ and $Xc + Ex < Cl$, the barrel will not be in contact with the bearing, and the bearing force, $Bf = 0$.

2. When $Xc - Ex < 0$ and $Xc + Ex < Cl$, the lower surface of the barrel will be pushing into the bearing, and the upper surface will be free. The resultant force acting on the barrel will be:

$$Bf = -(Xc - Ex).Kb$$

3. When $Xc - Ex \leq 0$ and $Xc + Ex \geq Cl$, both the upper and lower surface will be in contact with the bearings. The force on the barrel will have two components such that:

$$Bf = -(Xc - Ex).Kb - (Xc + Ex - Cl).Kb$$

or

$$Bf = -(2Xc - Cl).Kb$$

It will be noted that once the clearance has been taken up, the force component due to any more expansion disappears.

4. When $Xc - Ex > 0$ and $Xc + Ex \geq Cl$, the lower surface has risen off the bearing, but the clearance has been taken up on the other surface. Therefore,

$$Bf = -(Xc + Ex - Cl).Kb$$

The above equations within the limits indicated, give the force to be applied to the barrel at the bearing node if the barrel initially rests on the bottom of the bearing. A similar set of equations can be written when the barrel initially rests at the top of the bearing.

The barrel expansion is actually a dynamic situation, but unpublished studies by P King at RMCS suggest that for all practical purposes the expansion can be considered directly proportional to the internal pressure. For this study, a simple finite element model was

used to obtain an expansion coefficient, Ce, and the expansion given by:

$$Ex = Ce.\text{Instantaneous pressure}$$

The value used for the bearing stiffness was derived from earlier work carried out by King used in studies of a 120 mm barrel.

Computer Simulation

The simultion of the barrel expansion was applied to a typical 120 mm gun, similar to the Chieftain barrel. The pressure time curve was also typical of an APDS round in such a gun. Keeping the same bearing positions, the following cases were considered:

1. No expansion with pin jointed bearings.
2. No expansion with elastic bearings.
3. No expansion with elastic bearings and clearance of 0.25 mm.
4. As 3 above but with very large clearance of .0 mm so that impact with the other side of the bearing does not occur before shot exit.
5. Barrel expansion on solid bearings.
6. As 3 above but including barrel expansion.
7. As 6 above but with clearance of 0.15 mm.
8. As 6 above but with a clearance of 0.5 mm.
9. As 4 above but including barrel expansion.
10. A case with no transverse bearing restraint,(Free-Free).

The simulations all included the recoil acceleration and the resultant moments produced by the offset breech and muzzle reference sight.

Discussion of Results

Figures 1 and 2 demonstrate the effect of various bearing idealisations without barrel expansion included. Figure 1 shows the

vertical displacement of the muzzle for pin jointed bearings, elastic bearings, and elastic bearings with clearance. Figure 2 shows the displacement with typical clearance, very large clearance and no bearing restraint at all.

The large clearance case and Free-Free case produce very similar results. This is because the centre of gravity of the barrel is ahead of the front bearing, and therefore it normally sits on the bottom of the front bearing, and against the top of the rear bearing. When the breech moment is applied, the tendency is to lift away from each bearing and therefore have no restraint. However, there is an initial compression of the front bearing for a very short period which produces the slight difference between the two cases.

Figure 3 is shown for completeness and displays the probably unrealistic case of expansion on solid bearings compared with elastic bearings and 10 mm clearance.

Figure 4 shows the different responses for expansion with elastic bearings and various amounts of clearance. What is particularly interesting is the flattening of the responses around shot exit as the clearance is reduced. This has been observed in actual firings when measurement of muzzle movement was being taken. It occurred during a series of firings in relatively rapid succession. It could therefore have been caused by the barrel expanding as its temperature increased and hence the clearance reduced. Direct comparisons between expansion and no expansion are shown in Figures 5 and 6 for 0.25 mm clearance and 10 mm clearance. It can be seen that the expansion reduced the peak response of the barrel in both cases.

Confidence in the results is obtained when the barrel deflected

shapes are considered. These are shown in Figures 7,8, 9 and 10, and indicate the barrel shapes taken up at 0.5 ms intervals. The case of bearing clearance with no expansion, Figure 7, shows that at the front bearing the barrel moves across the clearance and, after compressing into the other side of the bearing, is deflected back across the clearance. When expansion is included, Figure 8, the barrel still moves across the clearance, but because the barrel has expanded and the clearance therefore reduced, the centre of line of the barrel does not get deflected back so easily.

The effect of the rear bearing is more obvious. The motion of the barrel downwards is assisted by the expansion of the barrel against the top of the rear bearing. The downwards motion of the breech is therefore increased by nearly 1.4 mm.

The case of a simple elastic bearing with no clearance is shown in Figure 9. The motion at each bearing has obviously been suppressed, as has the overall motion of the complete barrel. Figure 10 shows the Free-Free case for comparison.

Finally Figure 11 shows the jump characteristics for a simulation with and without expansion. The figure of jump is calculated as the muzzle angle plus the muzzle transverse velocity divided by the shot exit velocity. This is shown for the complete time period although the main area of interest is at shot exit. It enables an appreciation to be made of the possible change in jump if the shot exit point was not correct. It can be seen that for the simulation with barrel expansion, the exit time is not so critical. However, 0.5 ms difference for the no expansion case would produce a very different jump figure.

Conclusions

The effect of barrel expansion within the bearings and its effect on transverse response can be simulated relatively easily. It can be defined as additional forcing terms to the barrel, dependent upon the displacement of the barrel within the bearing.

Results show that inclusion of the barrel expansion produces a significant change in the barrel response and should therefore be considered in studies of gun jump characteristics.

References

1. TAYLOR B.

The use of Finite Element Based Model to Predict the Motion of the US 105 mm M68 Barrel.

TTCP WPT-2 (KTA6) BRL Aberdeen Maryland, October 1983.

2. SOIFER M. and BECKER R.

Development, Validation and Implementation of a Finite Element (Lumped Parameter) Model of the 75 mm ADMAG Gun System

TTCP WTP-2 (KTA6), BRL Aberdeen Maryland, October 1983.

3. FACAY C. THOMAS M.D. and KING W.P C.

A Model for Tank Gun Movement During Firing using an Implicit Difference Numerical Algorithm.

3rd US Army Symposium on Gun Dynamics, May 1982.

4. KING W.P.C. and THOMAS M.D.

A Gun Dynamics Model using Finite Difference Techniques

TTCP WPT-2 (KTA-6), RARDE Fort Halstead, September 1984.

5. BULMAN D.N.

Theoretical and Experimental Observations on the Effect of Bearing Spacing, Pressure Time Curve, Bearing and Barrel Damping on Barrel Motion.

TTCP WPT-2 (KTA-6) RARDE Fort Halstead, September 1984.

6. POWELL S.E.

A Simple Theoretical Model of Shot/Barrel Interaction Within a Smooth Bore Gun.

Fourth US Army Symposium on Gun Dynamics, May 1985.

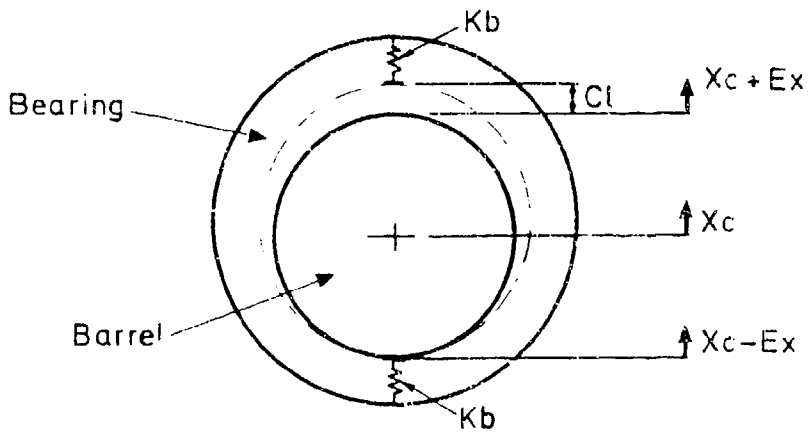

Xc ; Vertical displacement of barrel centre line

Ex ; Radial expansion of the barrel

Cl ; Initial clearance

Kb ; Bearing stiffness

Diag.1 REPRESENTATION OF BARREL EXPANSION WITHIN THE BEARING

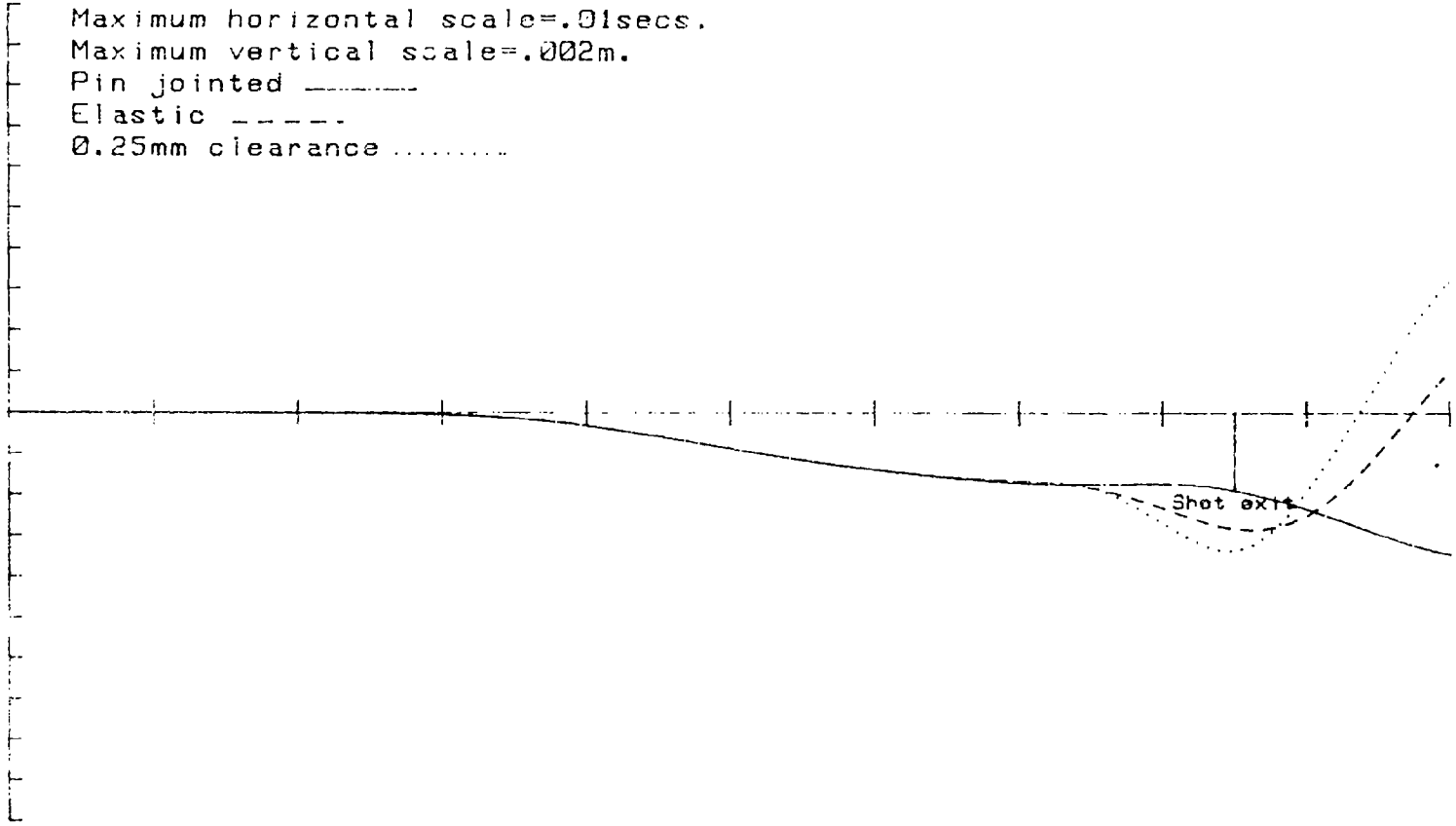

Fig 1 Pin jointed, elastic, or elastic with clearance
Vertical displacement of muzzle
No Expansion

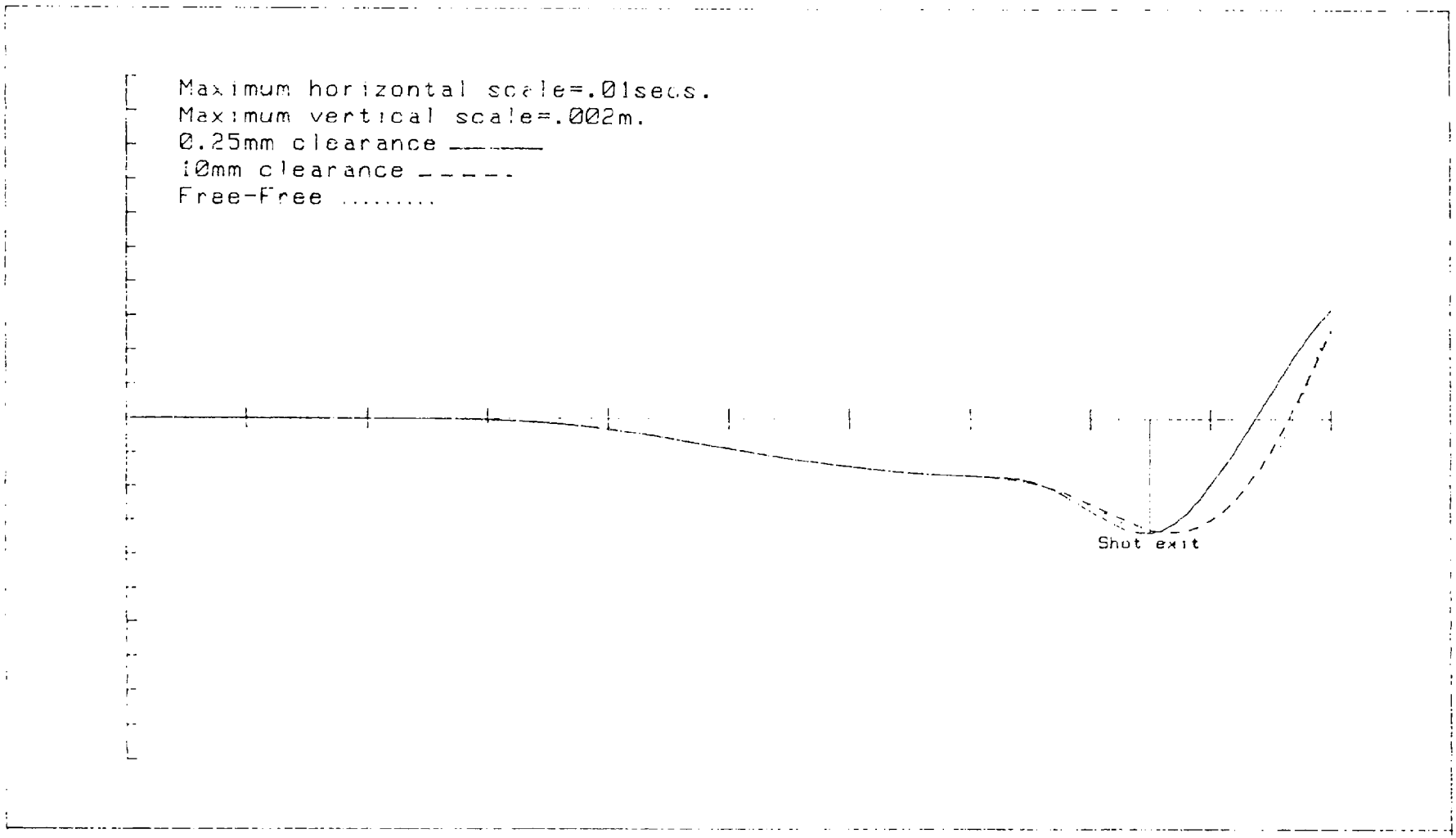

Fig 2 Elastic bearings with clearance and Free-Free
Vertical displacement of muzzle
No Expansion

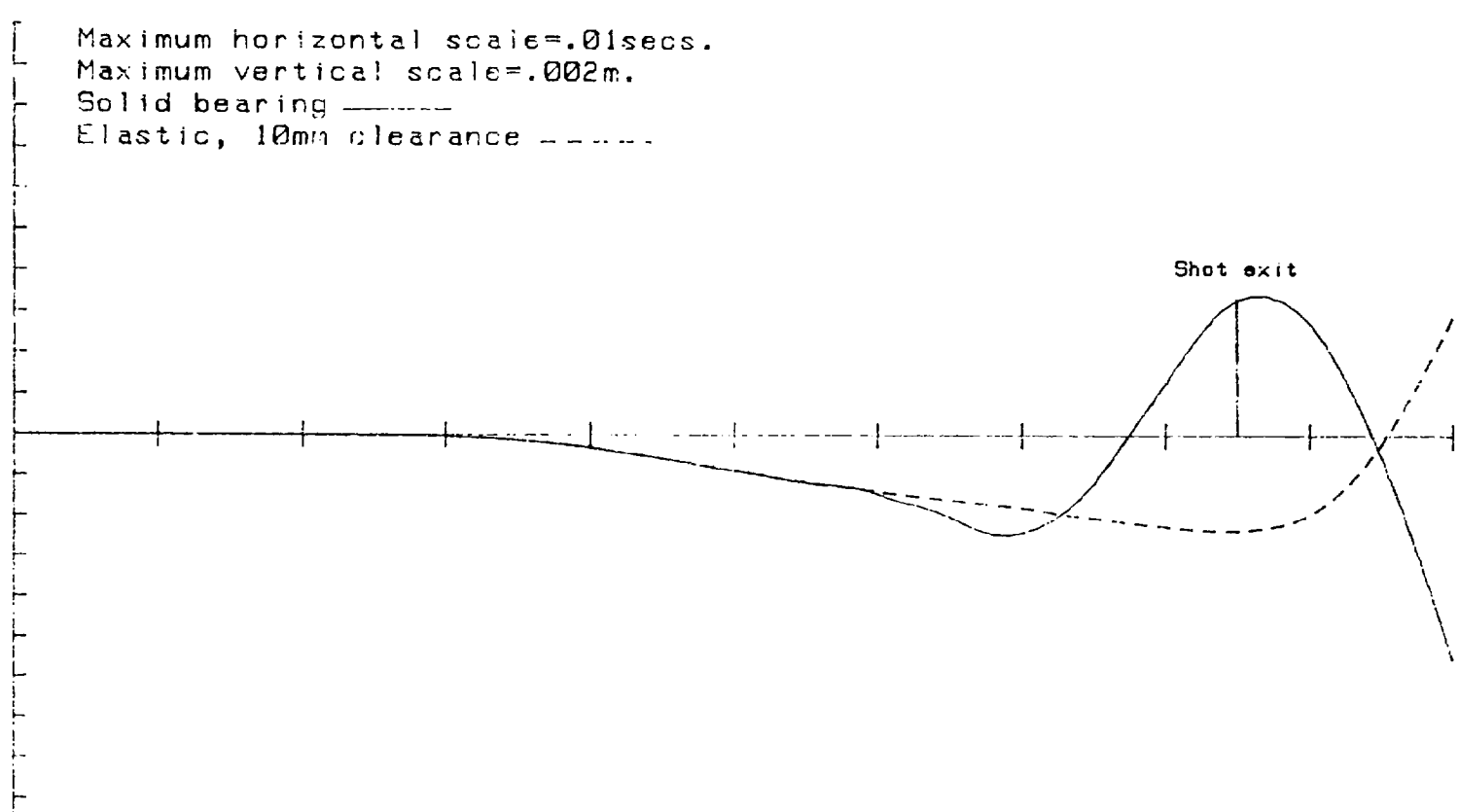

Fig 3 Expansion on solid bearing and elastic bearing
Vertical displacement of muzzle

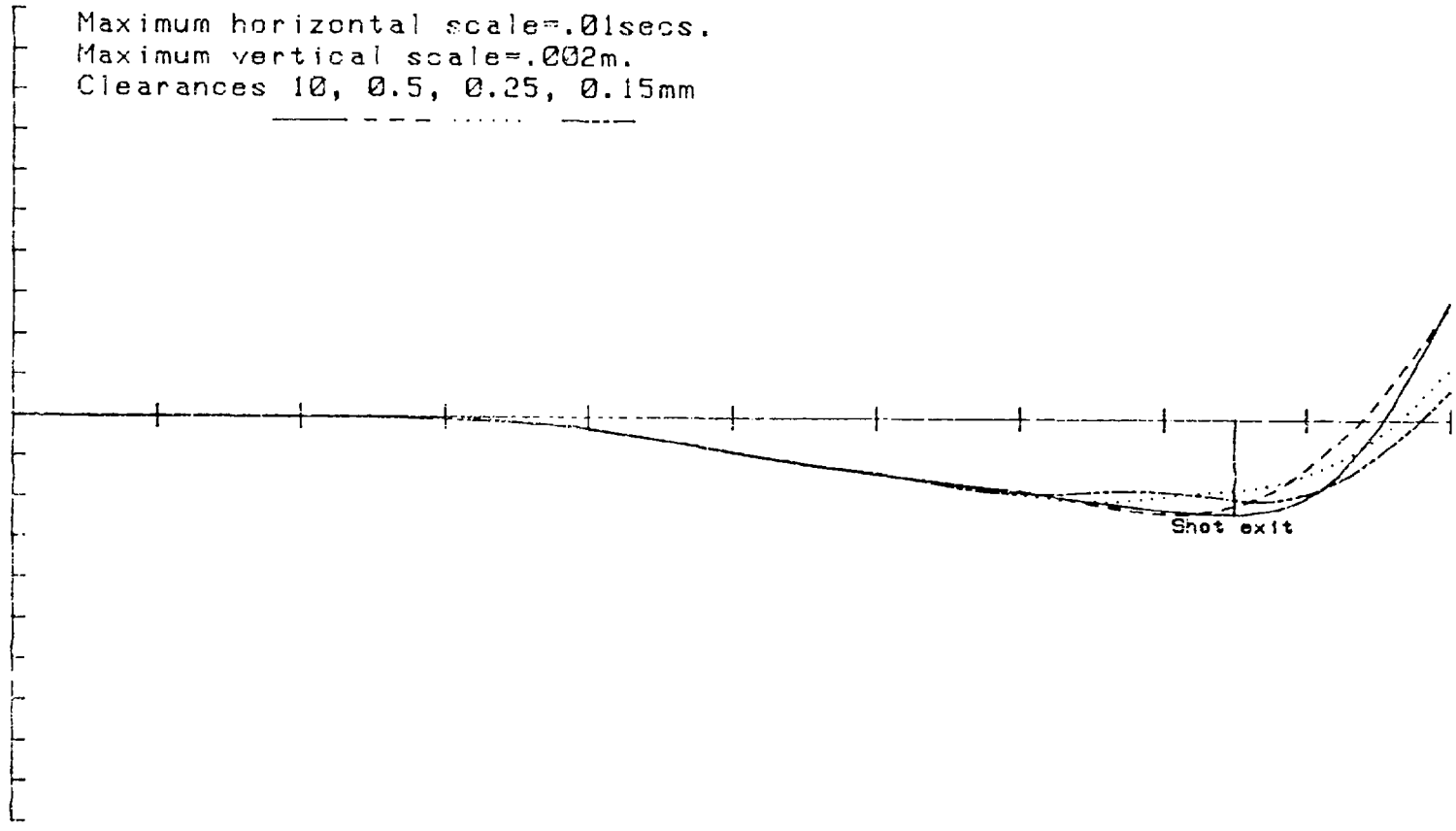

Fig 4 Expansion with various bearing clearances
Vertical displacement of muzzle

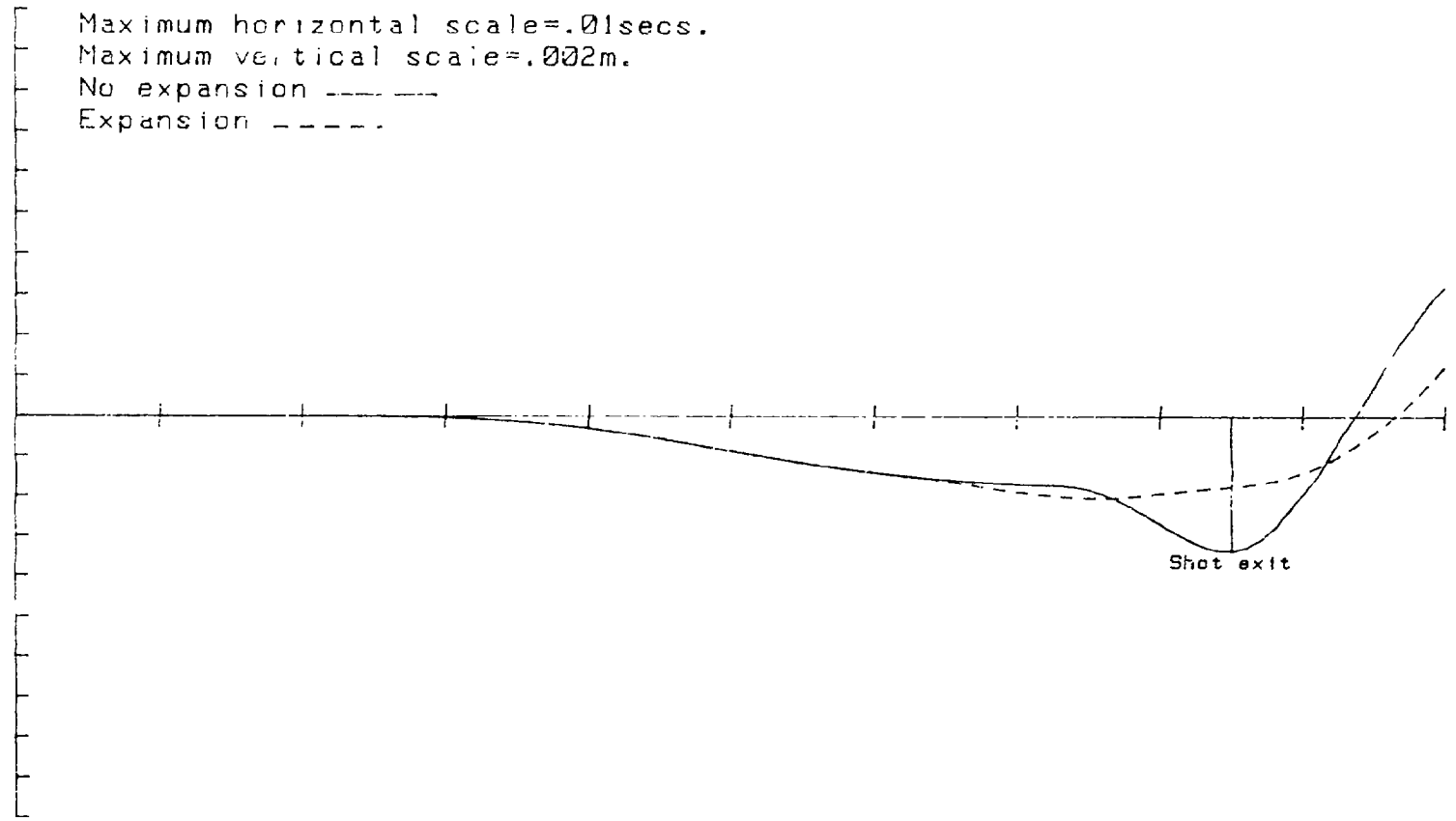

Fig 5 No expansion and expansion, 0.25mm clearance
Vertical displacement of muzzle

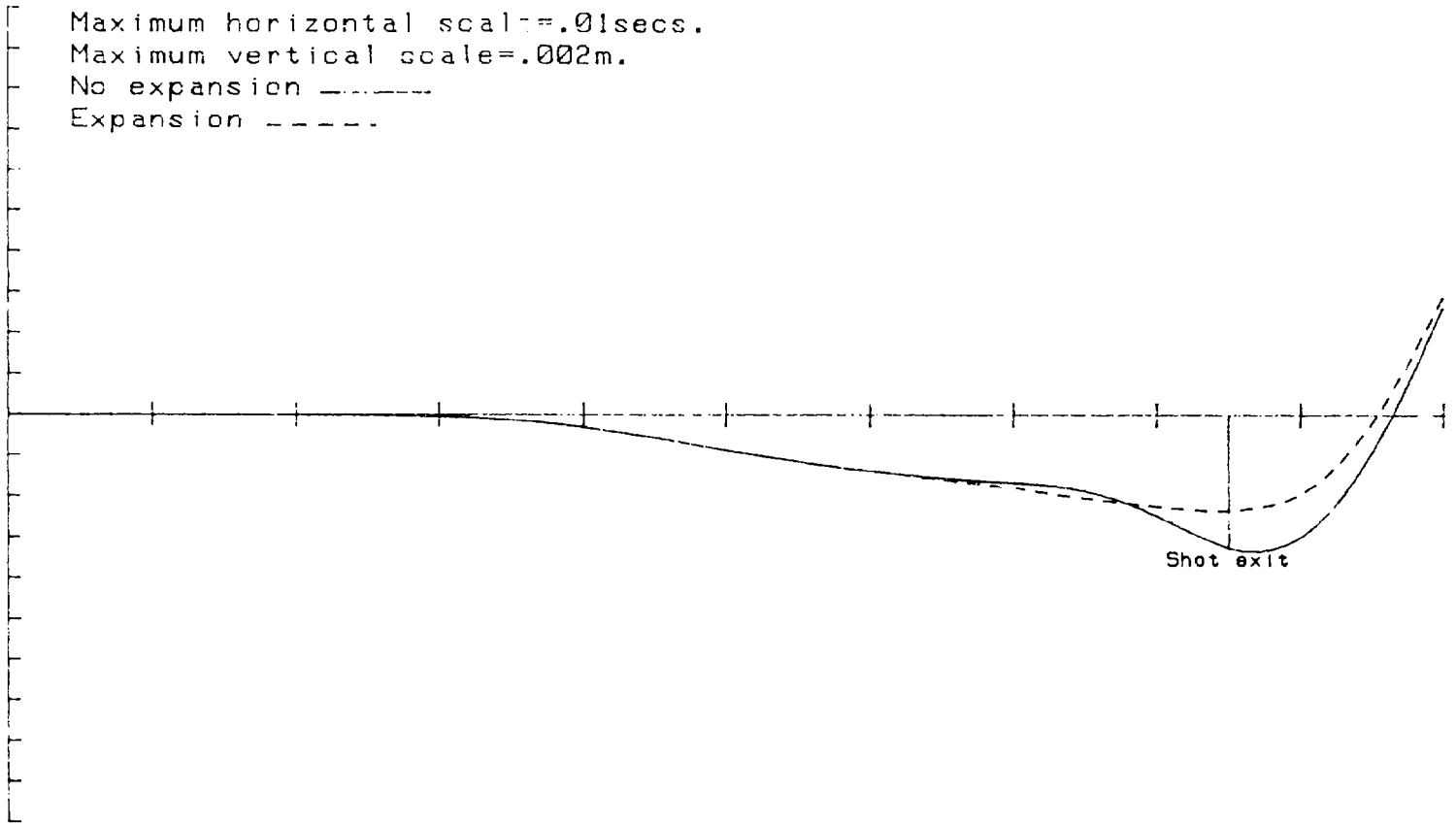

Fig 6 No expansion and expansion, 10mm clearance
Vertical displacement of muzzle

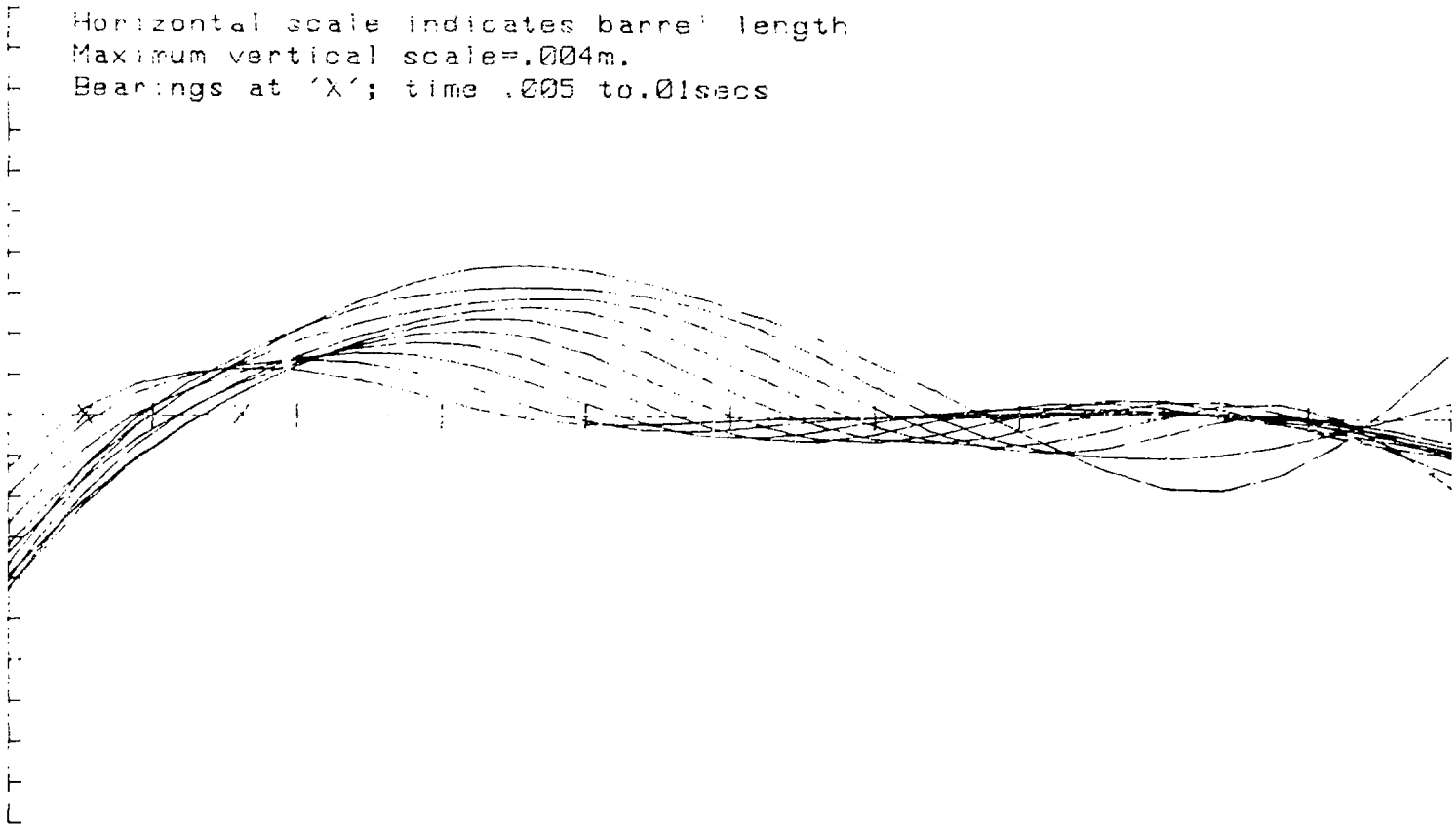

Fig 7 Bearings with 0.25mm clearance and no expansion
Barrel deflected shape

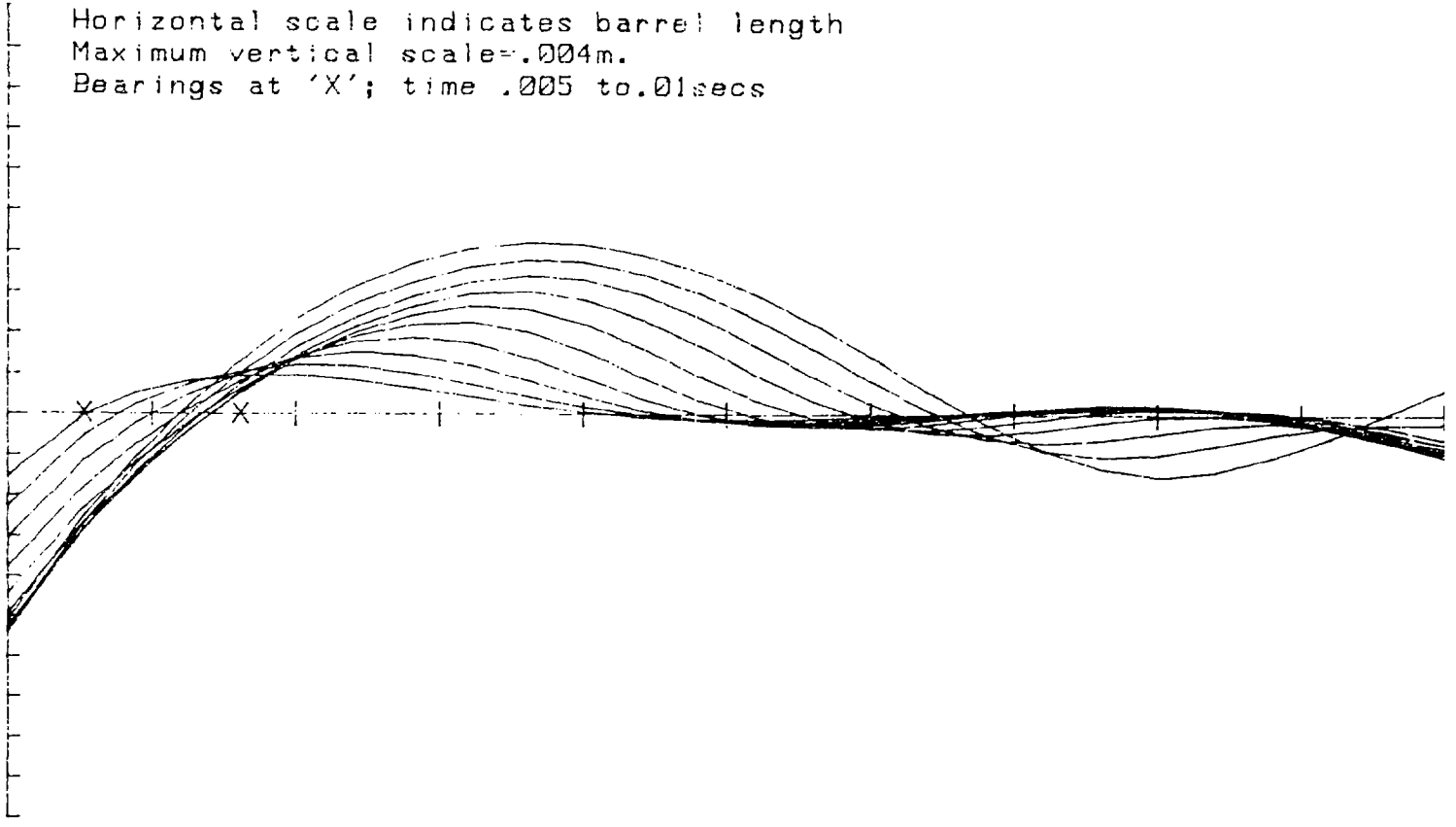

Fig 8 Bearings with 0.25mm clearance and plus expansion
Barrel deflected shape

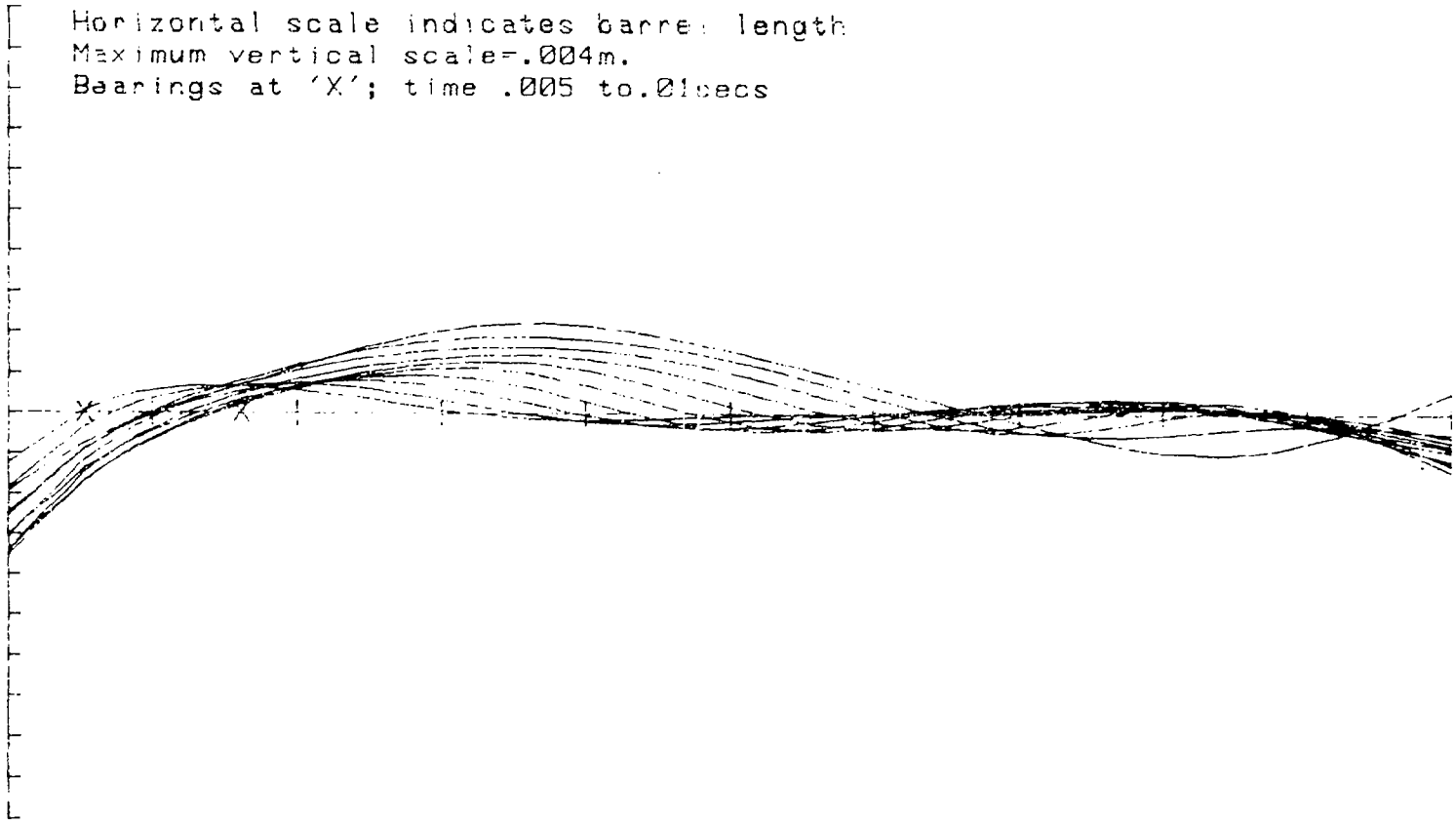

Fig 9 Simple elastic bearing simulation
Barrel deflected shape

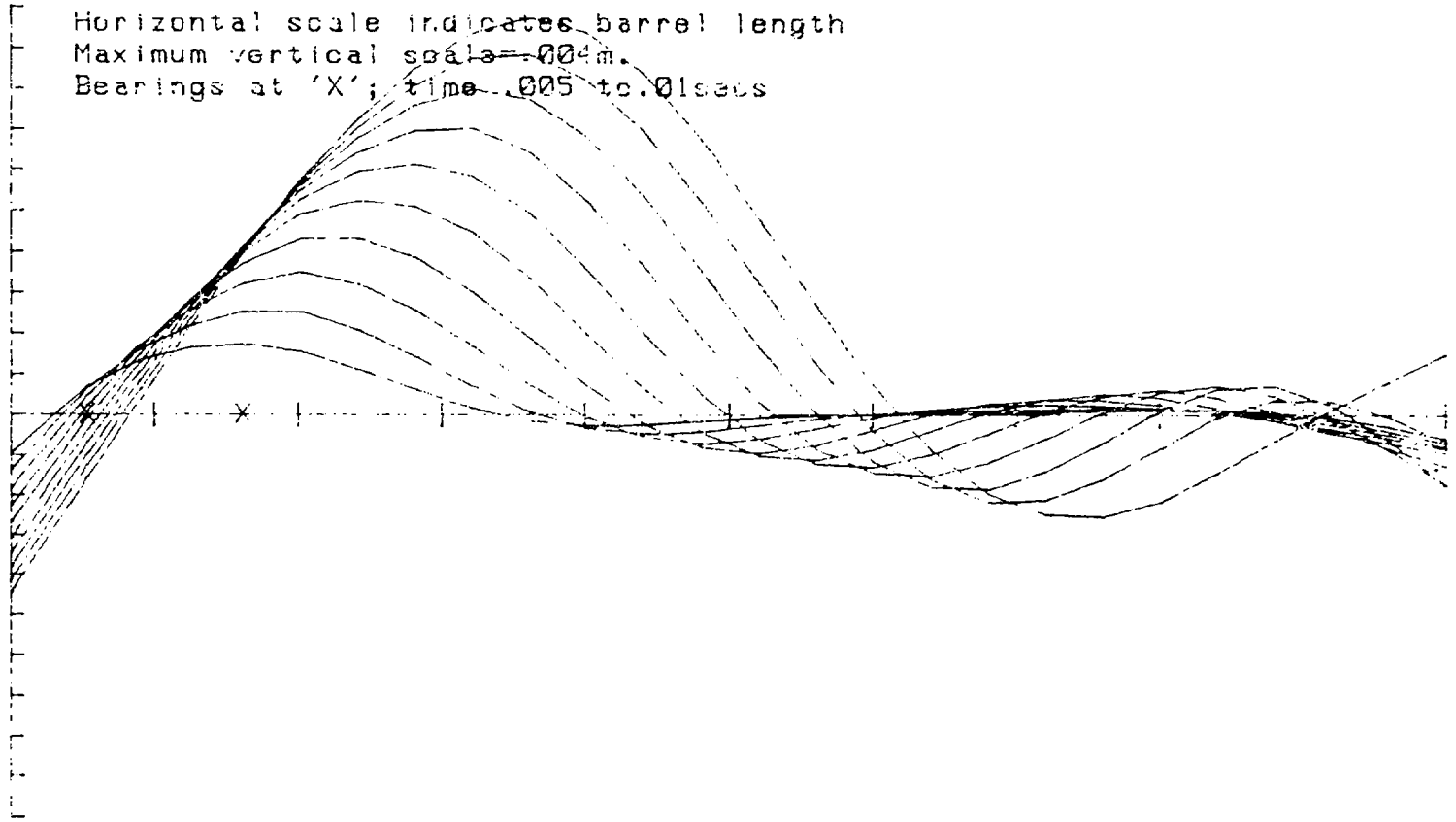

Fig 10 Free-Free Barrel Simulation
Barrel deflected shape

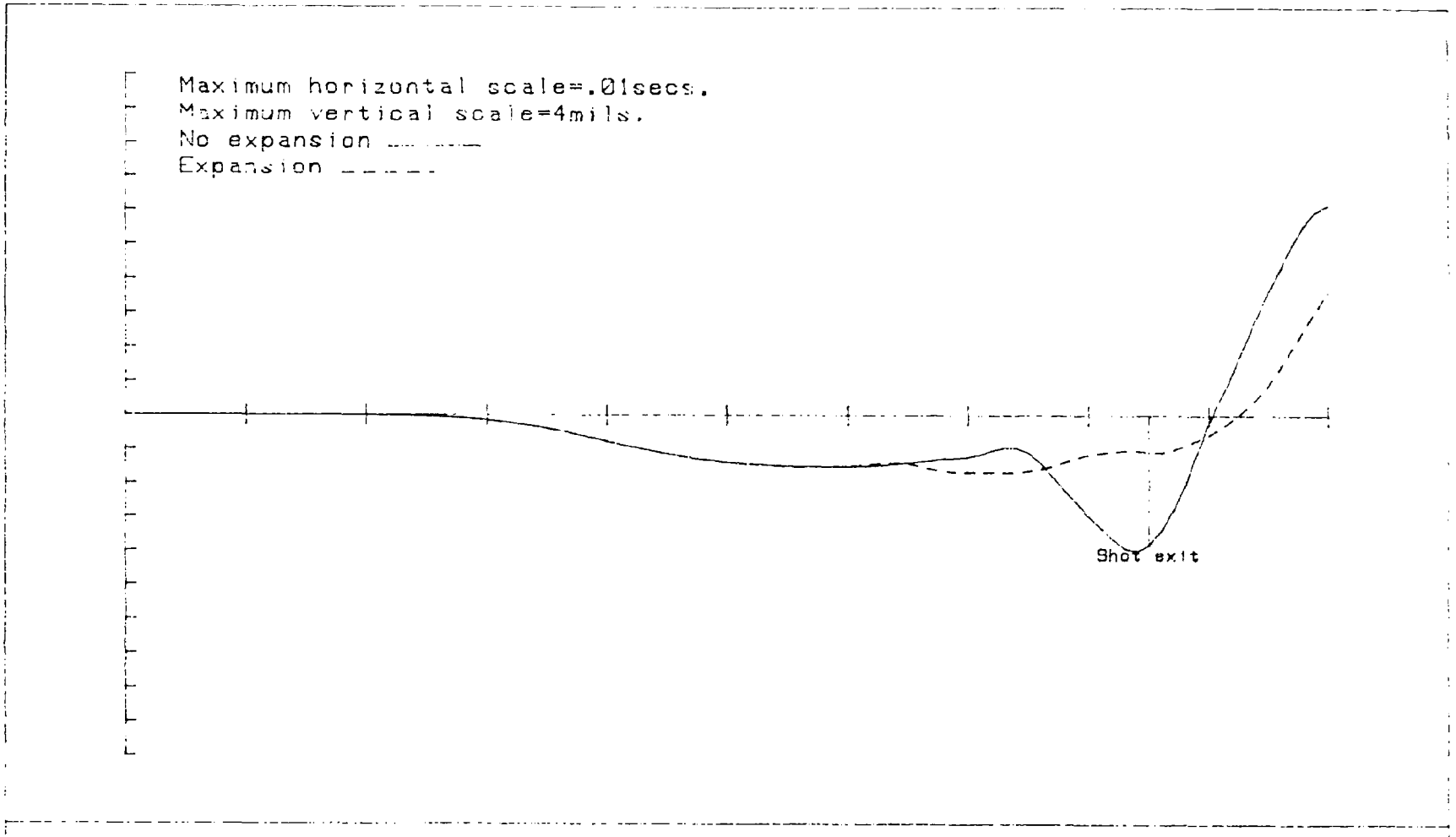

Fig 11 With and without expansion, 0.25mm clearance
Predicted gun jump

POWELL

A SIMPLE THEORETICAL MODEL OF SHOT/BARREL INTERACTION WITHIN A SMOOTH BORE GUN

ABSTRACT:

A model of a smooth bore barrel in one plane is developed. This involves the use of stiffness equations of single beam elements, similar to those used in finite element modelling. The equations of motion describing the pitch and bounce modes of the shot are stated and the two sets of equations are linked to predict the effects on the shot of shot-barrel interaction.

Data from a compressed air powered gun is used to validate the model.

BIOGRAPHY:
PRESENT ASSIGNMENT:

RESEARCH SCIENTIST ROYAL MILITARY COLLEGE OF SCIENCE

PAST EXPERIENCE:

PAST RESEARCH INCLUDES WORK ON GUN DYNAMICS AND AIRCRAFT SURVIVABILITY

DEGREES HELD:

B.A.

1. INTRODUCTION.

When considering modern tank guns one of the factors contributing to round to round dispersion is the yawing motion of the shot. Indeed Andrews(1) suggests that this motion is of major importance and Walker(2) makes the point that shot balloting (rattling in the bore) can cause severe shell engraving and wearing of the gun barrel. To understand the cause of yaw for an aerodynamically stable shot, it is necessary to study barrel movements, projectile in-bore motion and the interaction of the barrel and the projectile.

A considerable amount of experimental and theoretical work has taken place in the field of barrel motion. Mathematical modelling techniques using computers are now being used. These can be divided into those using finite difference equations, for instance Pagan(3), and King and Thomas(4) and those using the finite element method,such as Taylor,Thomason and Vance(5) in Great Britain and Soifer and Becker(6) in the United States.

A few theoretical barrel-projectile models have been produced. Notably by Soo Hoo and Anderson(7) who used equations of motion for the projectile dynamics obtained using Lagrange's method, coupled to a finite difference barrel model, and Chu(8) who used Euler's approach to obtain equations of motion for the shot. The potentially more powerful finite element barrel models produced in Great Britain and the United States are being modified to include the effects of shot/barrel interaction.

Another approach, suggested by Bulman(9) is to produce the stiffness equations similar to the finite element technique, include the inertia forces, and then solve the resulting set of simultaneous second order differential equations using one of the standard algorithms available.

In this paper Bulman's approach is used to produce a model of a smooth bore barrel in one plane. The equations of motion describing the pitch and bounce modes of a shot in one plane are stated and the two sets of equations are linked to predict the effects on the shot of shot-barrel interaction.

A compressed air powered apparatus which simulates many of the characteristics of a recoiling tank gun has been developed at RMCS(10). Data from this gun is used to test the theoretical results.

DERIVATION OF THE MATHEMATICAL MODELS

Barrel modelling

A two dimensional mathematical model of a barrel with constant bore and outer diameter was produced by considering a series of Euler-Bernoulli beam elements joined at the nodes. At this stage longitudinal vibrations were not included. This gives two degrees of freedom at each node. These are linear motion perpendicular to the barrel axis and angular motion about the horizontal axis. Using the sign convention shown below for the displacements,

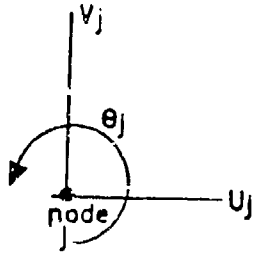

Fig 1. Displacement of node j

and letting the applied external forces on the barrel element at nodes j and j+1 be shear forces F_j and F_{j+1} and moments M_j and M_{j+1}, with the

... of figure 2,

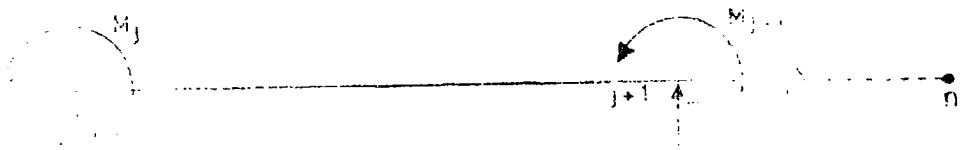

... Forces on the beam element at nodes ... and ... can be modelled by the three pairs of equations.

$$\left(+ \frac{\quad}{\quad}\theta_j - \frac{12}{L^2} V_j + \frac{6}{L}\theta_{j+1} \right)$$

$$\left(+ \frac{\quad}{\quad}\theta_j - \frac{6}{L^2} V_j + \frac{2}{L}\theta_{j+1} \right)$$

$$\left(- \frac{6}{L^2}\theta_{j-1} + \frac{12}{L^2} V_j - \frac{12}{L^2} V_{j+1} + \theta_{j+1} \right)$$

$$\left(- \frac{2}{L}\theta_{j-1} + \frac{6}{L}\theta_j - \frac{6}{L^2} V_{j+1} \right)$$

$$\left(\theta_{n-1} + \frac{12}{L^2} V_n - \frac{6}{L}\theta_n \right)$$

$$\left(+ \frac{6}{L}\theta_{n-1} - \frac{6}{L^2} V_n + \frac{4}{L}\theta_n \right)$$

... equations represent the barrel ... elements ... , similar equations can be produced ... split ... different lengths. These equations ... a computer program developed ... the ... applied external forces, damping ... inertia ... program uses a step method of solution ... 2nd Order Runge-Kutta routine

There is no requirement that the barrel elements need to be the same length. Indeed the program chooses element lengths so that the bearings are at barrel nodes.

Shot modelling

We first make the following assumptions.

1. There is no friction between barrel and shot.

2. The driving bands have no play in the barrel.

and 3. Yaw deflections are small such that sin $\theta = \theta$

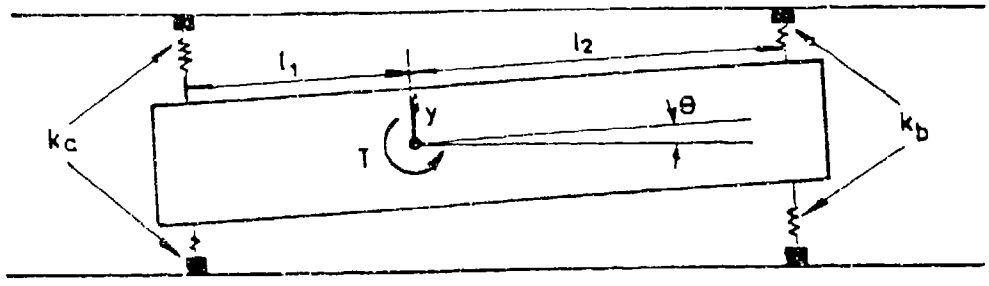

Fig 3. Schematic diagram of a shot in a smooth bore barrel.

Using the schematic diagram (figure 3) and considering shot 'bounce' and 'pitch' we can write the equations of motion for the shot.

$$M\ddot{y} = -k_a(y - \theta L_1) - k_b(y + \theta L_2) - C_a(\dot{y} - \dot{\theta} L_1) - C_b(\dot{y} + \dot{\theta} L_2) \quad \ldots\ldots\ldots\ldots \quad (4)$$

$$\ddot{\theta} I = T + L_1 k_a(y - \theta L_1) - L_2 k_b(y + \theta L_2) + C_a L_1(\dot{y} - \dot{\theta} L_1) - C_b L_2(\dot{y} + \dot{\theta} L_2) \ldots\ldots \quad (5)$$

These equations are solved using a 2nd order Runge-Kutta routine and the shot and barrel solutions are connected using the following method.

Shot barrel interaction

The position of the shot in the barrel is calculated from the pressure time curve and the position of each of the driving bands relative to element nodes is deduced.

a) Forces from the barrel on the shot

To include barrel effects in the equations of motion for the shot it is necessary to interpolate between the barrel nodes to give values for barrel motion at the driving bands.

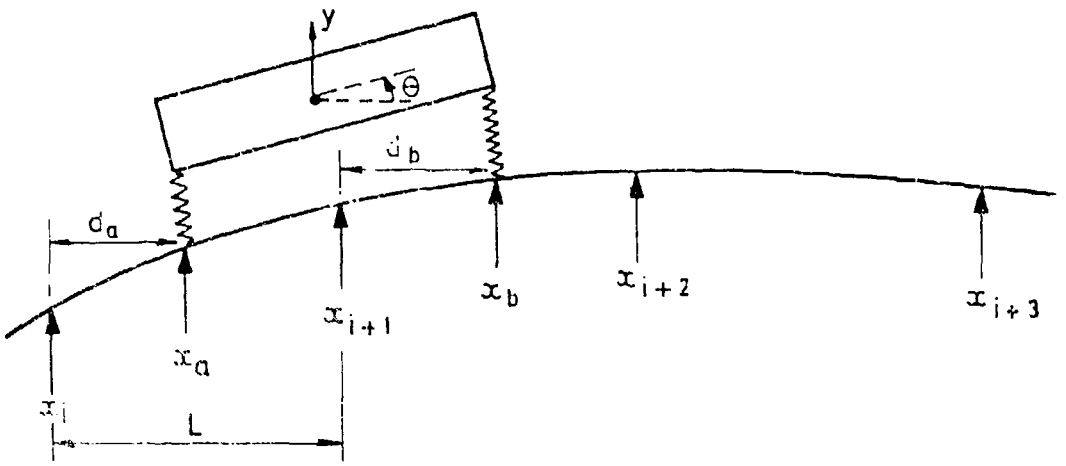

Fig 4. Displacement of the barrel at the shot driving bands.

Using figure 4, let the rear driving band be between nodes x_i and x_{i+1} and the front driving band be between nodes x_j and x_{j+1} then,

$$x_a = x_i + (x_{i+1} - x_i)d_a/L$$

$$x_b = x_j + (x_{j+1} - x_j)d_b/L$$

The vertical distance moved by the barrel is then incorporated into the shot 'bounce' equation (4) to give the new equation.

$$\ddot{M}\ddot{y} = -k_a(y-x_a-\theta L_1) - k_b(y-x_b+\theta L_2) - C_a(\dot{y}-\dot{x}_a-\dot{\theta}L_1) - C_b(\dot{y}-\dot{x}_b+\dot{\theta}L_2) \quad \ldots\ (6)$$

The equation for shot pitch becomes,

$$\ddot{\theta}I = T + L_1k_a(y-x_a-\theta L_1) - L_2k_b(y-x_b+\theta L_2) + C_aL_1(\dot{y}-\dot{x}_a-\dot{\theta}L_1) - C_bL_2(\dot{y}-\dot{x}_b+\dot{\theta}L_2) \quad \ldots\ (7)$$

b)Forces from the shot on the barrel

Vertical forces from a driving band are added to the barrel nodes either side of that driving band in proportion to the distance of the driving band from the nodes. Using figure 4 and letting F_{db} be the shear force from a driving band a distance d_a from node i the shear force on node i is calculated using the formula,

$$N_i = F_{bd}(1 - d_a/L)$$

and the shear force from the same driving band on node i+1 is.

$$N_{i+1} = F_{db}(d_a/L)$$

So that if the shot is within one barrel element, all of the forces from the shot are regarded to act at the nodes either side of that element. But if the driving bands are in separate barrel elements the forces are applied at three nodes.

EXPERIMENTAL PROGRAMME

A 30mm, muzzle loaded, compressed air powered gun has been developed at RMCS to simulate many of the characteristics of a recoiling tank gun. Many parameters can be varied easily, these include breech mass, breech inertia, buffer stiffness, bearing spacing, shot mass, bearing clearance and breech pressure/time profile. Barrels can be interchanged within a few minutes and these include a smooth bore mild steel barrel with a wall thickness of 10 cm, a thin walled aluminium smooth bore barrel and a rifled barrel.

The gun body is symmetrically balanced about both the horizontal and vertical axes but masses can be added above or below the axis to create an out of balance 'breech'.

Instrumentation has been designed which records the change in angle of the shot, about both the transverse horizontal axis and the vertical axis. To facilitate this the round was required to carry a 12 mm diameter mirror on its front face.

A round has been designed(11) to give a set of characteristics that include,

1, a pitch frequency of between 150 Hz and 300 Hz, to give sufficient number of cycles as the shot passes down the barrel,

2, a maximum pitch deflection of ± 4 mrad,

3, a damping ratio of .1, or less,

and 4, symmetry about the central axis with provision to attach oft axis masses to create an out of balance round.

A cross section of the design is shown in figure 5. It consists of an outer cup (AA) with machined driving bands (BB) and (CC), a 12mm diameter inner beam (D), a cantilevered beam (E) and an end mass (FF). The position of the mirror to be used when measuring the angle of the front face is shown at (G). In the experiments described here the cantilevered beam (E) was specified in silver steel, with the rest of the shot in aluminium alloy. However in future shots beams 'D' and 'E' are to be integrally machined from one material. The 'free' end of the beam is shaped to give a larger contact area with the mass. This is attached by a press fit and adhesive.

The driving bands were specified with a tolerance of .01 mm, this fit was designed to form a pressure seal and was considered tight enough for the balloting motion (rattling in the bore) of the shot outer cup to be neglected in theoretical predictions.

Except for two holes in the end mass (FF) the design is symmetrical about the central axis. Various masses can be screwed into these holes, to make the shot symmetrically balanced about the bore axis, or to give it an off-axis centre of gravity.

To give an initial test of the mathematical model two sets of firings of shots with a 2.1 gram mass, offset from the shot axis by 10.5 mm and positioned below the bore axis prior to firing, were chosen.These used,

1) The mild steel barrel with a muzzle support fitted so that the barrel can be regarded as inflexible and the shot studied in isolation, and

2) The flexible (aluminium) barrel with a balanced 'breech'.

RESULTS AND DISCUSSION

Figure 6 shows two theoretical traces for a shot with a 17mm x 2.6mm diameter cantilevered beam with an offset mass of 2.1 grams placed 10.5mm underneath the axis of the shot. One trace is for an inflexible barrel and the other for the flexible barrel. The theoretical predictions suggest that barrel motion will have a definite effect on the shot. In this case the effect of the flexible barrel is to rotate the nose of the shot downwards about the horizontal axis.

In figure 7 the theoretical prediction and an experimental result from the 'inflexible' barrel are plotted. As this figure shows the theoretical model is now giving reasonable predictions of shot motion within a solid barrel. The experimental trace shows a frequency of approximately 222 Hz, whilst the theoretical trace has a frequency of about 210 Hz.

Theoretical and experimental traces for a shot with a 20mm x 2.6mm diameter cantilevered beam, fired from the flexible barrel, are plotted in figure 8. The experimental result confirms that a downwards rotation of the shot nose, about the horizontal axis, does occur when the inflexible barrel is replaced by the flexible barrel.

One cause of inacurracy in the flexible barrel model is that the gun bearings were modelled as pin joints, and it has been shown(9), that the bearing stiffnesses and in particular damping at the bearings is an important factor when predicting barrel response.

A large scale firing programme to provide data to fully test the mathematical model will now be implemented.

CONCLUSIONS

Early comparisons with a few experimental results show encouraging results.

One of the advantages of the experimental apparatus described is that a large number of firings can be undertaken cheaply and quickly. A firing program will now be undertaken to provide large amounts of data both to test the simple mathematical model described and for the testing of other theoretical models.

ACKNOWLEDGEMENTS

The experimental programme described is being supported by the Royal Armament Research and Development Establishment (Fort Halstead).

NOTATION

For the barrel.

F_j	Shear force at node j
M_j	Moment at node j
E	Modulus of elasticity
I_b	Second moment of area of the barrel cross section
L_b	Length of barrel
L	Length of a barrel element
U_j	Horizontal displacement of node j
V_j	Vertical displacement of node j
θ_j	Angular displacement of node j
M_{be}	Mass of a barrel element

For the shot

θ	Angular displacement
L_1, L_2	Position of the body centre of gravity relative to the front and rear springs.
y	Vertical displacement of the shot centre of gravity.
T	Couple produced by the effect of an offset centre of gravity.
k_a, k_b	Stiffness coefficients for the driving bands
M	Mass of the shot body
I	Moment of inertia of the shot about its centre of gravity
C_a, C_b	Damping factors for the driving bands

Shot-barrel interaction

N_j	Shear force on barrel node j due to a driving band
F_{db}	Force from a driving band
d_i	Distance of the driving band from a barrel node

REFERENCES

1 ANDREWS T.O. (RARDE Fort Halstead)

Yaw of projectiles and effect on dispersion.

Private communication, 3 November 1982

2 WALKER E.H.

Yawing and Balloting Motion of a Projectile in the Bore of a Gun with application to Gun Tube Damage.

USA Ballistics Research Laboratories, September 1974

3 PAGAN G. THOMAS M.D. and KING W.P.C.

A Model for Tank Gun Movement During Firing using an Implicit Difference Numerical Algorithm.

3rd US Army Symposium on Gun Dynamics, May 1982

4 KING W.P.C. and THOMAS M.D.

A Gun Dynamics Model using Finite Difference Techniques.

TTCP WTP-2 (KTA-6), RARDE Fort Halstead, September 1984

5 TAYLOR B.

The use of a Finite Element Based Model to Predict the Motion of the US 105 mm M68 Barrel.

TTCP WTP-2 (KTA6) BRL Aberdeen Maryland, October 1983

6 SOIFER M. and BECKER R.

Development, Validation and Implementation of a Finite Element (Lumped Parameter) Model of the 75 mm ADMAG Gun System

TTCP WTP-2 (KTA6), BRL Aberdeen Maryland, October 1983

7 SOO HOO G. and ANDERSON L.P.

A Theoretical Model for In-bore Projectile balloting

US Naval Surface Weapons Center, June 1979

8 CHU S.H. (Large Caliber Weapons System Laboratory, Dover NJ)
Transverse Motion of 8 inch Projectile, XM673, in the XM201, M2A2 Gun Tube, MK-16 and MCL6 Gun. August 1973

9 BULMAN D.N.
Theoretical and Experimental Observations on the Effect of Bearing Spacing, Pressure Time Curve, Bearing and Barrel Damping on Barrel Motion.
TTCP WTP-2 (KTA-6) RARDE Fort Halstead, September 1984

10 POWELL S.E.
The use of the RMCS Compressed Air Powered Apparatus for the Measurement of In-bore Yaw.
TTCP WTP-2 (KTA6), BRL Aberdeen Maryland, October 1983

11 POWELL S.E.
An Experimental Round for In-bore Yaw Measurements.
TTCP WTP-2 (KTA6), RARDE Fort Halstead, September 1984

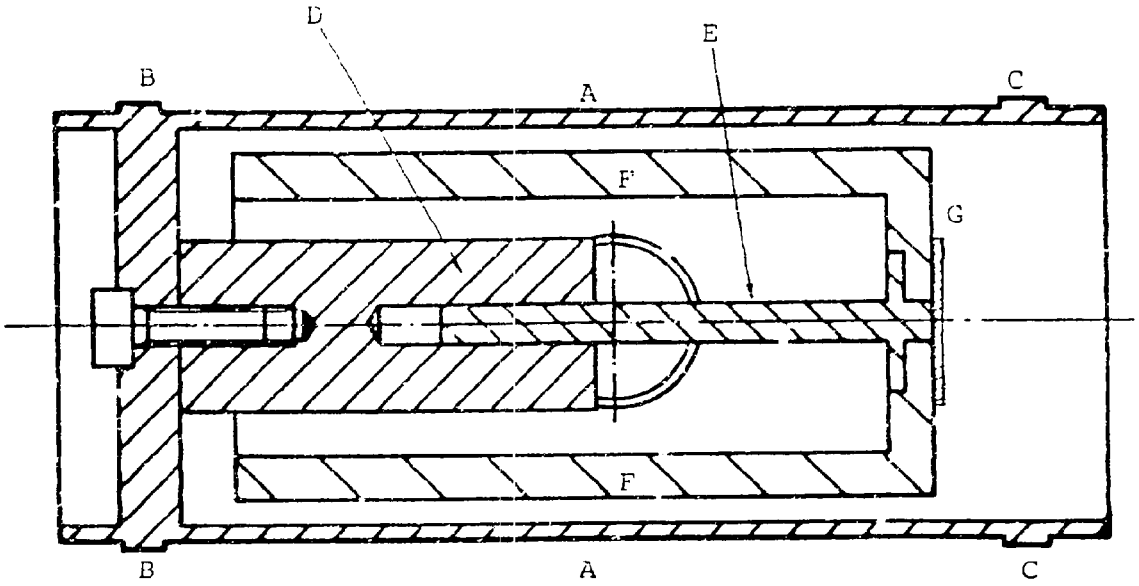

Figure 5. Cross section of a shot containing a cantilevered beam.

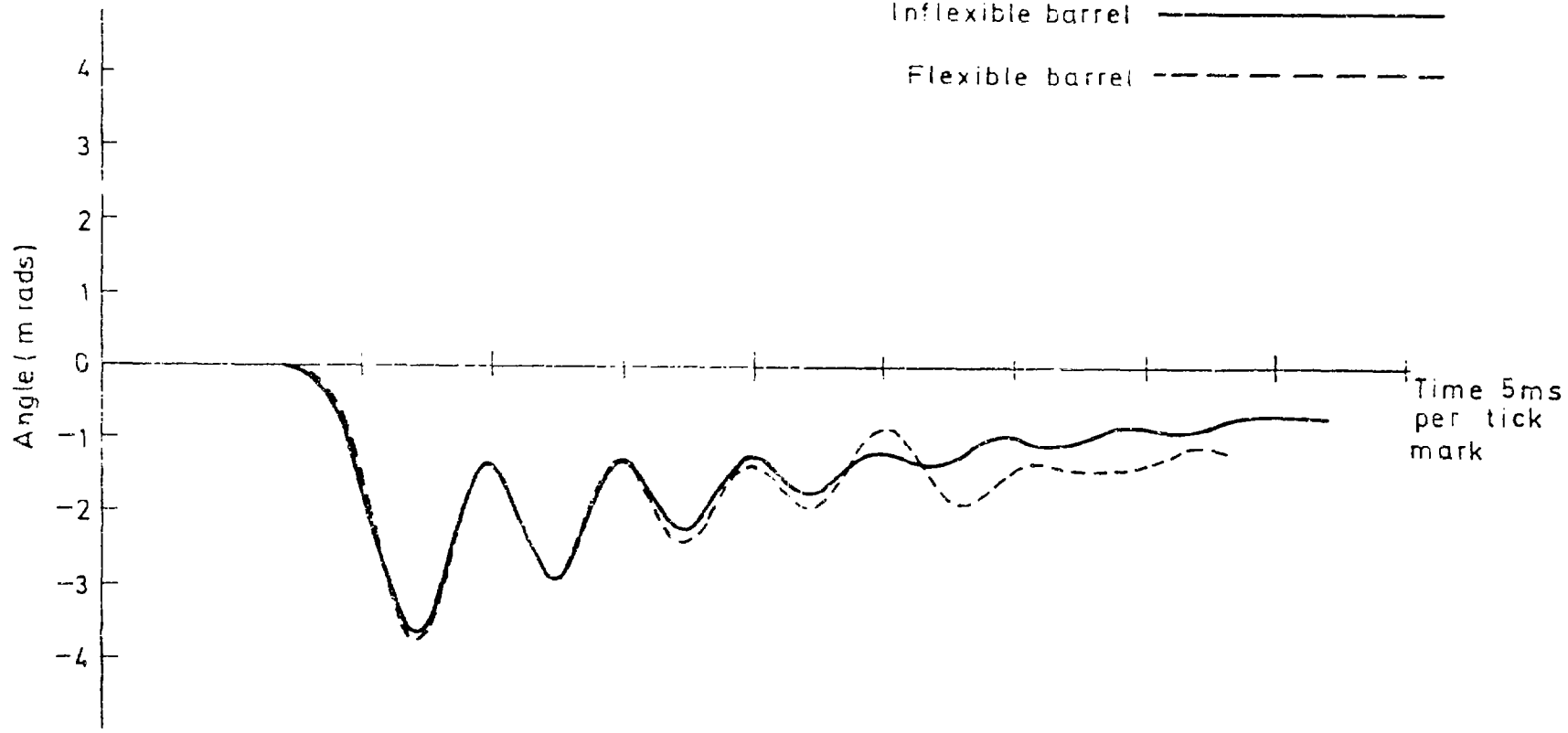

Figure 6

Theoretical yaw about the transverse horizontal axis. Shot containing a cantelevered beam with a 2.1 g mass initially positioned 10.5 mm below the bore axis.

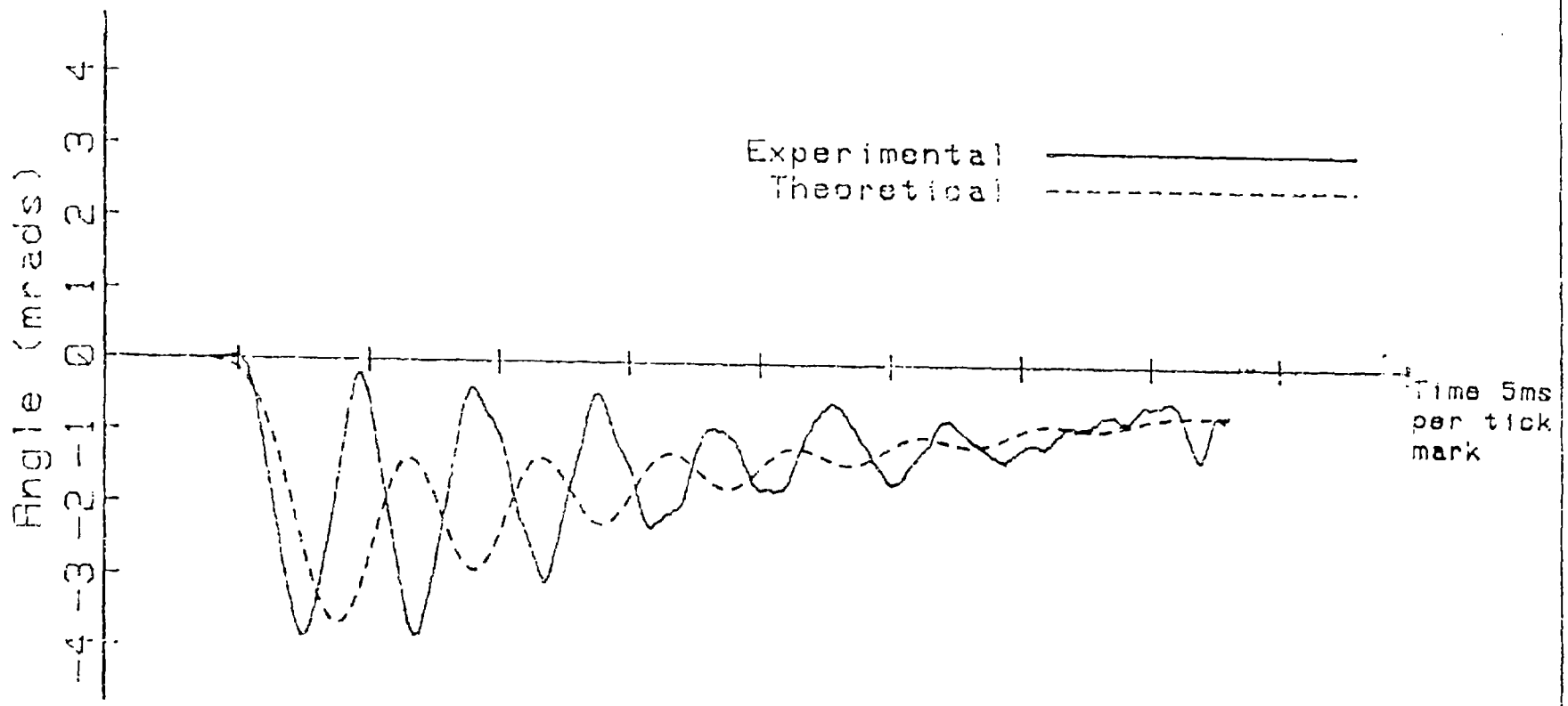

Figure 7

Theoretical and experimental yaw about the transverse horizontal axis. Shot containing a cantilevered beam with a 2.1 g mass initially positioned 10.5 mm below the bore axis. Fired from the 'inflexible' barrel.

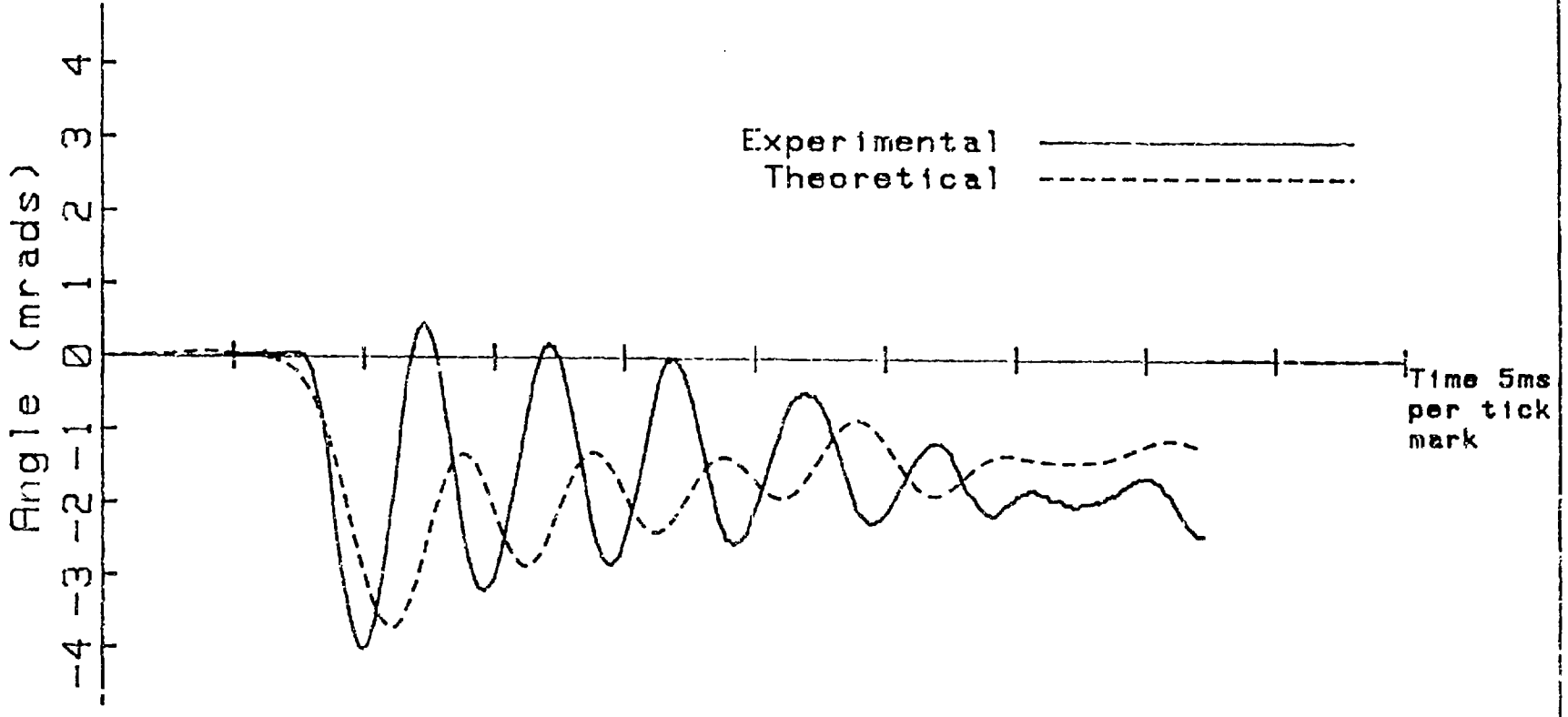

Figure 8

Theoretical and experimental yaw about the transverse horizontal axis. Shot containing a cantilevered beam with a 2.1 g mass initially positioned 10.5 mm below the bore axis. Fired from the 'flexible' barrel.

TITLE: Analysis of Sources of Error in Tank Gun Firing

EDWARD M. SCHMIDT and JOSEPH W. KOCHENDERFER
Ballistic Research Laboratory
U. S. Army Laboratory Command
Aberdeen Proving Ground, MD 21005-5066

ABSTRACT:

The sources of error in a representative modern tank are considered. Those processes occuring after shot ejection are treated in detail. Muzzle blast, sabot discard, and free flight aerodynamic perturbations are quantified. The influence of fire control system error is investigated.

BIOGRAPHY:

PRESENT ASSIGNMENT: Supervisory Aerospace Engineer, Ballistic Research Laboratory.

PAST EXPERIENCE: Captain, U.S. Army serving as R&D Coordinator, PM-UTTAS, (1969-1971).

DEGREES HELD: B.S.A.E. (1964), M.S. Astronautics (1965), and PhD Astronautics (1969), Polytechnic Institute of Brooklyn, N.Y.

ANALYSIS OF SOURCES OF ERROR IN TANK GUN FIRING

EDWARD M. SCHMIDT, PhD* AND JOSEPH W. KOCHENDERFER, MR
LAUNCH AND FLIGHT DIVISION
U. S. ARMY BALLISTIC RESEARCH LABORATORY
ABERDEEN PROVING GROUND, MD 21005-5066

1. INTRODUCTION

The capabilities of modern tank ammunition can be fully realized only when the rounds are delivered accurately. A primary source of error is the ability of the fire control system, including the gunner, to sense and locate the target then to lay the weapon to the proper orientation to insure ballistic intercept. However, even if this operation is performed to perfection, there are a number of perturbations which influence the launch and flight of the projectile. Some involve the dynamics of the tank/gun tube/projectile during inbore acceleration and subsequent separation. Others are dominated by the projectile aerodynamic characteristics. Also, the inability to sense and/or correct for the ambient conditions over the trajectory will cause disparity between the desired and actual points of impact. The present paper will address some sources of error in a representative modern tank, mainly considering perturbations following separation of the projectile from the launcher.

An illustration of some of the problems facing the analyst of in-bore dynamics of modern projectiles is provided in Figure 1. The weapon is a massive guide rail for the projectile; however, under the extreme loads of launch, the gun tube begins to respond while the shot is still in bore. In order to force a consistent sense to this response, cannon are generally fabricated with mass asymmetry. The tube is supported and constrained by the recoil system which may or may not be symmetric in design. Under gravity, the tube droops producing a curvature which is complicated by variations in bore straightness induced by manufacturing, installation, use, or the environment.

Upon firing the charge, the pressure within the tube builds up to thousands of bars causing both the projectile and gun tube to accelerate. Each of these moving bodies is subject to a gross rigid body motion upon which is superimposed flexural or vibrational modes. The linear and angular acceleration of the gun tube induces inertial loads which contribute to flexing. In addition, the motion of the projectile along the curved path of the tube results in transverse reaction loads which drive the gun motion. Historically, projectiles are assumed to undergo rigid body balloting motion as lateral clearances are taken up and rebound occurs. With long rod kinetic energy ammunition, this response is supplemented by longitudinal flexure of the sabot and of the projectile relative to the sabot.

In terms of accuracy, the critical moment of the in bore cycle is the separation of the projectile from the gun tube (Figure 1). Anything that influences the magnitude or direction of the projectile velocity vector could result in significant deviation from the intended trajectory. If the launch process terminated at the muzzle, the parameters of interest would be the

transverse velocity, angle, and angular rate of the gun tube plus the transverse linear and angular velocity of the projectile relative to the gun tube. Unfortunately, the projectile must disengage from the tube, pass through the reverse flow region of the muzzle blast, and then discard the sabot components before entry into unconstrained free flight. During transit of this near muzzle region, the trajectory may be further perturbed.

Once clear of the blast and sabot discard regions, the projectile free flight motion is reasonably well understood. Assuming that the projectile has not been damaged during launch, the trajectory can be well determined if the initial state is defined. The main source of error associated solely with the free flight of the round can be ascribed to the inability of the fire control system to accurately sense and provide appropriate corrections for ambient conditions over the flight path.

In order to complement the papers describing the contribution of gun and projectile in bore dynamics to launch conditions, the present paper will discuss the environment seen by the projectile following separation from the gun tube. Muzzle blast loads will be reviewed for weapons with and without muzzle brakes. Sabot discard interactions will be considered and related back to in bore properties. Finally, the free flight motion will be addressed.

2. MUZZLE BLAST LOADS

When problems are encountered in launching rounds from cannon, it is a common practice to ascribe the difficulty to loads encountered in the muzzle blast. In defense of this interesting gasdynamic phenomena, it must be made clear that care is required in diagnosing the origin of weapon launch problems. Muzzle blast may be the source of disturbance in some instances, particularly, for objects which are bluff, asymmetric, or of low density. However, in many cases, the extreme loads characterizing the in-bore environment are the real source of difficulty.

Once free of the gun tube, the projectile must transit the muzzle exhaust flow which consists of an outer air blast driven by the expanding propellant gas plume (Figure 2). The plume has the structure of a supersonic, underexpanded jet and is terminated at the shock layer consisting of the plume Mach disc, the propellant gas/air interface, and the outer shock of the blast wave. While inside the Mach disc, the projectile is subject to the plume flow wherein the gas velocity reaches values 2-3 times that of the projectile, i.e., the projectile is in reverse flow. Conventional wisdom dictates that for such a situation, finned projectiles would be unstable, but since the residence time within the plume is much lower than the inertial response times of the body, stability is not really of concern. Rather, it is the transverse impulse transmitted to the projectile that influences the subsequent trajectory.

The calculated variation [1] of the lift force, $\bar{L}$, with distance from the muzzle is illustrated in Figure 3 for different values of the ratio of the projectile exit velocity to the propellant speed of sound at shot ejection, Vp/c, i.e., the Mach number of the propellant gas prior to shot

exit. For values of the parameter equal to or greater than one, there is no in-bore interaction possible. For values less than one, the in-bore interaction occurs and may be important. Outside of the weapon, the behavior of the lift function is of interest. The relative flow velocity increases as the round moves through the plume causing the lift on the fins to increase. However, this increase due to the velocity, is offset by the rapid decrease in density of the propellant gas due to expansion. Under the influence of these two property variations, the lift function peaks and then decays to negligible values after only two exit diameters of travel.

Integration of the lift permits the computation of momentum tranferred to the projectile and the resultant deflection of the trajectory. The estimated trajectory deflection for a generic kinetic energy projectile is plotted as a function of launch velocity in Figure 4. The deflection in mils is ratioed by the launch angle of attack of the projectile in degrees. The lack of monotonicity in the plot is due to the assumed muzzle exit conditions which were taken from a variety of data sources. However, the result is striking. As the launch velocity increases, the trajectory deflection decreases significantly. For a typical tank round, the in-bore yaw angle should be quite low. Even if the angle were as large as 0.5 deg, the jump induced by muzzle blast would amount to only 0.05 mils.

3. MUZZLE DEVICE EFFECTS

When a weapon is equipped with a muzzle device, analysis of the flow becomes more difficult. A common device, the muzzle brake, reduces gun recoil by venting the propellant gas rearward. The device has a three-dimensional, confined geometry through which the propellant gases expand over the projectile. For sabot encapsulated rounds, the installation of a muzzle brake on the gun can create serious problems. First, the muzzle brake must not interfere with the sabot discard. Mechanical contact does extreme violence, both to the brake and to the round. Another, major difficulty can be the enhancement of muzzle gasdynamic loadings. Since muzzle brakes are under consideration for installation on a number of low recoil tank gun systems, it is of practical interest to consider the possible interactions.

Recently, tests were conducted on a medium caliber cannon with and without a triple baffle muzzle brake in place [2]. When the brake was installed, the dispersion of the system doubled. To determine if the flexural characteristics of the tube were altered, a mass simulating the brake was mounted at the muzzle. The mass did not interfere with the free expansion of the muzzle gases. Firings demonstrated that the dispersion returned to the level obtained with a bare tube indicating that the added mass was not the cause of the problem. A further investigation was conducted to investigate the influence of brake length. Successive baffles were cut off the device. As the baffles were decreased from three to one, the dispersion also decreased. It was found that a single baffle design produced no measurable increase in dispersion over the bare muzzle case. Apparently, enhanced gasdynamic loads associated with the confinement and length of the brake were altering the launch dynamics of the system.

Computations of the gasdynamic loads on the projectile as it passed through the brake, predicted a 20% growth in dispersion. Since dispersion doubled, this was not the sole effect. A series of orthogonal flash radiographs were taken of the sabot discard process for cases with and without the triple baffle brake in place. These data show that the presence of the brake produced a change in the sabot discard trajectory which was not treated in the computations. Mechanical contact between the sabot components and projectile occurred over a longer period and asymmetry in sabot discard was enhanced. The resultant asymmetry in the discard increased the loading upon the projectile and degraded precision. The tests demonstrated that care must be taken in the installation of muzzle devices upon weapon systems which are designed for precision fire.

4. SABOT DISCARD

The fact that sabot discard interactions influence the trajectory of fin stabilized projectiles can be demonstrated by considering measurements of free flight yawing motion (Figure 5). The data were acquired in the BRL Transonic Range on a typical kinetic energy projectile. The plots present the angle of attack versus the angle of sideslip as the round moves through the 200 m facility. With distance downrange, the yaw level decreases; therefore, the maximum yaw occurs near the weapon. Two plots are presented representing a case with low and high sabot discard perturbations, Figures 5a and 5b, respectively. The nature of this categorization can be seen if one considers the condition of the projectile at separation from the gun tube.

Within the bore, the projectile is constrained by clearances to yaw levels on the order of 0.1 deg; although the angular velocity may be appreciable. If a statically stable projectile enters into free flight with such initial dynamics (i.e., near zero initial yaw, but finite yaw rate) the resulting angular motion should be nearly planar yaw. In fact, this type yaw is well represented by the data shown in Figure 5a. This plot would suggest that sabot discard interactions either were not significant or are consistent with normal free flight aerodynamic loads.

In contrast, a second round of the same type demonstrates the effect of sabot discard interaction (Figure 5b). Here, the yawing motion is not planar, but elliptical. If one were to postulate initial launch dynamics for this round, they would be initial yaw of roughly 4 deg and a finite yaw velocity orthogonal to yaw angle. Obviously, the projectile did not have a 4 deg yaw at release from the gun tube; nor is it reasonable to assume that disengagement from the tube forced the yaw to build to such a level. Rather, the sabot discard process produced perturbations which significantly altered the launch dynamics of the round.

The sabot discard perturbations consist of both mechanical and aerodynamic interactions. At the muzzle of the weapon, the sabot components and projectile are in direct mechanical contact due to the constraints imposed by the tube and the various bands or seals of the sabot assembly. After clearing the tube, elastic decompression, spin, and gasdynamic loads act to break these bands and to lift the sabot away from the projectile. Depending

upon the design of the sabot, the lift process may be rapid and clean or may involve pivoting about a point of contact on the projectile. Alternatively, the sabot components may initially break contact only to reimpinge on the projectile at a later stage of discard. Asymmetry in the contact will generate lateral momentum transfer between the sabot components and the projectile. This alters both the projectile trajectory and the symmetry of sabot discard. Geometric asymmetry in the sabot discard results in aerodynamic asymmetry in the mutually interacting flowfields associated with the sabot components and the projectile.

The relative magnitudes of in bore and sabot discard perturbations have been estimated using data acquired from x-ray measurements of near muzzle projectile motion [3,4]. The results of a comparison of transverse angular impulse are presented in Table 1, below. The data indicate that the level of impulse due to sabot discard perturbations, is the same as that due to in bore disturbances. This conclusion is supported by data acquired by Biele [5] who measures the dynamics of a 120mm gun tube and the subsequent projectile trajectory. He finds that the gun muzzle motion accounts for roughly one-half of the measured trajectory jump angle. The remainder is associated with disengagement and sabot discard dynamics.

Table 1. Comparison of Transverse Angular Impulse

Round No.	In Bore Angular Impulse (rad/s)	Sabot Discard Angular Impulse (rad/s)
1	6.37	5.60
2	4.17	10.26
3	3.03	.21
4	3.58	3.28
5	7.45	1.82
6	1.71	6.30
7	14.28	5.88
8	1.29	9.04
9	5.97	9.08

Since sabot discard can significantly alter the projectile trajectory, it is of interest to consider the origin of asymmetry in discard. Conceptually, there could be asymmetry associated with the failure of bands or retaining rings; however, this behavior is difficult to measure or model. Alternatively, the asymmetry could be directly related to the initial state of the sabot and projectile upon disengagement from the bore. During travel within the gun, the projectile moves along a curved path determined by the tube bore profile and tube dynamic response. In addition, the projectile and sabot may be oscillating both relative to the bore and to each other. Finally, during release of constraints at shot exit, transverse loads may be imparted.

Plostins [4] assumed that a major factor influencing the sabot discard interactions was the in-bore oscillation of the projectile relative to the sabot. He examined the magnitude of measured sabot perturbation relative to the parameter δ'/δ. For small values of this ratio, the projectile is

assumed to be near the peak of its in-bore yaw. Conversely, large values of the ratio imply the projectile is being launched near the minimum of in bore yaw. The correlation indicates that sabot discard interactions are large for small values of δ_0' / δ_0. This would correspond to a condition where the projectile angular displacement is greatest and, presumably, where the differential strain in the sabot components is appreciable. The minimum discard interaction is measured for the case of large δ_0' / δ_0, which should be the case for low differential strain in the sabot components.

The results point out the need for a design tradeoff. To reduce aerodynamic jump, the launch angular rate must be minimized; however, Plostins' correlation suggests that as the rate is reduced the sabot discard interaction begins to build up. This implies that there could be an optimal launch condition for the minimization of the sum of the sabot discard interaction and aerodynamic jump.

5. FREE FLIGHT

In this section, consideration is given to the influence of the free flight aerodynamics upon accuracy. First, aerodynamic jump will be discussed. Second, the manner in which exterior ballistics is implemented in the fire control solution is addressed.

Aerodynamic jump is the deviation of the trajectory associated with the yawing motion of the projectile. As yaw builds up, a lift is produced which results in lateral acceleration and displacement of the round. Murphy [6] integrates the equations of motion to produce the following expression for the aerodynamic jump:

$$\theta = \frac{I_y}{m\ell^2} \frac{C_{L_\alpha}}{C_{M_\alpha}} [\delta_0' + H\delta_0]$$

To examine the importance of the initial angular rate and angle of attack, consider two cases representing the launch conditions of a fin-stabilized projectile:

Case 1: $\delta_0 = 5$ deg, $\delta_0' = 0$ rad/s

Case 2: $\delta_0 = 0$ deg, $\delta_0' = 14.5$ rad/s

To give yawing motion which is similar in magnitude (but not in phase) for each case, the first maximum of yaw will be roughly 5 deg. For Case 1, the projectile is assumed to be launched at this angle. For Case 2, the projectile is launched with an angular rate which will cause the yaw to build to a maximum of roughly 5 deg. In both cases, the initial velocity vector is assumed to be along the desired lay angle.

The resulting trajectory for each case was computed using a six-degree-of-freedom code (Figure 7). It is observed that the jump for Case 1 is negligible; however, for Case 2, there is significant trajectory

deflection. Since this case is more nearly that of typical gun launch, the computations indicate that the yawing motion of projectiles must be considered as an important source of deflection. This is especially true for yaw levels which are greater than one or two degrees. For comparison, the value of aerodynamic jump predicted by the above equation is shown on the plot. The two values are in good agreement. It is interesting to note that trajectory deflection angle is sensitive to projectile yaw for ranges less that 200 m. Beyond this distance, the jump approaches its asymptotic limit.

The second free flight effect to be considered is associated with the implementation of gun lay. The fire control system, inclusive of the tank crew, must sense the ambient conditions and correct the pointing angle of the gun to provide the correct trajectory. If the ambient conditions are not properly sensed or input to the fire control computer, then the round will deviate from the desired point of impact. Since the flight characteristics are sensitive to the projectile design and launch conditions, two typical fin stabilized tank rounds are considered: full bore, spike-nosed and sub-caliber, saboted long rod shapes. For a given level of uncertainty in ambient conditions, the shift in vertical target impact location is given as a function of range in Table 2.

Table 2. Shift in Vertical Target Impact Location (in mils) due to Error in Fire Control Inputs where FB = full bore round and SC = sub-caliber round.

Range (m)	10% error in density		10% error in ambient temp.		10 m/s muzzle velocity error		5 m/s crosswind estimation error	
	FB	SC	FB	SC	FB	SC	FB	SC
0	0	0	0	0	0	0	0	0
500	.018	.002	.004	.000	.036	.012	.290	.035
1000	.090	.005	.020	.002	.083	.022	.632	.072
1500	.245	.013	.059	.004	.139	.035	1.003	.107
2000	.560	.025	.141	.008	.220	.047	1.484	.146
2500	1.114	.040	.286	.013	.321	.060	2.003	.182
3000	2.184	.060	.558	.021	.478	.075	2.718	.226
3500	4.002	.084	1.000	.030	.686	.087	3.490	.268
4000	6.941	.116	1.617	.042	1.010	.104	4.545	.310

It is readily apparent that the sensitivity to errors in fire control inputs is significantly lower for the sub-caliber round than it is for the full-bore round. In addition, the variation with range is highly non-linear. To gauge the importance of these shifts in impact location, it is necessary to consider whether the estimation errors are reasonable. For example, a 10% variation in air temperature is about 30 deg C from the 15 deg C standard. This could reasonably result from a seasonal excursion or from a day to night change in a high desert environment. A 10% change in air density is at the extreme when variations are considered at a given altitude; however, if the weapon is moved from sea level to 1 km altitude, such a density change is possible. A 10 m/s variation in muzzle velocity has been observed in tank guns even with a correction for propellant temperature and

has been attributed to uncertainty in tube wear and propellant aging characteristics. A 5 m/s error in the estimation of crosswind is an upper bound on this property.

Due the short engagement ranges of tank cannon, the influence of rotation of the earth on the trajectory is neglected. The magnitude of this effect on the azimuthal fall of shot is illustrated in Fig. 7. Even at 3 km range for the slower round, the correction is relatively small.

The algorithm in the fire control system used to aim the weapon also influences the ability of the gunner to successfully engage targets. To compute gun lay angles, current systems use either a polynomial fitting to standard conditions plus corrections (unit effects) or solve two-dimensional equations of motion (with a closed form add-on equation for the cross plane). As long as computer memory space permits and the conditions are not widely different from standard, both solution methods yield comparable results. However, if there is a reasonably large divergence from standard such as a 15% density decrease coupled with a 10 m/s cross wind at an engagement range of 2000 meters when firing a full caliber finner, the interaction of density and wind, if uncompensated, would introduce an error of about one mil in the cross plane. Fire control algorithms which utilize polynomial fits for nonstandard conditions could suffer from the nonlinearity of the corrections but this shortcoming is minor and, generally, may be ignored. It should be pointed out that the fire control system attempts to compensate for the nonstandard effects addressed in Table 2; however, there is error in measuring each of these quantities which will influence the fall of shot. The perturbations listed, such as 10% in air density, can be properly accounted for if the correct value is input to the fire control. Unfortunately, the default values are often used in the solution of the aiming data because better data are unavailable or because the importance of these quantities is not recognized.

6. SUMMARY

The influence of perturbations to a projectile trajectory following separation from the gun tube is examined. Muzzle blast, sabot discard, and free flight effects are considered. Muzzle blast has a minimal influence. Sabot discard can cause changes in the trajectory similar to those due to transverse loads within the gun tube. Generally, free flight loads are well understood; however, uncertainty in ambient conditions can generate errors in the lay of the weapon which can be significant in some cases.

REFERENCES

1. E. M. Schmidt, K. S. Fansler, and D. D. Shear, "Trajectory Perturbations of Fin-Stabilized Projectiles due to Muzzle Blast," AIAA J. Spacecraft and Rockets, V. 14, No. 6, June 1977, pp 330-344.

2. E. M. Schmidt, F. J. Brandon, and S. C. Pearson, "Influence of Muzzle Brakes upon the Trajectory of Fin-Stabilized Projectiles," 8th Int'l Symp. on Ballistics, Orlando, FL, 23-25 October 1984.

3. E. M. Schmidt and L. D. Shear, "Aerodynamic Interference during Sabot Discard," AIAA J. Spacecraft and Rockets, V. 15, No. 3, May-June 1978, pp 162-167.

4. P. Plostins, "Launch Dynamics of APFSDS Ammunition," 8th Int'l Symp. on Ballistics, Orlando, FL, 23-25 October 1984.

5. J. K. Biele, "Gun Dynamics Effects to Jump of Smooth-Bore Tank Guns," 8th Int'l Symp. on Ballistics, 23-25 October 1984.

6. C. H. Murphy, "Free Flight Motion of Symmetric Missiles," R 1216, Ballistic Research Laboratories, APG, MD, July 1963. AD#42757.

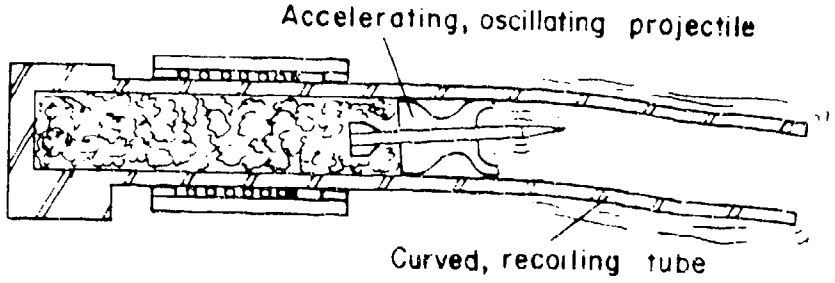

a. In-Bore

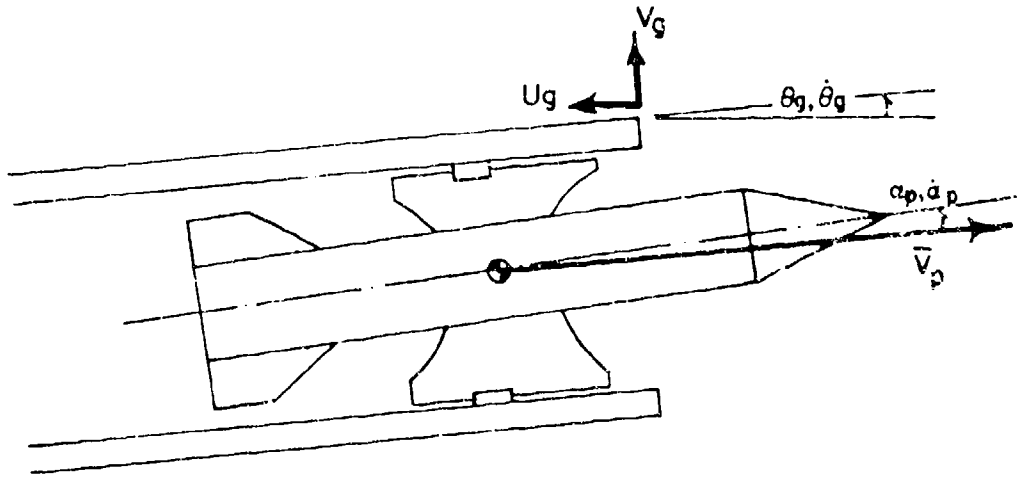

b. Muzzle Separation

Figure 1. Schematic of Launch Environment

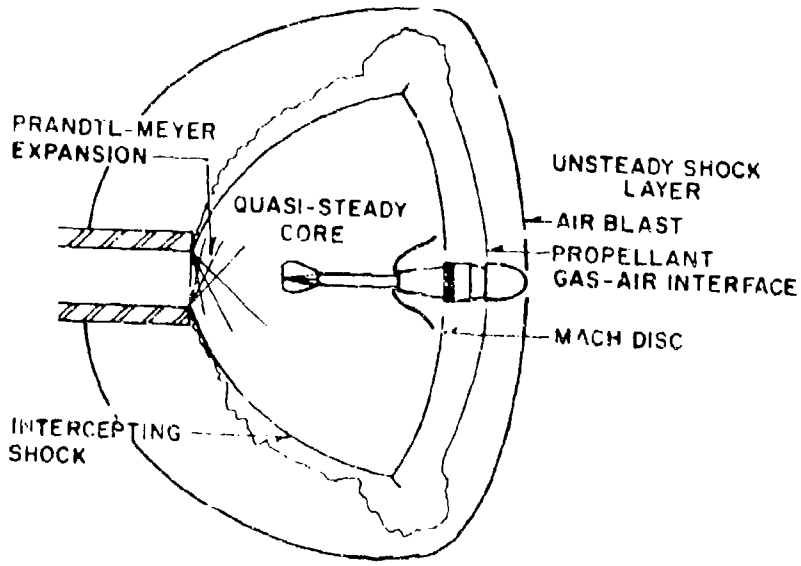

Figure 2. Muzzle Blast Flow Field

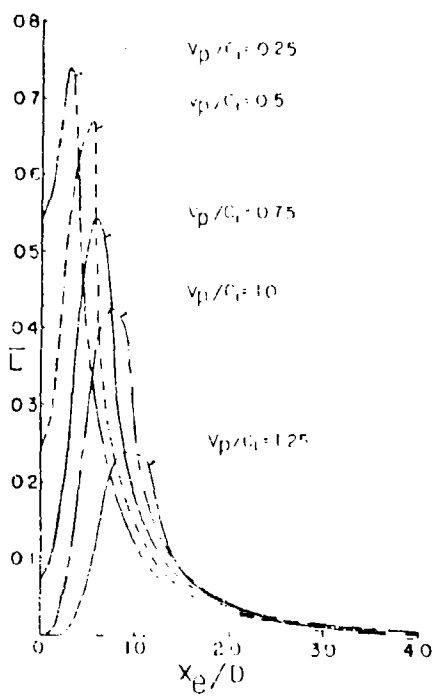

Figure 3. Variation of Transverse Force Through Muzzle Flow Field

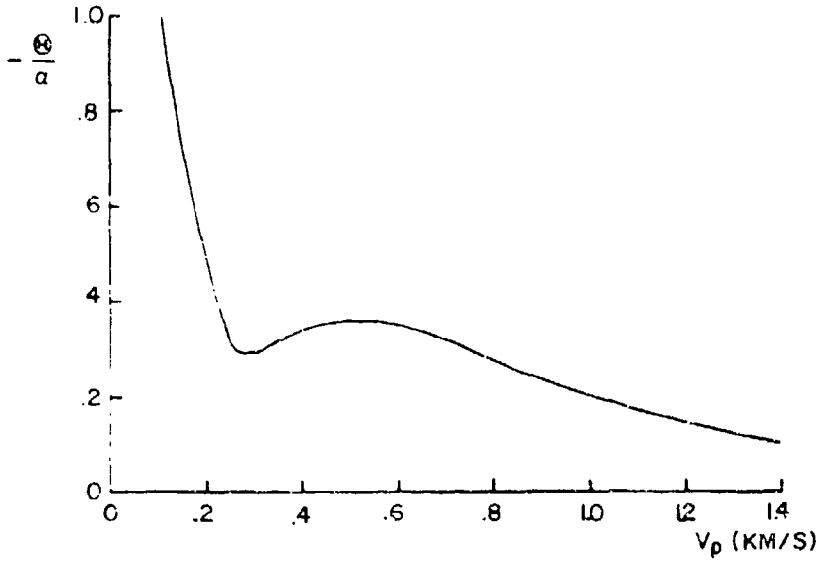

Figure 4. Trajectory Deflection Due to Muzzle Blast

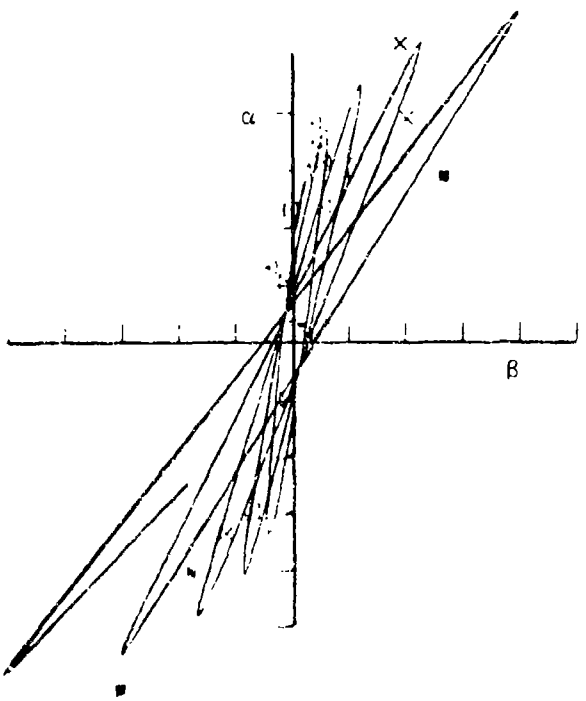

Figure 5a. Measured Yawing Motion for "Low Disturbance" Launch

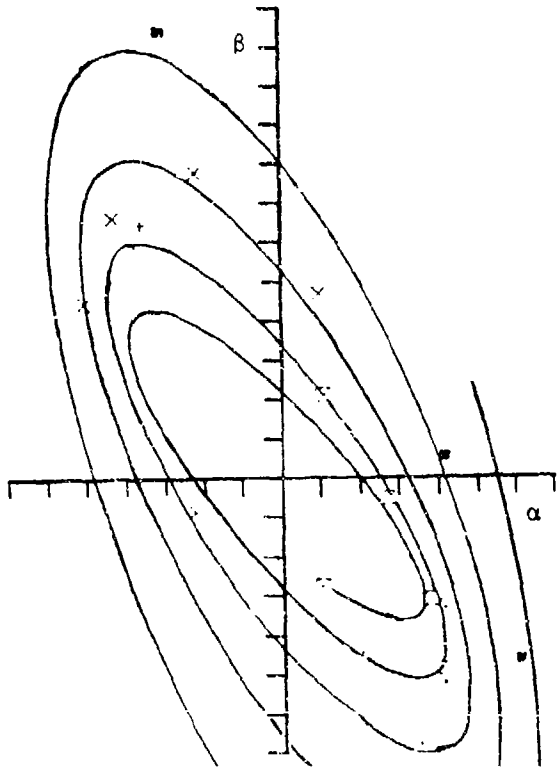

Figure 5b. Measured Yawing Motion for "Large Disturbance" Launch

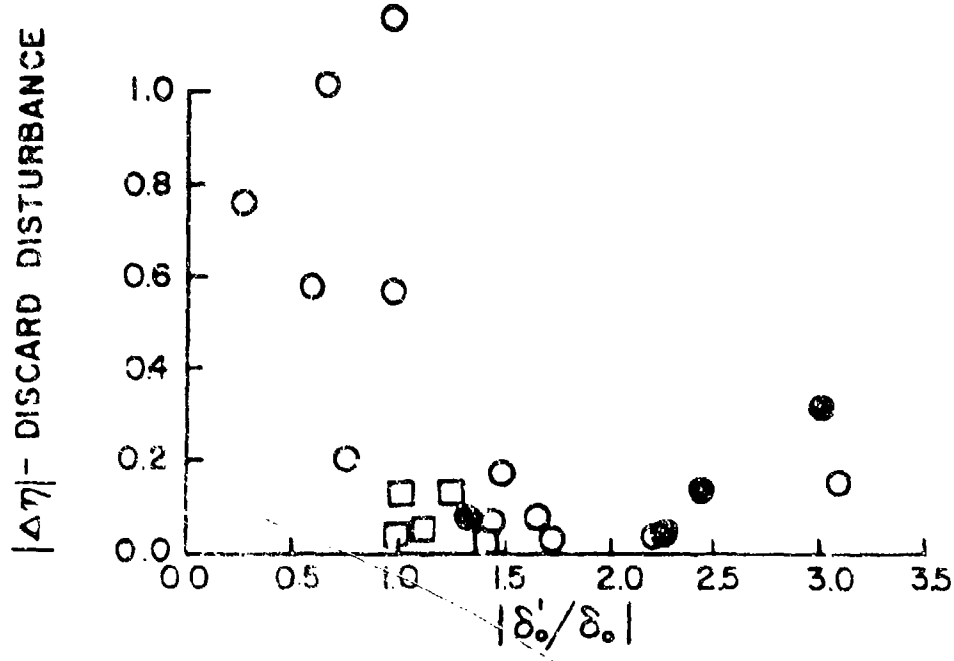

Figure 6. Correlation of Sabot Discard Disturbance with Launch State

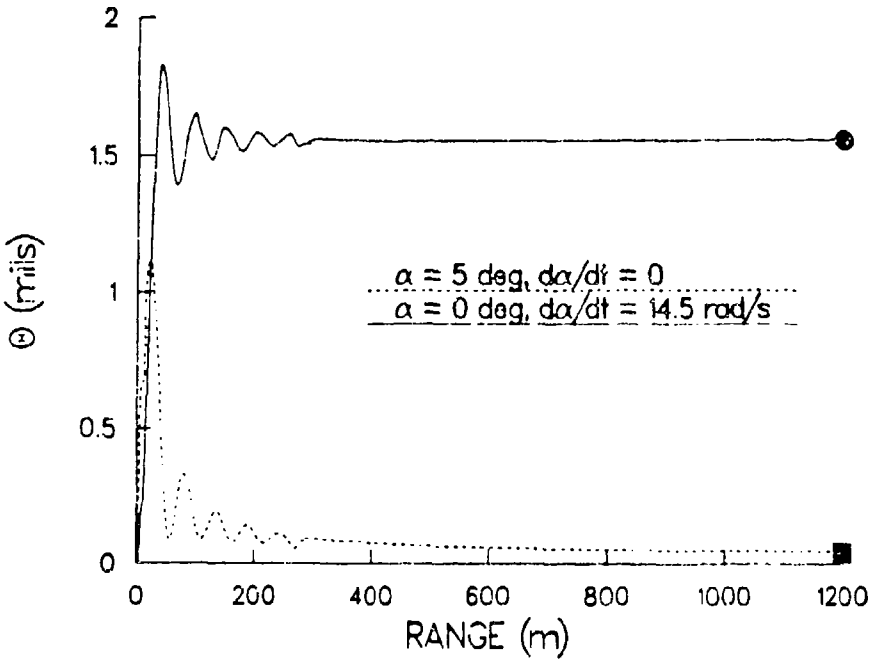

Figure 7. Jump Angle as a Function of Range for Two Different Launch Conditions

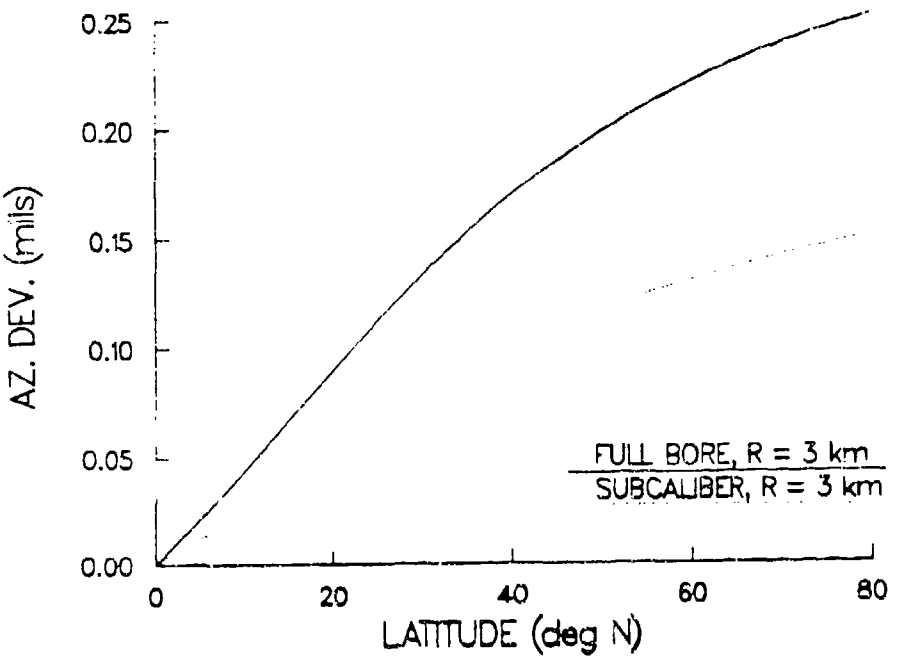

Figure 8. Azimuthal Deflection Due to Rotation of the Earth for 3 km Range

TITLE: A THREE-DIMENSIONAL COLOR COMPUTER GRAPHICS PROGRAM FOR DISPLAY OF PROJECTILE GUN DYNAMICS

Kathleen L. Zimmerman
U.S. Army Ballistic Research Laboratory
Aberdeen Proving Ground, MD 21005-5066

ABSTRACT:

Computer graphics is rapidly developing as an engineering design and analysis tool. The advent of interactive computing and array processing on minicomputers has made it possible to interface both experimental data and computer simulation with graphic displays to facilitate analysis. The use of color as a monitor of stress level or thermal effects, for example, provides an enhanced capability for the recognition and understanding of ballistic phenomena.

This paper describes a computer code which provides three-dimensional color output to display the dynamic motion of a gun tube. Using a description of the tube from a database and the centerline of the tube at rest, the static tube is displayed in both two and three dimensions. Data for the centerline, obtained from either a gun dynamics modeling program or experimental data, are used to calculate the gun tube display coordinates at a given time. Successive frames can be generated at appropriate time intervals to be used to make a film of the tube motion.

BIOGRAPHY:

PRESENT ASSIGNMENT: Mathematician, U.S. Army Ballistic Research Laboratory, Aberdeen Proving Ground, MD.

PAST EXPERIENCE: Mathematician, U.S. Army Ballistic Research Laboratory, Aberdeen Proving Ground, MD.

DEGREES HELD: B.S., Mathematics, Towson State University, 1965; M.S., Computer Science, Johns Hopkins University, 1982.

A THREE-DIMENSIONAL COLOR COMPUTER GRAPHICS PROGRAM FOR DISPLAY OF PROJECTILE GUN DYNAMICS

KATHLEEN L. ZIMMERMAN
U.S. Army Ballistic Research Laboratory
Aberdeen Proving Ground, MD 21005-5066

1. Introduction

Graphical representation of data is an old, widely used analysis tool. Computer algorithms to automatically generate 'X-Y' plots were developed quickly by the industry. The advent of the low-cost graphic terminal and development of mini- and micro- computers led to a tremendous growth in the graphics field during the early seventies. Graphics, suddenly available at a reasonable cost, captured the interest of many users from a host of disciplines. Almost instantaneously, computer graphics were being used to display three-dimensional objects in 'computer art', movies, and vendors' promotional material. Even the change in language from 'plotting routines' to 'computer graphics' reflects technological advances which allow us to make artistic use of color to show density, stress, temperature, texture, etc.

A survey of commercially available software was made before this project was undertaken in earnest. The leading contender, PATRAN, has a fantastic post processor for display of three-dimensional objects; the graphics modeling capability includes surface smoothing and highlighting which produce almost photographic quality results. Unfortunately the company which sells it does not plan to market a version which will run on any of our three candidate computer systems: an HP1000-F minicomputer, an HP9836C microcomputer, or a PE3252 minicomputer with a MEGATEK 7200 graphics engine. It took very little time to learn that buying software designed for our particular hardware combinations was next to impossible.

Since the ultimate goal of this project is to make a movie of the tube motion, it was decided to concentrate development efforts using the Perkin-Elmer minicomputer, the MEGATEK, and a MATRIX camera. DISSPLA, version 9, has been installed on the PE and is the current graphics package being used. It has the advantage of familiarity since it is also installed on the mainsite CYBER 173 and CYBER 825 computers. The 3-D graphics available with DISSPLA cannot be used for this application since DISSPLA expects a single-valued function to describe in x and y the surface.

The object of this paper is to present a simple, direct method for showing gun tube motion as predicted by a gun modeling code. The program has been written so that the user can generate the graphics picture using familiar two-dimensional plotting routines. Further, the program has been designed so that only one subroutine needs to be re-written when the code is 'ported' to other computers. With very little effort, the graphics subroutine has been converted to run on the HP 1000-F and the CYBER 825.

2. Graphic Concepts

The assumption has been made that gun modeling codes can produce centerline coordinates (x,y) for each node at a given time t and/or three-dimensional information which gives the centerline coordinates (x,y,z) and the rotation of point on the surface about each axis for each node at a given time t. The radius of the tube at each node is obtained from a database of gun tube descriptions. Surface coordinates are calculated at 25 points around the circumferenace of the tube at each node and stored in a three-dimensional matrix by node number, circuference point number, and axis coordinate. This tube matrix is similar to a finite element mesh and can be used to display a 'stick figure' representation of the tube.

In order to use the hardware polygon fill or software routines of a graphics package like DISSPLA, the data needs to be presented in a form so that consecutive vertices of a polygon are defined. A plotting matrix is computed using the information in the gun tube matrix just calculated. The surface coordinates are arranged so that each group of five describes a polygon where the fifth vertex is identical to the first and is used to close the polygon. The plotting matrix will become much larger than the tube matrix.

All that remains now is to transform this three-dimensional data into information which can be used for a two-dimensional display medium. At the present time, a 4 x 4 transformation matrix is calculated which performs an isometric projection of the plotting data and then projects it onto the z=0 plane. Every polygon is displayed and filled, including polygons which are not visible in the picture. This takes a lot of time, but does not alter the final view. In order to give the three-dimensional sense, the centerline of the tube as well as the surface circumference points at each node are drawn. A picture is taken of the tube at its initial position.

To calculate the plotting matrix for the next time step, it is necessary to perform the required translation of the centerline coordinates and the corresponding rotations at each node. This is done using the tube matrix and the plotting matrix is then defined again.

It is obvious that a hidden line or hidden surface routine must be added to this program in order to speed up the actual display of data on the graphics terminal. Since a gun tube is a series of convex volumes, the Roberts hidden line algorithm (reference 1) can be used to compute hidden lines. New endpoints are computed for partially visible lines and can replace the corresponding hidden vertices; thus a new polygon describing the visible portion of the original polygon is obtained. Totally invisible polygons, defined by the hidden vertices of their hidden edges, are not plotted.

Visibility, that is to plot or not to plot, is indicated by putting a one or zero in the fourth column of the plotting matrix. Even though the routine is CPU intensive, this should greatly reduce the plotting time for each frame. It must be emphasized that this addition will save time; it will not change the picture at each time step.

3. Program Details

The program reads input from units 5, 10, and 11. Unit 5 is usually the default input unit in FORTRAN and associated with the terminal in an interactive mode. Units 10 and 11 are attached to data files DTUBE and CTUBE. Each input required is described below.

The user is prompted for an enlargement factor (EF) and the desired tube name (RNAME). Response is expected on unit 5. The y coordinate of the centerline (and eventually the rotations) are multiplied by EF so that the movement will be noticeable to the user. RNAME is used to pick the correct tube description data from the file DTUBE.

The database of tube descriptions is created by the user from the engineering drawings and recorded in the file DTUBE. This input file is attached to unit 10. Each tube is described in the following manner:

Line 1: (A20,I5)
- DNAME = Name of gun tube, i.e. 105mm - M68
- NSEC = Number of sections in tube

Line 2: (I2,1X,A1,1X,4F10.4) - repeated NSEC times
- ISEC = Section number
- TYPE = Cross-section description
  - R -> rectangular
  - T -> trapezoidal
  - D -> discontinuous
- XB = x coordinate at beginning of section
- YB = y coordinate at beginning of section
- XE = x coordinate at end of section
- YE = y coordinate at end of section

Figure 1 shows the diagram of the 105mm gun tube and Table 1 shows the data as entered in the file DTUBE.

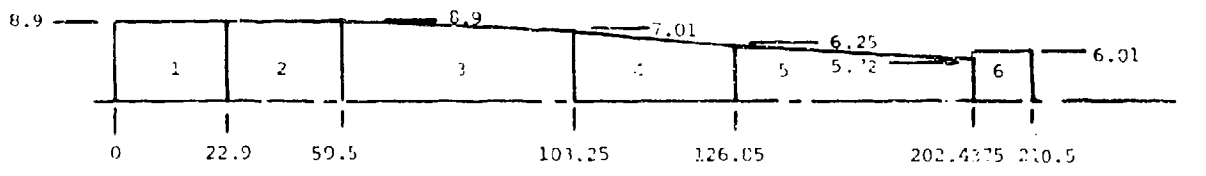

Figure 1. Illustration of the 105mm - M68 Gun Tube.

Table 1. Example of data as entered in file DTUBE.

105mm - M68			6		
1	R	0.0000	8.9000	22.5000	8.9000
2	R	22.5000	8.9000	59.5000	8.9000
3	T	59.0000	8.9000	103.2500	7.0100
4	T	103.2500	7.0100	126.8500	6.2500
5	T	126.8500	6.2500	202.4375	6.0500
6	D	202.4375	6.0500	210.5000	6.0500

The file CTUBE, which is attached to unit 11, is created by the gun modeling program. It must contain the following information:

Line 1: CNODES (6X,I5) = Number of nodes chosen (does not change during the run)

Line 2: TIME (6X,E17.10) = time at each step

Line 3: (6E12.7) -> to be used for a 3-D modeling program
C(J,1) = x coordinate on centerline
C(J,2) = y coordinate on centerline
C(J,3) = z coordinate on centerline
R(J,1) = rotation of point on surface about x axis
R(J,2) = rotation of point on surface about y axis
R(J,3) = rotation of point on surface about z axis
where J = nodal point number < 20 and this line is repeated for each nodal point.

Data at subsequent time steps repeat line 2 once and line 3 CNODES number of times. Line 1 is never repeated. Table 2 shows the data generated by the Boresi modeling program (reference 2) for the 105mm at time zero. This is a 2-D program and the format of line 3 is (11X,2E18.10) since only the x and y coordinates of the centerline are provided.

Table 2. Example of data as expected in file CTUBE from the Boresi model.

8	CNODES	
.0000000000E 00	INITIAL CONDITIONS	
1	.0000000000E+02	.3167988028E-04
2	.2250000000E+02	.2731650263E-03
3	.4090000000E+02	-.1280901859E-03
4	.5950000000E+02	-.1519039589E-02
5	.1032500000E+03	-.8859127947E-02
6	.1268500000E+03	-.1497079945E-01
7	.2024375000E+03	-.4300180835E-01
8	.2105000000E+03	-.4623445425E-01

The program uses the gun tube description data to find the radius at each of the centerline nodal points. It has been assumed that the modeling program will include the end points of each tube section in the nodal point set. The program will create two points at the beginning of each discontinuous section.

Table 3 shows the plotting nodes which have been determined from the tube description data and the gun model data. Note that the y coordinates have been multiplied by the enlargement factor EF=1000.

Table 3. Plotting nodes determined from DTUBE and CTUBE input.

Plotting Node	x	y	z
1	0.00000	0.03168	0.00000
2	22.50000	0.27317	0.00000
3	40.89999	-0.12809	0.00000
4	59.50000	-1.51904	0.00000
5	103.25000	-8.85913	0.00000
6	126.85000	-14.97080	0.00000
7	202.43750	-43.00182	0.00000
8	202.43750	-43.00182	0.00000
9	210.50000	-46.23455	0.00000

The (y,z) coordinates on the surface of the tube at each node x are calculated in subroutine CIRCLE. This subroutine uses a parametric equation of a circle so that the coordinates are evenly spaced around the circumference of the circle rather than evenly spaced on the y-axis. The results are stored in the tube matrix G(KJ,KC,I) where KJ is the node number, KC is the number of the circumference point on the surface, and I indicates the x, y, or z coordinate. The first and last points are identical in order to close the circle.

The plotting array ZP(N,3) is created from the tube matrix G(KJ,KC,3). As stated above, the surface coordinates are arranged in groups of five to describe the polygons which approximate the surface of the tube. The size of N is determined by

5 x (# pts on circle -1) x (# plotting nodes -1).

Assuming that 19 nodes are specified by the gun modeling program and that there is just one discontinuous section, then the number of plotting nodes is 20. The program always calculates 25 points on the circle. Therefore, in this case, N = 5 x 24 x 19 = 2280 and 6840 words are required to store the entire plotting array. It is obvious that the size of N grows quickly and that care must be exercised to keep the arrays within the memory limits of the computer being used. The current limit for N is 2500.

Subroutine GRAPH3D is the driver routine for calculating the homogeneous coordinates which will be displayed on a two-dimensional medium. It expects data in an N x 4 plotting matrix where the first three columns define the x, y, and z coordinates and the fourth column indicates if the point is to be plotted. The subroutine call is

SUBROUTINE GRAPH3D(ZP,IR,T9,ZH,INITL)

where ZP = input data matrix
IR = number of rows in ZP
T9 = 4x4 transformation matrix from subroutine TRANS
ZH = homogeneous coordinate matrix
INITL = 0.

Normally, options can be selected to describe the type and order of transformations to be made to the data. For this application, an isometric projection of the data onto the z=0 plane has been preset. In general, the transformation matrices T(4,4) are calculated and concatenated in the order specified by the user. The options supplied by GRAPH3D are used in subroutine TRANS to select successive 4 x 4 matrix multiplications until the final transformation matrix is calculated. These multiplications are done first in order to avoid successive matrix multiplications with the much larger plotting matrix. It is important that the options specify the transformations in the correct order. The last transformation matrix for a given set of options

$$[T] = [T_1] \times [T_2] \times \ldots \times [T_i]$$

is used in GRAPH3D to calculate the transformed data:

$$[ZP]_{N\times4} \times [T]_{4\times4} = [ZT]_{N\times4}.$$

All transformations assume a right-handed coordinate system; the user is responsible for making any adjustments for left-handed coordinate systems.

The homogeneous coordinates are determined by dividing the elements of each row by the fourth element of that row:

ZH(IROW,ICOL) = ZT(IROW,ICOL)/ZT(IROW,4)
where ICOL = 1 to 4.

Thus, all fourth column elements now equal one. Since the transformation usually includes a projection onto the z = 0 plane, the homogeneous coordinate matrix [ZH] contains the two-dimensional representation of the three-dimensional data in the form [x y 0 1].

Detailed descriptions of the mathematics used for the translation, rotation, and projection matrices used in subroutine GRAPH3D and TRANS can be found in reference 3. This is an excellent text for mathematical techniques required to develop computer graphic algorithms.

Now, since the fourth column information has been preserved in the array ZP(N,4), it can be inserted in the fourth column of the homogeneous array ZH. Finally, the data is ready to be displayed on whatever medium chosen. This data can be passed to a subroutine for actual plotting or written to an output file to be plotted later. Because of the amount of computation required, this program writes to file DGRPGP on unit 12. This decision has given the flexibility to try the graphics using different graphics packages on other computers without worrying about user program space or memory size.

If the user wants to remove hidden lines, this must be done before the data is projected onto the z=0 plane and after all other transformations are calculated. An option is available to do just that in GRAPH3D. Subroutine ROBERT is the implementation of a hidden line algorithm [reference 1] developed by L.G. Roberts at M.I.T. in 1963. This algorithm looks to see if an edge or line is hidden from view by any object in the scene. Each volume or object must be convex in itself; the total scene need not be. Each object is described in several ways:

1. By a volume matrix composed of the plane equations for each plane in the object,
2. By a corner matrix which gives the x, y, and z coordinates of each vertex, and
3. By a plane/vertex matrix which contains the vertex numbers describing each plane.

The general equation for a plane

$$A_j x + B_j y + C_j z + D_j = 0$$

provides the coefficients for each column of the volume matrix

$$[V] = \begin{bmatrix} A_j & A_{j+1} & \cdots \\ B_j & B_{j+1} & \cdots \\ C_j & C_{j+1} & \cdots \\ D_j & D_{j+1} & \cdots \end{bmatrix}$$

where j counts the planes. Using the plotting matrix, which is conveniently ordered by vertices defining each plane, this volume matrix is determined in subroutine VOLMAT. Three vertices on each plane are used to calculate the plane equation coefficients A, B, and C; coefficient D is set to one. The following is applied

$$\begin{bmatrix} X_1 & Y_1 & Z_1 \\ X_2 & Y_2 & Z_2 \\ X_3 & Y_3 & Z_3 \end{bmatrix}^{-1} \begin{bmatrix} -1 \\ -1 \\ -1 \end{bmatrix} = \begin{bmatrix} A \\ B \\ C \end{bmatrix}$$

to each of the j planes describing the object. Since an arbitrary 25 points were chosen for the circumference points, there are 24 planes around the tube and one at each end; therefore the volume matrix is 4 x 26. The volume matrix must be adjusted so that the dot product of the position vector of a point inside the volume and the volume matrix yields a positive result. The point s is found by taking the average for each X, Y, and Z:

$$x = (X_1 + X_2 + \ldots + X_j)/j$$

$$y = (Y_1 + Y_2 + \ldots + Y_j)/j$$

$$z = (Z_1 + Z_2 + \ldots + Z_j)/j$$

and its position vector **s** = [x y z 1]. If **s** [V] < 0, then the corresponding column of the volume matrix is multiplied by -1.

The corner matrix is calculated in subroutine CORMAT. This matrix is simply a reordered subset of the vertices contained in the plotting matrix.

The plane/vertex matrix is determined in subroutine PVMAT. This is another bookkeeping type routine which orders the vertex numbers of each plane counterclockwise. The 'sides' of each object, which is the section of the gun tube between each node, are planes with 24 vertices.

As previously stated, the transformations required are concatenated up to the point of projection onto the z=0 plane. The inverse of the transformation matrix [T] is stored in matrix [T9]. The volume matrix is pre-multiplied by the inverse transformation matrix to give the volume matrix in the transformed space:

$$[T]^{-1} = [T9]$$
$$[T9]\ [V] = [VT].$$

The corner matrix is transformed by post-multiplying it by the transformation matrix:

$$[CN]\ [T] = [CT].$$

Using the plane/vertex matrix, an edge matrix is computed which gives the two vertices describing the edge, the two planes which intersect at the edge, and a flag indicating visibility of the edge. Initially, the flag is set to one to indicate visibility.

The determination of hidden planes is made in subroutine HIDE1. The transformed volume matrix is pre-multiplied by the eye point vector

$$\mathbf{C} = [0\ 0\ 1\ 0]$$

to yield a vector

$$\mathbf{C}\ [VT] = \mathbf{PP}.$$

If each component of the resulting vector, **PP**, is positive, then the planes are not seen. The edges formed by the intersection of these planes are also invisible. The flag for that edge is then set to zero in the edge matrix for the volume being tested.

Testing for visible and non-visible lines begins in subroutine HIDE2. A quick test for complete visibility is done first. Given the two endpoints **s**

and p_2 of an edge, the line between them is visible is both endpoints are visible. The following vectors are calculated:

$$\mathbf{d} = \mathbf{p}_2 - \mathbf{s}$$

$$\mathbf{p}_j = \mathbf{s}\ [VT]$$

$$\mathbf{q}_j = \mathbf{d}\ [VT]$$

$$\mathbf{w}_j = \mathbf{G}\ [VT].$$

If, for any j, the two conditions

1. $\mathbf{P}_j \leq 0 \quad \mathbf{P}$

2. $\mathbf{p}_j + \mathbf{q}_j \leq 0 \quad$ and $\quad \mathbf{w}_j \leq 0 \quad \mathbf{w}$

   where $\mathbf{G} = [0\ 0\ 1\ 0]$

are satisfied, then the line is visible. If the edge is visible, its flag in the edge matrix remains set to one and the next edge is processed. If the edge is not visible, the flag is set to two and further testing is done.

At this point, use is made of a parametric represencation of a line to determine its visibility. Given

$$P(t) = P_1 + (P_2 - P_1)t \text{ where } 0 \leq t \leq 1 \qquad (1)$$

$$\mathbf{V} = \mathbf{s} + \mathbf{d}t$$
$$\text{where } 0 \leq t \leq 1, \quad \alpha \geq 1,$$
$$\mathbf{s} = P_1, \quad \text{and} \quad \mathbf{d} = P_2 - P_1$$

$$Q(\alpha, t) = \mathbf{u} = \mathbf{s} + \mathbf{d}t + \alpha\,\mathbf{G}$$

Substituting,

$$\mathbf{u}\ [VT] = \mathbf{s}\ [VT] + t\mathbf{d}\ [VT] + \alpha\ \mathbf{G}[VT]$$
$$\mathbf{u}\ [VT] = \mathbf{p}_j + t\mathbf{q}_j + \alpha\ \mathbf{w}_j \qquad (2)$$

Equation (2) yields a set of j linear equations to be solved for α and t. Each pair of equations is solved in HIDE3. If there is a solution for the given pair of equations subroutine TLIMIT is called to determine if t is a minimum or a maximum. This subroutine determines the $MAX(t_{min})$ and $MIN(t_{max})$ for the entire set of solutions to equation (2). The portion of the line which is visible is given for the region of t

$$0 \leq t < t_{min} \quad \text{and} \quad t_{max} < t \leq 1$$

and the invisible portion for values of t

$$t_{min} \leq t \leq t_{max}.$$

The endpoints are calculated using $t = t_{min}$ and $t = t_{max}$ and substituting the values in equation (1). The values of t_{min} and t_{max} are used to determine the number of visible segments from each edge. Invisible segments are discarded. Visible segments from each edge are stored in a temporary array and are tested against any remaining volumes before proceeding to the next edge. Those segments which are found to be totally visible are stored in a line matrix in subroutine HIDE2.

After all the edges are checked against all the volumes, except its own, the line segments from the line matrix and any edges which were found to be totally visible after the quick check are put into an array for plotting. Projection onto the z=0 plane is done just prior to writing the plotting array.

4. Conclusions

Although calculations have not been done with as small a time step as will be necessary to produce enough frames for a movie, the method has been demonstrated. The hidden line algorithm has not been applied to this specific problem, but it has been tested for a scene composed of three rectangular parallelipipeds. The routine will have to be modified to handle the 24-sided planes of each tube section.

Only the Boresi gun model has been used for input so far. Thus there has been no test of the rotations; again, the subroutine involved has been used to calculate rotations of other objects and its results have been confirmed.

Simple enhancements are planned like using a contrasting colored stripe on the surface of the tube to show twist and a marker of some sort to show the position of the projectile. Eventually, the motion of the projectile will also be displayed. In this case, the invisible section of the tube will be drawn with the visible portion of the projectile. Highlighting, shading, and surface smoothing are desirable but not planned for the near future.

REFERENCES:

1. L. G. Roberts, "Machine Perception of Three-Dimensional Solids", Lincoln Laboratory, Massachussets Institute of Technology, Technical Report No. 315, May 1963.

2. A. P. Boresi, "Transient Response of a Gun System under Repeated Firing", ARO Contractor Report DAAK-10-77C-0210.

3. David F. Rogers and J. Alan Adams, Mathematical Elements for Computer Graphics, McGraw-Hill, 1976.

CHU

TITLE: An Insight Into Gun Tube Vibrations

DR. Szu Hsiung Chu

Applied Sciences Division

Large Caliber Weapon Systems Laboratory, U.S. ARDC

Dover, New Jersey 07801

ABSTRACT:

A study of the projectile-gun tube interactions using a two point force technique was presented at the Third US Army Symposium on Gun Dynamics. It showed that the large computation-experimental discrepancy of one to two orders of magnitude for vibrations in the M68 gun tube could be eliminated.

This paper presents the work related to the two point force formulation of the general case of the transverse vibration of an elastic gun tube with uniform rifling. It outlines the formulations of projectile motion and tube vibration, presents correlations of computations and tests, and discusses the theory of formulation. The success of the formulations is in the use of elastic deformations to replace the stereomechanical impact for projectile motion and the use of a two point force technique to replace the point mass approximation for tube vibration. The computations show the important effect of projectile c.g. eccentricity and tube-projectile clearance. A detailed computation of the muzzle motion of the M68 gun tube is obtained using a typical pressure-time curve. From the computed results it is seen that the gun vibrations fluctuate depending on the variations of initial conditions. For given realistic initial condition, the computed results are comparable to the test data and there exists no computation-test data discrepancy. The wide range in the variation of the computed results can be explained by recalling the principles of resonance of vibration. The evaluation of the computed results gives an insight into gun tube vibrations.

BIOGRAPHY:

PRESENT ASSIGNMENT: Mechanical Engineer, Applied Sciences Division, Large Caliber Weapon Systems Laboratory, ARDC, Dover, New Jersey

PAST EXPERIENCE: Research studies in applied mechanics related to the analysis of complex gun and ammunition dynamics since joining ARDC (formerly Picatinny Arsenal) in 1967.

DEGREES HELD: B.S., National Chiao-Tung University, Republic of China; M.S., Kansas State University; Ph.D., Polytechnic Institute of Brooklyn, NY

AN INSIGHT INTO GUN TUBE VIBRATIONS

SZU HSIUNG CHU, PH.D.
US ARMY ARMAMENT RESEARCH AND DEVELOPMENT CENTER
LARGE CALIBER WEAPON SYSTEMS LABORATORY
DOVER, NEW JERSEY 07801

INTRODUCTION

The existing state in gun dynamics is that the computation of the transverse gun tube vibration generates results that are one to two orders of magnitude less than the corresponding experimental data (1, 2)*. However, the torsional vibrations of the gun tube have good computation-test agreement (2, 3). In order to improve the computations, a two point force technique was proposed at the Second Meeting of the Gun Dynamics Steering Committee (4). This technique considers a projectile as a rigid body except at the bourrelet and the rotating band where elastic deformations may occur. The transverse projectile-gun tube interactions computed from a six degrees of freedom formulation of such projectile motion are then used as the two exciting forces with opposite sign at the bourrelet and the rotating band locations of the gun tube. Thus, in addition to the effect of the conventional point mass forces, the effect of a moment induced by the base pressure resultant and the projectile c.g. eccentricity is also included. The M483 projectile computations (4) show that the results are dependent on the projectile c.g. eccentricity and agree with the available test data. This technique together with a simple example was later presented at the Third U.S. Army Symposium on Gun Dynamics (5). Reference (6) shows the effect of a moving couple introduced by the projectile eccentricity and (7) presents a six degrees of freedom formulation. Both use similar concepts, and indicate that the technique has many advantages.

This paper documents in more detail the two point force technique and the related gun dynamics work performed in the Applied Sciences Division of the LCWSL, ARDC. Its aim is to present some observations and insights into the gun dynamics field. The modification of current formulations using the point mass approximation may be easily done by substituting the original forcing function with the two transverse interactions at the bourrelet and the rotating band, or by an equivalent force and moment.

This paper will emphasize the principles of problem formulation, descriptions of forces and deformations, and correlations of computations and tests. The equations of motion will be mentioned briefly, since the derivation is rather a general mathematical manipulation once forces and masses are defined.

---

*Numbers in brackets ( ) in the text denotes the reference listed at the end of the paper.

The presentation begins with the formulation of the projectile motion. After the motion and forces are determined, the opposite of the transverse forces acting on the projectile are used to formulate the transverse vibration of an elastic gun tube with uniform rifling. Methods and examples of solution are presented. A detailed result of the computation of the muzzle motion of a M68 gun tube is obtained using a typical pressure-time curve. Various cases of different initial conditions are considered. Some correlations between the computations and the field tests are mentioned. The discussions of the formulations and the computed results indicate the advantages of this formulation and may give some insight into the complicated gun dynamics problem.

FORMULATION OF PROJECTILE MOTION

The forces acting on a projectile during launch are the base pressure, gravity, projectile-tube interaction, air resistance and the inertia force. Knowing these forces are essential for designing projectiles and fuzes, defining initial conditions of exterior ballistics and generating tube vibrations.

In 1971, a research program was initiated to determine the forces to be used in fuze and projectile design. After surveying related literatures, an extensive formulation was performed and documented (8). This formulation has the following features:

1. Six degrees of freedom to replace the conventional three degrees of freedom;

2. Physical reasoning is used to define the applied forces instead of mathematically assuming the three components of a force;

3. Introduction of elastic deformation instead of traditional stereomechanical impact at the bourrelet contact;

4. Emphasis of the projectile c.g. eccentricity from its geometrical axis;

5. Consideration of the effect of non-uniform band engraving of the rotating band;

6. Inclusion of the influence of tube curvature generated by its own weight or temperature difference;

7. Initial position of the projectile;

8. Using the base pressure directly as input to the system of motion equations;

9. Including the effect of transverse tube vibration;

10. Considering rifling effects; and

11. Throw off at muzzle.

The program has undergone successive improvements and documented in (4, 5, 9-15). Additional features as follows are considered:

1. The air resistance or aerodynamic forces at the front portion of the projectile;

2. The friction forces at the bourrelet and the rotating band;

3. The effect of tube wear and copper deposit in a worn tube;

4. The center of the engraved rotating band is not confined to move along the tube axis, and lateral motion is permitted; and

5. The effect of the resisting moment of the rotating band, which opposes the transverse rotation of the projectile.

The six degrees of freedom formulation (8, 11, 15) is based on the basic principles of rigid body dynamics, that is, Newton's second law of motion for translational motions and its complement in the law of moment of momentum for rotational motions. For economic purposes, the products of inertia of the projectile is ignored. Consequently the following Newton's and Euler's equations of motion are used,

$$ma_x = F_x \tag{1}$$

$$ma_y = F_y \tag{2}$$

$$ma_z = F_z \tag{3}$$

$$\dot{h}_1 - \Omega_3 h_2 + \Omega_2 h_3 = M_1 \tag{4}$$

$$\dot{h}_2 - \Omega_1 h_3 + \Omega_3 h_1 = M_2 \tag{5}$$

$$\dot{h}_3 - \Omega_2 h_1 + \Omega_1 h_2 = M_3 \tag{6}$$

where

m = mass of projectile,

a_x, a_y, a_z = accelerations in the x, y, z directions,

F_x, F_y, F_z = forces in the x, y, z directions,

h_1, h_2, h_3 = angular momenta in the 1, 2, 3 directions,

Ω_1, Ω_2, Ω_3 = angular velocities in the 1, 2, 3 directions,

M_1, M_2, M_3 = moments in the 1, 2, 3 directions, and

dot over a quantity denotes its time derivative.

In addition, spinning is governed by the rifling equation,

$$\dot{W}\tan\gamma = R(\dot{\psi} + \dot{\phi}\cos\theta) \qquad (7)$$

where

W = displacement of rotating band in z direction,

γ = twisting angle of rifling,

R = bore radius, and

ψ, ϕ, θ = Euler's angles.

To properly define the motion and forces, several sets of fixed and moving right-handed rectangular coordinate systems and Euler's angles are employed. These coordinate systems are described in Tables 1 and 2. The fixed X, Y, Z coordinate system is the basic reference system and it is fixed to the stationary portion of the gun tube or the ground. The moving X', Y', Z' system is parallel to X, Y, Z system but its origin moves with the driving band. The moving X_1, Y_1, Z_1 system translates with the rotating band but rotates so that the Z_1-axis is always tangent to the gun tube axis. The moving coordinate system, 1, 2, 3 and 1', 2', 3' are parallel to each other but with different origins. The body-fixed 1", 2", 3" system is fixed in the projectile and is equivalent to the 1', 2', 3' system rotated an angle ϕ_1 about its 3'-axis.

The Euler's angles, ψ, ϕ and θ, are defined as follows:

1. ψ is the angle of precession, which is the angle between the nutation axis (intersection line of the driving band plane and the X-Y plane of system X, Y, Z) and the X-axis;

2. ϕ is the angle of spin, which is the angle between the body-fixed 1"-axis in the rotating band plane and the nutation axis, and

3. θ is the angle of nutation which is formed by the Z-axis and the spin axis.

Superscript ' and subscript 1 are used for Euler's angles with respect to the reference coordinate systems X', Y', Z' and X_1, Y_1, Z_1 respectively.

The forces and moments acting on the projectile are basically visualized on the assumption that the projectile has elastic deformation at the bourrelet and the rotating band, and otherwise rigid everywhere. All forces and moments considered are shown in Fig. 1*. The subscripts used in this figure have the following meanings:

A = aerodynamic force or air resistance,

a = inertia force due to motion of gun system,

BRT = bourrelet normal and friction force,

---

*Figures are shown at the end of the paper

TABLE 1. RIGHT-HANDED CARTESIAN COORDINATE SYSTEMS-GUN TUBE AXES

SYSTEM NAME	ORIGIN	FIRST AXIS	SECOND AXIS	THIRD AXIS
X,Y,Z (fixed)	Fixed at point where gun tube axis intersects rotating band plane at t=0	Horizontal, pointing to right when viewed facing muzzle	In vertical plane	Tangent to gun tube axis
X',Y',Z' (moving)	Always at moving point where gun tube axis intersects rotating band plane	Parallel to X-axis	Parallel to Y-axis	Parallel to Z-axis
X_1,Y_1,Z_1 (moving)	Same as origin of X',Y',Z' system	Same as X-axis	In vertical plane	Tangent to tube axis

TABLE 2. RIGHT-HANDED CARTESIAN COORDINATE SYSTEMS-SHELL AXES

SYSTEM NAME	ORIGIN	FIRST AXIS	SECOND AXIS	THIRD AXIS
1,2,3 (moving)	At shell C.G	Parallel to nutation axis 1'	Normal to shell axis	Parallel to shell axis
1',2',3' (moving)	At moving point where gun tube axis intersects rotating band plane. Same as origin of X',Y',Z'	Nutation axis in center plane of rotating band	Parallel to 2-axis	Parallel to 3-axis
1",2",3" (body-fixed)	Fixed on shell at point coinciding with origin of 1',2',3' system	Intersects 3-axis at negative side	Normal to shell axis	Parallel to shell axis (coincides with 3'-axis)

g = gravity force,

p = base pressure,

RB = rotating band normal and friction force,

RF = rifling normal and friction force, and

x,y,z = components in the x,y,z directions

The forces at the bourrelet is worthy of special attention. An elastic deformation or spring force is introduced instead of the traditional use of rigid body contact or stereomechanical impact force (see Discussion section). This technique avoids the jerky computed results. A general configuration of bourrelet deformation is determined by the contact condition for an unevenly engraved rotating band case. The associated bourrelet force is the force resultant acting on the contact area. The simple expression for the normal bourrelet force is:

$$N_b = k_b \delta_b \tag{8}$$

where

N_b = normal bourrelet contact force,

k_b = spring constant, and

δ_b = deflection at the contact.

The rotating band forces may be obtained by integration around the rotating band. To avoid not including the effect of the uniformly distributed forces, the formulation computes the uniformly distributed force and an unbalanced force due to the lateral motion separately. The unbalanced normal force has an expression similar to the normal bourrelet force. Furthermore, for a rotating band of very narrow width, the resisting moment due to uneven force distribution in the tube axis direction may be ignored. In case this moment is not neglected, it is expressed by

$$M_r = C_r \theta \tag{9}$$

where

M_r = resisting moment,

θ = yaw angle, and

C_r = coefficient of resisting moment.

The air resistance or aerodynamic force at the front portion of the projectile is not formulated in the same manner as the base pressure. Rather, it is considered as forces acting on an inclined object moving in the air confined inside the gun tube. Consequently, equations similar to the aerodynamic force formula are used.

The rifling force is determined from the rifling condition (8). When a

projectile is launched in a smooth gun tube, the situation is quite different and the formulation is much simpler (14).

The equations of motion for both drooped and vibrating gun tube cases present additional computation problems over and above the original equations programmed for the fixed straight gun tube. These problems were solved by referring the motion to the ground fixed coordinate systems and using a number of coordinate conversion equations. A simpler set of equations have resulted from considering the relative motion with respect to a moving coordinate system which translates and rotates as it moves along the gun tube axis. This technique computes the projectile c.g. acceleration according to the following general acceleration expression and makes corresponding modifications in the formulation.

The general vector expression for the accleration, a, of a point referred to a moving coordinate system is from the theory of dynamics of a rigid body,

$$a = \ddot{R}_c + \omega \times (\omega \times \rho) + \dot{\omega} \times \rho + \ddot{\rho}_r + 2\omega \times \dot{\rho}_r \tag{10}$$

where

$\ddot{R}_c$ = acceleration vector of origin of the moving coordinate system,

ω = rotation vector of the moving coordinate system,

ρ, $\dot{\rho}_r$, $\ddot{\rho}_r$ = displacement, velocity, acceleration vector of the point relative to the moving coordinate system.

Manipulating the cross product operation and separating the acceleration and associated components in the X_1, Y_1, Z_1 directions, these components of acceleration are

$$a_{X_1} = \ddot{R}_{cX_1} + \ddot{X}_1 - 2\dot{Y}_1\omega_{Z_1} + 2\dot{Z}_1\omega_{Y_1} - X_1(\omega_{Y_1}^2 + \omega_{Z_1}^2) + Y_1(\omega_{X_1}\omega_{Y_1} - \dot{\omega}_{Z_1}) + Z_1(\omega_{Z_1}\omega_{X_1} + \dot{\omega}_{Y_1}) \tag{11}$$

$$a_{Y_1} = \ddot{R}_{cY_1} + \ddot{Y}_1 - 2\dot{Z}_1\omega_{X_1} + 2\dot{X}_1\omega_{Z_1} - Y_1(\omega_{Z_1}^2 + \omega_{X_1}^2) + Z_1(\omega_{Y_1}\omega_{Z_1} - \dot{\omega}_{X_1}) + X_1(\omega_{X_1}\omega_{Y_1} + \dot{\omega}_{Z_1}) \tag{12}$$

$$a_{Z_1} = \ddot{R}_{cZ_1} + \ddot{Z}_1 - 2\dot{X}_1\omega_{Y_1} + 2\dot{Y}_1\omega_{X_1} - Z_1(\omega_{X_1}^2 + \omega_{Y_1}^2) + X_1(\omega_{Z_1}\omega_{X_1} - \dot{\omega}_{Y_1}) + Y_1(\omega_{Y_1}\omega_{Z_1} + \dot{\omega}_{X_1}) \tag{13}$$

In the case of a drooped gun tube which is considered stationary with curvature in the vertical Y_1- Z_1 plane, the motion of the X_1, Y_1, Z_1 coordinate system is confined in this plane and hence its acceleration components are only $\ddot{R}_{cY_1}$ and $\ddot{R}_{cZ_1}$, and the angular velocity and acceleration components are only ω_{X_1} and $\dot{\omega}_{X_1}$. Consequently, the acceleration componen s of the mass center of the projectile reduce to:

$$a_{x_1} = \ddot{X}_1 \tag{14}$$

$$a_{Y_1} = \ddot{R}_{cY_1} + \ddot{Y}_1 - 2\dot{Z}_1\omega_{x_1} - Y_1\omega_{x_1}^2 - Z_1\dot{\omega}_{x_1} \tag{15}$$

$$a_{Z_1} = \ddot{R}_{cz_1} + \ddot{Z}_1 + 2\dot{Y}_1\omega_{x_1} - Z_1\omega_{x_1}^2 + Y_1\dot{\omega}_{x_1} \tag{16}$$

The moving coordinate translation and rotation terms in these equations are determined by differentiating the equation of the tube axis with respect to time and the travel of the projectile. The curvature of the gun tube axis may be experimentally determined or computed. A simpler method is as follows:

The non-uniform gun tube is divided into many segments or stations, counted from the fixed end. The deflection and slope of the gun at station n are determined from the equations for a general cantilever beam, namely (25),

$$Y_n = Y_{n-1} + \theta_{n-1}\ell_n + \frac{M_n\ell_n^2}{2EI_n} + \frac{S_n\ell_n^3}{3EI_n} \tag{17}$$

$$\theta_n = \theta_{n-1} + \frac{M_n\ell_n}{EI_n} + \frac{S_n\ell_n^2}{2EI_n} \tag{18}$$

where

Y = deflection,

θ = slope,

M = moment,

ℓ = length of beam element,

I = section area moment of inertia,

S = shear force, and

n = subscript to denote station.

In the case of a transversly vibrating gun tube the complete Equations (11), (12) and (13) are used. These equations show that the transverse and the torsional vibrations are coupled, since they contain terms with ω_{z_1} and $\dot{\omega}_{z_1}$, which are due to the rotation of gun tube about its axis or torsion. When torsion is not considered, these terms are omitted, and the acceleration components become:

$$a_{x_1} = \ddot{R}_{cx_1} + \ddot{X}_1 + 2\dot{Z}_1\omega_{Y_1} - X_1\omega_{Y_1}^2 + Y_1\omega_{x_1}\omega_{Y_1} + Z_1\dot{\omega}_{Y_1} \tag{19}$$

$$a_{Y_1} = \ddot{R}_{cY_1} + \ddot{Y}_1 - 2\dot{Z}_1\omega_{x_1} - Y_1\omega_{x_1}^2 - Z_1\dot{\omega}_{x_1} + X_1\omega_{x_1}\omega_{Y_1} \tag{20}$$

$$a_{Z_1} = \ddot{R}_{cz_1} + \ddot{Z}_1 - 2\dot{X}_1\omega_{Y_1} + 2\dot{Y}_1\omega_{x_1} - Z_1(\omega_{x_1}^2 + \omega_{Y_1}^2) - X_1\dot{\omega}_{Y_1} + Y_1\dot{\omega}_{x_1} \tag{21}$$

These equations contain coupling terms ω_{x_1} and ω_{Y_1} and their time derivatives. This means that the transverse vibrations in the vertical and

horizontal planes will not be independent and the usual separate computation technique is indeed only an approximation. The moving coordinate system translation and rotation terms are determined by the gun tube vibration which is described in the next section.

At the same time Picatinny Arsenal started this work in 1971, similar investigations were also performed at the Sandia Laboratories, Albuquerque, NM (16, 17, 18), later at Naval Surface Weapons Center, Dahlgran Laboratory, VA (20, 21), and recently at S&D Dynamics, Inc., Huntington, NY (7).

FORMULATION OF TUBE VIBRATION

In most transverse tube vibration studies, the projectile is considered to be a point mass since it is small compared to the gun tube, and the gun tube is approximated as a cantilever beam since it is a long tube with the breech end supported. In reality the transverse vibration of the gun tube is not confined to a plane. However, to simplifiy the formulation, it is usually considered that the tube vibration has components in two perpendicular planes and may be analyzed separately. In general, Euler's or Timoshenko's beam theory is used in the formulation of the equation of vibration. The general equation derived from Euler's theory for the X-Y (vertical) plane vibration is

$$(EIY'')'' + m\ddot{Y} = \delta(X_p - X)F_p \qquad (22)$$

where

m = mass of the gun tube per unit length,

E = Young's modulus,

I = area moment of inertia of the gun tube element section,

X = location of the gun tube element,

X_p = location of the projectile c.g.,

Y = normal or Y-axis displacement of the gun tube element,

F_p = projectile-gun tube interaction force exerted on the gun tube by the projectile, and

$\delta(X_p - X)$ = Dirac delta function.

The gravity force of the beam is usually ignored in the formulation. A similar equation is used for the X-Z (horizontal) plane vibration.

The interaction force F_p may be derived from the point mass approximation (22). An important point is that this formulation ignored the effect of a moment which is the product of the base pressure resultant and the projectile c.g. eccentricity (see Discussion section). This moment is not small for high base pressure cases. Consequently, there is no satisfactory agreement between the computed results and the experimental data (1, 2, 3, 23). Nevertheless, the computation of torsional tube vibration did show good agreement with the test data (3). This difference of agreement is perplexing since all theories and techniques of dynamics are well developed and available.

To improve the formulation, the technique or concept of a two point force approach is introduced (4, 5, 15). The equation of vibration becomes

$$(EIY'')'' + m\ddot{Y} = -\delta(X_p - \ell - X)N_{oy} - \delta(X_p + h - X)N_{by} \tag{23}$$

where

ℓ = axial distance of the projectile c.g. to the rotating band center section,

h = axial distance of the projectile c.g. to the bourrelet,

N_{oy} = Y component of normal force acting at the rotating band, and

N_{by} = Y component of normal force acting at the bourrelet.

The forces $-N_{oy}$ and $-N_{by}$ are the components of the two projectile-gun tube interactions acting at the rotating band and the bourrelet location respectively. They are computed from the projectile motion but with opposite sign. They may also be represented by an equivalent force and a moment at the projectile c.g., since the equivalent of two parallel forces is a force and a moment. However, the two point force representation is preferred, since they represent completely the force actions until the rotating band leaves the muzzle.

The acceleration and rotation of the gun tube are obtained by differentiating the displacement and the slope respectively. These quantities are used in the equations of motion of the projectile as mentioned before.

METHOD OF SOLUTION

Traditionally the computations of the projectile and tube vibration are performed separately. Usually, the equations of motion of the projectile are solved first to obtain the displacement, velocity and acceleration data without considering the effect of tube vibration. The computed projectile data are then used as known values to solve the equation of tube vibration. In reality, there is a coupling effect between the projectile and the tube. This may be seen from the appearance of the coupling terms such as interaction forces in the vibration equation, and tube accelerations and rotation terms in the equations of motion of the projectile. Therefore, for accurate results, all these equations should be solved simultaneously.

The computation time of solving simultaneous equations increases with the number of equations involved. To utilize the existing projectile analysis program and save some computation time, an alternate numerical integration technique is used. This approach solves the equations of motion of the projectile and the tube vibration alternately at each time step of numerical solution. The only data required from the interior ballistics computation or test is the base or chamber pressure. At the first time step the projectile equations are solved with the gun tube at rest or no vibration. At the second time step, the result of the projectile solution at the previous time step is used as the known input data to solve the vibration equations of the tube. The results of this solution is then used to solve the projectile equation. The same procedure is repeated for each time step until the projectile rotating band is out of muzzle. This technique has the advantage of both

simplifying the computation and computing the effect of projectile-tube interaction since the time step of integration is taken small.

Any of the standard numerical integration methods may be used in the solution. A simpler technique is the Euler's method and the constant acceleration technique (24). The basic equations used are

$$\dot{y}_{n+1} = \dot{y}_n + \ddot{y}_n \Delta t \tag{24}$$

$$y_{n+1} = y_n + \dot{y}_n \Delta t + \tfrac{1}{2}\ddot{y}_n (\Delta t)^2 \tag{25}$$

where

Δt = time step size, and

n, n+1 = subscript to denote the time step number.

Modal analysis is used to solve the equation of motion of the gun tube. The natural frequencies and normal functions are solved using the Myklestad's technique. These techniques are well documented in many text books and technical reports, such as Reference 25, and not repeated here. These techniques transform the tube vibration equation into the following equations:

$$Y = \sum_{i=1}^{n} Y_i(X) q_i(t) \tag{26}$$

$$\ddot{q}_i + \omega_i^2 q_i = -\frac{1}{M_i}(N_{oy} Y_{io} + N_{by} Y_{ib}) \tag{27}$$

$$M_i = \sum_{j=1}^{n} m_j Y_{ij}^2 \tag{28}$$

where

Y_i = ith normal function or mode,

q_i = ith normal coordinate or modal response,

ω_i = ith natural frequency,

m_j = jth lumped mass of the gun tube,

M_i = ith generalized mass,

Y_{io}, Y_{ib} = ith normal function or mode at the rotating band, the bourrelet contact point location, and

n = total number of lumped mass of the gun tube.

Computer programs have been generated based on the above mentioned technique to solve the following examples of computations.

EXAMPLES OF COMPUTATIONS

The input data for the computations are the geometrical dimensions, physical properties, initial conditions of the projectile and the gun tube, and the firing pressure. They are obtained from design data, test results or interior ballistic computations of propellant charges. The equations of motion are solved by standard numerical integration methods.

The solution of the projectile motion can calculate all components of the motion and forces. Some of these terms are: projectile travel, velocity and acceleration; c.g. and bourrelet center displacement (polar diagram), bourrelet contact point and deflection; absolute lateral velocity of c.g., normal accelerations of c.g. and some specified axial points; yaw angle, velocity and acceleration; cross spin rate; force components at bourrelet and rotating band; total forces at c.g., etc. These computations could not be obtained with previous formulations. The computed values from this formulation are used as design reference values for projectiles and fuzes. Examples of projectiles that have been computed are the XM673, XM712, M392A2, XM829, M107, M483, M549 and so forth. Some typical curves of the computed values are shown on Fig. 2.

In the computation of gun tube vibration only fixed breech end cases are considered at present. The input data include the outside diameters, area moment of inertia at different element stations along the tube in addition to those required for projectile analysis. The computed results represent the tube configuration at any time, that is displacement, velocity and acceleration of different station points. Special attention is paid to the muzzle motion and its displacement, slope, velocity and acceleration are computed. Some of the computed results of the 120mm and M68 105mm guns are shown in Fig. 3-5 and Table 3.

CORRELATION OF FIELD TESTS

Most of the test data used for cases mentioned in this paper are from design drawings, similar items, and simplifications since no actual test data are available. Even in cases which test data are available, many parameters or constants required in the formulation are not recorded during the test. Therefore, exact comparison between the computations and the tests are not feasible. However, some correlations may be mentioned to show the advantages of this formulation.

During 1974, a thorough flight evaluation was conducted on the 155mm M483 projectile fired in the M185 gun to determine the cause of short rounds previously encountered in cold weather test at Nicolet, Canada. In order to determine the importance of interior ballistic factors on this program, the balloting motion of the projectile was analyzed using the method described in this paper. Interior ballistic performance from various M185 tubes was calculated, including a new tube and tubes with a significant amount of wear. It is noted that tube no. 22530 (11) had a restriction in its center portion (180" to 75" from muzzle), due to the deposit of copper, which tended to reduce the in-bore clearance between projectile and tube. Due to this condition, the frequency of impacts at the bourrelet tended to increase compared to the other tubes of better wear conditions and the magnitude of the contact force at the bourrelet was significantly higher. A comparison of the calculated balloting behavior with test firings is indicated in the following Table 4. It is noted that the coppered tube (Tube No. 22530) produced a higher cross spin rate and higher bourrelet force than a tube with significantly higher wear in both the origin of rifling and the muzzle, and that the calculated performance corresponded with the higher first maximum yaw and higher incidence of short rounds noted in the field firings. After firing an additional 800 rounds, however, the star gaging of the tube indicated that the reduced diameter section was removed and performance appeared to improve.

TABLE 3. PEAK MUZZLE DISPLACEMENTS OF M68 105 MM GUN LAUNCHING M455A2 PROJECTILE

Case No.	Tube Bourrelet Contact	Spring Cogstant 10^5 N/cm	C.G. Eccentricity m	C.G. Position O'Clock	Until Shot Exit				Until Band Exit			
					Vertical Disp. m		Horizontal Disp. m		Vertical Disp. m		Horizontal Disp. m	
					Max	Min	Max	Min	Max	Min	Max	Min
1	No	.49	0	6	.60	-.07	.02	-.48	.60	-.11	.02	-.48
2	No	.49	.01	6	.39	-.25	2.48	-.01	.65	-.25	2.48	-.03
3	No	.49	.013	6	.62	-.40	1.01	-.03	.70	-.40	1.01	-.32
4	No	.49	.015	6	1.47	-.06	.65	-3.52	1.47	-.06	.65	-3.28
5	Yes	.49	.01	6	.01	-.41	.03	-.23	.05	-.56	.03	-.23
6	Yes	.49	.015	6	1.25	-.17	.30	-.01	1.48	-.17	.80	-.30
7	Yes	49	.018	6	1.38	-.07	.51	-1.91	1.38	-.07	.51	-2.22
8	No	.49	.01	3	.21	-.28	.20	-.03	.21	-.28	.20	-.05
9	No	.49	.01	9	.05	-2.30	.47	-.31	.05	-2.87	.92	-.31
10	No	.49	.01	12	1.26	-.02	.67	-.31	1.26	-.28	.67	-.34
11	Yes	.49	.01	3	.02	-.46	.49	-.06	.02	-.51	.65	-.21
12	Yes	.49	.01	9	.05	-.31	.14	-.08	.28	-.32	.40	-.08
13	Yes	.49	.01	12	.03	-.76	.01	-.48	.03	-.97	.14	-.52
14	No	.61	.015	6	1.74	-.58	.35	-2.91	1.74	-.69	.35	-2.91
15	No	.70	.015	6	1.79	-1.93	.21	-2.35	1.79	-3.53	.21	-2.35

NOTE: Tube-bourrelet contact = Yes means that bourrelet is contacting tube initially
= No means that there is no bourrelet-tube contact and projectile axis is nearly parallel to tube axis initially

CHU

TABLE 4. EFFECT OF GUN TUBE CONDITION - M185 GUN

Tube No.	Type	Computation: Peak Bourrelet Impact Force (lbs.)	Computation: Gross Spin Rate at Muzzle (rad/sec)	Field Experience: 1st Max. Yaw, Avg. (deg.)	Field Experience: Short Rd. Rate
22535	New	3100	.71	1.6	1/20
22530	Coppered	8900	1.69	4.7	4/20
22530	600 rds later	5700	1.19	Not Taken	3/60
2282-11	Condemned	5100	1.01	2.0	0/10

An additional instance of correspondence between the analytical predictions and the field experience was found. The M483 projectile used in the field tests at Yuma Proving Ground were all tested for projectile mass balance, and the position and degree of unbalance recorded. It is noted that for initial values of the precession angle, ψ , and spin angle, ϕ , of 0^{o}, 90^{o}; 90^{o}, 0^{o}; 180^{o}, 270^{o}; and 270^{o}, 180^{o} respectively, the center to gravity of an eccentric projectile is in the 12 o'clock position in the gun tube. Average calculated values for initial conditions with the heavy shell side located in the 3, 6, 9 and 12 o'clock positions are given in Table 5. It is noted that the initial orientation calculated to yield a higher value of cross spin rate was found to produce a higher value of first maximum yaw in the field firings.

TABLE 5. EFFECT OF INITIAL PROJECTILE CENTER OF GRAVITY ORIENTATION M483 PROJECTILE

Center of Gravity Orientation (o'clock)	Computed Peak Bourrelet Force (lbs)	Computed Cross Spin Rate (rad/sec)	Field Test Average 1st Max Yaw (deg.)
3	4500	1.08	Not taken
6	4700	.96	3.4
9	3500	1.06	Not taken
12	6900	1.36	4.7

The 155mm projectiles M107, M483A1, and M549, fired in the M198 howitzer, perform differently, especially in the bourrelet engravings found in field tests. An analysis was performed to identify and compare their in-bore lateral motion characteristics (12). Three projectiles with an assumed c.g. (actual data not available) unbalance of 141mm-N (20 in-oz) and 353mm-N (50 in-oz) were analyzed. Both new and worn gun tubes were considered. The computed results are presented in plots and tables for the peak values and variations of the yaw angle and velocity. The computed items include cross-spin rate, the normal accelerations at two axial points (6.35 cm and 25.4 cm to the projectile nose), the lateral forces acting at the rotating band, the

bourrelet (Fig. 2C) and the c.g., and the paths of the c.g. and bourrelet center. These results show that the M549 projectile has the largest balloting effect of the three projectiles, and agree with the field test results that the M549 rounds have more severe engraving at the bourrelet.

All analyses of projectiles with large c.g. eccentricity fired in a new rifled gun tube, show that the bourrelet and the rotating band forces increase toward the muzzle (Fig. 2B). The tube wear at the muzzle end region are due to the friction between the projectile and tube. Consequently, with the rotating band and bourrelet forces increased, the tube wear will be increased accordingly. This corresponds well to the general observation of more tube wear near the muzzle.

A computation in 1977 of the M344A1 projectile in the 106mm M206 cannon showed the bourrelet and the rotating band forces has a maximum value as shown in Fig. 2A. Later, a gun tube failed at the location where the computed force is maximum.

Another interesting correlation may be mentioned here. As shown by computation results, the bourrelet force (Figs. 2B and 2C) is increased with c.g. eccentricity, and travel along the rifling. Therefore there are many pulses of bourrelet force acting along the rifling during launch. If the force pulse is large enough there will be many dents or local bending along the rifling. This may explain the test fact that local bending was observed in the vicinity of the projectile (pp 14 of (27)), and these deflections are not predicted by the Bounoulli-Euler theory.

Tube vibration is of primary concern in gun tube dynamics. The large discrepancy between the computed results and the experimental measurements puzzled investigators for a long time. The computations based on the point mass approximation are much less than the test data (1, 23). However, the computations from the two point force technique are well comparable to the test data depending on the parameters of c.g. eccentricity, projectile-tube clearance, spring constants and so forth. For example, the BRL test data (26) of mean vertical muzzle deflection of the M109A1 howitzer at shot exit is 2.029mm and the computed result with several c.g. eccentricity values are shown in Table 6. The average value of the four computations is 1.972mm.

TABLE 6. COMPUTED MUZZLE VERTICAL DISPLACEMENTS OF 155MM, M109A1 HOWITZER WITH M483 ROUND AT EXIT

Case No.	c.g. Ecc mm (in)	c.g. Imb. mm-N (in-oz)	Defl. mm (in)
1	.154 (.006)	70.61 (10)	.93 (.04)
2	.184 (.007)	84.73 (12)	1.54 (.06)
3	.203 (.008)	91.80 (13)	2.03 (.08)
4	.231 (.009)	105.92 (15)	3.30 (.14)

NOTE: Projectile launched with zone 3 charge, c.g. at 6 o'clock position

The most described and computed case in literature is the transverse gun vibration of the M68 105mm gun with a M392A2 projectile. Test data and computations are well reported (23). A detailed computation on the fixed breech end case using the method mentioned in this paper are performed to compare the results. The peak test data for the vertical and the horizontal muzzle displacements are 2.25 and .25mm respectively (Test No. Ident 06 of (23)). The input data used for analyses are from design drawings, similar items, and simplifications. Some of the computed results are shown in Table 3 and also shown in Figures 4 to 5. From the table and figures it is seen that depending on the bourrelet contact conditions, e.g. eccentricity, spring constants and initial projectile positions, the computed peak muzzle displacement values are either larger or smaller than the test data. Whereas the computations of point mass approximation always give smaller values. This shows that the method mentioned in this paper has the capability to compute the comparable values. The problem is how to obtain proper input data of computation.

DISCUSSIONS

A major difficulty in solving gun dynamics problems is how to define the force relations among the various components of the gun system and how they behave during firing.

The point mass approximation has the advantage of simplifying the formulation and the subsequent solution of the resulting equations. However, in considering an object as a point mass, some characteristics of the object may be inadvertently ignored. In gun dynamics, the projectile is small compared to the gun tube and the yaw motion is severely restricted by the tube-bourrelet clearance, and hence traditionally the point mass approximation is used. This leads to two disadvantages in the solution.

The first adverse effect is in the formulation of the motion of the projectile. Traditionally, a projectile is first considered as a point mass to compute the forward acceleration. To compensate for spin effect, an equivalent (heavier) mass is used. Later, the centrifugal force is added to account for the c.g. eccentricity effect. Furthermore, to compute the yaw effect, it is considered as a spinning body with a yaw motion. The point mass approximation excludes body deformation. This leads to the solid body contact force or the stereomechanical impact formulation to describe the bourrelet and rotating forces. The solid body contact force formulation computes a less varied or fixed yaw angle while the stereomechanical impact approach computes jerky motion. The stereomechanical impact formulation is incapable of describing the transient forces or deformations produced, and is limited to a specification of initial and terminal velocity states of the objects and the applied linear or angular impulse (28). Furthermore, the gun is fired in a rather short time duration, and thus not including the transient deformation leads to inaccurate computation. Satisfactory computations are therefore unobtainable. The method mentioned in this paper uses the six degrees of freedom formulation and considers the projectile as a rigid body except at the bourrelet and the rotating band where deformation exists, and consequently introduces the elastic contact or spring forces instead of the stereomechanical impact forces. The successful computations mentioned in previous sections and the fact that the stereomechanical impact formulations

are subsequently replaced by similar elastic forces by others in the field show that this technique of formulation is practical and useful. However, the small time step size of numerical integration is essential to the computation. Unless some check measure is employed in the computer program to make sure the time step size is small enough, the computation will be incorrect.

Next, the point mass approximation has a great influence on the transverse tube vibration formulation. Traditionally the projectile is always considered as a point mass in the problem formulation since, as mentioned above, the projectile is apparently very small compared to the gun tube and there is serious restrictions of yaw motion. The approximation does have the advantage of simplifying the formulation by reducing the number of equations of motion. However, the tube-projectile interactions or the transverse forces exerted on the gun tube by the projectile are only one force resultant. Consequently, the moment effect which is the product of the base pressure resultant and the projectile c.g. eccentricity, is inadvertently ignored. Unfortunately, this moment is so large that it should not be ignored for large guns or in cases when high base pressure is used. An approximate computation of this neglected moment of several projectiles is shown in Table 7.

TABLE 7. MOMENTS DUE TO PROJECTILE C.G. ECCENTRICITY AND BASE PRESSURE

Projectile	Time, ms	Base Pressure, psi (MPa)	Moment, in-lb (m-kg)
M106	4.9	37300 (257)	18590 (214)
M107	4.9	35350 (244)	10240 (118)
M392A2	3.9	49600 (342)	4480 (52)
M456	2.2	54140 (373)	7230 (84)
XM549	5.0	38250 (264)	11020 (127)

NOTE: All moments computed with .01 in c.g. eccentricity and firing pressure from Heppner, Leo D., "Methodology Investigation on Setback and Spin for Artillery Mortar, Recoilless Rifle, and Tank Ammunition", TECOM Proj. No. 9-CO-011-075, Report No. APG-MT-4503, Materiel Testing Directorate, APG, MD, Sept. 1974.

The tube vibration depends on the forcing function. With less exciting force the vibration decreases accordingly. This is why all computations using the point mass approximation gave results of much less value than the

experimental data (1, 2, 23).

The concept of point mass approximation is deeply rooted in gun tube vibration investigations. This is seen by the fact that though the rotating band and bourrelet forces have been computed using the six degrees of freedom formulation, yet these forces are not used as the two interaction forces to excite the tube vibration. Instead, a single force which is their resultant is used.

Tables 3 and 6, and Figs. 4 and 5 show that the computation results of gun vibrations fluctuate depending on the variations of initial conditions. For certain initial conditions, the computed result may be larger, less than or match the test data, and there exists no computation-test data discrepancy. The wide range of variation of the computed results is not difficult to explain if one recalls the principle of resonance of vibration. The balloting motion, spinning, rifling reaction and different natural frequencies of vibration may cause many variations. This insight into gun vibrations may help to pin-point important conditions for good weapon system design. The successful computations using the method described in this paper and the apparent importance of the initial conditions indicate that this method is a proper way to persue more accurate computations. The problem now is how to obtain more accurate data to be used for computations and perform more tests to get actual data to refine the details of the formulation.

Many coefficients or constants used in the method are assumed to be obtained, before computation, from experimental measurements, similar items or may be computed using general elasticity equations or finite element programs. Either average value or tabulated values may be used. The method of computing coefficients at each time step is not used and these constants are saved once they have been computed previously. This reduces computing time.

The resisting moment at the rotation band which acts against the transverse turning of the projectile may be obtained by either test or computations. Since the yaw angle is rather small, this moment is ignored in the computation by using a zero coefficient of resistant moment. This omittance may have rather small effect when the width of the rotating band is small compared to the bourrelet-rotating band distance.

In the formulation of the aerodynamic forces or air resistance, which acts on the front portion of the projectile, a technique similar to that of aerodynamics is used instead of computing a uniformly distributed air pressure on a flat surface. The air is compressed through the uneven tube-bourrelet clearance and acts on the cylindrical portion of the projectile, in addition to acting on the nose portion. The projectile is not always parallel to the tube axis, or there is a yaw motion. Thus the air pressure is not necessarily uniformly applied on the front portion of the projectile. In theory the total force should be obtained from the integration of air pressure on all surfaces of this front portion. This procedure is similar to computing aerodynamic forces. The problem now is how to determine experimentally the related coefficients and parameters. At present, there is no data available, and some assumed values based on test data of solid objects moving in air are used, or the forces are ignored by using zero coefficients.

From all computations, it is seen that the projectile c.g. eccentricity and bourrelet contact are essential to the projectile motion and the tube vibration. The moment induced by the base pressure resultant or setback force at the projectile c.g., depends on the location of the projectile c.g. with respect to the projectile itself and the tube axis. The spring constants, tube-bourrelet clearance, engraving of rotating band, etc., further affect this state. To reduce the projectile balloting motion and tube vibrations it is essential to decrease c.g. eccentricity, and the tube-bourrelet clearance.

CONCLUSION

Successful computations in gun dynamics depends on the proper formulations of forces acting at the projectile, and the description of the projectile-gun tube interaction forces which excite the tube vibration. The introduction of an elastic deformation force at the bourrelet and the rotating band instead of the traditional stereomechanical impact make the computation practical and accurate. Projectile in-bore motions, such as that of M483, XM673, XM712, M107, etc., have been computed. There are many correlations between the computations and the field tests.

The introduction of the two point force technique to replace the point mass approximation includes the important effect of moment which is the product of the base pressure resultant and the projectile c.g. eccentricity. This increases the exciting force of tube vibration and thus the computed results are no longer small as computed with the traditional point mass approximation. Thus, this technique can eliminate the computation-test discrepancy which has long puzzled scientists and engineers in the field. The computations of the M109A gun with the M483 projectile and the M68 gun with the M392A2 projectile both show that the computed results can exceed, be less than or match the test data, depending on the variations of parameters, such as spring constants, projectile-gun tube clearance, etc., and especially the projectile c.g. eccentricity.

From all computations, it is seen that the magnitude of the projectile c.g. eccentricity and tube-projectile clearance have a large effect on the projectile balloting motion and the tube vibration. The moment induced by the base pressure resultant or setback force at the projectile c.g. depends on the location of the projectile c.g. with respect to the projectile itself and the tube axis. The spring constants, tube-bourrelet clearance, and the engraving of rotating band further affect the condition. To reduce the projectile balloting and tube vibrations, it is essential to decrease the effect of these parameters, especially the c.g. eccentricity and tube-projectile clearance.

ACKNOWLEDGEMENTS

The author would like to express his special appreciation to Mr. Bruce Knutelsky for his advice and assistance in preparing this paper. Mrs. Donna Baker and Mrs. Carol Pellegrino are hereby thanked for their patience in word processing of the manuscript.

REFERENCES

1. Simkins, T. E., "Minutes of First Meeting, Gun Dynamics Steering Committee - 26 June 1979", ARRADCOM LCWSL, Benet Weapons Laboratory, Watervliet, NY,

June 1979.

2. Boresi, A. P., "A Review of Selected Works on Gun Dynamics", Contract Report ARBRL-CR-00500, BRL, APG, MD, Jan 1983.

3. Haden, H. G., "Some Theoretical Studies of Gun Barrel Vibration", Royal Armament Research and Development Establishment Memorandum (P) 45/63, August 1963.

4. Chu, Szu Hsiung, "A New Concept in Gun Dynamics", presentation at the Second Meeting of Gun Dynamics Steering Committee, BRL, APG, MD, Oct 9, 1980.

5. Chu, Szu Hsiung, "New Approach for Analysis of Transverse Projectile-Tube Interactions", pp. III-105 to III-125 of Proceedings of the Third U.S. Army Symposium on Gun Dynamics, Vol. II of II, Report No. ARLCB-SP-82005, US ARRADCOM, LCWSL, Benet Weapons Laboratory, Watervliet, NY, May 1982.

6. Wu, Julian J., "On Dynamic Forces in Gun Tube Motions Analysis", pp. III-86 to III-104 of Proceedings of the Third U.S. Army Symposium on Gun Dynamics, Vol. II of II, Report No. ARLCB-SP-82005, US ARRADCOM, LCWSL, Benet Weapons Laboratory, Watervliet, NY, May 1982.

7. Seifer, Martin T. and Becker, Robert S., "Projectile Motion in a Flexible Gun Tube", Contract Report BRL-CR-536, BRL, APG, MD, Oct. 1984.

8. Chu, S. H. and Soechting, F.K., "Transverse Motion of an Accelerating Shell", Technical Report 4314, Picatinny Arsenal, Dover, N.J., June 1972.

9. Chu, S. H., "Transverse Motion of 8-inch Projectile, XM673, Inside XM201, M2A2 Gun Tube, MK-16 and MCLG Gun", Technical Memorandum 2103, Picatinny Arsenal, Dover, NJ, August 1973.

10. Chu, S. H., "Transverse Motion of Eight-Inch Projectile, XM753, in Gun TubeXM201", Technical Report 4918, Picatinny Arsenal, Dover, NJ, December 1975.

11. Chu, S. H., "Balloting Motion of an Accelerating Shell", preprints of papers to be presented at the Fuze/Munitions Environment Characterization Symposium II, U.S. Army Armament Research and Development Command, Picatinny Arsenal, Dover, NJ, 7-9 October 1975, pp 648-670.

12. Chu, S. H., "In-Bore Motion Analysis of XM712 Projectile in the M198 Gun", Technical Report ARLCD-TR-80005, ARRADCOM, Dover, NJ, November 1981.

13. Chu, Szu Hsiung, "In-Bore Motion Analysis of 155mm Projectiles M107, M483A1 and M549 in M198 Gun", Technical Report ARLCD-TR-80048, ARRADCOM, Dover, NJ, October 1981.

14. Chu, Szu Hsiung, "Mathematical Modeling of In-Bore Projectile Motion in a Smooth Gun Tube", Technical Report ARLCD-TR-83023, ARRADCOM, Dover, NJ, June 1983.

15. Chu, Szu Hsiung, "In-Bore Projectile Motion in a Transversely Vibrating Gun Tube", Technical Report in preparation.

16. Perdreauville, F. J., "Analysis of the Lateral Motion of a Projectile in the Gun Tube", Research Report SC-RR-710071, Sandia Laboratories, Albuquerque, NM, April 1971.

17. Perdreauville, F. J., "Analysis of the Lateral Motion of an Unbalanced Projectile in a Rigid Gun Tube", Report SAND 74-0361, Sandia Laboratories, Albuquerque, NM, December 1974.

18. Perdreauville, F. J., "Analysis of the Lateral Motion of an Unbalanced Projectile in an Elastic Gun Tube", Report SAND 74-0362, Sandia Laboratories, Albuquerque, NM, December 1974.

19. Haug, E.J., editor, "Proceedings, First Conference on Dynamics of Precision Gun Weapons", Report No. P-TR-77-008, US Army Armament Research and Development Command, Dover, NJ, February 1977.

20. Hoo, G. S., "A Theoretical Model for In-Bore Projectile Balloting and Barrel Motion", pp. 46-80 of (19).

21. Hoo, George Soo & Anderson, Leon P., "A Theoretical Model for In-Bore Projectile Balloting", Report No. NSWC TR-79-186, Naval Surface Weapons Center, June 1979.

22. Simkins, T., Pflegl, G., and Scanlon, R., "Dynamic Response of the M113 Gun Tube to Travelling Ballistic Pressure and Data Smoothing as Applied to XM150 Acceleration Data", Technical Report WVT-TR-75015, Benet Weapons Laboratory, Watervliet Arsenal, Watervliet, NY, April 1975.

23. Cox, P.A., and Hokanson, J.C., "Muzzle Motions of the M68 105mm Tank Gun", Contract Report ARBRL-CR-00418, US Army Armament Research and Development Command, Ballistic Research Laboratory, Aberdeen Proving Ground, Aberdeen, MD.

24. Greenwood, Donald T., Principles of Dynamics, Prentice-Hall, Inc., Englewood Cliffs, NJ, 1965.

25. Timoshenko, S.P., Vibration Problems in Engineering, 3d ed, Van Nostrand, Princeton, NJ, 1955.

26. Haug, Bailey T. and Brosseau, Timothy L., "Muzzle Motion of the 155mm, M109A1 Self-Propelled Howitzer during the Firing of the M483 Round", Interim Memorandum Report No. 306, BRL, APG, MD, Nov. 1974.

27. Elder, A. S., "Historical Review and Survey of Current Problems in Weapon Dynamics", pp. 1-26 of (19).

28. Goldsmith, Werner, Impact - The Theory and Physical Behavior of Colliding Solids, Edward Arnold (Publishers) Ltd, London, 1960.

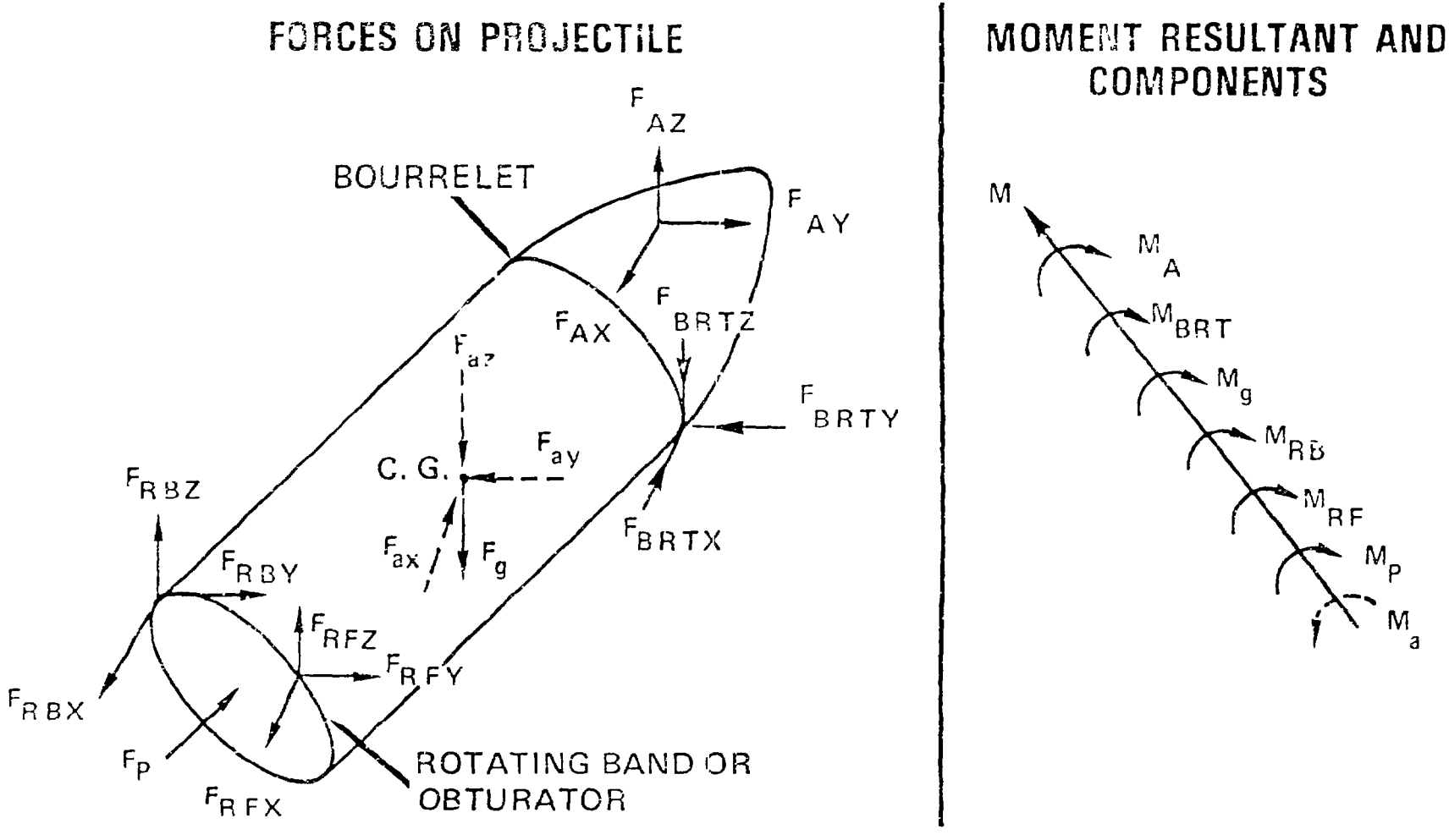

FIGURE 1. FORCES AND MOMENTS ON PROJECTILE

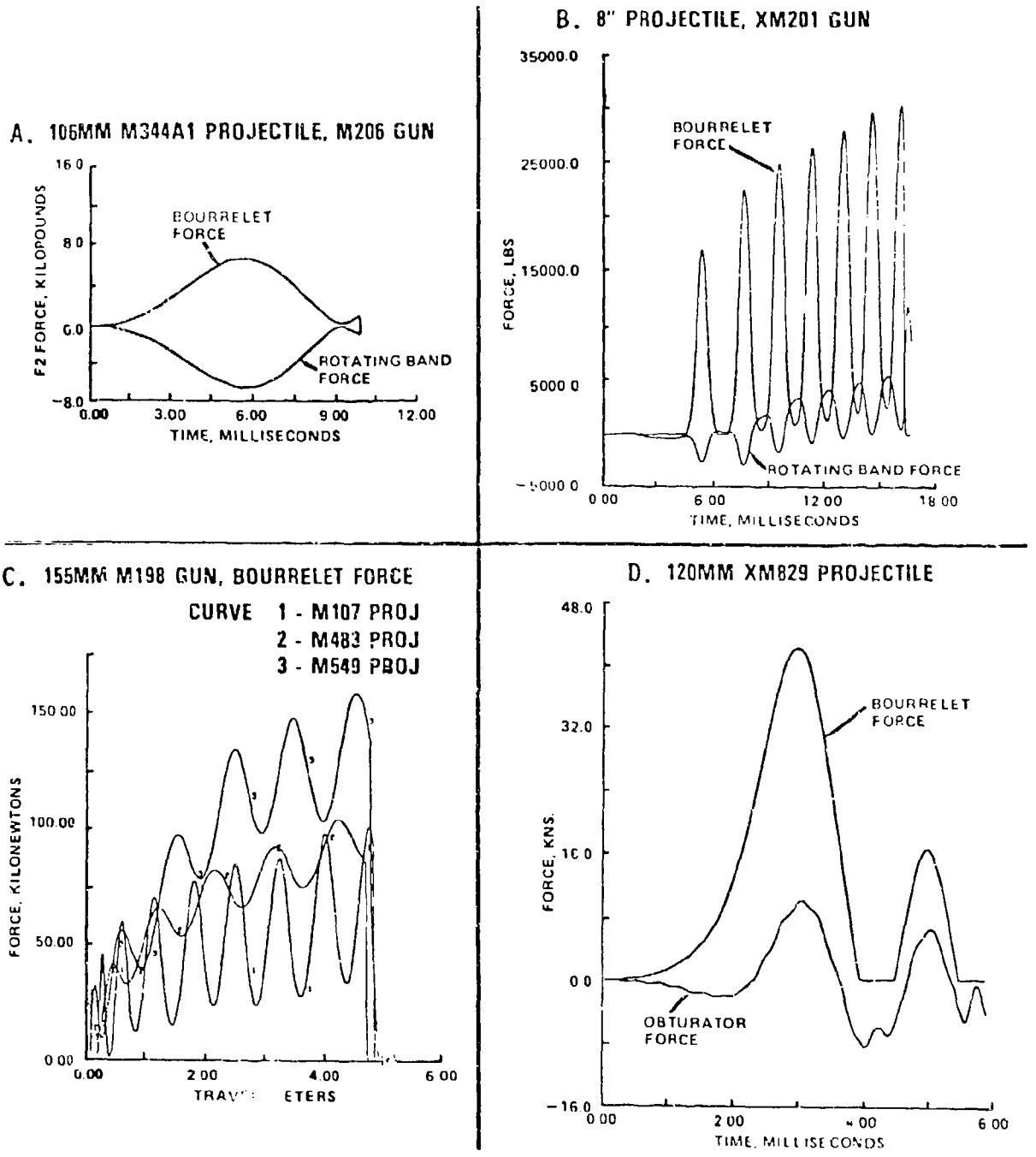

FIGURE 2. LATERAL FORCES ON PROJECTILES

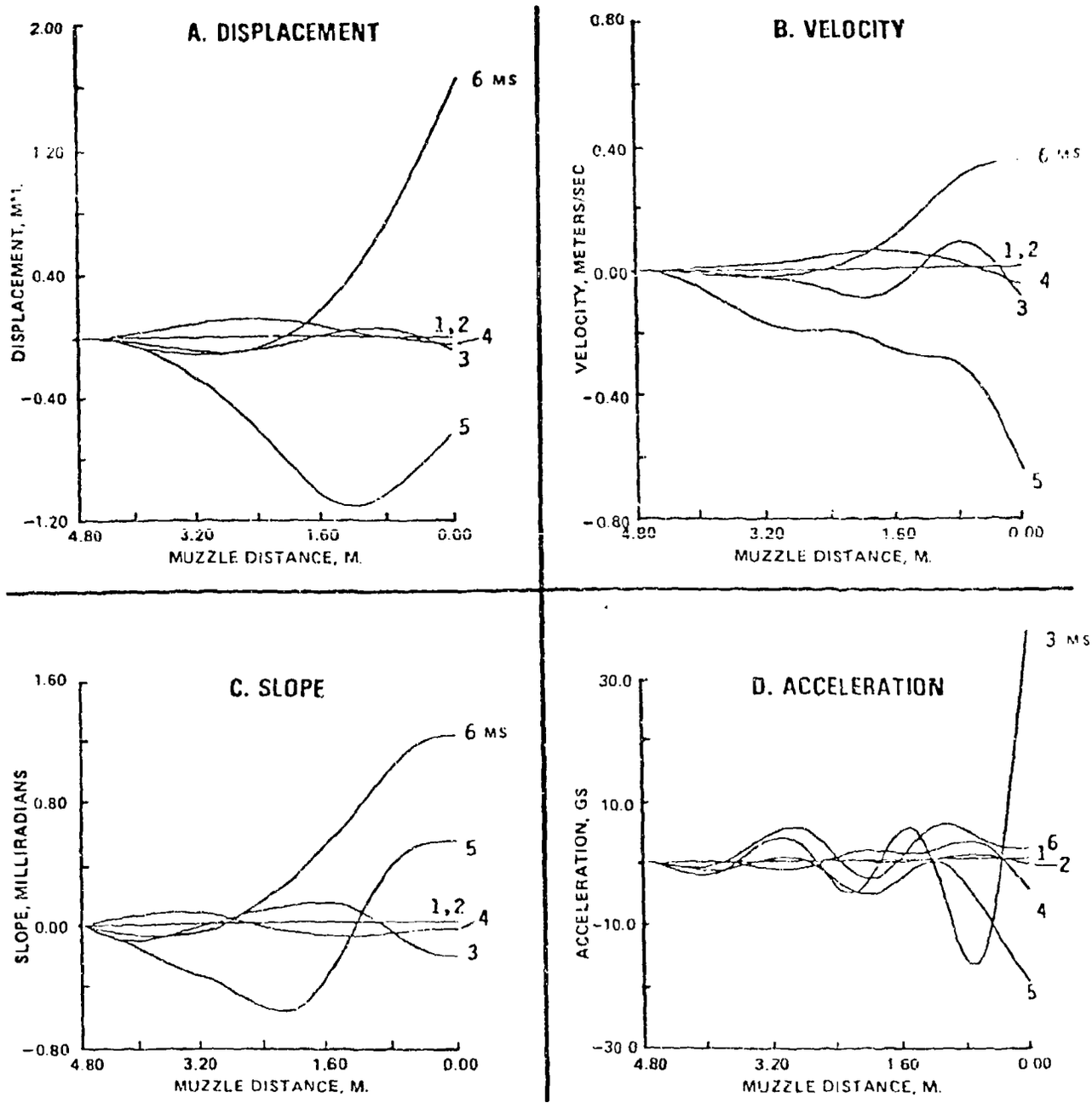

FIGURE 3. 120mm GUN TUBE VIBRATION WITH XM829 PROJECTILE

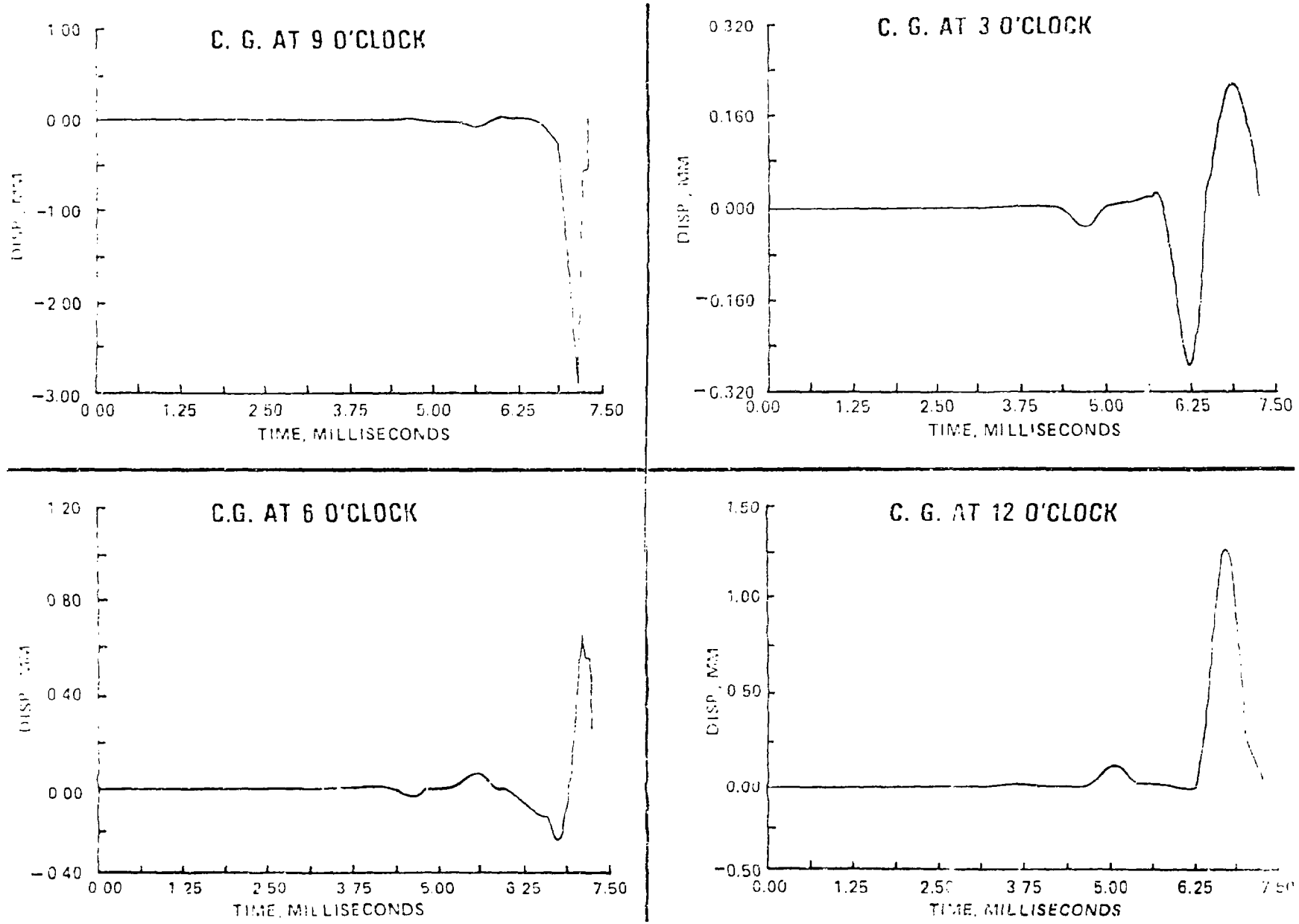

FIGURE 4. VERTICAL MUZZLE DISPLACEMENT - M68 TUBE, M392A2 PROJECTILE (INITIAL PROJ C.G. POSITION EFFECT)

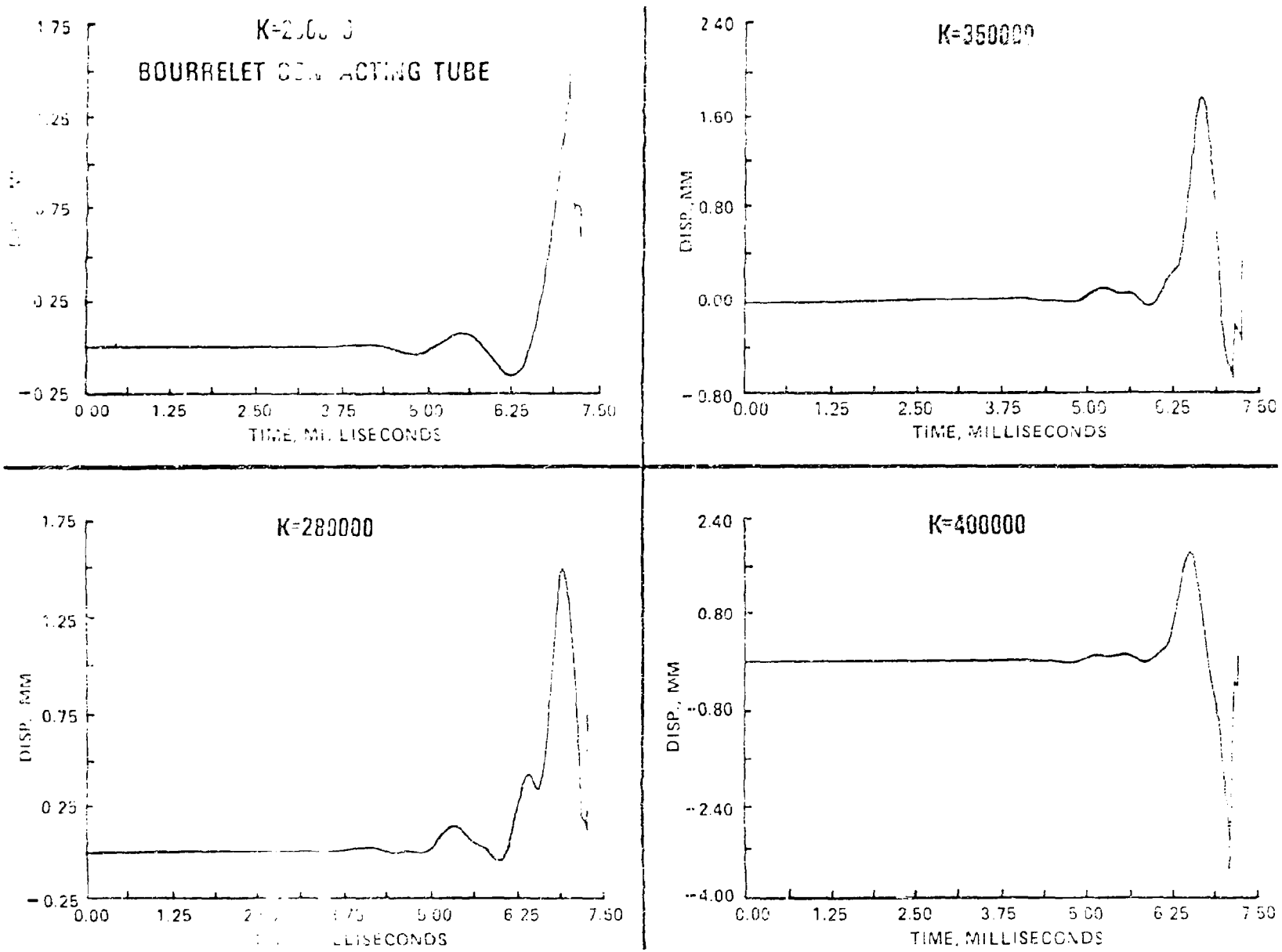

FIGURE 5. VERTICAL MUZZLE DISPLACEMENT - M68 TUBE, M392A2 PROJECTILE (BOURRELET SPRING CONSTANT EFFECT)

FLOROFF-LIONETTI

TITLE: Light Artillery Recoil Mechanisms

STEPHEN G. FLOROFF
NORMAN T. LIONETTI
U.S. Army Armament Research and Development Center
Large Caliber Weapons Systems Laboratory
Dover, NJ 07801-5001

ABSTRACT:

Traditionally, the terms lightweight and long range, when applied to artillery weapons, have been mutually exclusive goals. To obtain a significant increase in range, the impulse applied to the weapon structure must also increase. This increased impulse negatively affects the stability of the piece. Compounding the stability problem is the decreased weapon mass due to the lightweight system requirement. Significant weight reduction can be accomplished through the use of lightweight materials (i.e. composites), a reduction in design safety factors, or a combination of both. The load applied to the weapon structure becomes critical as safety factors and state-of-the-art lightweight materials are utilized.

Traditional recoil design involves throttling hydraulic oil through a variable orifice. This orifice is a function of recoil stroke and is mechanically a fixed system. In essence, the orifice profile is pre-programmed and designed around ideal parameters which rarely exist. The result is a non-optimized energy dissipation system which cannot be tolerated in a lightweight weapon.

This paper presents the concept of a microprocessor controlled servovalve, which, through closed loop feedback control principles will ensure consistent operation. Two control algorithms are presented and their application to recoil mechanism design are discussed. Finally, the concept of "super-long" recoil and "soft" recoil, augmented with microprocessor control, are investigated.

BIOGRAPHY:

PRESENT ASSIGNMENT: Mechanical Engineer, Army Research and Development Center, DRDAR, Weapons Division, Dover, NJ

DEGREE HELD: BSME Newark College of Engineering, New Jersey Institute of Technology (1978).

LIGHT ARTILLERY RECOIL MECHANISMS

STEPHEN G. FLOROFF
NORMAN T LIONETTI
U.S.ARMY ARMAMENT RESEARCH AND DEVELOPMENT CENTER
LARGE CALIBER WEAPONS SYSTEMS LABORATORY
WEAPONS DIVISION
DOVER, N.J. 07801-5001

1 Introduction

Traditionally, the terms lightweight and long range, when applied to artillery weapons, have been mutually exclusive . In order to obtain long range capability, the impulse applied to the projectile must be large. Due to the realities of conservation of momentum, this same impulse is also imposed upon the supporting structure. This applied impulse has a negative affect upon stability. Compounding the stability problem is a decrease in weapon mass resulting from lightweight design requirements. Reduced firing loads are mandatory if truly lightweight artillery with acceptable range characteristics is to be realized. Consequently novel approaches to recoil energy management are necessary.

The numerous design considerations essential to attaining a lightweight, long range weapon are outlined in the following sections of this paper.In section 2, performance characteristics for a lightweight 155mm howitzer are discussed and methods of obtaining these characteristics are described. In section 3, basic recoil mechanism design is reviewed and shortcomings of present systems are presented. In section 4, the concept of electronic feedback recoil control is introduced. Finally, in section 5, two approaches to lightweight recoil mechanism design, augmented with electronic control, are described.

2. Design Approach for a Lightweight Howitzer

The Army Research and Development Center, Dover, NJ, is developing a full scale lightgweight, 155mm towed howitzer feasibility demonstrator. The weapon must have the same performance characterisitcs as the M198 towed howitzer but weigh 9,000 pounds. Selected performance criteria of the M198 are listed below.

M198 Towed Howitzer

Total weight -	16,000 lb
Maximum breech force -	1,500,000 lb
Maximum applied impulse- (with muzzle brake)	11,400 lb-sec
Weight of recoiling parts-	7,000 lb
Maximum trunnion force-	80,000 lb

Thus, overall weight reduction of approximately 44 percent is the desired goal. The use of state-of-the-art composite materials including glass/epoxy, graphite/epoxy, Kevlar and metal matrix are being investigated as alternatives to more traditional homogeneous metal construction. Further weight savings can be realized by reducing structural safety factors. Through the use of finite element analysis, critical areas of the weapon can be determined and maximum stress levels can be established. This analysis presupposes a specific input force; this force being generated through the recoil mechanism. If structural safety factors are reduced it is imperative that the applied load be consistent. Unfortunately traditional recoil mechanism design cannot be relied upon to provide consistent applied force.

3. Recoil Mechanism Design

Conventional large caliber artillery recoil mechanisms are comprised of three basic components; a recoil brake, a counterrecoil mechanism, and a counterrecoil buffer. The recoil brake provides controlled resistance to weapon recoil by throttling hydraulic fluid through a variable orifice. The counterrecoil mechanism, or "recuperator" returns the recoiling parts to the initial firing position by storing and releasing a portion of the recoil energy. The counterrecoil buffer reduces counterrecoil velocity of the moving parts to zero through a hydraulic fluid throttling process similar to the recoil brake.

Ideally the recoil brake should throttle hydraulic oil such that a rectangular retarding force verses recoil distance is obtained. See figure 1. Since the area under this curve represents the work necessary to stop the recoiling mass , a rectangular curve will yield the lowest retarding force for a given recoil length. Theoretically, the only limit to this reduction in retarding force is the physical constraints associated with length of recoil. These constraints are attributable primarily to weapon configuration.

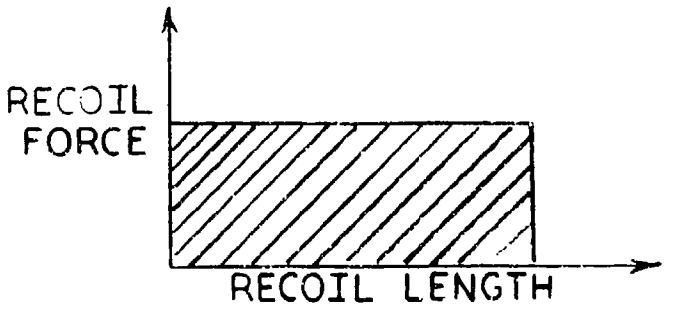

Figure 1 -"Ideal" Force Versus Stroke Relationship

The M198 towed howitzer, as an example, can accomodate the following recoil lengths

Propelling Charge Designation	Nominal Recoil Length (in)
M3	25
M4	45
M119	62 (reduced to 50 for high elevation)
M203	70 (reduced to 50 for high elevation)

Reduced recoil length at high firing elevations is necessary to prevent the recoiling parts from striking the ground. Thus the weapon supporting structure must be designed to withstand this "worst case" retarding force. In the instance of the M198 towed howitzer, the worst case is the retarding force associated with the impulse from the M203 charge and a 50- inch (nominal) recoil length.

In order to generate a constant retarding force, a variable throttling orifice is required. This is necessary due to the very high input force which must be attenuated. The procedure for determining a preliminary orifice "profile" is well established, (refs. 1,2,and 3) and is not repeated here. However, it must be stated that for any preliminary recoil brake orifice profile design, two parameters are essential:

- Total applied impulse (lb-sec)
- Total length available for recoil (in)

This information is just the first of numerous assumptions

made in the design process. Ultimately due to practical realities of machining operations, hydraulic fluid compressibility, and turbulent fluid flow, many iterations are necessary to obtain a workable system. Computer models must be modified with fluid discharge coefficients to obtain a suitable match to live fire data.

As discussed previously, maximum force reduction is possible only when maximum recoil stroke is utilized. While the orifice profile is designed to do just that, many system variables tend to upset this ideal force versus stroke relationship. These include

- Variations in maximum impulse due to production tolerances in propellant manufacture.
- Propellant temperature variations due to varying climatic conditions which change the maximum impulse profile.
- Manufacturing tolerances in the throttling orifice(s).
- Temperature induced hydraulic fluid viscosity changes.

In essence, the recoil brake throttling orifice is a pre-programmed device designed around ideal parameters which rarely exist. This may result in a non-optimized force versus stroke relationship during firing. If weapon weight and stability are not concerns, this approach to recoil design is satisfactory. The lightweight artillery challenge however, requires an effective and consistent energy dissipation system.

4. Microprocessor Control of Weapon Recoil Energy

In order to ensure consistent recoil operation regardless of the system variables mentioned above, the concept of closed-loop feedback control has been investigated. The concept of throttling recoil oil through a constantly variable orifice controlled by a feedback system is not new. It was described in a 1977 Rock Island Arsenal Technical Report (ref.4) but was never pursued. The reason for this, in the author's opinion, was twofold.

- Microprocessor technology was not then sufficiently developed
- The high degree of "finesse" alluded to was unnecessary

The advantages of electronic control include the following:

a. Variable recoil length - Many artillery recoil mechanisms have provision to shorten the recoil stroke for high elevation firings. As discussed in section 3, this is necessary to prevent the recoiling parts from contacting the ground during recoil. The mechanism necessary to accomplish this reduction in stroke adds considerable mechanical complexity to the recoil system. This can be alleviated by providing the microprocessor with a weapon elevation input. The microprocessor could then perform the trigonometric calculations necessary to determine available recoil length. Recoil resistance could be adjusted accordingly.

b. Counterrecoil control - The system used to control recoil could be used to control counterrecoil as well. Throttling of hydraulic oil can be programmed to ensure consistent buffing action and return-to-battery. This would eliminate the need for separate counterrecoil passages, thus further reducing mechanical complexity.

c. Elimination of control orifices - Traditional artillery recoil mechanisms employ control rods or grooves to throttle oil. These orifices are precision machined and therefore costly to manufacture. Furthermore the final design is often done by tedious iteration with prototype hardware. This is both expensive and time consuming. Precision-made control orifices can be eliminated through incorporation of a constantly variable throttling orifice.

d. "Tailoring" of the recoil force versus stroke profile- As discussed in section 2, one approach to weight savings to to apply a consistent load such that structural safety factors can be reduced. The weight savings gained through incorporation of reduced safety factors is of little value, however, if weapon stability is not maintained. Practically speaking, the weapon must not "jump" or "hop" when fired. Unfortunately, a lightweight artillery piece is, by nature, more prone to instability due to the reduction of overall mass. Consider the free body diagram of forces acting on the weapon (fig.2.)

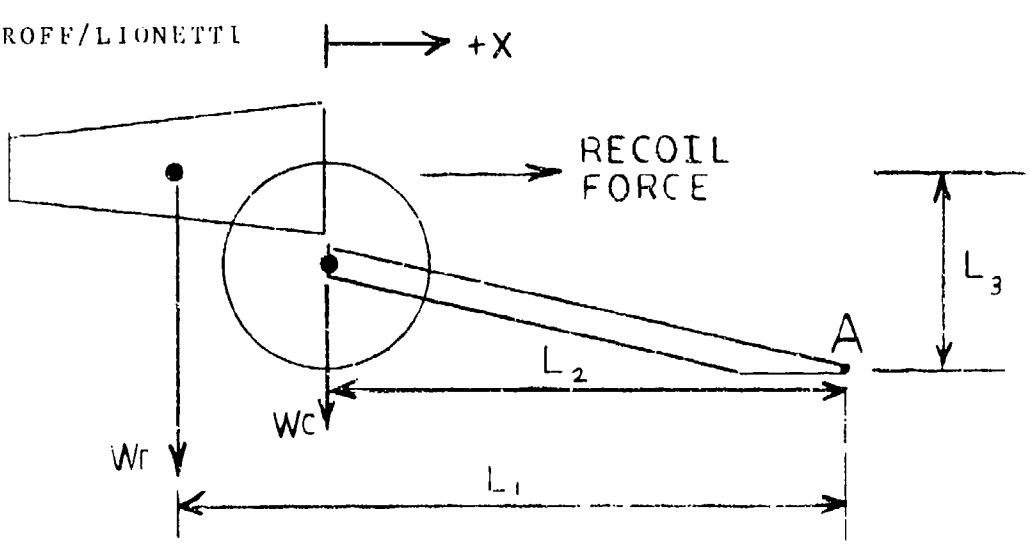

FIGURE 2. - WEAPON STABILITY CRITERIA

By summing moments about point A it can be seen that the gun system will remain rotationally stable as long as the counter-clockwise moments from the weights of the recoiling parts (Wr), and carriage assembly (Wc) exceed the clockwise moment from the force that the recoiling mass exerts on the carriage. The condition for stability is

$$\text{RECOIL FORCE}(L_3) < W_r(L_1 - x) + W_c L_2 \qquad (1)$$

Note that as recoil progresses to the right, the counter-clockwise moment from the recoiling weight decreases due to the moving center of gravity of the recoiling parts; therefore the condition for stability is most critical at the end of the recoil stroke. While this condition does not override the primary goal of maintaining a consistent recoil force as low as possible, it demonstrates that the recoil force should not increase during the final portion of the stroke. It would be entirely possible for the microprocessor to tailor the force versus stroke profile to improve stability of a lightweight weapon.

The constantly variable fluid throttling orifice thus described is envisioned as a microprocessor-activated servovalve operating as a fluid bypass. A schematic of this system is shown in figure 3.

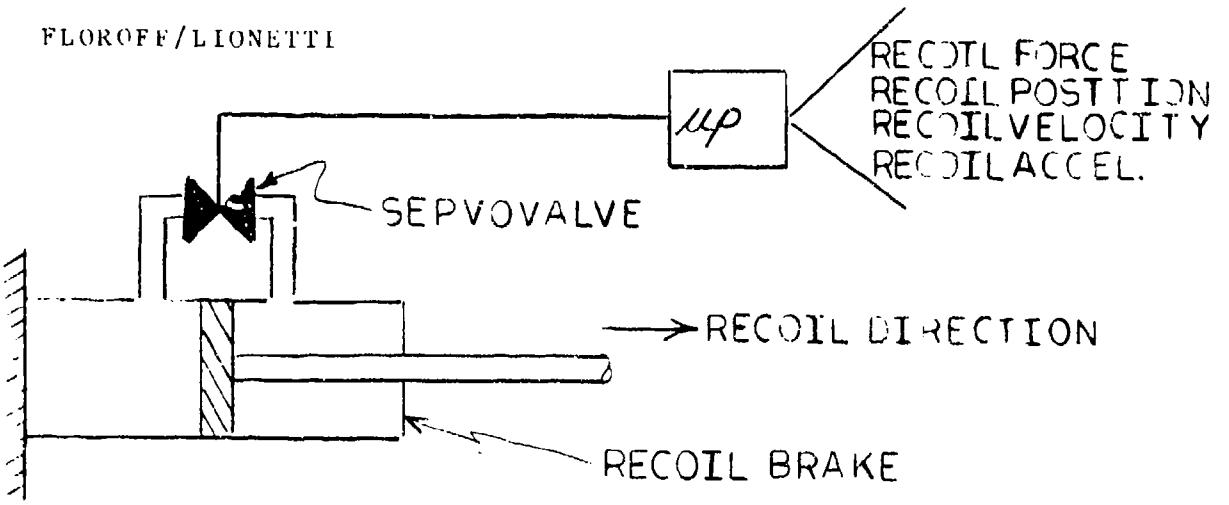

FIGURE 3. - MICROPROCESSOR-CONTROLLED BYPASS VALVE

Assuming various factors such as recoil force, position, velocity and acceleration are available to the microprocessor in real time during the recoil stroke, optimum recoil energy dissipation can be programmed. Two control algorithms have been developed (ref 5) to accomplish this and are described below

Level 1 Control - Maintain a Preset Recoil Force. The recoil force or the force transmitted to the weapon supporting structure can be monitored and maintained at a preselected value. This value could be mathematically or empirically determined such that the total available recoil stroke is always utilized for a specific impulse input. If actual recoil force is less than the preselected value, the servovalve would be commanded to shift to the closed position If recoil force is greater than the preselected value the valve would shift to the full open position.

The control algorithm described above is very simple, yet it has the potential for true optimization of each recoil stroke through the concept of closed loop feedback control.

Level 2 Control- Compute Recoil Force During Firing A more sophisticated approach to effective recoil energy dissipation is to dynamically determine required recoil force during recoil . This has the advantage of not requiring advance knowledge of what impulse is to be expected.

This technique equates the mechanical energy of the recoiling mass to the amount of work necessary to stop the recoiling parts. The work energy relationship is first established. For a simple, one-dimensional recoil mechanism, motion is governed by Newton's second law

$$F = M_r \ddot{X} \tag{2}$$

where: F= sum of all forces acting on the recoil mechanism in the direction of motion (lb)
M_r= Mass of recoiling parts (slugs)
$\ddot{X}$= Acceleration of recoiling parts (ft/sec).

Figure 4 illustrates a free body diagram of forces acting on a typical artillery recoil mechanism.

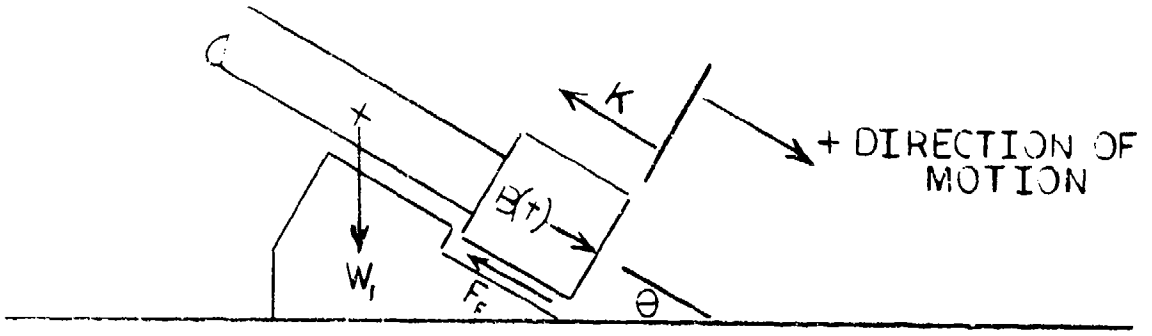

Figure 4. - Forces Acting on an Artillery Recoil Mechanism

where: B(t)=Propellant gas force as a function of time (lb)
K =Recoil resistance (lb)
F_F =Mechanical friction due to recoil mechanism movement (lb)
W_r =Weight of recoiling parts (lb)
θ =Angle of elevation of weapon (degrees)

Arbitrarily assuming a positive direction as shown in figure 3, equation 2 can be re-written as

$$M_r \ddot{x} = B(t) + W_r \sin\theta - K - F_F \tag{3}$$

Recoil distance is introduced with the following substitution:

$$\ddot{x} = \frac{dv}{dt} = \frac{dx}{dt}\frac{dv}{dx} = v\frac{dv}{dx} \tag{4}$$

yielding

$$M_r v\frac{dv}{dx} = B(t) + W_r \sin\theta - K - F_F \tag{5}$$

Integration with respect to distance yields

$$-\frac{1}{2}M_r V^2\Big|_1^2 = \int_1^2 B(t)\,dx + \int_1^2 W_r \sin\theta\,dx - \int_1^2 k\,dx - \int_1^2 F_F\,dx \quad (6)$$

By selecting an initial integration condition at some arbitrary distance, x, (where the velocity is V), a final condition at maximum recoil stroke, xmax (where recoil velocity is zero), and assuming recoil force (k) is to be maintained at a constant value, equation 6 becomes

$$-\frac{1}{2}M_r V^2 = \int_x^{xmax} B(t)\,dx + W_r \sin\theta(xmax-x) - K(xmax-x) - \int_x^{xmax} F_F\,dx \quad (7)$$

Solving this equation for recoil resistance (k) results in

$$K = \frac{1}{xmax-x}\left[\frac{1}{2}M_r V^2 + \int_x^{xmax} B(t)\,dx - \int_x^{xmax} F_F\,dx\right] + W_r \sin\theta \quad (8)$$

Equation 8 becomes the "control equation" used to compute recoil resistance during the recoil process. While the microprocessor could probably update the computation quickly enough, the mechanical transducers, A-D converters and servovalve action may be "too slow" to effect the proper change. Although this has not yet been established through test, it certainly would be desirable to simplify equation 8 to reduce computation time. This could be accomplished using the following logic.

A comparison of the magnitude of forces used in equation 8 as a function of recoil stroke for a typical artillery recoil mechanism is depicted in figure 5. It is evident that the friction and weight terms are not large contributers to the work-energy relationship. Realizing that friction tends to reduce the recoil resistance force while the weight contribution tends to increase it, it would be prudent to include the weight computation and to simplify equation 8 ,omit friction. This will ensure the stability requirement is met since recoil force will not increase as recoil action progresses.

Further simplification of equation 8 is possible if the breech force component is ignored. This may appear radical since the breech force is the largest force applied to the weapon; however, it acts for only a fraction of the total recoil stroke. Furthermore, the computed value would only be correct after B(t) becomes negligible. Ignoring breech force would require the servovalve to control recoil force to a preset value until the majority of it (the breech force) has been applied. This value could be the maximum recoil force the weapon is designed to handle. Incorporating these decisions; equation 8 can be rewritten as

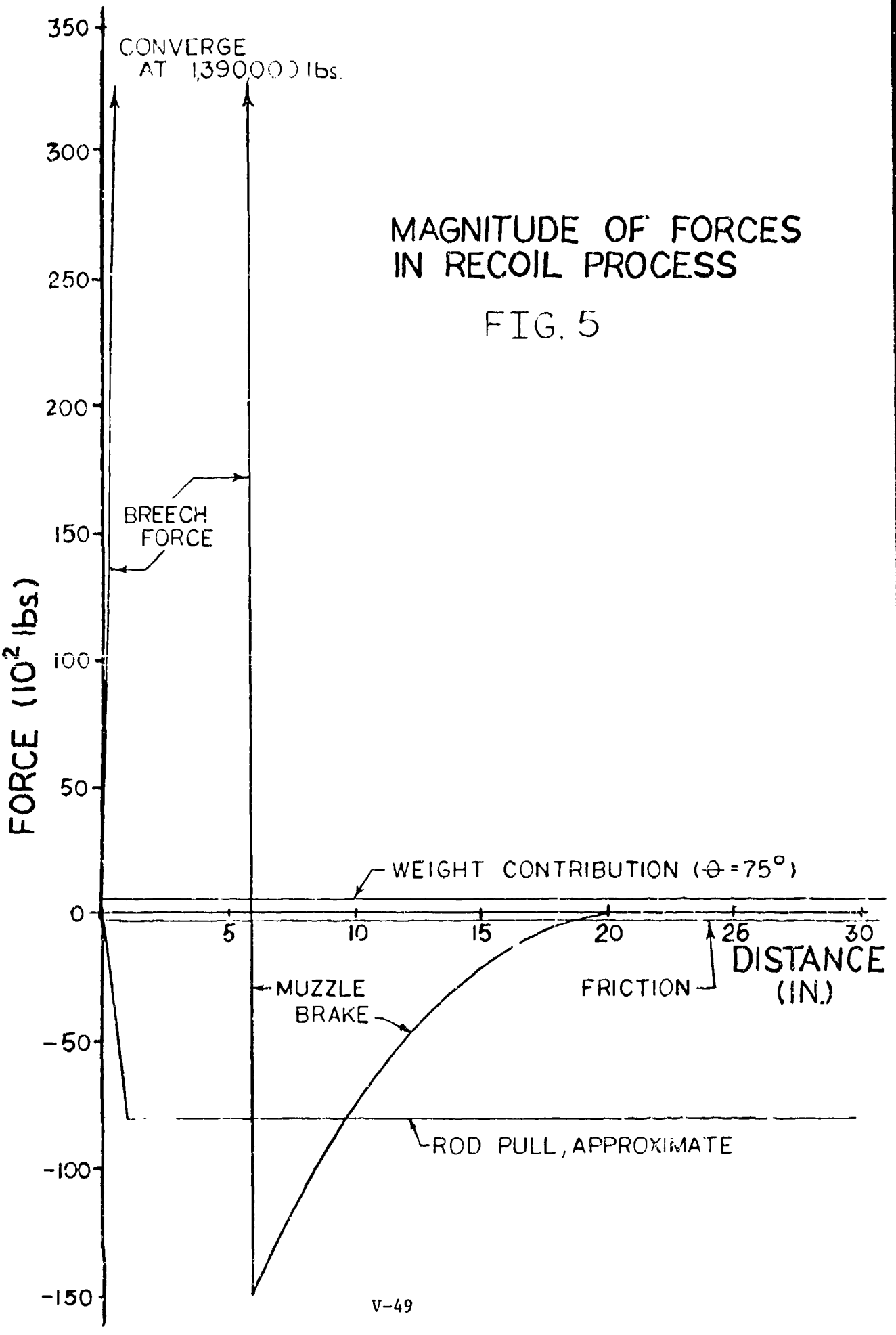
MAGNITUDE OF FORCES IN RECOIL PROCESS
FIG. 5
CONVERGE AT 1,390000 lbs.
BREECH FORCE
FORCE (10^2 lbs.)
350
300
250
200
150
100
50
0
-50
-100
-150
WEIGHT CONTRIBUTION ($\theta = 75°$)
5
10
15
20
25
30
DISTANCE (IN.)
MUZZLE BRAKE
FRICTION
ROD PULL, APPROXIMATE

$$K = \frac{1}{x_{max} - x}\left[\frac{1}{2} M_r V^2\right] + W_r \sin\theta \qquad (9)$$

The obvious question is at what point during recoil should control transition from preset rodpull to the calculated rodpull computed in equation 9. This could occur when the acceleration of the recoiling parts changes sign from positive to negative. If the weapon employs a muzzle brake, transition would occur when the muzzle brake activates. If a muzzle brake is not used, acceleration will change sign when the breech force is reduced to a level below the combined recoil resistive force and frictional force

There are both physical and computational problems with equation 9 during the final portion of the recoil process which need to be addressed. Due to the inevitable leakage of piston seals and variations in frictional and recuperator forces the recoiling mass would never stop at precisely the specified xmax. This, in turn, causes k to become undefined as xmax is approached. In order to prevent this, a controlled closure of the servovalve should be provided at a specified distance from xmax.

This approach to recoil mechanism control has been simulated (ref.5). The results are encouraging, and prove the viability of this approach to recoil control.

Implementation of the microprocessor recoil approach results in some concerns. They include:

a. The substitution of electronic complexity for mechanical complexity. It must be acknowledged however, that electronics have proven their dependability in the aerospace and automotive fields. therefore,This may not be a deterrent.

b. Input of energy is necessary to "manage" recoil energy dissipation.(Electrical energy is required to power the microprocessor and a high pressure fluid source is required to shift the servovalve.)

c. Microprocessor failure could be critcal if a redundant backup is not provided.

These comments are not meant to discourage the approach, but merely to point out unique problems not previously encountered in recoil mechanism design.

5. Lightweight Artillery Recoil Mechanisms

Lowered recoil force is mandatory for a lightweight artillery piece. There is no magic involved in achieving this; lowered force levels can be achieved only by increasing effective recoil

length. If this can be accomplished, the microprocessor can supervise the recoil process to ensure that the total recoil stroke is always utilized.

Two approaches to lightweight recoil mechanisms are described in the following paragraphs. These concepts are not new but with the addition of microprocessor control, become viable alternatives for a lightweight artillery application.

Super Long Recoil - Using a conventional cycle; i.e. fire-recoil-return to battery, but incorporating 120 inches for recoil travel, the force imparted to the weapon can be reduced by 50 percent. This reduction in force is due to more than doubling the length of recoil. An artists sketch of one possible approach is shown in figure 6.

Utilization of this approach does have drawbacks. These include:

a. Drastic changes when compared to a conventional weapon carriage. For example, a significant increase in weapon height. This would, in turn, negatively affect the vehicle's silhouette, making it more "spottable".

b. Loading the weapon would be more difficult because the breech is 10 ft. off the ground. This problem could be alleviated by programming the microprocessor to bring the recoiling parts to a load position, followed by re-positioning for firing.

Soft Recoil- Perhaps the most intriguing approach to lightweight artillery recoil systems is the concept of soft recoil. The basic idea of soft recoil is embodied by its fundamentally different sequence of operations when compared to the conventional recoil cycle. This difference is graphically illustrated in figure 7.

In conventional recoil mechanisms, the firing momentum is directly transferred to recoiling parts that are at rest prior to firing. This momentum is then absorbed by the supporting structure, and the recoiling parts are brought to rest. In soft recoil, approximately half the momentum of the projectile is applied to the recoiling parts by accelerating them in the firing direction prior to firing the projectile. Firing momentum thus transferred to the foward moving recoiling parts stops and propels them to the rear. In effect, recoil length is doubled and imparted foward momentum is absorbed. The soft recoil cycle can reduce forces applied to the supporting structure by more than half that imposed by a conventional system.(ref. 6)

"SUPER LONG" RECOIL CONCEPT

FIGURE 6

CONVENTIONAL RECOIL CYCLE

FIGURE 7

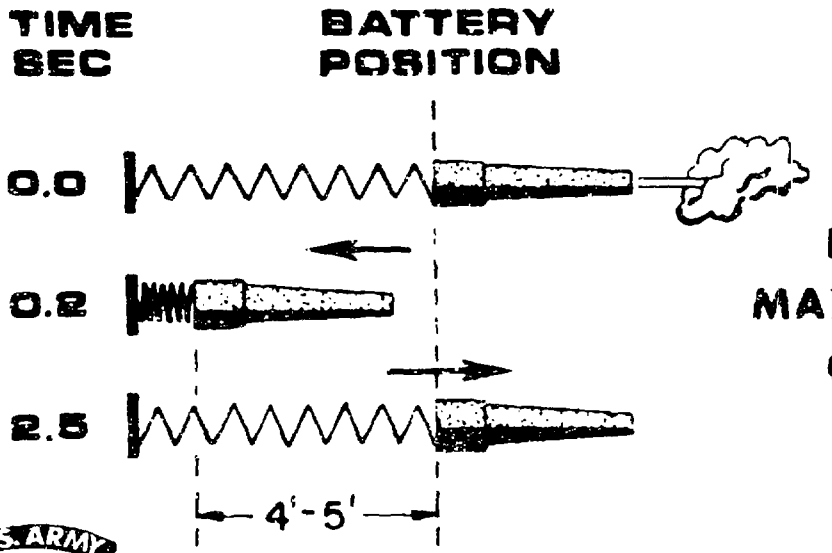

SOFT RECOIL CYCLE

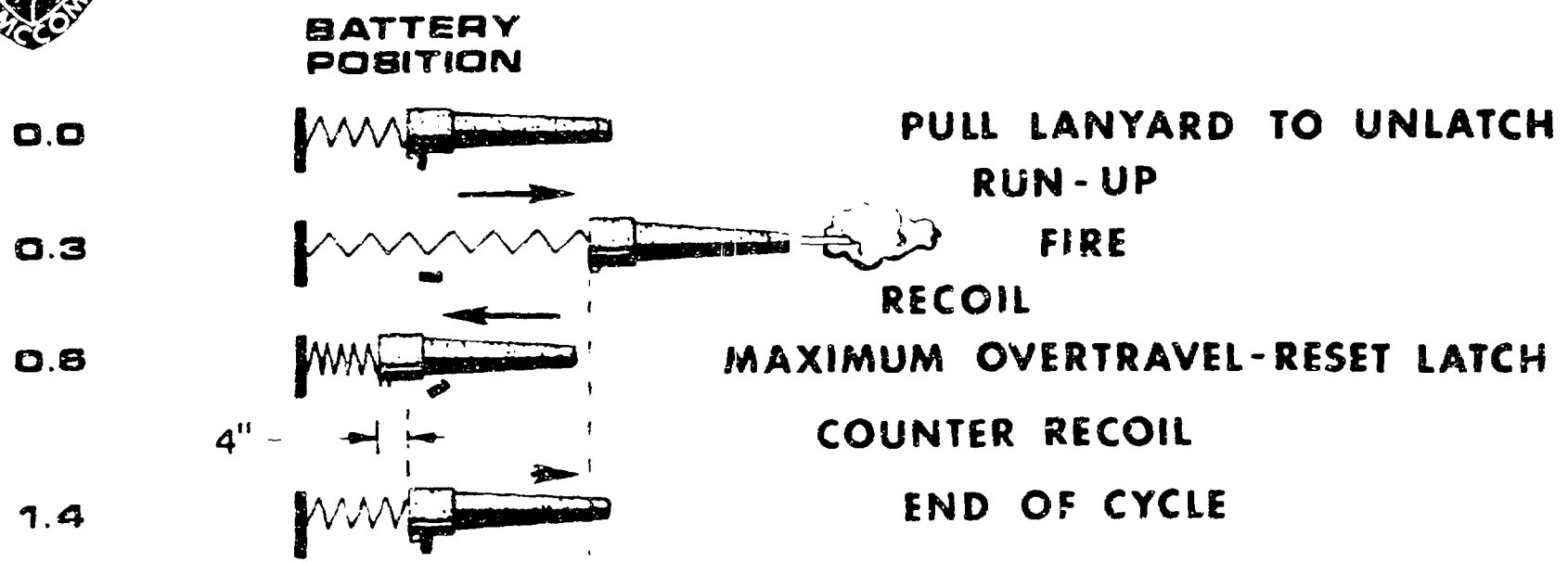

Due to fail-safe devices incorporated in past soft recoil mechanisms, the existing mechanisms tend to be heavy and complex simply due to the practical realities of building such a weapon. Specifically, two conventional "recoil mechanisms" are required, one at each end of travel. This is due to the potential for two overload conditions which may occur as follows:

a. The weapon must be programmed to fire at a foward recoiling parts velocity commensurate with the propelling charge energy released during combustion. The possibility exists to fire the highest zone (maximum impulse) at lowest foward velocity. This results in a rear overload condition. This condition can also occur due to propellant "cook off", in a hot tube prior to the initiation of foward velocity. In either case the imparted energy must be dissipated, usually through a traditional oil throttling process.

b. After foward velocity is initiated, ignition delay or misfire (failure to fire) will cause a forward overload condition. This energy must also be dissipated again, usually through an oil throttling process.

In essence, the soft recoil approach requires a high degree of control during the recoil process. Timing is critical. In addition, stability problems are inherent in the design if it does not function properly.

It is suggested that microprocessor technology can be incorporated to "manage" the entire soft recoil cycle. This management could consist of the following:

a. Prior to firing, ensure that the proper zone, i.e. required foward velocity, is input into the weapon control. This could consist of a keyboard excerise, or manual verification of a firing command. This could eliminate the rear overload condition.

b. Electronically monitor foward velocity and initiate firing. The microprocessor could monitor propellant temperature, changing frictional forces and store past firing performance so that firing is initiated at just the right instant based on the action of the particular weapon. This will ensure optimum energy dissipation.

c. Assuming a misfire or ignition delay occurs, a controlled shutdown is initiated by throttling oil through a servovalve. The recoil shutdown force profile could be designed such that weapon stability will be maintained. This could be accomplished with "tipping" sensors to maintain overall stability.

d. On-board diagnostics will ensure the weapon will not be destroyed due to failure of a replacable fail-soft component. Assuminmg an overload condition occurred, such that a sacrificial energy absorber was used, for instance, in lieu of, or in addition to, servovalve throttling, firing would be prohibited until a replacement was made.

These "management" options are only suggestions of what is possible with microprocessors controlling soft recoil. It is essential to review state-of-the-art soft recoil to fully appreciate the problems associated with this concept. The U.S. Army has constructed and type classified a 105mm soft recoil howitzer, designated M204. An excellent synopsis concerning the development of this weapon and can be found in reference 6.

REFERENCES

1, "Engineering Design Handbook:-Carriages and Mount Series, Recoil Mechanisms," AMCP 706 342, U.S. Army Material Command, Washington, D.C. September 1963.

2. MG Thomas J. Hayes, "Elements of Ordnance" John Wiley & Sons NY , 1938.

3. Jasbir S. Arora and Edward J Haug Jr. "A Guide to Design of Artillery Recoil Mechanisms," U.S. Army Armament Research and Development Command, Dover, NJ, September 1977.

4. S.M. Wu, A.N. Madiwale "Optimal Control of Active Recoil Mechanisms". Technical Report R-TR-77 024, Rock Island Arsenal, Illinois February 1977.

5. LTC George Y. Jumper USAF and Stephen G. Floroff "Feasibility Study of a Microprocessor Controlled Recoil Mechanism for Large Caliber Artillery Weapons." Technical Report ARLCD-TR-85007. US Army Armament Research & Development Center, Dover, NJ (To be published-May 1985)

6. Robert E. Seamands "Exploratory Development of Howitzer Light,Towed 105 mm soft recoil XM204. Technical Report RE TR 70-179, Rock Island Arsenal Illinois July 1970.

Title: Effect of the Flick Ramming Environment on Selected Artillery Fuzes

Robert X. Brennan
US Army Research and Development Command
Large Caliber Weapon Systems Laboratory
Nuclear and Fuze Division
Picatinny Arsenal, Dover, NJ 07801-5001

Abstract

In order to arrive at a decision in regard to the development of a flick rammer for the Howitzer Improvement Program the compatibility of the flick ramming environment with large caliber fuzes was investigated. The fuzes investigated were the M557, M739, M577, XM762, M732 and M572. The only possible area of concern uncovered in this investigation was the M1 delay plunger (used in the M557, M572 and M739 fuzes) and its successor the impact delay module (IDM) which is used in the M739A1 fuze.

The centrifugal pin in the M1 delay plunger has been undercut to prevent functioning in the absence of a spin environment. A range of setforward decelerations, plunger spring preloads and frictional forces were simulated. In all cases the undercut on the centrifugal pins caused the plunger assembly to lock up before it could function.

Biography

Present Assignment: Mechanical Engineer, US Army Armament Research & Development Command, LCWSL, Picatinny Arsenal, Dover, NJ 07801-5001.

Past Experience: Diplom Physiker, Brown-Boveri Corp, Baden Switzerland 1967-1969, Physicist General Electric, Valley Forge, PA. 1965-1967, Physicist MIT, Cambridge, Massachusetts 1963 - 1965.

Degrees Held: BS Physics Bkln Polytechnic Inst 1960, MS Physics Stevens Institute of Technology 1963, MS Mathematics Stevens Institute of Technology 1976.

Effect of Flick Ramming Environment on Selected Artillery Fuzes

Robert X. Brennan

US Army Research and Development Command
Large Caliber Weapon Systems Laboratory
Picatinny Arsenal
Dover, New Jersey 07801-5001

1. Introduction

To insure the interchangeability of current and future US & NATO artillery fuzes ammunition used in the flick ramming/autoloading environment, PM-CAWS at Picatinny Arsenal initiated an experimental and theoretical investigation of the compatibility of the M557, M739, M577, XM762, M732 and M572 fuzes with the flick ramming environment.

In May 1983 the deceleration G-level required to seat the 155mm round in the M199 gun tube of the M198 Towed Howitzer equipped with a flick rammer was measured with triaxial accelerometers. Figure 1 shows the accelerometers mounted in the fuze well of the 155mm M107 projectile.

Ten ramming tests were conducted through a range of elevation angles 0 to 70 degrees in steps of 10 degrees. These tests yielded a total of 80 deceleration-time traces. The traces were digitized by the Hybrid Division of ARDC. A subset was used to provide a quantitative time dependent forcing function for the computer simulation. The highest magnitude of pulse observed on these traces was 1800 G's.

As part of the study the fuze mechanisms were discussed with the respective project engineers. Those components about which there was some doubt as to whether they could withstand the flick ramming environment were subjected to analysis and/or testing.

Forcing Function

The first step in determining the response of fuze mechanisms was to measure the deceleration G's required to seat the 155mm round in the M199 gun tube of the M198 towed Howitzer equipped with a "Flick Rammer". In the fuze well of the 155mm round the deceleration G's were monitored by a triaxial accelerometer. The mounting of the accelerometer is shown in figure 1. Ten flick ramming tests were conducted at quadrant elevation angles of 0^{o}, 10^{o}, 20^{o}, 30^{o}, 40^{o}, 50^{o}, 60^{o}, and 70^{o}.[1] These tests yielded a total of 80 deceleration-time traces. The results of these tests are shown in figures 2 and 3. Figure 2 shows the maximum measured values of the deceleration at the fuze well as a function of the quadrant elevation angle of the gun tube. Figure 3 gives the range of ramming speeds generated by the flick rammer.

These 80 analog traces were digitized and processed by the Hybrid Division of ARDC using a program called "Hydra"[2]. The maximum axial deceleration amplitude was about 1800 G's. A typical trace for quadrant elevation angle 30^{o} is shown in figure 4. The x and y axis are transverse to the round and they represent balloting forces The z component is directed along the longitudinal axis of the round. The HYDRA program can expand the time scale and the plot is shown with the expanded time scale. Since the round decelerates when being seated by the flick rammer the sign associated with the G's should be negative. Accordingly, in the analysis only the negative portion of the z component was used as input to the analysis. The positive portion of the trace was assumed to be noise. These pulses have a typical time duration of 2 milliseconds. These durations agree well with the measurements conducted by GE for the Bundesamt fur Wehrtechnik and Beschaffung (BWB) 1981 [3] which resulted in pulse durations of 1.8 milliseconds. In a series of tests conducted at Meppen in 1983[4] by the BWB, 40 rounds with the M739 fuze set in the delay mode were flick rammed at 33 feet/second and all the rounds subsequently functioned properly on impact. Twenty fuzes were mounted on the L15A1 projectile and fired at high and low temperatures. Another 20 were fired with the M549A1 RAP round at high and low temperatures. The ramming G's were not measured, but they could have been as high as 4,000 G's.

As a comparison, measurements were also made in the M185 gun tube equipped with a hydraulic rammer[5]. This trace was also processed by the HYDRA program. The pulse duration is again 2 milliseconds, but its peak is only 218 G's.

Fuzes Investigated

The fuzes which were checked for compatibility with the flick rammer were the M557[6], M739[6], M577[7], XM762[8], and M732[9] fuzes. Discussions were held with the project engineers on these fuzes, and those sub-assemblies which could possibly fail as a result of the flick rammer set-forward force were identified. The following sections of this report summarize the analysis and laboratory testing of these parts.

M557 PD Element

Figure 5 shows a sketch of the firing pin in the M557 PD element. Under set forward deceleration it is possible that the firing pin could be forced

through the washer and the crimp on the nose. Using a spring tester the load on the firing pin head was increased until the crimp sheared. The shearing force measured was 69 lbs and since the firing pin weight is 0.021 oz it would require 52000 G's of setforward deceleration to drive the firing pin through the crimp. Since the highest flick ramming G's never exceeded 1833 G's, this failure mode can be disregarded.

M739 Fuze Firing Pin

A possible mode of failure in the M739 fuze is for the firing pin head to come off the firing pin. According to the drawing specifications for part #9294606, it would take 80 lbs to pull the head off the pin. In the actual assembly as shown in figure 6 more force would be required since the firing pin head is also held by the firing pin tube. Since the pin weighs 0.03 oz, using 80 lbs as a conservative estimate it would require 42000 G's setforward deceleration for this mode of failure to occur. Therefore, this type of failure can also be ruled out.

M739 Fuze, Firing Pin Support

Another potential mode of failure in the M739 fuze is for the firing pin support to collapse. According to the drawing part number 9258614, it takes about 100 lbs to collapse the firing pin holder. Since the detonator housing weighs 0.075 ounces, this mode of failure would require a set forward deceleration of 21,000 G's.

M577 Fuze Time Assembly

In the M577 fuze the weakest elements appeared to be the timer hairspring tube and the timer hairspring. A sketch of this mechanism is shown in figure 7. According to drawing part number 9236712, the timer hairspring tube must be able to withstand a load of 800 lbs. The weight of the tube was calculated to be 0.054 ounces. To break this press fit would require a setforward deceleration of 235000 G's. According to the same drawing, it would require 9 lbs to pull the timer hairspring free of its collar. The weight of the hairspring was calculated to be 0.002 ounces. It would, therefore, require 65000 G's to pull the hairspring free.

M732 Fuze

Three M732 inert fuzes were mounted on inert 155mm projectiles and rammed. All three fuzes looked undamaged, hadn't turned and felt tight in a hand grip. The three fuzes were disasembled and nothing unusualy was observed. Recent air gun tests at Picatinny Arsenal [10] indicate that the time setting torque could be seriously degraded when the fuzes were subjected to setforward decelerations between 1000 G's and 2000 G's for a duration of 5 milliseconds.

XM762 Fuze

This fuze is in the engineering development phase. Discussions with the project engineer did not point to any part of the mechanism as being possibly subject to failure.

M1 Delay Plunger

The M1 delay plunger which is built into the inventory of M557, M572 and M739 fuzes provides a functioning time delay. A sketch of this device is shown in figure 8. Since the delay element is designed to function due to the setforward deceleration generated when the projectile impacts and penetrates a wall, it is possible that it could also function when the projectile is seated by flick ramming. The major difference is that the projectile has a high spin when it impacts a target whereas there is no spin when it is flick rammed. As a result the setforward deceleration would have to be sufficient to retract the centrifugal pins. Since the centrifugal pins are skewed at an angle of 15 degrees in the direction of flight it is possible that there would be a component of the deceleration G's sufficiently large to cause the pins to retract. As the centrifugal pins retract, the spin lock detent (not shown in the figure) will play no role since the plunger immediately rides forward over the plunger support. Once the plunger goes forward the delay element would be driven into the firing pin. The initiation of the delay element would in turn damage the S&A causing the round to be a "dud". Qualitatively there is the possibility of a malfunction of the M1 Delay Plunger and the question remains to be answered if quantitatively there is enough energy for this to occur.

Centrifugal Plunger Pin and Spring

In order to proceed quantitatively the differential equations for the motion of the centrifugal pins as well as for the plunger are required. The differential equation for the centrifual pins is given by:

$$1)\quad m\ddot{x} = -kx - mg\,G_{sp} - \mu_x mg\,G_z(t)\cos\theta_o - mg\,G_r(t)\cos\theta_o + mg\,G_z(t)\sin\theta_o$$

$$\dot{x}(o) = o$$

$$x(o) = o$$

m is the mass of the centrifugal plunger pin, 0.116×10^{-4} lb $sec^2/inch$

x is the displacement of the centrigual plunger pin, inches

k is the centrifugal plunger pin spring rate, 0.19 lb/inch

g is the gravitational acceleration, 386.4 inches/sec

G_{sp} centrifugal plunger pin spring preload, 17 G's (MIL-P-10480)

$G_z(t)$ is the longitudinal component of setforward deceleration

μ_x coefficient of friction

θ_o angle between the centrifugal plunger pin and the perpendicular to the spin axis, 15 degrees (see figure 8)

$G_r(t)$ transverse or balloting component of deceleration

For the purposes of analysis equation 1 can be written in the form

2) $\ddot{x} = -\omega_o^2 x - g G_{sp} - \mu_x g G_z(t) \cos\theta_o + g\left(G_z(t)\sin\theta_o - G_r(t)\cos\theta_o\right)$

where

3) $\omega_o = \sqrt{\frac{k}{m}} = 28.4$ herz

Plunger Assembly

The differential equation for the motion of the plunger is

4) $m_p \ddot{y} = -k_p y - m_p g G_s + m_p g G_z(t) - \mu_y m_p g G_r(t)$

m_p mass of the plunger body 2.74×10^{-4} lb-sec/inch

k_p plunger restraining rate 3.9 lb/inch

G_s plunger restraining spring preload 13 G's

For the purpose of integration equation 4 can be written as

5) $\ddot{y} = -\omega_p^2 y - g G_s + g G_z(t) - \mu_y g G_r(t)$

where ω_p = 20 herz

Results of the Computer Simulation

The differential equations 1 and 4 were solved simultaneously employing a special purpose computer program for solving ordinary differential equations called ACSL[11]. The results for test 29 rammed at QE of 30° are shown in figure 9. In figure 9 three curves are superimposed. These are the axial setforward G's (650 G's max.) and the displacement of the centrifugal plunger pins together with the plunger displacement. To cause initiation of the delay element the centrifugal pins must displace 0.095 inches before the pin and plunger assembly are rammed against the plunger support. In figure 9 the coefficients of friction of both the centrifugal pins, μ_x, and the plunger body, μ_y, were taken equal to 0.1. The relationship of the plunger assembly with respect to the plunger support is shown in figure 10. The centrifugal pins must release before the plunger moves 0.059 inches. In figure 9 the pins displace only 0.044 inches before being rammed against the plunger support.

If the G trace were to be multiplied by 1.5 it would peak at 1000 G's. Maintaining the coefficients of friction μ_x and μ_y equal to 0.1 the results of a simulation are shown in figure 11. Once again the pins are rammed against the plunger support before they free the plunger.

The simulation was rerun using the 630 G pulse and the coefficient of plunger friction was set equal to 0.5. Again the M1 delay plunger does not function. The simulation was repeated with the same coefficients of friction and a 1000 G pulse. Although the pins displace somewhat further there is no functioning of the M1 delay.

However, if the preload on the plunger spring is increased from 13 G's to 100 G's the M1 delay will almost function. The main effect of the high preload is to delay motion of the plunger until the pins release.

A higher preload on the plunger spring (150 G's) allows the pins to clear the plunger support permitting the plunger to move forward. However, as shown in figure 12 the plunger does not close the 0.2 inch gap to the firing pin as the plunger spring is too stiff.

If the conditions of the previous simulation are repeated except that the peak G's are increased to 2000 G's the M1 plunger assembly will function. This is shown in figure 13. The peak kinetic energy is over 200 inch ounces which would initiate the M1 delay element. On the other hand a 2000 G pulse and a 13 G preload on the plunger causes the pins to jam the plunger.

In conclusion, the race between the plunger and the centrigual pins is won by the plunger unless the plunger spring stiffness is increased by a factor of 10.

Effect of Plunger Support Interference

The question remains to be answered as to whether the M1 delay assembly can function when the retraction of the centrifugal pins is interfered with by the plunger support. The head of the centrifugal pin is undercut by 13° which produces an additional normal force on the pins. Taking this additional normal force into account makes the free body diagram two dimensional as shown in figure 14. For convenience the angle of the pin and the angle of the undercut were both taken as $\theta_o = 15^{\circ}$. From this figure the equation of equilibrium can be read directly.

6a) $N\cos\theta_o - mg\,G_z\cos\theta_o - mg\,G_r\sin\theta_o = 0$

6b) $m\ddot{x}' = mg\,G_z\sin\theta_o - kx' - mg\,G_{sp} - mg\,G_r\cos\theta_o - \mu_x N\cos\theta_o - N\sin\theta_o$

In these two equations terms of the order of $\mu_x \sin\theta_o$ have been neglected. Combining these equations yieids:

7) $\ddot{x}' = -\omega_o^2 x' - g\,G_{sp} - g\,G_r\sec\theta_o - \mu_x g\,(G_z\cos\theta_o + G_r\sin\theta_o)$

Since all the terms in this equation are negative the pins cannot move. Only the ballotting force $G_r(t)$ can change sign. Since the two pins are diametrically opposed, it the ballotting drives one pin out, it drives the other pin into engagement with the plunger support.

References

(1) Project Engineer, S. Floroff, Future Weapon Systems Branch, Weapons Division, LCWSL

(2) Hybrid Data Reduction and Analysis, "HYDRA", MISD UM 83-3, April 1983, F. Traverni, Hybrid Division, ARRADCOM, NJ.

(3) "Flick Ramming for Artillery Ammunition" Becker WM IV 4-90-13-90 18 January 1982.

(4) "Testing the Safety and Reliability of the Munitions for the 155mm Howitzer Utilizing a Flick Rammer", Brinkmann, WM VI 90-13-20-05.

(5) Project Engineer, R. Koppman, Self Propelled Artillery Branch, WD, LCWSL

(6) Project Engineer, W. Pellet, LCWSL, Tube Fired Fuze Branch

(7) Project Engineer, R. DeBlock, LCWSL, Tube Fired Fuze Branch

(8) Project Engineer, P. Weldon, LCWSL, Tube Fired Fuze Branch

(9) Project Engineer, C. Sun, HDL, DELHD-DE-OM

(10) Ddiscussion with R. Shaffer, LCWSL, Tube Fired Fuze Branch, 2/85.

(11) "ACSL" Advanced Continuous Simulation Language, Mitchell and Gauthier Assoc., Inc., PO Box 635, Concord, MA 01742

(12) MIL-D-46486F (PA)

TRIAXIAL ACCELEROMETER MOUNTED ON MK7 PROJECTILE

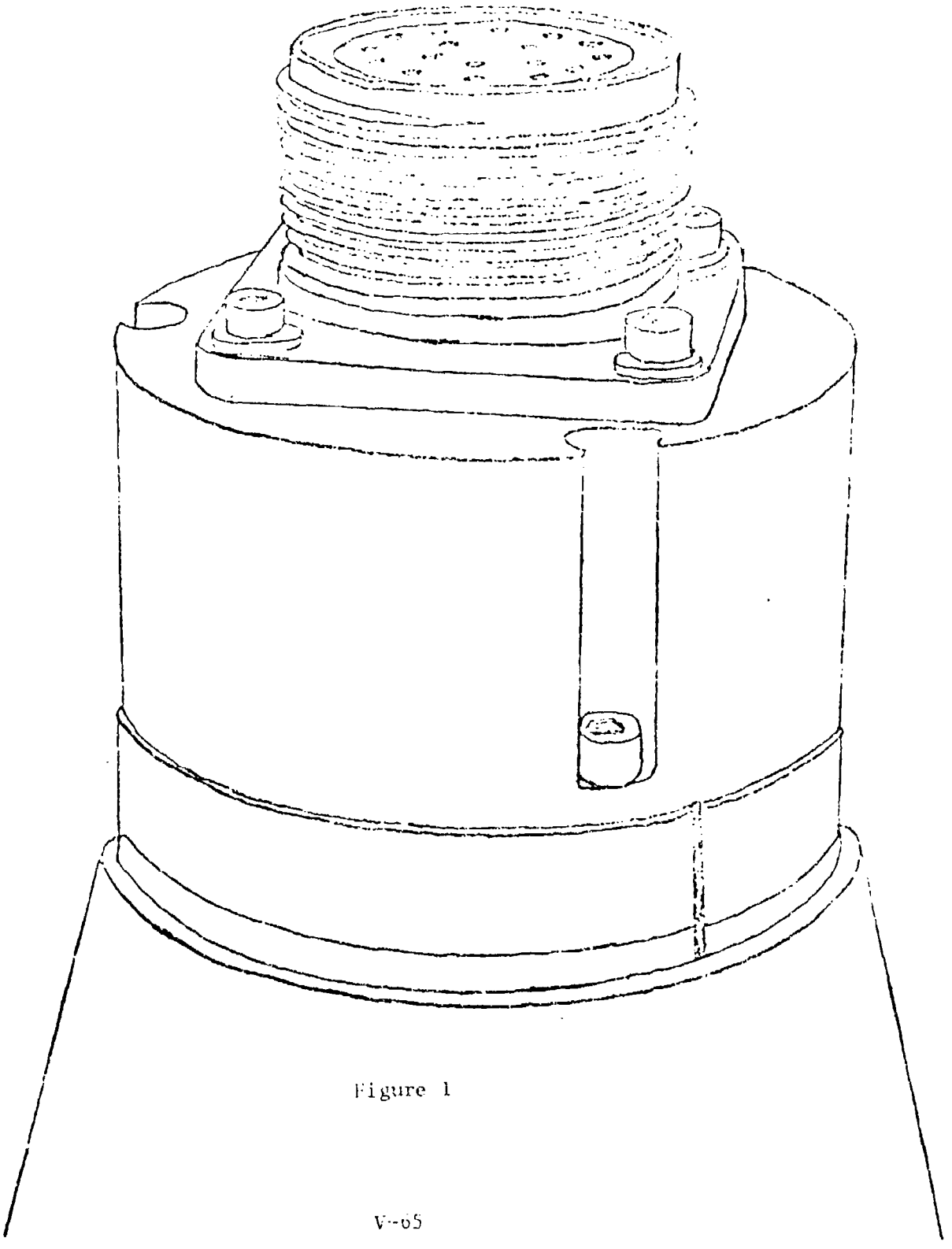

Figure 1

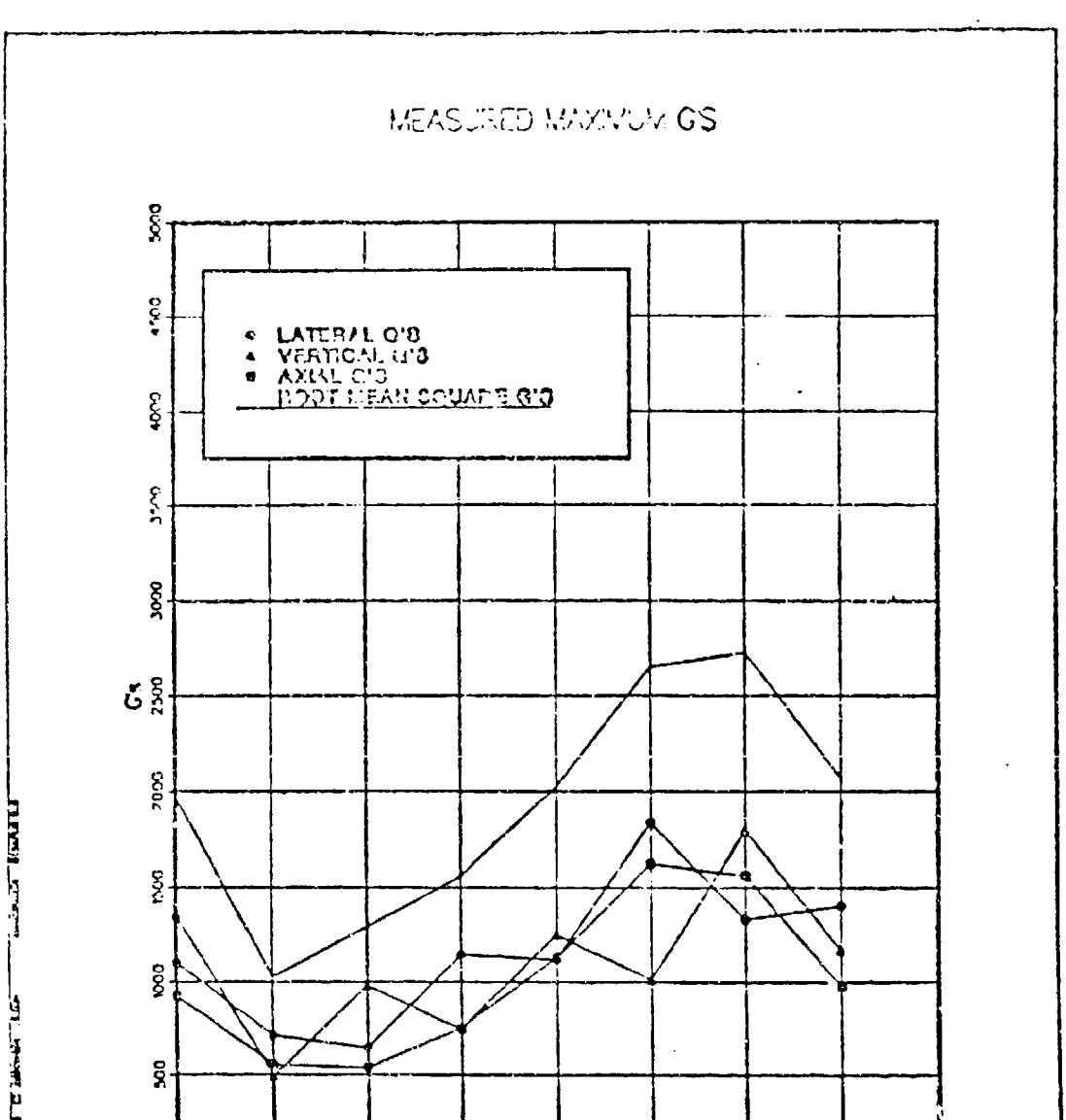
MEASURED MAXIMUM GS
LATERAL G'S
VERTICAL G'S
AXIAL G'S
ROOT MEAN SQUARE G'S
Gs
0
500
1000
1500
2000
2500
3000
3500
4000
4500
5000
0
10
20
30
40
50
60
70
80
CE ANGLE DEGREES

Figure 2

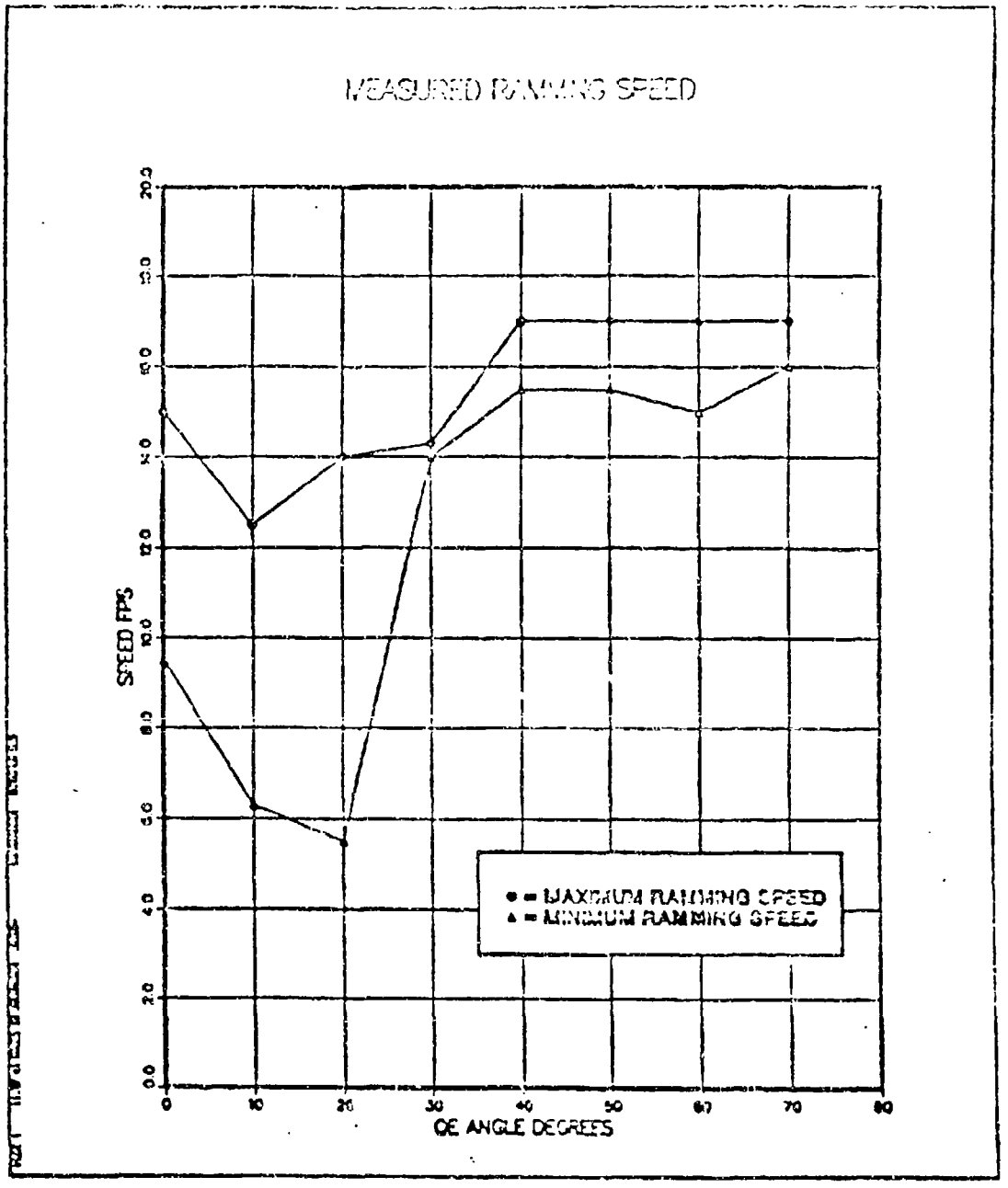
MEASURED RAMMING SPEED
SPEED FPS
QE ANGLE DEGREES
0
10
20
30
40
50
60
70
80
0.0
2.0
4.0
6.0
8.0
10.0
12.0
14.0
16.0
18.0
20.0
● = MAXIMUM RAMMING SPEED
▲ = MINIMUM RAMMING SPEED

Figure 3

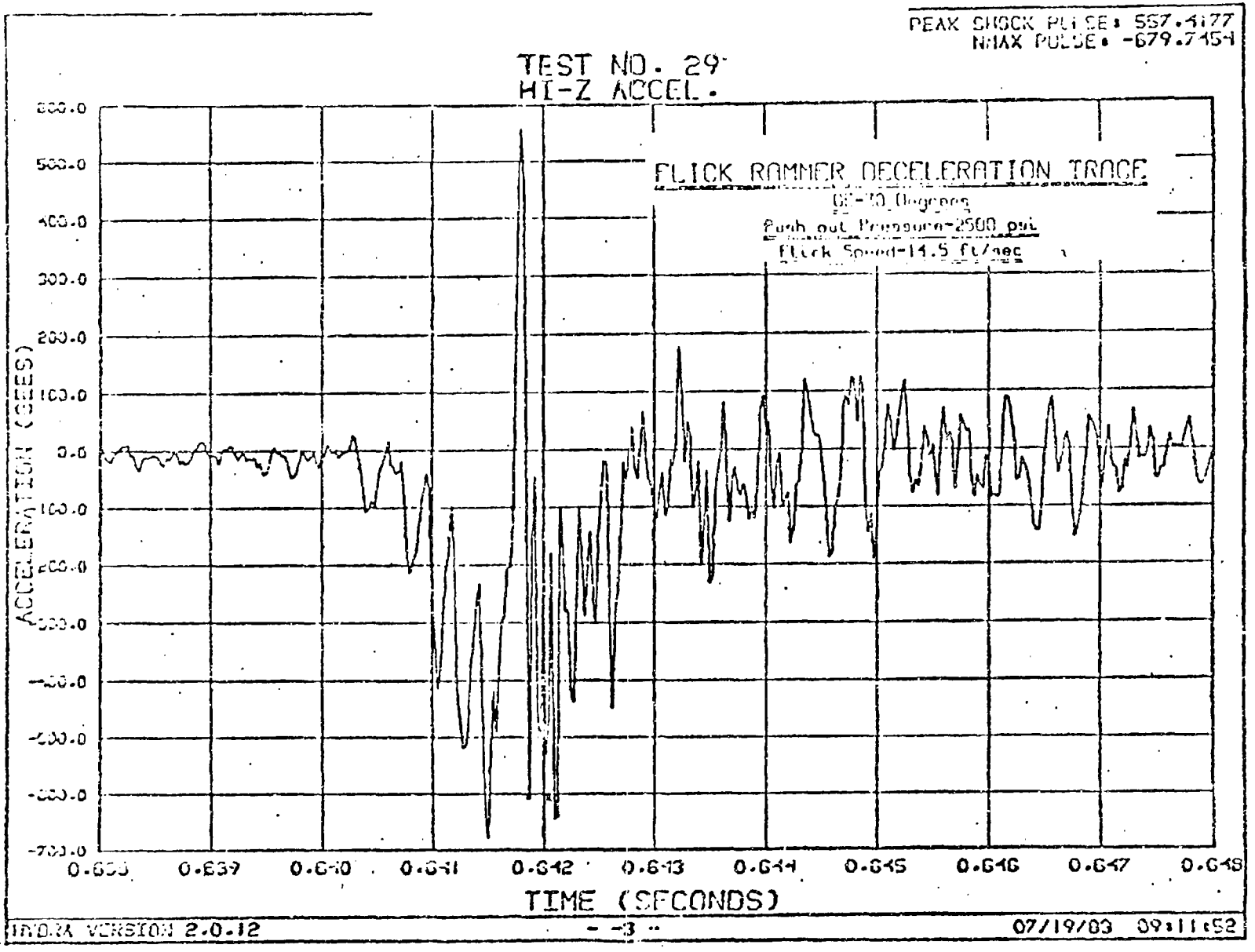
PEAK SHOCK PULSE: 557.4177
NMAX PULSE: -679.7454
TEST NO. 29
HI-Z ACCEL.
FLICK RAMMER DECELERATION TRACE
Push out Pressure=2500 psi
Flick Speed=14.5 ft/sec
ACCELERATION (GEES)
TIME (SECONDS)
07/19/83 09:11:52

Figure 4

M557 FUZE PD ELEMENT

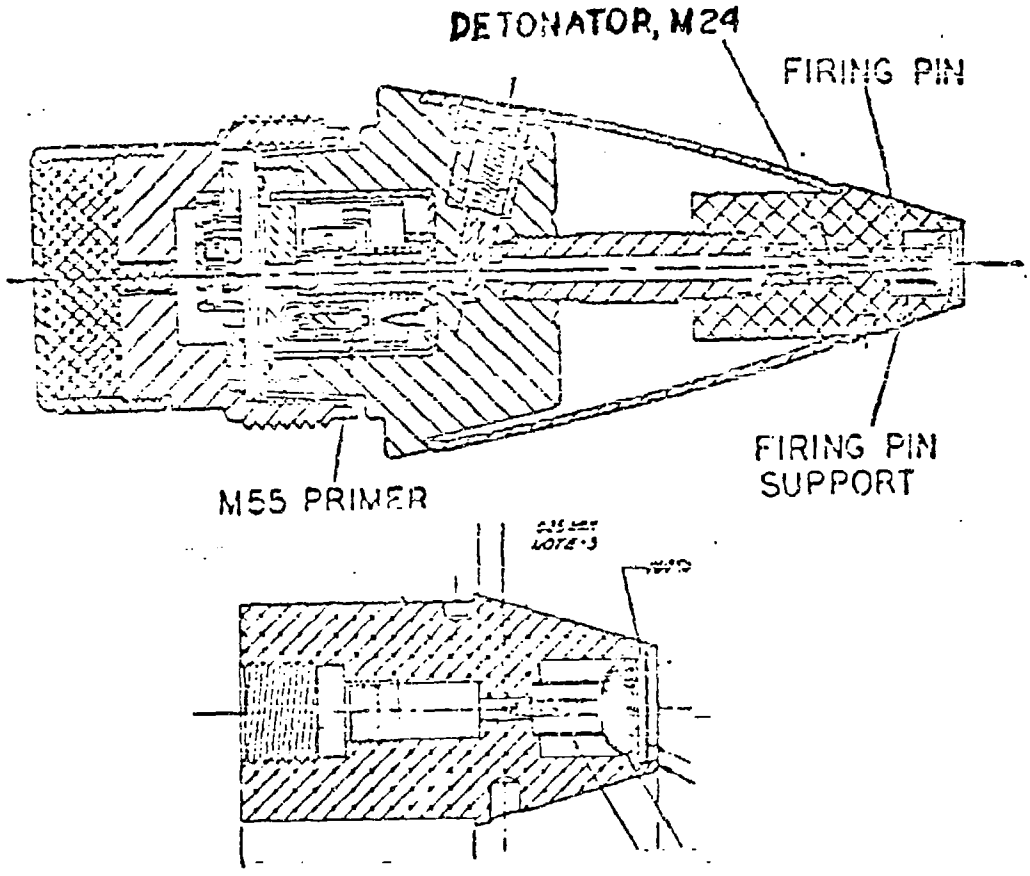

Figure 5

M739 FUZE FIRING PIN

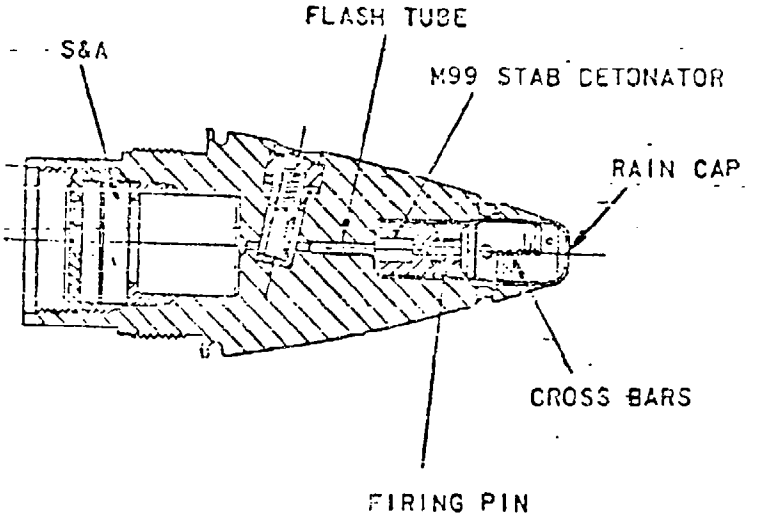

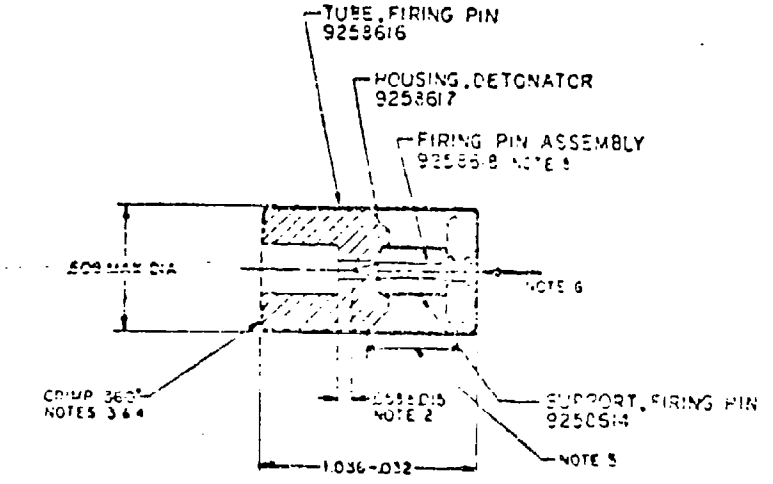

Figure 6

M577 FUZE TIMER ASSEMBLY

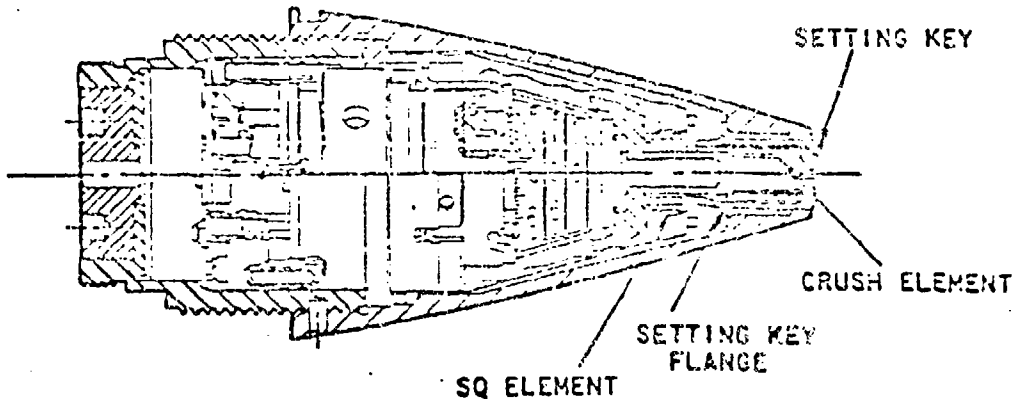

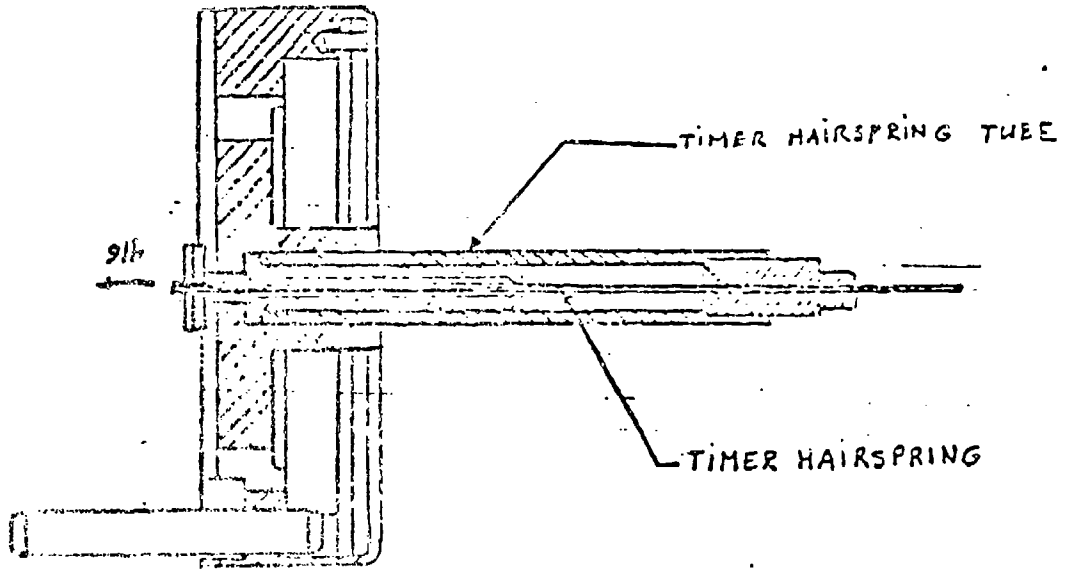

Figure 7

M1 DELAY PLUNGER M557 AND M739 FUZES

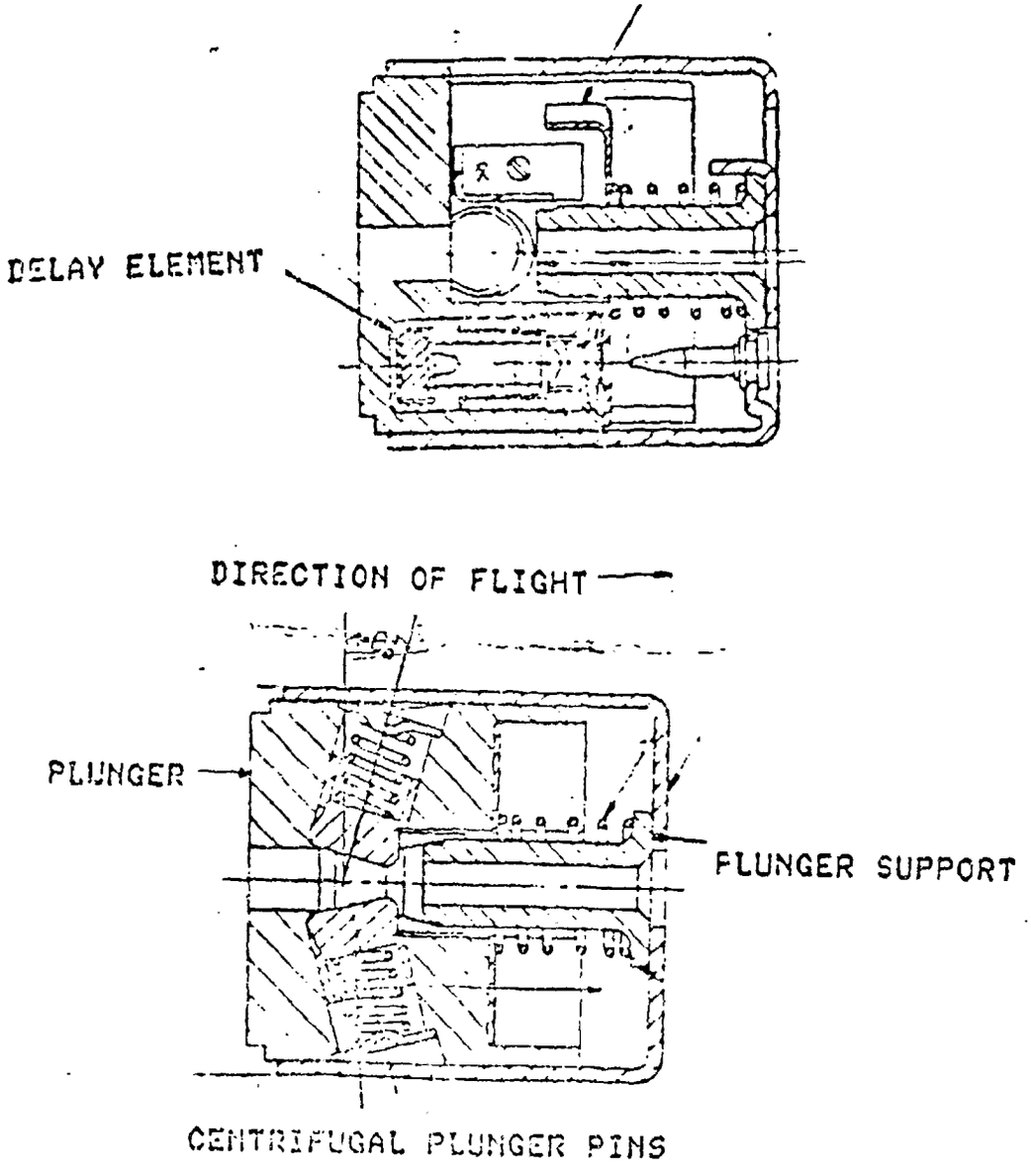

Figure 8

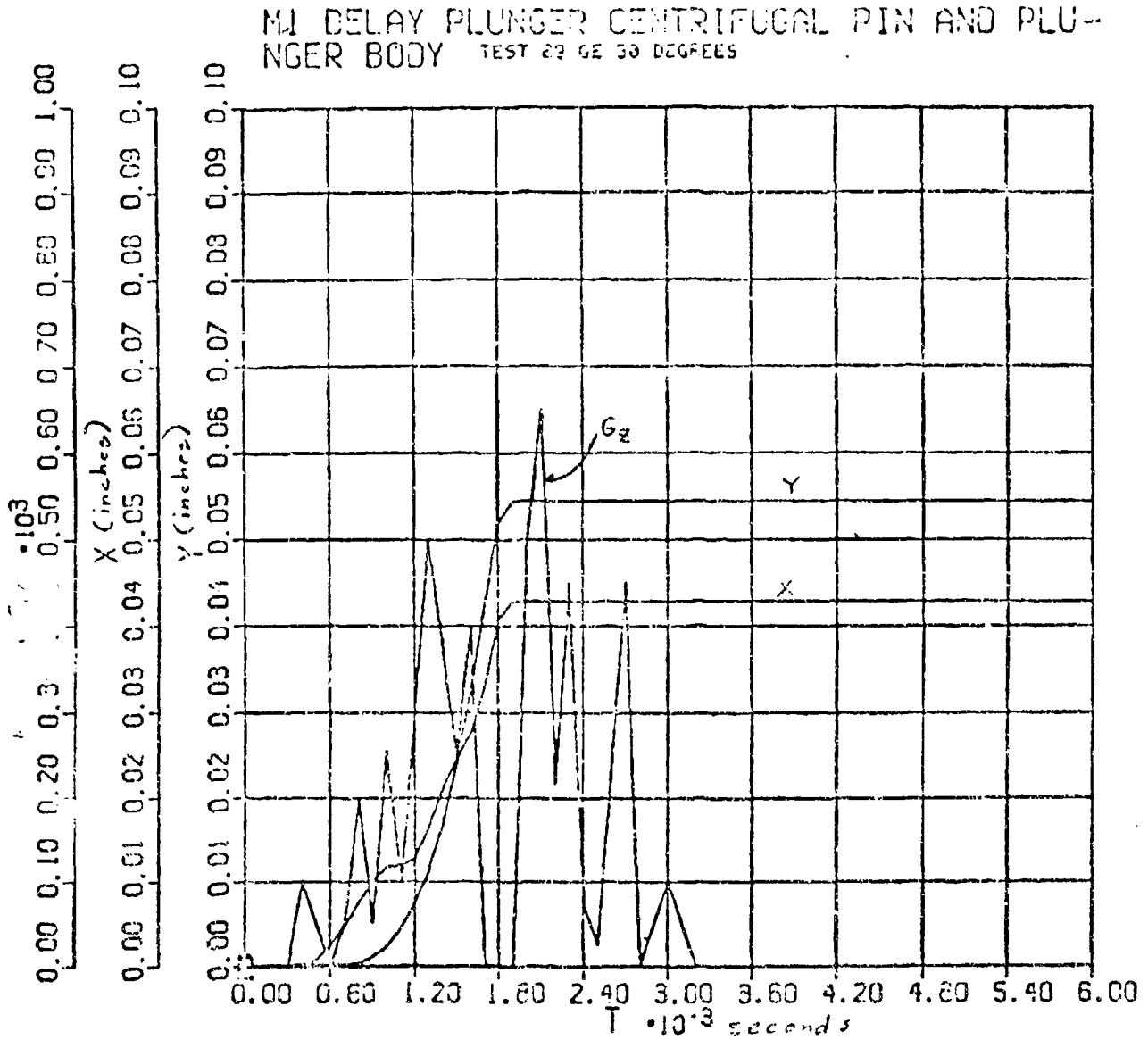
MJ DELAY PLUNGER CENTRIFUGAL PIN AND PLUNGER BODY TEST @ 6E 30 DEGREES
X (inches)
Y (inches)
•10^3
0.00 0.10 0.20 0.30 0.40 0.50 0.60 0.70 0.80 0.90 1.00
0.00 0.01 0.02 0.03 0.04 0.05 0.06 0.07 0.08 0.09 0.10
Gz
Y
X
0.00 0.60 1.20 1.80 2.40 3.00 3.60 4.20 4.80 5.40 6.00
T •10^-3 seconds

Figure 9

KINEMATIC DIAGRAM

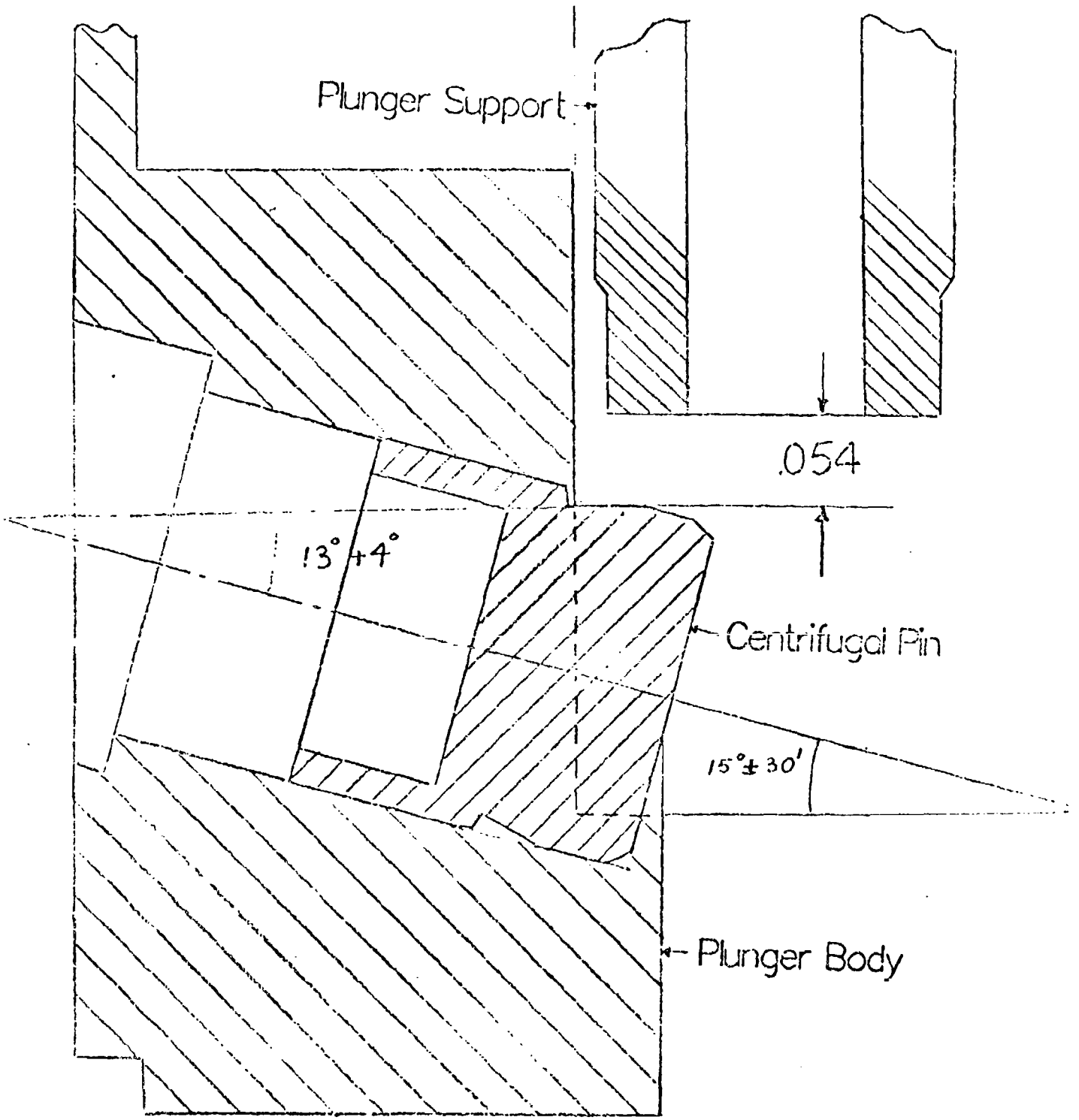

Figure 10

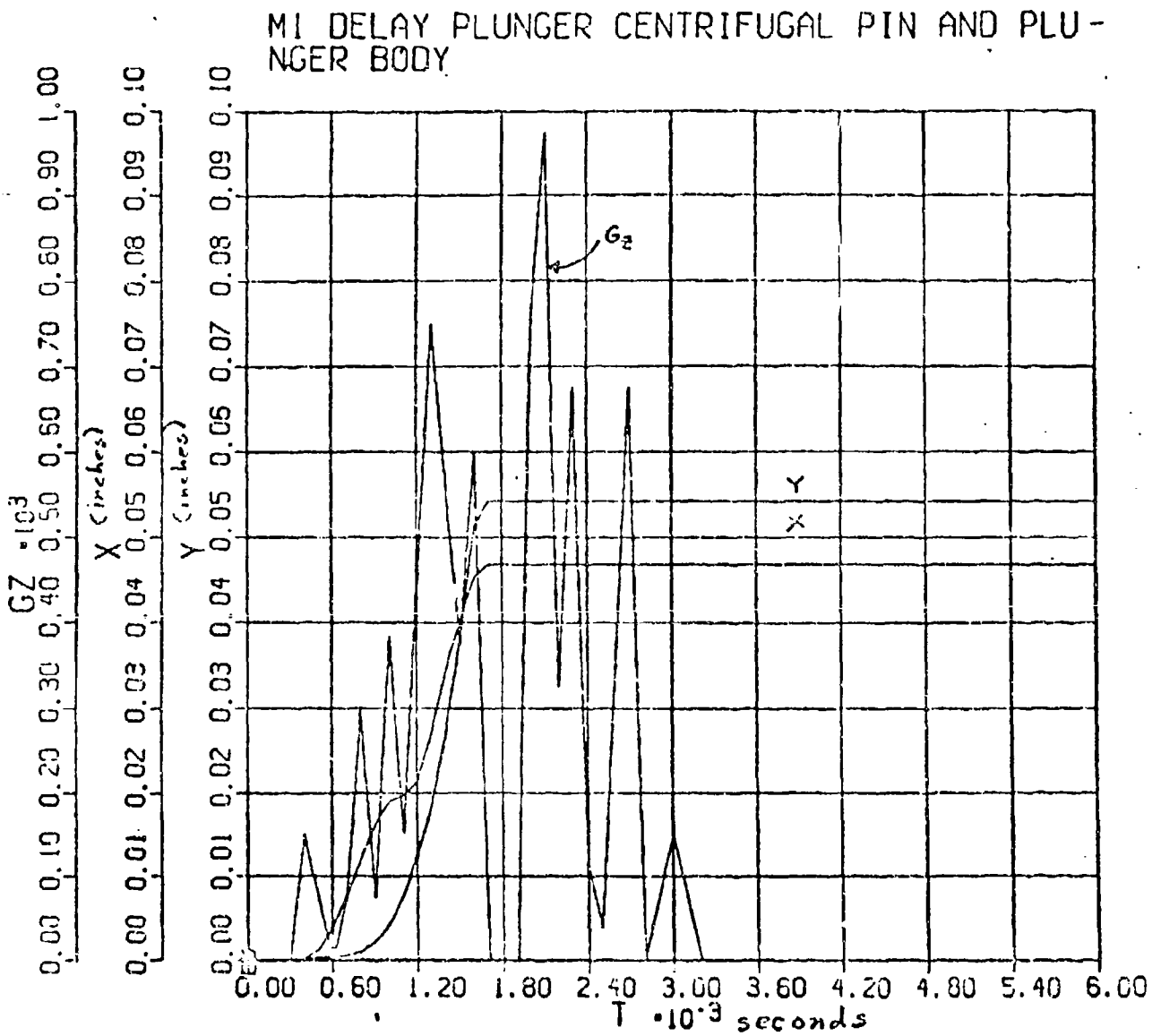
MI DELAY PLUNGER CENTRIFUGAL PIN AND PLUNGER BODY
GZ •10³
X (inches)
Y (inches)
0.00 0.10 0.20 0.30 0.40 0.50 0.60 0.70 0.80 0.90 1.00
0.00 0.01 0.02 0.03 0.04 0.05 0.06 0.07 0.08 0.09 0.10
G_z
Y
X
0.00 0.60 1.20 1.80 2.40 3.00 3.60 4.20 4.80 5.40 6.00
T •10⁻³ seconds

Figure 11

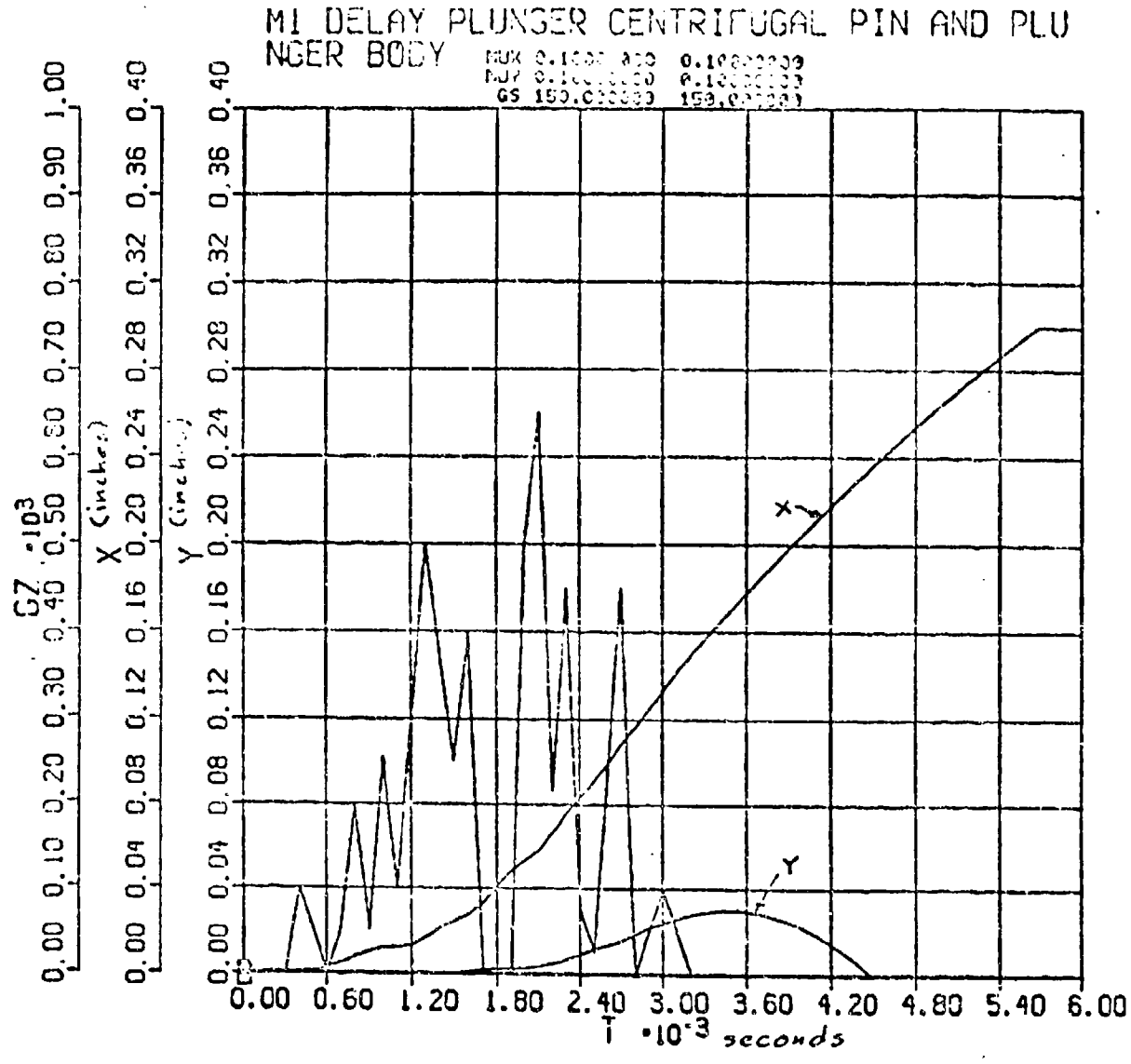
MI DELAY PLUNGER CENTRIFUGAL PIN AND PLU
NGER BODY
GZ •10^3
X (inches)
Y (inches)
0.00 0.10 0.20 0.30 0.40 0.50 0.60 0.70 0.80 0.90 1.00
0.00 0.04 0.08 0.12 0.16 0.20 0.24 0.28 0.32 0.36 0.40
0.00 0.60 1.20 1.80 2.40 3.00 3.60 4.20 4.80 5.40 6.00
T •10^-3 seconds
X
Y

Figure 12

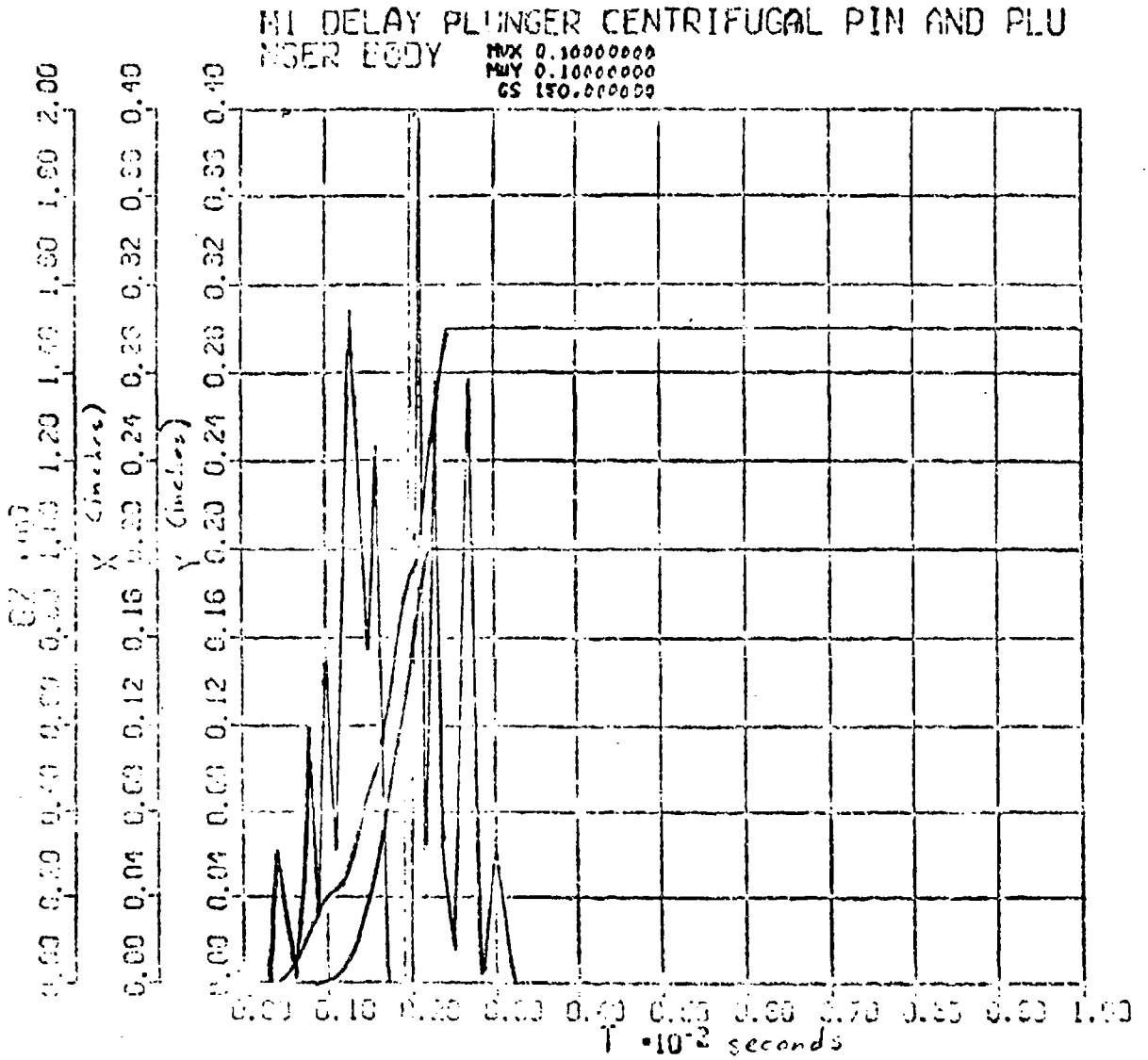
MI DELAY PLUNGER CENTRIFUGAL PIN AND PLU
NGER BODY
MVX 0.10000000
MVY 0.10000000
GS 150.000000
X (inches)
Y (inches)
T •10⁻² seconds

Figure 13

FREE BODY DIAGRAM

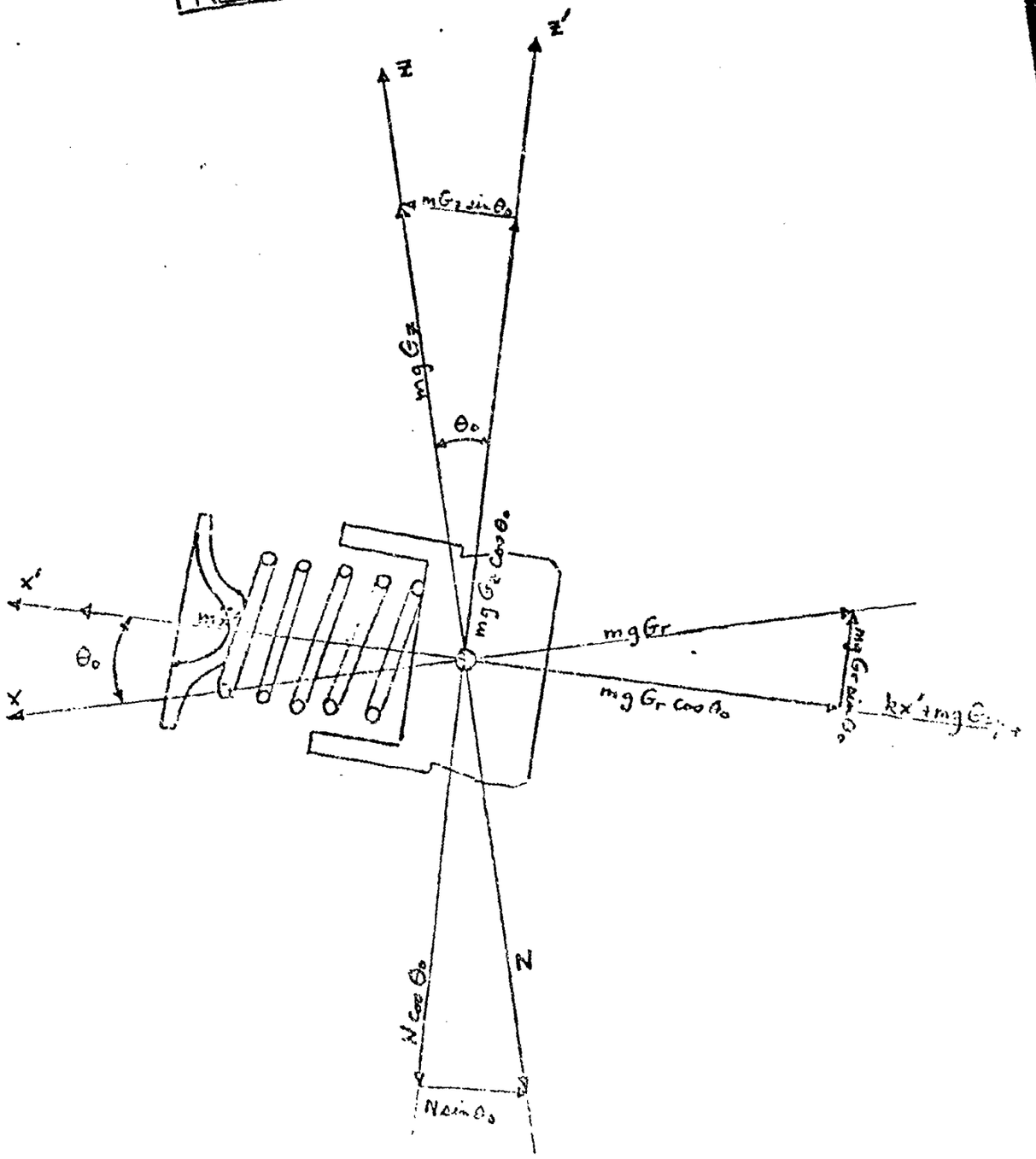

Figure 14

BROOKS

TITLE: A Systems Analysis of Liquid Propellant in a 155mm SP Artillery System

JACK BROOKS
U.S. Army Armament Research and Development Center
Large Caliber Weapon Systems Laboratory
Systems Division
Dover, NJ 07801-5001

ABSTRACT:

A systems analysis is presented on a liquid propellant application to an artillery system. The study attempts to answer the question: "Would we field a Liquid Propellant Gun system if it worked?" It addresses fundamental system considerations, cost, performance, vulnerability, logistics, producability, engineering implications, fielding implications, potential risks and problems, etc. The work was performed in early FY1984.

BIOGRAPHY:

PRESENT ASSIGNMENT: Supervisory Armament Engineer, U.S. Army Armament Research and Development Center, LCWSL, Systems Division.

PAST EXPERIENCE: Systems Analysis, Picatinny Arsenal, 1968-1977; Chemical Engineer, Picatinny Arsenal, 1958-1968.

DEGREES HELD: B.CH.E. Polytechnic Institute of Brooklyn, 1958.

*This paper was classified Distribution Limited to US Government Agencies. Only the abstract appears in these Proceedings. Contact the author for further information.

AN INTEGRATED WEAPON ARMORED VEHICLE MODEL (IWAVM) AND COMPUTER SIMULATION

MR. JOHN GROFF, CHIEF, ENGINEERING
SYSTEMS ANALYSIS SECTION
US ARMY MATERIEL SYSTEMS ANALYSIS ACTIVITY (AMSAA)
ABERDEEN PROVING GROUND, MD 21005-5071

DR. JAMES WALBERT
US ARMY BALLISTIC RESEARCH LABORATORY (BRL)
ABERDEEN PROVING GROUND, MD 21005-5066

MR. THOMAS DOLCE*, OPERATIONS RESEARCH ANALYST
US ARMY MATERIEL SYSTEMS ANALYSIS ACTIVITY (AMSAA)
ABERDEEN PROVING GROUND, MD 21005-5071

1. INTRODUCTION

The importance of computer simulations of performance of complex mechanical systems has long been recognized. The Army Materiel Systems Analysis Activity (AMSAA) has developed an armored vehicle model for studies of automotive performance, hit probability estimations, and related parameters. Since gun dynamics is known to play an important role in weapon accuracy, it was deemed appropriate to replace the rigid gun tube portion of the AMSAA model with a relatively simple gun dynamics model supplied by the Ballistic Research Laboratory (BRL).

In this paper we describe the integrated model, including the limitations and simplifying assumptions concerning the gun dynamics portion, and present comparisons between computer simulation output of muzzle motion with actual recorded muzzle motion from a moving vehicle over various types of terrain.

2. OVERVIEW OF THE INTEGRATED WEAPON ARMORED VEHICLE MODEL (IWAVM)

The gun dynamics model used in the simulation has as its basis a modeling technique developed by Boresi (1). This technique involves the use of a finite element method to simulate the dynamic response of the gun tube to mount motion and ballistic loading. For the purposes of the current computer model, numerous significant changes have been

made by one of the authors to the original modeling technique. In particular, the recoil, the interior ballistics, and the mount motion sections of the model were completely reworked to reflect more realistic conditions.

The original interior ballistics portion of the model used the so-called standard equations for pressure and projectile acceleration and travel from Corner (2). These equations suffer from two main difficulties. Namely, the phasing between pressure and acceleration is not accurate, and an additional inflection point which results in incorrect curvature near the critical muzzle exit point. To correct this problem, the simulation was modified to use actual pressure, acceleration, velocity and travel curves for particular projectiles.

Figures 1 through 4 depict the modified and augment Corner interior ballistic responses for the M392 projectile used in the simulation. These data curves were obtained by averaging, using ammunition lot acceptance data. The fact that the interior ballistics were modified necessitated reworking the recoil section of the code, since the interior ballistic forces drive the recoil mechanism. In this case, the same scaling between projectile acceleration and recoil acceleration was used as in the original version. The breech is modeled as a solid mass with axis offset from the bore axis.

To accommodate vehicle motion input to the trunnions, the model was modified to accept time series data, instead of using a Fourier expansion as forced base motion. In this way, actual data recorded from vehicle road and cross-country tests could be input to the gun dynamics portion of the model for comparison with response to simulated vehicle motion. This also allows actual firing data from moving vehicles to be compared with the simulation. It should be noted that in the current model, only gun tube motion in the vertical plane is simulated. It is anticipated that future developments will include a full six-degree-of-freedom gun dynamics model, for more realistic simulation.

The gun dynamics model has been run independently of the vehicle model for verification of its output in terms of response to ballistic loading. On the basis of available experimental data for comparison, the model gives an adequate representation of the actual firing dynamics of the M68 105mm tank cannon. Comparisons of test data with computer runs of the full simulation show good correlation, especially of muzzle vibration frequencies.

The motivation for integrating the Boresi gun dynamics model into a detailed engineering model/simulation of an armored vehicle stems from an analytical need to:

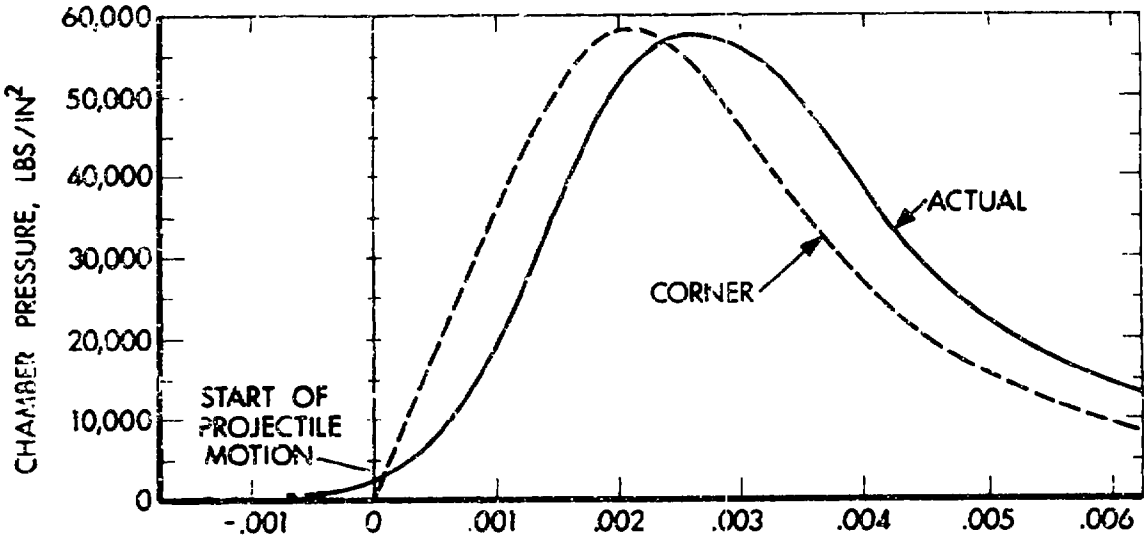

Figure 1. Interior Ballistic Data for M392 Projectile Chamber Pressure (PSI).

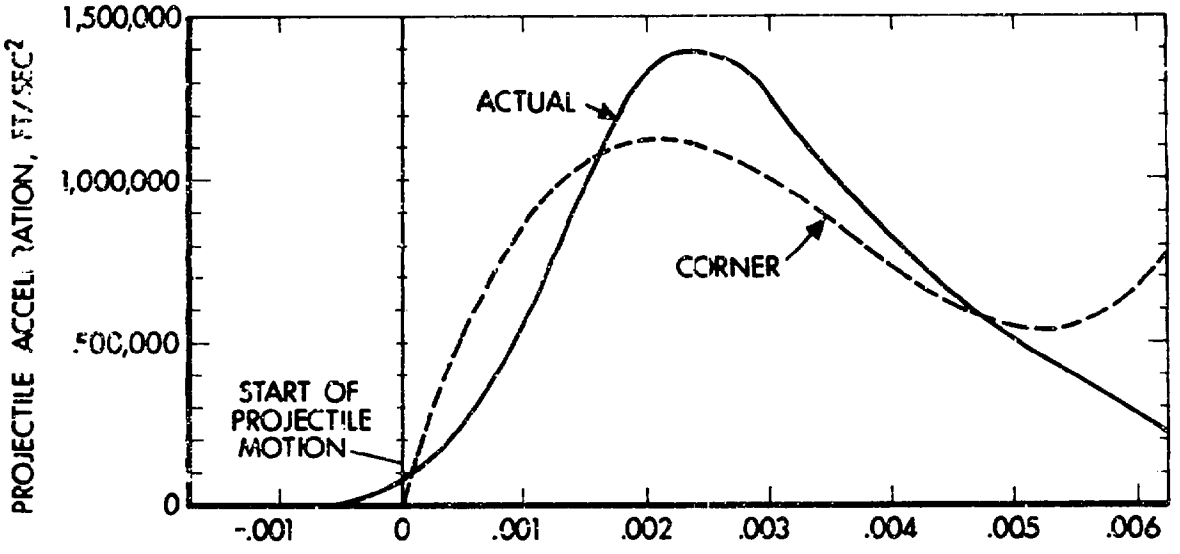

Figure 2. Interior Ballistic Data for M392 Projectile Acceleration (Ft/Sec/Sec)

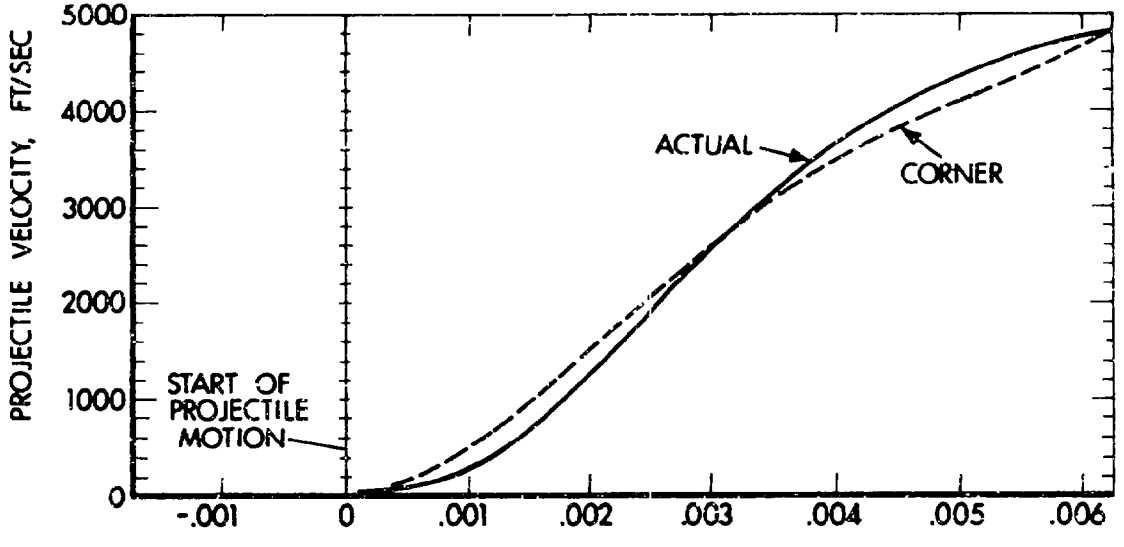

Figure 3. Interior Ballistic Data for M392 Projectile Velocity (Ft/Sec)

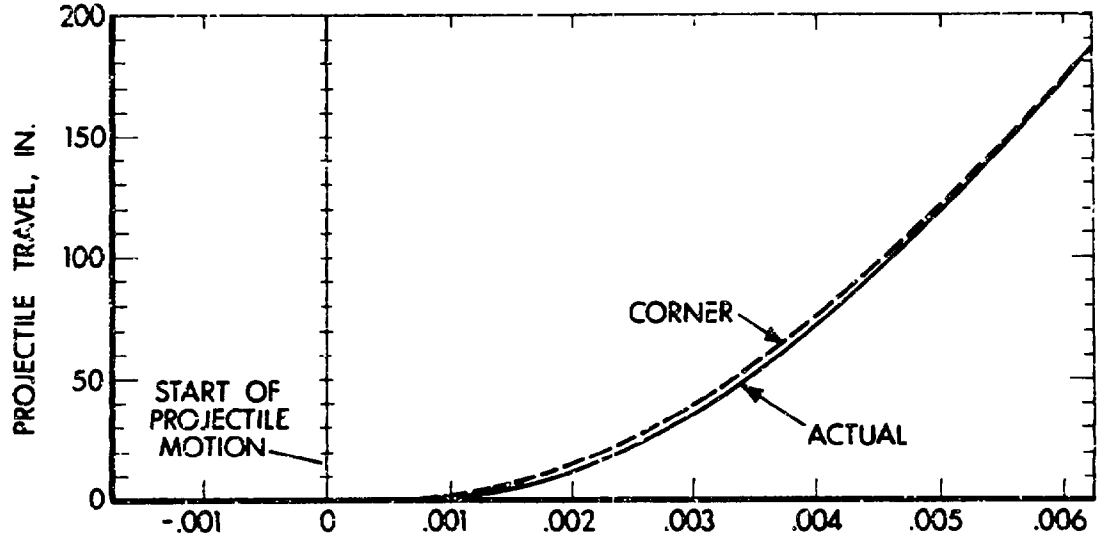

Figure 4. Interior Ballistic Data for M392 Projectile Travel (in.)

a. Characterize/Quantify this error source and it's impact on weapon system delivery accuracy, especially for dynamic situations such as firing on the move, and

b. Study possible fire control modifications/algorithms designed to correct for muzzle flexure induced errors resulting from base motion disturbances and interior ballistic efforts. Besides enhancing the delivery accuracy capability of a weapon study, this study has the potential of increasing target servicing rates by allowing firing of the weapon under extreme base motion disturbances resulting from high terrain severity conditions. Figure 5 depicts the functional block diagram of the "Integrated Weapon Armored Vehicle Model" (IWAVM) that has been jointly developed by the US Army Materiel Systems Analysis Activity and US Army Ballistic Research Laboratory.

The digital computer simulation of an armored vehicle weapon system that is being used in the study contains representations of the vehicle and target motion, suspension characteristics, weapon/turret servo drives, fire control, sight/reticle servo drives, human gunner model, human driver performance characteristics and terrain profiles. Briefly, the basic subroutine modules are:

a. SUBROUTINE FIRST, in which total weights, inertias, center of gravity, mass unbalance and scenario conditions for a run are initialized.

b. SUBROUTINE MOTION, which generates the motion of the road wheel over either an APG Bump Course or Micro Terrain Profile and the angular motion of the hull on the suspension. In turn it calls SUBROUTINE BUMP, in which the terrain or APG Stabilization Bump Course is modeled, and SUBROUTINE SUSPEN, in which the torsion bar, volute springs, suspension stops, and dampers are described.

c. SUBROUTINE DRIVE, which describes both the elevation and azimuth stabilization drives to include the analog compensation networks, hydraulic servo valves, load dynamics, gear box characteristics and sensors.

d. SUBROUTINE GUNNER, in which the human dynamical responses, decision making, and action and visual thresholds are modeled.

e. SUBROUTINE SIGHT, which simulates the gun-director type fire control in the elevation sight axis and the driven-reticle model in the azimuth sight axis.

f. SUBROUTINE RETCON, which simulates the digital control laws programmed in the ballistic computer for commanding the azimuth reticle servo.

g. SUBROUTINE OFFSET, which emulates the M1 elevation and azimuth algorithms for computing the ballistic offsets for the kinetic-energy and heat rounds.

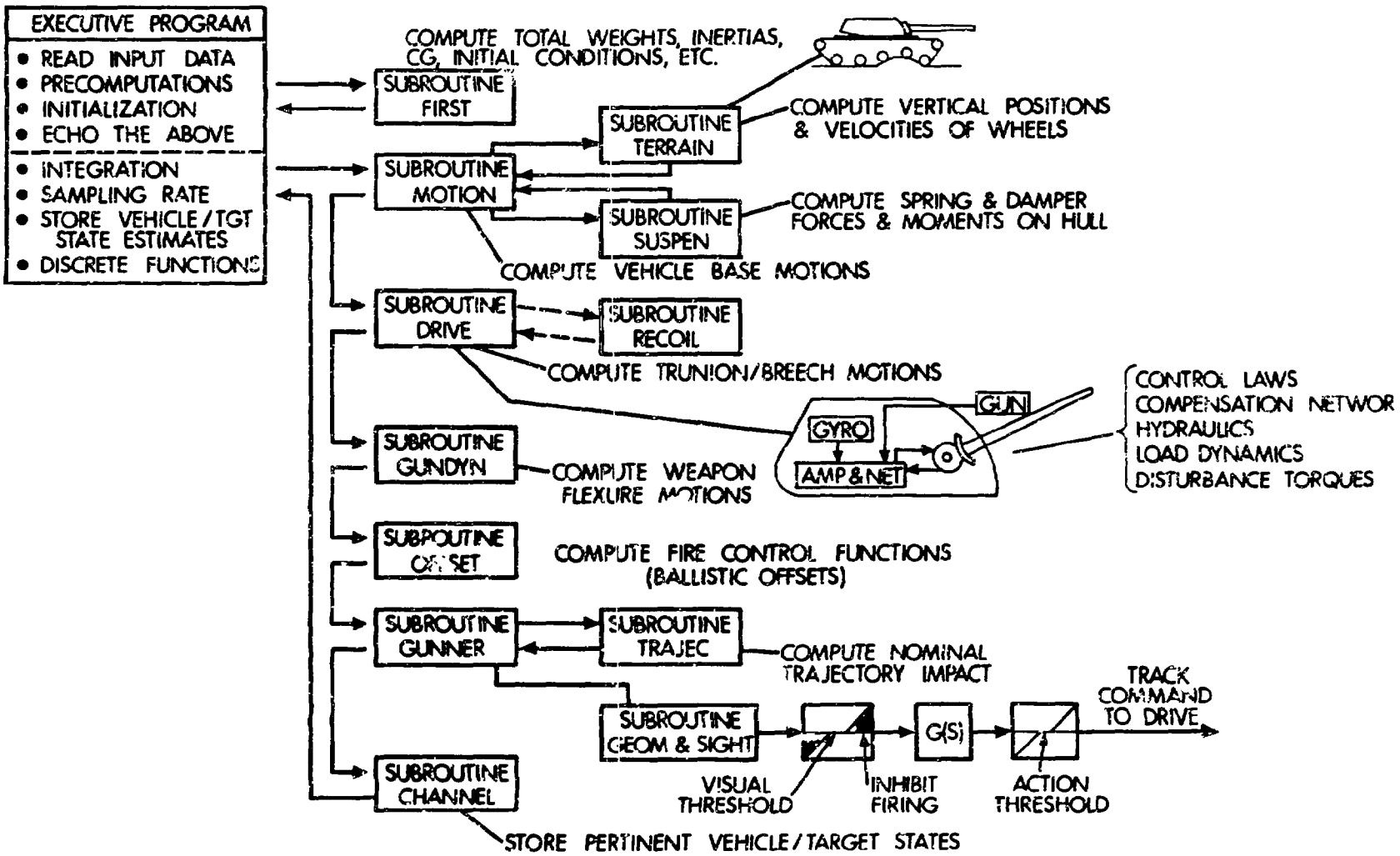

Figure 5. Functional Block Diagram of Integrated Weapon Armored Vehicle Model (IWAVM)

h. SUBROUTINE TRAJEC, which computes required weapon to target offsets and takes into account target motion as well as additional velocity components imparted to the projectile.

i. SUBROUTINE GUNDYN, which simulates the independent weapon tube flexure responses based on the Boresi model formulations. The model has been modified to accept vertical and gun tube translational motion generated at the trunnions by the armored vehicle simulation.

3. SUMMARY

To date the Boresi gun dynamics model has been successfully integrated with the M1 engineering armored vehicle model and exercised for various verificaiton/validation scenarios. Figures 6 and 7 depict actual and simulated power spectral analysis responses for the M68 105mm weapon. The scenario conditions were gravel road (0.5 inch RMS - Waterways Experimental Station Terrain Severity Criterion) at 15 mph. Both simulated and actual responses generally exhibit the same resonance frequency range and amplitude levels.

Further verification and validation work as well as additional refinements to the model are being pursued prior to application of the IWAVM simulation. Future work will focus on extending the model to include the extended 105mm as well as the 120mm gun tubes.

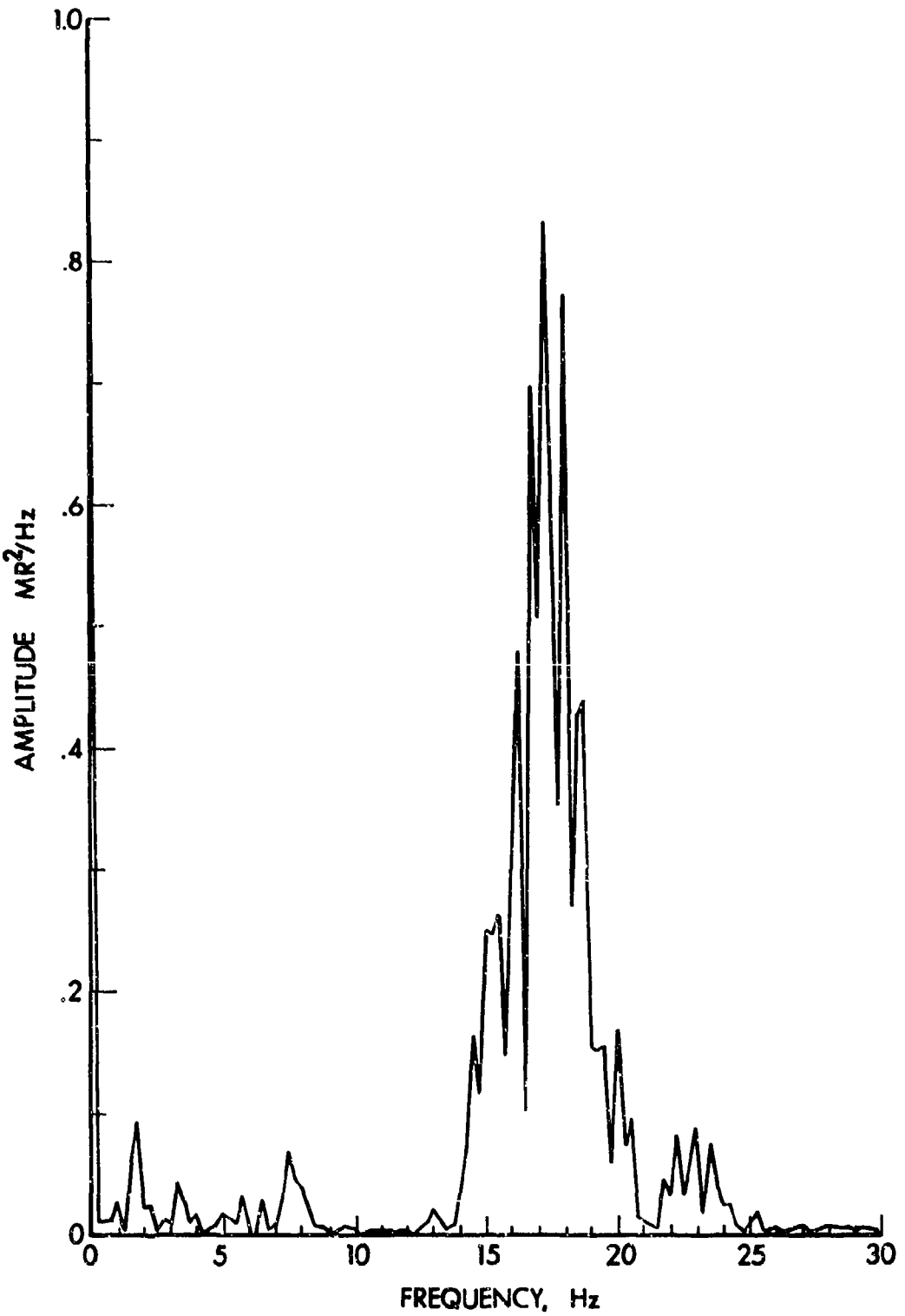

Figure 6. Power Spectral Density / Actual Test Data / Scenario: Gravel Course / 15 mph.

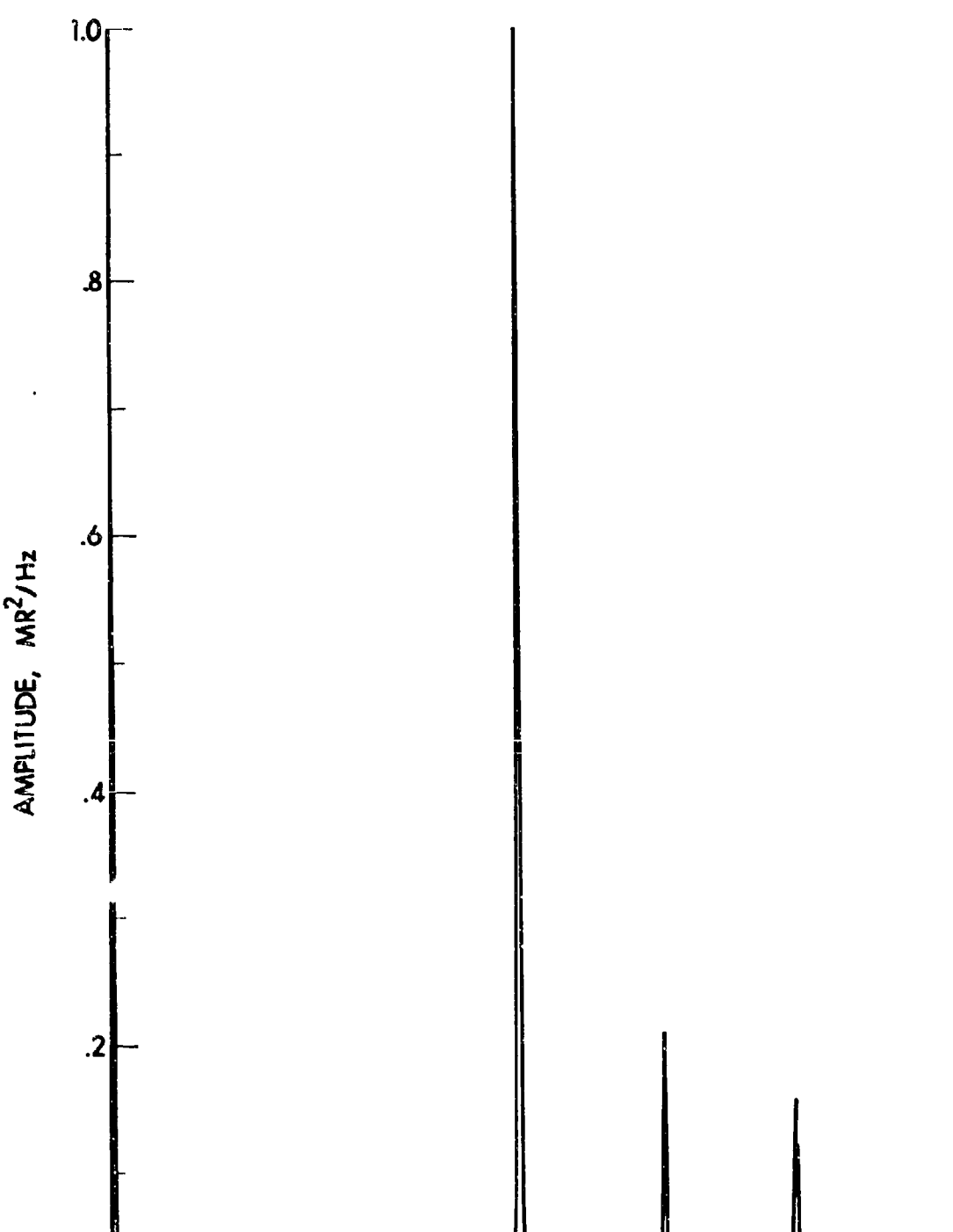

Figure 7. Power Spectral Density / Simulation Results / Scenario: Gravel Course / 15 mph.

BIBLIOGRAPHY

1. Boresi, A.P., "Transient Response of a Gun System under Repeated Firing", ARO Contractor Report DAAK-10-77C-0210.
2. Corner, J., "Theory of the Interior Ballistics of Guns", Wiley, 1950.
3. Cushman, P., P. Kester, and G. Grackis, "Description of HITPRO Model and Computer Simulation for the XM-1 Tank", General Electric Company, December, 1980.
4. Cushman, P., "Memo - Data and Program Changes for HITPRO M1 Simulation", General Electric Company Memo, November, 1983.

TITLE: The Predicted Effect on 'Gun Jump' Due to Changes in Gun Cradle Bearings and Gun Barrel Stiffness.

Peter H G Penny
Royal Armament Research & Development Establishment
Chobham Lane, Chertsey, Surrey. KT16 0EE
United Kingdom of Great Britain & Northern Ireland.

ABSTRACT: A computer programme is used to investigate the changes which occur to the variables which contribute to the term 'gun jump' and the manner in which these variables change with changes to the gun barrel and cradle bearing stiffness and the bearing location. Attention is drawn to the undesirability of high rates of change of certain varisbles just as the projectile exits the barrel.

BIOGRAPHY:

PRESENT ASSIGNMENT:		Section Head, Gun Systems Division, RARDE(Chertsey)
DEGREES HELD:	BSc	City University, London, UK (1972)
	PhD	City University, London, UK (1978)

THE PREDICTED EFFECT ON 'GUN JUMP' DUE TO CHANGES IN GUN CRADLE BEARINGS AND GUN BARREL STIFFNESS.

P H G PENNY
Royal Armament Research & Development Establishment (Chertsey)
Chobham Lane, Chertsey, Surrey, KT16 0EE
United Kingdom of Great Britain & Northern Ireland

W P C KING
Royal Military College of Science,
School of Management and Mathematics, Shrivenham,
Swindon, Wiltshire, SN6 8LA,
United Kingdom of Great Britain & Northern Ireland

1. INTRODUCTION

Since the seventeenth century many people have noticed that gun projectiles do not always land on their expected target. Attempts to improve gun accuracy are concerned with the sources and mechanisms which cause a given projectile impact distribution at the target.

The flight of the projectile to the target can be considered in three phases:

(a) Interior ballistics - projectile motion within the barrel.
(b) Intermediate ballistics - projectile launch, propellant gas blast and, for sub-calibre rounds, sabot separation.
(c) Exterior ballistics - downrange flight and target impact.

In this paper we will consider the motion of the gun barrel and its mounting up to projectile launch. The computer program RAMA 84 was used. This program was written and developed by The Royal Military College of Science and a paper describing an earlier version was presented to the 3rd US Army Symposium on Gun Dynamics (1).

2. DESCRIPTION OF COMPUTER MODEL

The mathematical model represents a flexible gun barrel mounted in a rigid body cradle. The cradle is able to rotate about its trunnions, its rotational movement being resisted by an elevating gear stiffness coupled to a slipping clutch (see Figure 1). The barrel can have breech and muzzle masses attached to it.

At the barrel/cradle interface are two identical cylindrical elastic bearings of finite length. The bearing positions and parameters can be varied.

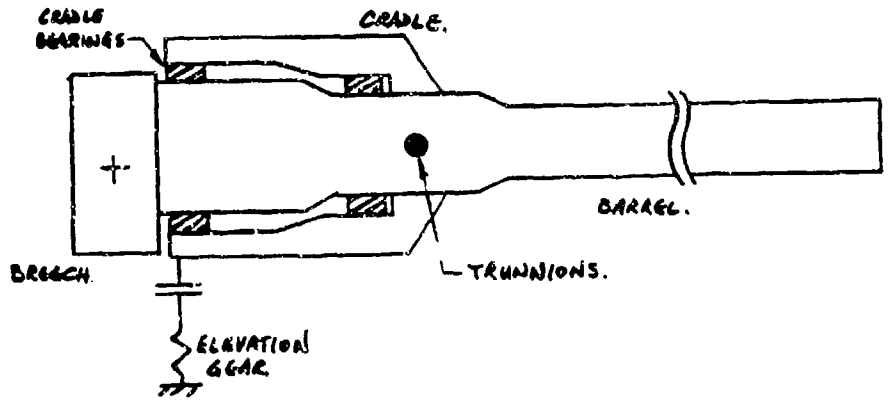

Figure 1 Schematic of the Breech, Barrel and Cradle

The theoretical basis of the model is the Euler-Bernoulli theory of thin beams. The model is subject to both flexural and axial vibrations. The resulting differential equations with their boundary conditions are numerically solved using an implicit finite difference algorithm. The program is now very user friendly and data files are easily compiled, edited and recorded.

The algorithm used for the solution of the differential equations is efficient and robust. The method of solution was described in the earlier paper.

3. PARAMETERS INVESTIGATED

In a previous paper presented to the TTCP MTA6 Second Workshop in September 1984 (2), the predicted effect of local stiffening and mass redistribution of the gun barrel was examined. One parameter not examined in the MTA6 paper was that of cradle bearing stiffness.

It should be emphasized that the gun system parameters used in this investigation are for illustrative purposes only and do not represent a current tank gun nor any proposed future tank gun. The effects due to changes in three parameters will be examined:

(a) Gun barrel stiffness
(b) Cradle bearing spacing
(c) Cradle bearing stiffness

4. CHOICE OF OUTPUT VARIABLES

If we intend to produce a 'better' gun we must decide what measured criteria we will accept as producing an improvement. In this paper the vibration and yaw angle of the projectile within the gun barrel will not be considered, although some work in this area does look promising. The assessment will simply compare gun muzzle transverse velocity, muzzle slope and gun cradle rotation.

It could be claimed that a gun system giving a consistently high 'gun jump' figure (see Figure 2), would give a constant bias which could be compensated for within the sighting system. It should be mentioned, however, that a gun which is sensitive to small production variations will probably lead to variable accuracy whereas a gun which demonstrates a lower sensitivety to changes in these parameters would probably be termed an 'improvement'.

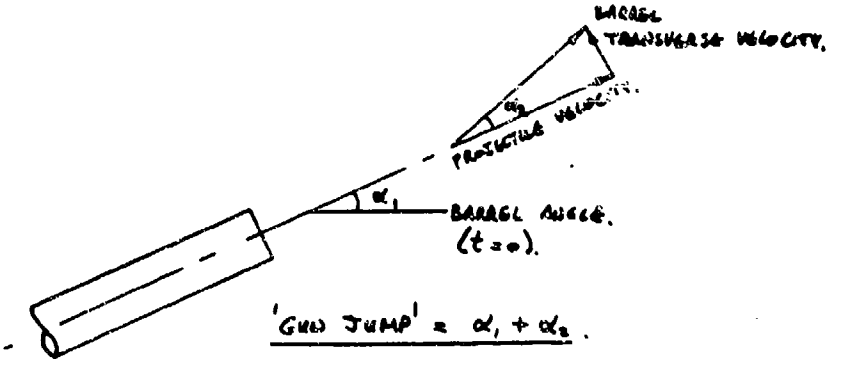

Figure 2 Definition of 'Gun Jump'

5. RESULTS

5.1 Gun barrel stiffness

Two gun barrel configurations were examined and are shown in outline in Figure 3.

The first configuration was used to examine the effect of inserting a more compliant barrel section between the breech and the forward cradle bearing whilst retaining the same recoiling mass. The barrels, of course, no longer retain the same degree of balance.

In almost every case Configuration No.1 is the worst case in terms of the maximum disturbance amplitude, although close to shot exit (just over 7ms), there is often little difference. A comparison of barrel transverse velocity at the muzzle is

shown in Figure 4; note the difference in the rates of change at shot exit. At 9ms the cradle rotation is about double that of the second configuration.

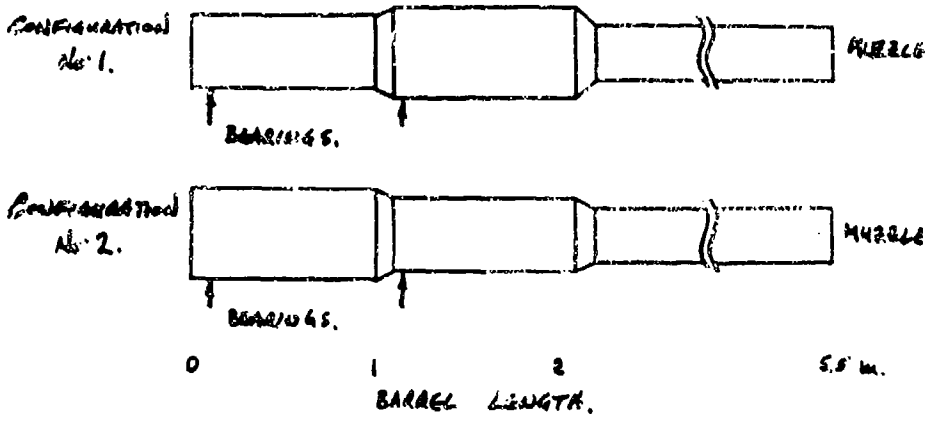

Figure 3 Barrel Configurations

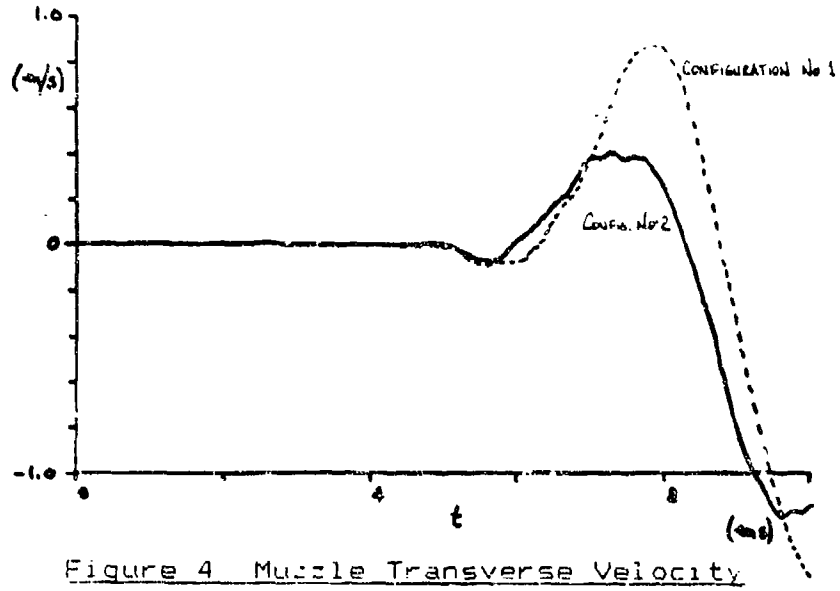

Figure 4 Muzzle Transverse Velocity

A more detailed examination of the results is confined to Configuration No.2.

5.2 Forward cradle bearing position

The forward cradle bearing position was increased in 0.5m increments from 1m to 2m. The muzzle transverse velocity does not exhibit a marked change before shot exit (see Figure 5). The muzzle slope figures also show the major differences to occur after shot exit (see Figure 6). The cradle rotation reaches a maximum value earlier as the cradle bearing spacing is increased (from 9.5ms down to 8ms) and the maximum

amplitude is reduced from 0.8mr to 0.5mr. At shot exit, however, the cradle rotation increases with the cradle bearing spacing since larger moments are being passed into the cradle.

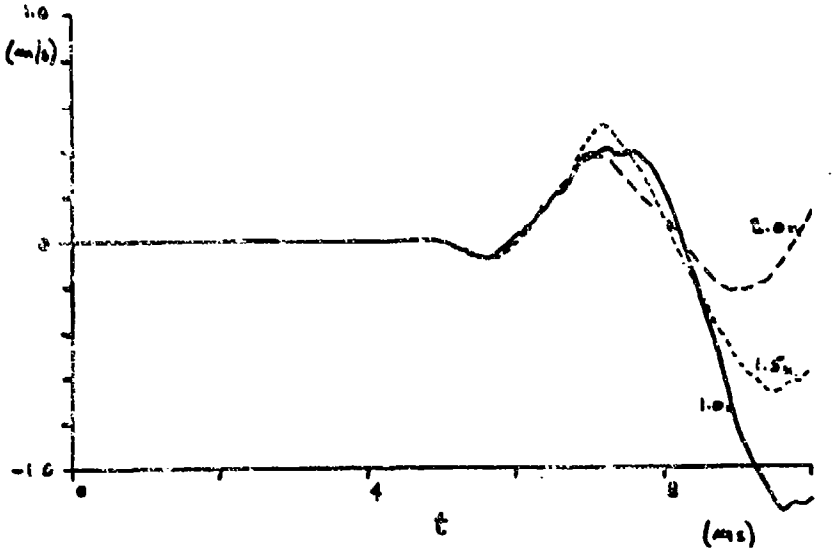

Figure 5 Muzzle Transverse Velocity
Graph numbering denotes cradle bearing spacing in metres

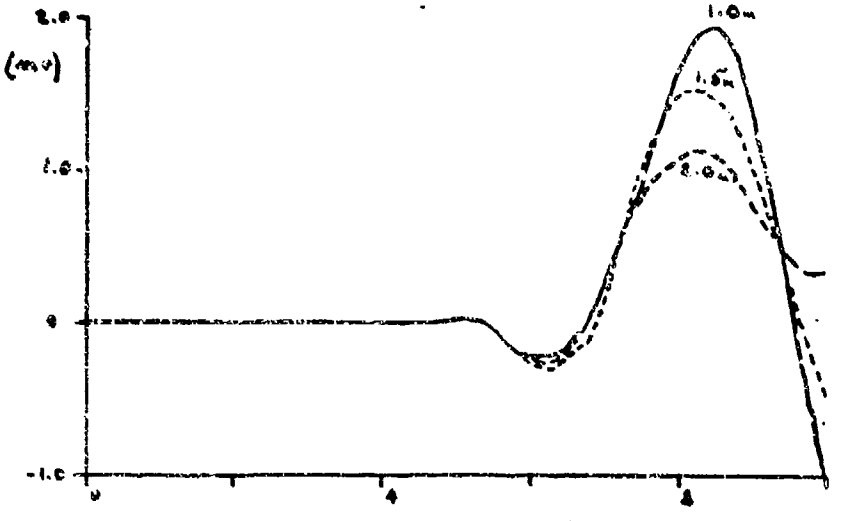

Figure 6 Muzzle Slope
Graph numbering denotes cradle bearing spacing in metres

5.3 Cradle bearing stiffness

A number of cradle bearing stiffnesses were examined but only three are shown. The units of bearing stiffness are Newtons per metre deflection per metre length of bearing. The figure

of 1.0×10^5 Nm/m is often used and these results are compared with 0.5×10^9 Nm/m and 5.0×10^9 Nm/m.

Examination of the muzzle transverse velocity, muzzle slope and cradle rotation graphs indicated that the effect of the softer bearings was small, whereas the effect of the stiffer bearing was quite noticeable; in particular note the lower rates of change with the stiffer bearings. It should be noted that the stiffer bearings were much stiffer from the standard figure than the degree of softening. The results are shown in Figures 7, 8 and 9.

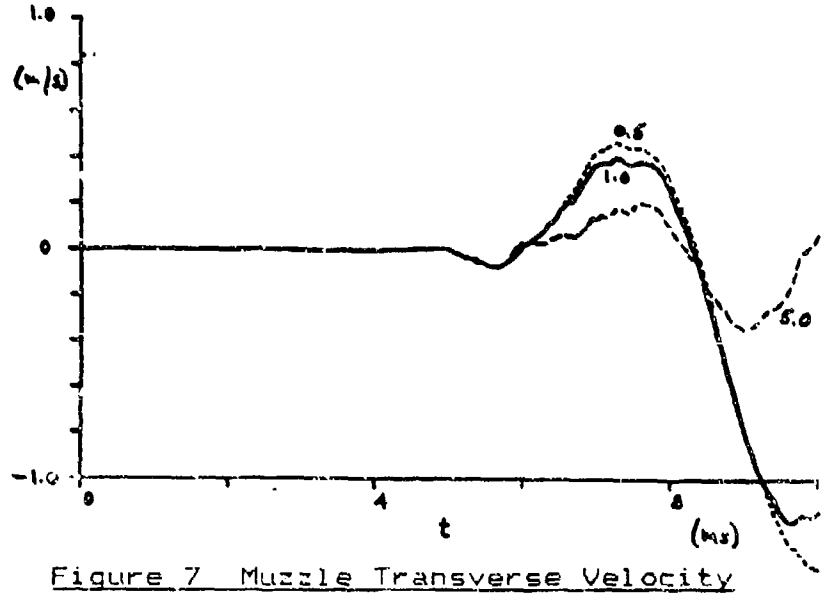

Figure 7 Muzzle Transverse Velocity
Graph numbering denoted cradle bearing stiffness $\times 10^{-9}$ N/m

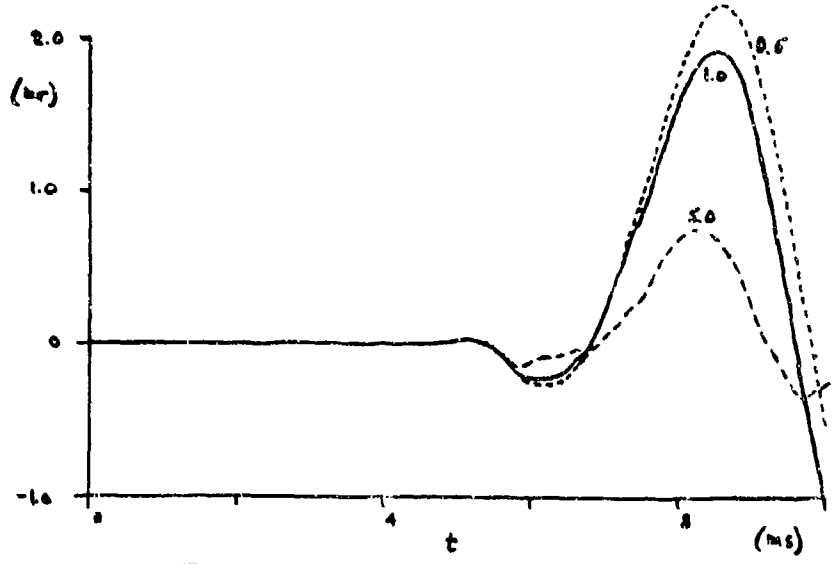

Figure 8 Muzzle Slope
Graph numbering denotes cradle bearing stiffness $\times 10^{-9}$ Nm/m

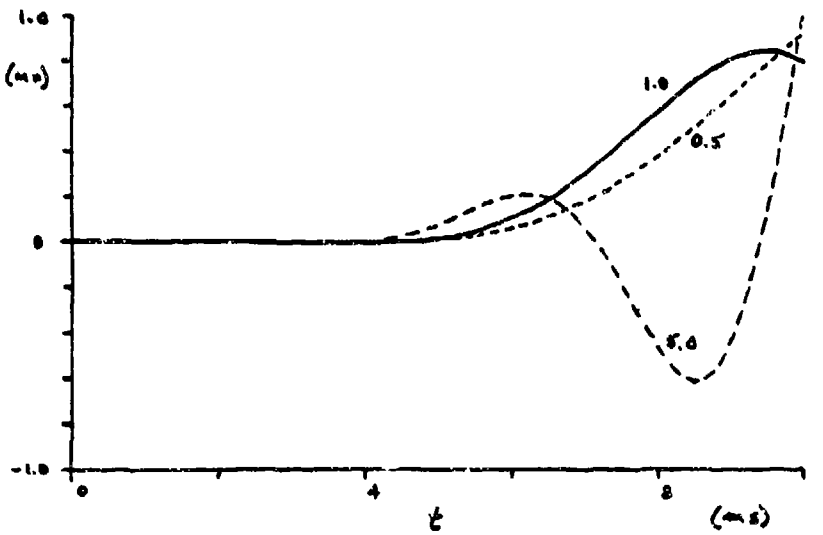

Figure 9 Cradle Rotation
Graph numbering denotes cradle bearing stiffness $\times 10^{-9}$ Nm/m

6. CONCLUSIONS

The results are only true for the combinations of barrel and bearing stiffnesses together with the gun balance and bearing locations.

The computer model used for this work had linear elastic bearings with no backlash. The model indicates a substantially changed response with different stiffness cradle bearings. The program is in the process of incorporating a cradle bearing model which includes backlash. A paper by Bulman indicates the possible effects of bearing backlash (3).

Since the cradle is considered as a rigid body the quoted bearing stiffness includes the effective cradle stiffness.

The output variables chosen are not the only variables that can be examined and some projectiles are known to be sensitive to certain launch conditions. As Powell demonstrates, the projectile dynamics within the gun barrel can be important (4). However, based on our simple criteria the preferred system would be Configuration No.2 with the stiffer cradle bearings.

It is considered that the computer model has improved our appreciation of the dynamic interactions within the weapon system and that properly supported by trials results it will assist us in producing a more effective weapon system.

REFERENCES

1. A model for tank gun movements during firing using an implicit difference numerical algorithm'; W F King, G Pagan and M D Thomas. 3rd US Army Symposium on Gun Dynamics, Rensselaerville, NY, May 1982.

2. 'Observations on the effects of parameter changes to the RMCS gun dynamics computer program';F H G Penny. Paper presented to TTCP, KTA6 Second Workshop on Gun Dynamics, RARDE, Fort Halstead, UK, September 1984.

3. The effect of bearing clearance and barrel expansion on barrel response'; D N Bulman. 4th US Army Symposium on Gun Dynamics, Riviera Beach, Florida, May 1985.

4. A simple theoretical model of shot/barrel interaction within a smooth bore gun'; S E Powell. 4th US Army Symposium on Gun Dynamics, Riviera Beach, Florida, May 1985.

AUTHOR INDEX

TECHNICAL REPORT INTERNAL DISTRIBUTION LIST

	NO. OF COPIES
CHIEF, DEVELOPMENT ENGINEERING BRANCH	
ATTN: SMCAR-LCB-D	1
-DA	1
-DP	1
-DR	1
-DS (SYSTEMS)	1
-DS (ICAS GROUP)	1
-DC	1
-DM	1
CHIEF, ENGINEERING SUPPORT BRANCH	
ATTN: SMCAR-LCB-S	1
-SE	1
CHIEF, RESEARCH BRANCH	
ATTN: SMCAR-LCB-R	2
-R (ELLEN FOGARTY)	1
-RA	1
-RM	2
-RP	1
-RT	1
TECHNICAL LIBRARY	5
ATTN: SMCAR-LCB-TL	
TECHNICAL PUBLICATIONS & EDITING UNIT	2
ATTN: SMCAR-LCB-TL	
DIRECTOR, OPERATIONS DIRECTORATE	1
DIRECTOR, PROCUREMENT DIRECTORATE	1
DIRECTOR, PRODUCT ASSURANCE DIRECTORATE	1

NOTE: PLEASE NOTIFY DIRECTOR, BENET WEAPONS LABORATORY, ATTN: SMCAR-LCB-TL, OF ANY ADDRESS CHANGES.

TECHNICAL REPORT EXTERNAL DISTRIBUTION LIST

	NO. OF COPIES
ASST SEC OF THE ARMY RESEARCH & DEVELOPMENT ATTN: DEP FOR SCI & TECH THE PENTAGON WASHINGTON, D.C. 20315	1
COMMANDER DEFENSE TECHNICAL INFO CENTER ATTN: DTIC-DDA CAMERON STATION ALEXANDRIA, VA 22314	12
COMMANDER US ARMY MAT DEV & READ COMD ATTN: DRCDE-SG 5001 EISENHOWER AVE ALEXANDRIA, VA 22333	1
COMMANDER ARMAMENT RES & DEV CTR US ARMY AMCCOM ATTN: SMCAR-LC	1
SMCAR-LCE	1
SMCAR-LCM (BLDG 321)	1
SMCAR-LCS	1
SMCAR-LCU	1
SMCAR-LCW	1
SMCAR-SCM-O (PLASTICS TECH EVAL CTR, BLDG. 351N)	1
SMCAR-TSS (STINFO) DOVER, NJ 07801	2
DIRECTOR BALLISTICS RESEARCH LABORATORY ATTN: AMXBR-TSB-S (STINFO) ABERDEEN PROVING GROUND, MD 21005	1
MATERIEL SYSTEMS ANALYSIS ACTV ATTN: DRXSY-MP ABERDEEN PROVING GROUND, MD 21005	1
COMMANDER US ARMY AMCCOM ATTN: SMCAR-ESP-L ROCK ISLAND, IL 61299	1
COMMANDER ROCK ISLAND ARSENAL ATTN: SMCRI-ENM (MAT SCI DIV) ROCK ISLAND, IL 61299	1
DIRECTOR US ARMY INDUSTRIAL BASE ENG ACTV ATTN: DRXIB-M ROCK ISLAND, IL 61299	1
COMMANDER US ARMY TANK-AUTMV R&D COMD ATTN: TECH LIB - DRSTA-TSL WARREN, MI 48090	1
COMMANDER US ARMY TANK-AUTMV COMD ATTN: DRSTA-RC WARREN, MI 48090	1
COMMANDER US MILITARY ACADEMY ATTN: CHMN, MECH ENGR DEPT WEST POINT, NY 10996	1
US ARMY MISSILE COMD REDSTONE SCIENTIFIC INFO CTR ATTN: DOCUMENTS SECT, BLDG. 4484 REDSTONE ARSENAL, AL 35898	2
COMMANDER US ARMY FGN SCIENCE & TECH CTR ATTN: DRXST-SD 220 7TH STREET, N.E. CHARLOTTESVILLE, VA 22901	1

NOTE: PLEASE NOTIFY COMMANDER, ARMAMENT RESEARCH AND DEVELOPMENT CENTER, US ARMY AMCCOM, ATTN: BENET WEAPONS LABORATORY, SMCAR-LCB-TL, WATERVLIET, NY 12189, OF ANY ADDRESS CHANGES.

TECHNICAL REPORT EXTERNAL DISTRIBUTION LIST (CONT'D)

	NO. OF COPIES
COMMANDER US ARMY MATERIALS & MECHANICS RESEARCH CENTER ATTN: TECH LIB - DRXMR-PL WATERTOWN, MA 01272	2
COMMANDER US ARMY RESEARCH OFFICE ATTN: CHIEF, IPO P.O. BOX 12211 RESEARCH TRIANGLE PARK, NC 27709	1
COMMANDER US ARMY HARRY DIAMOND LAB ATTN: TECH LIB 2800 POWDER MILL ROAD ADELPHIA, MD 20783	1
COMMANDER NAVAL SURFACE WEAPONS CTR ATTN: TECHNICAL LIBRARY CODE X212 DAHLGREN, VA 22448	1
DIRECTOR US NAVAL RESEARCH LAB ATTN: DIR, MECH DIV CODE 26-27, (DOC LIB) WASHINGTON, D.C. 20375	1 1
COMMANDER AIR FORCE ARMAMENT LABORATORY ATTN: AFATL/DLJ AFATL/DLJG EGLIN AFB, FL 32542	1 1
METALS & CERAMICS INFO CTR BATTELLE COLUMBUS LAB 505 KING AVENUE COLUMBUS, OH 43201	1

NOTE: PLEASE NOTIFY COMMANDER, ARMAMENT RESEARCH AND DEVELOPMENT CENTER, US ARMY AMCCOM, ATTN: BENET WEAPONS LABORATORY, SMCAR-LCB-TL, WATERVLIET, NY 12189, OF ANY ADDRESS CHANGES.

NOTE: COPY TO EACH SYMPOSIUM ATTENDEE.